EXPLICIT INFLUENCE OF WATER MICROSOLVATION ON CHARGE TRANSFER AND DYNAMICS IN GROUND AND EXCITED ELECTRONIC STATES OF MOLECULAR SYSTEMS

Dissertation

zur Erlangung des Doktorgrades

der Naturwissenschaften

von

Maxim Zakharov

vorgelegt beim Fachbereich
Chemische und Pharmazeutische Wissenschaften
der Johann Wolfgang Goethe-Universität
in Frankfurt am Main

Frankfurt am Main

2009

D30

vom Fachbereich FB 14 Biochemie, Chemie und Pharmazie der Johann Wolfgang Goethe–Universität als Dissertation angenommen.

Dekan: ……Prof. Dr. Dieter Steinhilber

Gutachter: ……Prof. Dr. Bernd Brutschy

Datum der Disputation: ……..… 07.07.2010

Dedicated to the bright memory of my father…

Acknowledgements

I would like to acknowledge the following persons whom I had the pleasure to know and work with during the last years.

Prof. Dr. Andreas Dreuw for his systematic, and same time, creativity-stimulating manner of supervision.

Our collaboration partners from Frankfurt (Prof. Dr. Brutschy, Dr. Yevgeniy Nosenko), Mainz (Dr. Anke Hoffman) and Orlando (Dr. Artëm E. Masunov), especially the experimentalists, without whose intriguing experiments this work would not exist.

Current and former members of the AK Brutschy, AK Dreuw, AK Stock and AK Wachtveitl (especially Alexandros, Jan Hendrik, Jürgen, Maxim, Michael, Philipp, Roman, Stefan and Victor) for sharing experiences – often productive.

Special thanks to Dr. Pedro Salvador (Girona) for teaching me BSSE-free way of thinking and to our system administrator, Dr. Rainer Hegger, for the MS-free, yet comfortable, computational environment.

Sincere gratitude to my family members, whose constant support during the study and tolerance at its final stage, I appreciate so much.

Contents

Contents i

Kurzdarstellung (German Abstract) v
Abstract vii

Einleitung und Zusammenfassung (German Introduction and Summary) ix
Introduction and Summary xiv

Chapter 1 1
Theoretical Methods: an Overview 1
Part 1.1 1
Molecular Schrödinger Equation 1
1.1.1 Molecular Wave-Function: a General Form 1
1.1.2 Adiabatic Expansion and Born-Oppenheimer Approximation 3
1.1.3 Characterization of Adiabatic Potential Energy Surfaces 7
1.1.4 Harmonic Approximation and Beyond 8
Part 1.2 11
Electronic Schrödinger Equation: Ground State 11
1.2.1 Wave function of Noninteracting Electrons 11
1.2.2 Hartree-Fock Approximation 14
1.2.3 Electron Correlation 18
1.2.4 Perturbation Theory 23
1.2.5 Coupled-Cluster Theory 27
1.2.6 Density-Functional Theory 29
Part 1.3 34
Electronic Schrödinger Equation: Excited States 34
1.3.1 An Overview 35
1.3.2 Introduction to Response Theory 36
1.3.3 Time-Dependent Coupled-Cluster Theory 42
1.3.4 Time-Dependent Density-Functional Theory: Formal Foundations 44
1.3.5 Time-Dependent Density-Functional Response Theory 49
1.3.6 Time-Dependent Density-Functional Theory: Properties and Limitations 51
Part 1.4 53
Basis-Set Effects 53
1.4.1 Basis-Sets Types and Basis-Set Errors 53
1.4.2 Methods for Basis-Set Superposition Error Correction 58
1.4.3 Counterpoise Correction for Basis-Set Superposition Error 60
1.4.4 Basis-Set Superposition Error: Uncommon Implications 65

Chapter 2 69
Water Deficient Environment Accelerates Proton Exchange: Acetone-Water Reaction Catalyzed by Calix[4]hydroquinone Macromolecules 69
2.1 Introduction 69
2.2 Theoretical Methods 73
2.3 Proton Exchange via Concerted Proton Transfer in CHQ 75
2.4 Keto-Enol Tautomerism via Concerted Proton Transfer in Hydrated Acetone Clusters 77
2.5 Keto-Enol Tautomerism in Hydrated Hydroquinone-Acetone Clusters 83

2.6 Stability of the Hydrated Acetone and Hydrated Hydroquinone-Acetone Clusters 85
2.7 Proton Exchange via Concerted Mechanism: Summary 86
2.8 Proton Exchange via Ionic Mechanism Triggered by CHQ Dissociation: Possible Scenarios 87
2.9 Proton Exchange via Zwitterionic Intermediates 92
2.10 Proton Exchange via Anionic Intermediates 93
2.11 Proton Exchange via Cationic Intermediates 95
2.12 Rate Constants of the Proton Exchange via Ionic Intermediates 96
2.13 Catalysis of Acetone-Water Proton Exchange by Strong and Weak Acids in Aqueous Solutions 97
2.14 Summary and Conclusions 98

Chapter 3 103
Specific Microsolvation Triggers Dissociation-Mediated Red-Shifted Fluorescence of Methyl 4-*N*,*N*-dimethylaminobenzoate Ester in the Gas Phase 103
3.1 Introduction 103
3.2 Theoretical Methods 107
3.3 Assignment of the Infrared Spectra of DMABME•••$(H_2O)_2$ Complexes 109
3.4 Excited Electronic States of the DMABME•••$(H_2O)_2$ Complexes 113
3.5 Dissociation-Mediated TICT Formation in DMABME 119
3.6 Summary and Conclusions 123
3.7 Addendum 126
Influence of Electron Correlation, Anharmonicity and Basis-Sets on 126
Calculated IR Spectra of H-bonded Prototype Systems 126

References 135

Abbreviations

Chap.……chapter
Eq.……equation
Fig.……figure
Ref.……reference
Sch.……scheme
Sec.……section
Tab.……table

ADC(2)……algebraic diagrammatic construction (**1.3.1**)[1]
ALDA……adiabatic local-density approximation (**1.3.4**)
AU……atomic units (**1.2.2**)
B3LYP……Becke-Lee-Young-Perdew 3-parameter hybrid density functional (**1.2.6**)
BO……Born-Oppenheimer (**1.1.2**)
BSIE……basis-set incompleteness error (**1.4.1**)
BSSE……basis-set superposition error (**1.4.1**)
CC……coupled-cluster (**1.2.3**)
CC2……approximated coupled-cluster with singles and doubles (**3.2**)
CDFT……current density-functional theory (**1.3.6**)
CGF……contracted Gaussian functions (**1.4.1**)
CHA……chemical Hamiltonian approach (**1.4.2**)
CI……configuration-interaction (**1.2.3**)
CHQ……calix[4]hydroquinone (**2.1**)
CP……counterpoise (correction) (**1.4.2**)
CT……charge transfer (**1.3.6**)
DE……deprotonation energy/enthalpy (**2.2**)
DFT……density-functional theory (**1.2.3**)
DMABME……methyl 4-*N*,*N*-dimethylaminobenzoate ester (**3.1**)
DMABN……4-*N*,*N*-dimethylaminobenzonitrile (**3.1**)
EA……electron affinity (**3.3**)
GF……Gaussian-type functions (**1.4.1**)
GGA……generalized-gradient approximation (**1.2.6**)
HA……harmonic approximation (**1.1.4**)
H-bond……hydrogen bond (**1.2.3**)
HF……Hartree-Fock (**1.2.2**)
HK……Hohenberg-Kohn (**1.2.6**)
ICT……intramolecular charge transfer (**3.1**)
IP……ionization potential (**3.3**)
IR……infrared (**1.1.3**)
IVR……internal vibrational energy redistribution (**3.5**)

[1] Here and below: first detailed entry (section).

KET……keto-enol tautomerism (**2.1**)
KS……Kohn-Sham (**1.2.6**)
LDA……local-density approximation (**1.2.6**)
LE…… locally-excited (electronic states) (**1.3.6**)
LIF……laser-induced fluorescence(spectroscopy) (**3.1**)
MBPT……many-body perturbation theory (**1.2.3**)
MCSCF……multiconfiguration self-consistent field (**1.2.1**)
MP2……Møller-Plesset perturbation theory of second-order (**1.2.4**)
MPPT……Møller-Plesset perturbation theory (**1.2.4**)
NEO……nuclear-electronic orbitals (approach) (**1.1.2**)
NMR……nuclear-magnetic resonance (**2.1**)
NOON……natural-orbitals occupation number (**2.2**)
PA……proton affinity (**2.2**)
PE……proton exchange (**2.1**)
PICT……planar intramolecular charge transfer (**3.1**)
PT……proton transfer (**2.1**)
PES……potential energy surface (**1.1.2)**
R2PI……resonant two-photon ionization (spectroscopy) (**3.1**)
RG……Runge-Gross (**1.3.4**)
RSPT……Rayleigh-Schrödinger perturbation theory (**1.2.3**)
SCF……self-consistent field (**1.2.2**)
SF……Slater-type functions (**1.4.1**)
TDDFT……time-dependent density-functional theory (**1.3.4**)
TD-DFRT……time-dependent density-functional response theory (**1.3.5**)
TD-KS……time-dependent Kohn-Sham (**1.3.5**)
TICT……twisted intramolecular charge transfer (**3.1**)
***xc*-kernel**……exchange-correlation kernel (**1.3.4**)
ZPVE……zero-point vibrational energy (**1.1.4**)

Kurzdarstellung

Moderne computergestützte molekulare quantenchemische Studien, wie die vorliegende, verwenden in der Regel ein breites Spektrum theoretischer Methoden. Die letzteren sind oft sehr komplex und man sollte generell nicht erwarten, dass ein praxisorientierter Wissenschaftler im Bereich der physikalischen Chemie – ein potentieller Leser dieser Arbeit – mit all diesen Methoden vertraut sein muß. Um das Lesen dieser Dissertation in einem solchen Fall zu vereinfachen, und sie *autark* zu machen, ist sie mit einem Überblick über die verwendeten theoretischen Methodologien versehen (Kapitel **1**). In diesem Überblick werden quantenchemische *Grundbegriffe* erläutert, auf die in der gesamten Arbeit immer wieder verwiesen wird, die theoretischen *Grundlagen* verwendeter Methoden dargelegt und deren *Eigenschaften* und *Beschränkungen* skizziert. Im Abschnitt **1.1** werden allgemeine Ansätze zur Lösung der molekularen Schrödingergleichung eingeführt, und in den Teilen **1.2** und **1.3** werden spezifische Ansätze zur Lösung der elektronischen Schrödingergleichung zur Bestimmung des elektronischen Grundzustands und angeregter Zustände präsentiert. Teil **1.4** ist der Beschreibung von *Basissatzeffekten*, die in Elektronenstrukturrechnungen im Allgemeinen auftreten, gewidmet. Dieser Abschnitt enthält eine Reihe von verschiedenen Einblicken und Konzepten, die im Rahmen dieser Arbeit vorgeschlagen werden, und welche den Experten in der Quantenchemie aufschlußreich sein können.

Im Kapitel **2** wird das Phänomen der Katalyse von Aceton-Wasser *Protonenaustausch* durch selbstaggregierende Calix[4]hydrochinon (CHQ)-Nanotubes sowie durch amorphe Aggregate von CHQ, welche in NMR-Versuchen (Ref. **1**) beobachtet wurde, mit Hilfe von modernen quantenchemischen Methoden untersucht. Der erste Teil dieser Studie (Abschnitt **2.3**-**2.7)** betrachtet den *konzertierten* Protonentransfer, unterstützt von mehreren *ursprünglich neutralen* OH-Gruppen innerhalb der wasserstoffgebundenen Netzwerke der CHQ-Aggregate. Der zweite Teil der Studie (Abschnitt **2.8**-**2.13**) ist dem dem *schrittweisen* Protonentransfer mittels Bildung von *ionischen* Zwischenprodukten infolge der CHQ- Prädissoziation gewidmet. CHQ-anwendungsspezifische Schlußfolgerungen, sowie allgemeine Aspekte, die für das Hauptthema dieser Dissertation relevant sind (*i.e.* Einfluß spezifischer Mikrosolvatation auf die betrachteten Protonentransferprozesse), werden im Abschnitt **2.1.4** zusammengefasst.

Das Phänomen der *dualen Fluoreszenz*, das in Komplexen von 4-*N*,*N*-Dimethylaminobenzoesäuremethylester (DMABME) und zwei Wassermolekülen in der Gasphase beobachtet wurde, wird im Kapitel **3** untersucht. Im Abschnitt **3.3** werden zunächst berechnete Grundzustandsinfrarotspektren verschiedener DMABME*2H_2O Isomere präsentiert, die zum einen die Identifikation aller in der Gasphase vorliegenden Isomeren erlauben, und zum anderen vor allem die Charakterisierung des für das Auftreten der dualen Fluoreszenz verantwortlichen Isomer ermöglichen. Um weiter den Reaktionsmechanismus der dualen Fluoreszenz zu verstehen, wurden die Potentialenergieflächen der relevanten Isomere im angeregten Zustand entlang der sogenannten TICT-Koordinate (TICT: engl. *twisted intramolecular charge transfer)* berechnet und der Mechanismus der Energierelaxation dieser Komplexe erforscht (Abschnitt **3.4-3.5**) (Ref. **3**). Eine kurze Zusammenfassung der wichtigsten Ergebnisse dieses Kapitels und die wichtigsten Schlußfolgerungen finden sich in Abschnitt **3.6**. Zum Abschluß wird im Abschnitt **3.7** eine Vergleichsstudie der Qualität der Potentialenergieflächen von prototypischen wasserstoffgebundenen Systemen im elektronischen Grundzustand (Ammoniak-Wasser und Ameisensäure-Wasser) zusammengefasst, in der die Qualität der Potentialenergieflächen hinsichtlich des verwendeten atomaren Basissatzes, der Behandlung der Elektronenkorrelation und der Anharmonizität der Potentialflächen getestet werden. Vor allem wurde festgestellt, dass die zum Studium der IR-Spektren der hydratisierten DMABME-Komplexe verwendete Methode hinreichend genau ist, um die einzelnen Isomere zu unterscheiden und die experimentellen Spektren eindeutig zuzuordnen (Abschnitt **3.3**).

Abstract

Modern computational molecular quantum chemical studies, such as the present one, typically employ a wide range of theoretical techniques. The latter are often rather complicated and one should not generally expect that an experimental scientist in the area of physical chemistry, a potential reader of this work, should be familiar with all these techniques. To simplify the reading of the Thesis and to make it *self-sufficient*, it is supplied with an overview of the employed theoretical methodologies (Chapter **1**). The overview explains basic quantum-chemical *terminology* referred to throughout the Thesis, introduces theoretical *foundations* of the methods and outlines their *properties* and *limitations*. In Part **1.1** of Chapter **1**, methods for the solution of the molecular Schrödinger equation are introduced, while in the subsequent Parts **1.2** and **1.3** methods for the solution of the electronic Schrödinger equation are presented to find the ground and excited states, respectively. Part **1.4** is dedicated to *basis-set effects* which are omnipresent in electronic-structure calculations. It contains a number of unusual insights and concepts proposed by the author and, thus, may be insightful also to experts in quantum chemistry.

In Chapter **2**, the phenomenon of acetone-water *proton exchange* catalyzed by tubular as well as amorphous aggregates of calix[4]hydroquinone (CHQ) macromolecules, which has been observed previously in NMR experiments (Ref. **1**), is investigated by means of correlated quantum-chemical methods. The first part of the study (Section **2.3**-**2.7**) considers *concerted* proton transfer, assisted by several initially *neutral* OH-groups in the hydrogen-bonded networks of CHQ aggregates. The second part of the study (Section **2.8**-**2.13**) is dedicated to a second mechanism of proton exchange: *step-wise* proton transfer via formation of *ionic* intermediates resulting from CHQ pre-dissociation. CHQ application-specific as well as general conclusions, relevant to the main topic of the Thesis (*i.e.* influence of specific microsolvation on the considered proton transfer processes), are presented in Section **2.14**.

The phenomenon of *dual fluorescence* observed in clusters of methyl 4-*N*,*N*-dimethylaminobenzoate ester (DMABME) and two water molecules in the gas phase, is studied in Chapter **3**. Experimentally, the dual fluorescence was detected in experiments combining optical and ground-state ion-depletion infrared spectroscopies in ultracold molecular beams (Ref. **2**). In Section **3.3**, calculated ground-state infrared spectra are presented that allow to identify the structures of those isomers, which are present in the gas-

phase, as well as the structure of the isomer responsible for dual fluorescence. To further understand the reaction mechanism of dual fluorescence, excited-state potential energy surfaces of the identified isomers were computed along the relevant *twisted intermolecular charge-transfer* formation coordinate and the mechanism of energy dissipation in these complexes was investigated (Section **3.4**-**3.5**) (Ref. **3**). A brief summary of the main results of this chapter and conclusions are given in Section **3.6**. Finally, in Section **3.7** a complementary benchmark study of the quality of ground-state potential energy surfaces of prototypical hydrogen-bonded systems (ammonia-water and formic acid-water dimers) obtained at the level of BSSE-corrected MP2 combined with moderate basis sets, has been conducted. The quality of potential energy surfaces was tested with respect to basis-set size, level of electron correlation and anharmonicity effects and the applied methodology to identify the IR spectrum of hydrated DMABME complexes (Section **3.3**) has been found to be sufficient to uniquely assign the IR spectra.

Einleitung und Zusammenfassung

Emergenz ist unvermeidlich...

Die modernen Fortschritte in der chemischen Kinetik besagen, dass die so genannten *elementaren Reaktionen* wie *Protonen-* und *Elektronentransfer* oft durch Interaktionen der *gelösten Substanz* mit dem *Lösungsmittel* bestimmt (*e.g.* Ref. **4**, **5**, **6**, **7**, **8**, **9**, **10**, **11**) sind. Obwohl diese Interaktionen ungefähr um eine Größenordnung schwächer als *kovalente Bindungen* sind, können sie die Energie der Edukte und Produkte, Reaktionsraten und damit sogar die zugrundeliegenden Reaktionsmechanismen beträchtlich ändern. Wenn das Lösungsmittel *polar*, *protisch* oder *basisch* ist, dann können seine Moleküle Komplexe mit dem gelösten Stoff bilden, oder höhere Aggregate, durch, zum Beispiel, *dative* oder *Wasserstoff-Bindungen*. Die geometrische oder elektronische Struktur von den Reagenten kann beträchtlich beeinflusst werden (Ref. **8**, **9**, **11**). Folglich kann das System elementare Reaktionsszenarien aufweisen, die sich von solchen in *isolierten* Molekülen oder im *dielektrischen/polaren Kontinuum* unterscheiden. Dies impliziert, dass Experimente an *einzelnen* Molekülen umgeben von einer geringen Anzahl an Lösungsmittelmolekülen, sogenannter Cluster, entscheidend sind für das Verständnis des direkten Einflußes des Lösungsmittels auf die Elementarreaktionen auf *molekularer* Ebene. Dieses Verständnis erlaubt dann oft Rückschlüsse auf die in der *kondensierten Phase* ablaufenden Reaktionen zu ziehen. Technisch gesehen, kann man solche Bedingungen durch Experimente an in Molekularstrahlen gebildeten Clustern bei niedrigen Temperaturen realisieren. Oft können aufwändige laserspektroskopische Verfahren die notwendige *spektrale, temporale* und *strukturelle* Auflösung liefern, um die Reaktionsmechanismen detailliert zu untersuchen, während quantenchemische *ab-initio*-Berechnungen oft komplementär sind und aussagekräftige Einblicke zur Interpretation von Versuchsdaten liefern können.

Unter vielen anderen polaren Lösungsmitteln, spielt Wasser in Elementarreaktionen eine besondere Rolle. Erstens, da es in der Natur omnipräsent ist, ist Wasser in viele fundamentale chemische und biologische Prozesse involviert. Zweitens, Wassermoleküle sind *bifunktionell,* d.h. sie besitzen *protonenabgebende* sowie *protonakzeptierende* Gruppen, die unmittelbar in die Protonenübertragungsreaktionen involviert werden können (*e.g.* Ref. **8**, **9**, **12**, **13**, **14**, **15**, **16**). Solche Reaktionen treten normalerweise entlang der *intra-* oder *intermolekularen* Wasserstoffbrücken auf. In dieser Arbeit sind zwei Beispiele mittels moderner

quantenchemischer Methoden untersucht worden, die die zentrale Bedeutung der *Mikrosolvatation* des Wassers demonstrieren.

Das erste Beispiel (Kapitel **2**) ist das Phänomen des *Protonenaustauschs* im Gemisch von Aceton, Wasser, katalysiert durch selbstaggregierende Nanotubes sowie amorpher Aggregate von Calix[4]hydrochinon (CHQ), welches in NMR Experimenten beobachtet werden konnte (Ref. **1**). Hier treten Protonenübertragungsreaktionen zwischen Wasser und *Gast*-Acetonmolekülen, eingelagert in den CHQ-*Wirts*-Molekülen, im elektronischen Grundzustand auf. Da das Phänomen in *spezifischen* wasserstoffgebunden Netzwerken auftritt, die durch die OH-Gruppen vom eingebetteten Wasser und CHQ gebildet werden, bedarf es einer expliziten Analyse der Mikrosalvation. Obwohl die Katalyse des Protonenaustauschs in der kondensierten Phase beobachtet wurde, gibt es Argumente dafür, dass sie dank der *Desolvatationseigenschaft* der CHQ Makromoleküle auftritt. Daher kann man davon ausgehen, dass die Protonentransferprozesse, die in wasserstoffgebundenen Netzwerken stattfinden, denen in Gasphasenclustern ähnlich sind.

Zwei grundlegende Mechanismen des Protonenaustauschs wurden analysiert. Der erste Mechanismus ist die *keto-enol-Tautomerie* von Aceton durch *konzertierten* Protonentransfer, unterstützt von mehreren, ursprünglich neutralen OH-Gruppen innerhalb der wasserstoffgebundenen Netzwerken der CHQ-Aggregate. Es wird gezeigt, dass diese OH-Gruppen tatsächlich den Protonentransfer katalysieren. Die Herkunft dieser Katalyse wurde dem kooperativen Effekt der permanenten elektrischen Dipolmomente der bifunktionnellen OH-Gruppen zugeschrieben. Der zweite in Betracht gezogene Mechanismus ist der *schrittweise* Protonentransfer durch die Bildung von *ionischen* Zwischenprodukten, die aus der CHQ-Dissotiation resultieren (Ref. **17**). Die durchgeführten Rechnungen haben offenbart, dass die von der Dissoziation produzierten ionischen Intermediate: das *Anion* der CHQ, das *Kation* des protonierten Acetons und ein aus beiden letzeren bestehendes *Zwitterion*, den Protonenaustausch viel stärker katalysieren, als dies im Rahmen des konzertierten Mechanismus passiert. Das Zustandekommen der Katalyse wurde durch die Polarisierung der Reaktanden erklärt: durch die relevanten Protonentransfernetzwerke (anionischer Mechanismus), durch die Schwächung der CH-Bindung des protonierten Acetons (kationischer Mechanismus) und durch die Präsenz von unabgeschirmten Anionen und Kationen (zwitterionischer Mechanismus).

Die spezifische Rolle der nicht-katalysierenden Wassermoleküle in wässriger Lösung wird aufgezeigt. Zum einen depolarisieren die permanenten Dipolmomente der

Lösungsmittelmolekülen diejenigen bifunktionnellen OH-Gruppen, die in den Protonentransfer involviert sind und mindern somit die Effizienz der Katalyse sowohl in konzertierten neutralen als auch in schrittweisen ionischen Transfermechanismen. Zum anderen wird durch vollständige Solvatation der geladenen Teilchen und vor allem der Protonen die Entstehung der effizienten katalytischen ionischen Intermediate verhindert.

Ein zweites Beispiel für die Bedeutung der Mikrosolvatation für Moleküleigenschaften ist das Phänomen der *dualen Fluoreszenz*, welche zum Beispiel in mikrosolvatisierten Gasphasenclustern des 4-N,N-Dimehylaminobenzoesäuremethylesters (DMABME) (Ref. **2**) beobachtet wurde. DMABME gehört zu den berühmten *push-pull* Benzolderivaten, die nach Anregung in den ersten elektronisch angeregten Zustand *intramolekularen Ladungstransfer* (ICT) vollziehen. Diese Moleküle weisen typischerweise in *wässrigen* Lösungen eine anomale *rotverschobene* duale Fluoreszenz auf (Ref. **18**). Dagegen zeigen einzelne, isolierte Moleküle von DMABME keine duale Fluoreszenz in der Gasphase, erst nach Mikrosolvatation durch mindestens zwei Wassermoleküle (1:2) ist duale Fluoreszenz wieder beobachtbar. Die Infrarot (IR) *Ion-Depletion* Spektroskopie ermöglicht es grundsätzlich die IR-Spektren des Grundzustand-*Vorläufers* des 1:2 Komplexes zu erhalten, der für die duale Fluoreszenz verantwortlich ist (Ref. **2**).

Tatsächlich sind jedoch zwei unterschiedliche Isomere des 1:2 Komplexes zu fast gleichen Mengen im Molekularstrahl gefunden worden, wobei jedoch nur eines rotverschobene Fluoreszenz zeigt. Um festzustellen welches Isomer für die rotverschobene Fluoreszenz verantwortlich ist und um den zugrundeliegenden Mechanismus zu untersuchen, ist eine gründliche theoretische Untersuchung unternommen worden (Kapitel **3,** Ref. **3**). Die berechneten Grundzustand-IR-Spektren haben die Identifizierung der experimentell beobachteten Isomere möglich gemacht. In diesen Komplexen ist ein Wasserdimer entweder an den Carbonylsauerstoff der Esterfunktion oder an den Aminostickstoff des DMABME wasserstoffgebunden. Die Mikrosolvatation durch das Wasserdimer hat natürlich einen Einfluß auf die angeregten ICT-Zustände der Isomere: es kann sie abhängig vom Bindungsmuster stabilisieren oder destabilisieren. Dieser Effekt ist dem oben beschriebenen (Kapitel **2**) Effekt des Wassers in Protonentransferreaktionen konzeptionell ähnlich.

Noch erstaunlicher ist es, dass die Berechnungen gezeigt haben, dass das N-gebundene Isomer für die rotverschobene Fluoreszenz verantwortlich ist, obwohl der entsprechende ICT-Stand durch das Wasserdimer destabilisiert wird. Um dieses überraschende Verhalten der Isomere zu verstehen, sind der Mechanismus der Bildung eines *twisted intramolecular Charge-Transfer* (TICT) Zustands und mögliche Energiedissipationwege ausführlich studiert

worden. Denn um rotverschobene fluoreszieren zu können, muß der N-gebundene Komplex imstande sein Energie abzugeben und sich in einer für die Fluoreszenz verantwortlichen TICT-Struktur stabilisieren. In der Gasphase kann das *strahlungsfrei* nur durch *Photodissoziation* passieren. *Tatsächlich* zeigen unsere Rechnungen, dass nur das N-gebundene Isomer schnell genug in isoliertes DMABME und ein Wasserdimer dissoziiert, aufgrund der sofortigen Repulsion zwischen dem Aminostickstoff und dem Wasserdimer im TICT-Zustand. Im Gegensatz dazu wird das O-gebundene Isomer im ICT Zustand sogar stärker gebunden, da es zu zusätzlicher elektrostatische Anziehung im ICT-Zustand kommt. Dieses verhindert die Photodissoziation des O-gebundenen Isomers und somit auch die Bildung eines TICT-Zustands. Dieses Beispiel demonstriert eine andere wichtige, aber oft vergessene Eigenschaft der Lösungsmittelmoleküle, nämlich als *Energieakzeptor* in der Gas- und Flüssigphase zu dienen, was den spezifischen Verlauf chemischer Reaktionen entlang bestimmter Reaktionspfade erst möglich macht (Ref. **3**).

Die beiden Beispiele der Kapitel **2** und **3** unterstützen uneingeschränkt die These, dass Ladungstransferreaktionen mit Hilfe von unterschiedlichen Mechanismen optimiert werden können, im Hinblick auf Anzahl und spezifische Bindungsmuster der involvierten Wassermoleküle. Die Ergebnisse von effizienteren Reaktionsszenarien könnnen nur in der Gasphase oder in *wasserknappen* makromolekularen Architekturen beobachtet werden, da die Szenarien in den wässrigen Lösungen durch die Gegenwirkung des Wassers als Lösungsmittel unterdrückt werden können. *Im Allgemein können Elementarreaktionen, die in wässriger Lösung ablaufen, oft weder durch die Eigenschaften der einzelnen zu lösenden Moleküle noch durch Berechnungen in polaren Kontinuumsmodellen theoretisch beschrieben werden.*

Die theoretische Beschreibung von Ladungstransferreaktionen in Komplexen von Lösungsmittel und gelöstem Stoff benötigt im Allgemeinen eine quantenmechanische Untersuchung der elektronischen Struktur auf hoher theoretischer Ebene (Abschnitt **1.2.3**). Derzeit ist die quantenchemische Berechnung *mittelgroßer* molekularer Systeme auf Methoden beschränkt, die hinsichtlich der Genauigkeit und des Rechenaufwandes mit der *Møller-Plesset Störungstheorie* zweiter Ordnung vergleichbar sind (Abschnitt **1.2.4**). Es ist dabei zu beachten, dass bereits mittelgroße Systeme praktisch relevant sind, da sie oft grundlegende Eigenschaften von größeren realen (z. B. biologischen) Systemen abbilden.

Die meisten der üblichen quantenchemischen Rechenmethoden verwenden *atom-zentrierte* Basissätze (Abschnitt **1.4.1**). Dies beinhaltet einen zusätzlichen Berechnungsfehler – den sogenannten Basissatzsuperpositionsfehler (Engl. *basis-set superposition error* (BSSE))

(Abschnitt **1.4.1**), der durch die wechselseitige Erweiterung der Fragmentbasissätze innerhalb eines Komplexes zu Stande kommt. Zwangsläufig sind Wellenfunktion und damit Moleküleigenschaften des Komplexes BSSE-kontaminiert, die absolute Energie des Komplexes wird zu negativ und die *Potentialenergieflächen* verfälscht. Potentialenergieflächen von Komplexen, die sogenannte *nicht-kovalente* Wechselwirkungen besitzen, sind besonders BSSE-empfindlich (Abschnitt **1.4.3**) und zeichnen sich durch ein sogenanntes *Overbinding* aus. Bisher gab es bereits mehrere Beispiele, die demonstriert haben, dass die Berücksichtigung des BSSE die Qualität der Potentialenergieflächen von schwach gebundenen, insbesondere wasserstoffgebundenen Komplexen, die mit Hilfe der Møller-Plesset Störungstheorie zweiter Ordnung (MP2) (Abschnitt **1.2.4**) (siehe Ref. **19** für Überblick) erhalten wurden, beträchtlich verbessert.

Die Botschaft der vorliegenden Arbeit ist, dass die Qualität der MP2 Potentialenergieflächen von wasserstoffgebundenen Komplexen nach der BSSE-Korrektur nicht nur höher wird, sondern praktisch *gleich* zu denjenigen BSSE-bereinigten Flächen wird, die mit genaueren und rechnerisch wesentlich anspruchsvolleren Methodologien berechnet wurden. Dies wurde anhand prototypischer wasserstoffgebundener Systeme im Rahmen einer Vergleichsstudie gezeigt (Abschnitt **3.7**), die eine Grundlage zur Entschlüsselung des IR-Spektrums der 1:2-Komplexen von DMABME geschaffen hat. Im Prinzip ist diese Aussage ziemlich intuitiv, wenn man realisiert, dass der fehlerhafte BSSE-*Beitrag* zur *Stabilisationsenergie* eines supermolekularen Komplexes normalerweise meist in etwa dieselbe Größe hat wie der der *Elektronenkorrelation*. Nichtsdestotrotz wurde diese Tatsache von der quantenchemischen wissenschaftlichen Gemeinschaft bislang nicht wahrgenommen.

Introduction and Summary

Emergence is inevitable...

Contemporary advances in chemical kinetics suggest that so-called *elementary reactions* such as *proton* and *electron transfer* are often determined by the interactions of *solute* with *solvent* (*e.g.* Ref. **4**, **5**, **6**, **7**, **8**, **9**, **10**, **11**). Although these interactions are about an order of magnitude weaker than *covalent bonds*, they can alter energy, rates or even underlying mechanisms of reactions considerably. When the solvent is *polar*, *protic* or *basic*, its molecules can form *solute-solvent* complexes, or larger aggregates via, for example, *dative* or *hydrogen bonds*. The geometric or electronic structure of the reagents can be affected significantly (Ref. **8**, **9**, **11**). Consequently, the system can exhibit elementary reaction scenarios, different from those in *isolated* molecules, or in *dielectric/polar continuum*. It proposes that the experiments on *individual* solute molecules, as well as on the solute molecules surrounded by a small number of solvent molecules, is the key for understanding the direct influence of solvent on the elementary reactions at a *microscopic* level. This understanding often allows to draw conclusions about the behaviour of the reactions in *condensed phase*. Technically, such conditions can be realized in the experiments on the *gas-phase* molecular clusters formed in *supersonic beams* at low temperatures. Elaborate spectroscopic techniques can often provide sufficient *spectral*, *temporal* and *structural* resolution to investigate the reaction mechanisms in great details, whereas high-level *ab-initio* quantum-chemical calculations are often complimentary and can provide meaningful insights for the interpretation of experimental data.

Among many other polar solvents, water plays a special role in elementary reactions. Firstly, since it is ubiquitous in nature, water is involved in many fundamental chemical and biological processes. Secondly, water molecules are *bifuctional i.e.* they possess *proton-donating* as well as *proton-accepting* groups which can be directly involved in proton-transfer reactions in both ground and electronically-excited states (*e.g.* Ref. **8**, **9**, **12**, **13**, **14**, **15**, **16**). Such reactions normally occur along *intra-* or *intermolecular* hydrogen bonds. In the present Ph. D. Thesis, two examples which demonstrate the paramount importance of water *microsolvation* in charge-transfer processes have been investigated by means of high-level quantum-chemical methodology.

The first example (Chapter **2**) is the phenomenon of acetone-water *proton exchange* catalyzed by tubular as well as amorphous aggregates of calix[4]hydroquinone (CHQ) macromolecules, observed in nuclear magnetic resonance experiments (Ref. **1**). Here, proton-transfer reactions occur between water and *guest* acetone molecule trapped by the CHQ *host* macromolecules in the ground electronic state. Since the phenomenon occurred in *specific* hydrogen-bonded networks formed by the OH-groups of embedded water and CHQ, it required an explicit analysis of microsolvation. Although the proton exchange catalysis was observed in condensed phase, arguments are given that it occurs due to the *desolvation* property of CHQ macromolecules. Thus, the proton-transfer processes are taking place in the hydrogen-bonded networks of CHQ similar to those in gas-phase clusters.

Two principle mechanisms of the proton exchange are analyzed. The first mechanism is *keto-enol tautomerism* of acetone via *concerted* proton transfer assisted by several, initially neutral, OH-groups in the hydrogen-bonded networks of CHQ aggregates (Ref. **1**). It is shown, that these OH-groups, indeed, catalyze proton exchange. The origin of the catalysis was attributed to the cooperative effect of permanent electric dipole moments of bifunctional OH-groups. The second considered mechanism is *step-wise* proton transfer via formation of *ionic* intermediates resulting from CHQ dissociation (Ref. **17**). The simulations revealed that the ionic moieties produced by the dissociation: the *anion* of CHQ, the *cation* of protonated acetone and the *zwitterion* comprising the latter two ions, catalyze proton exchange much stronger than in the case of the concerted mechanism. The nature of catalysis was then explained by polarization of the reagents by relevant proton transfer networks (anionic mechanism), by weakening the CH-bond of protonated acetone (cationic mechanism) and by the presence of unscreened anions and cations (zwitterionic mechanism).

The specific role of the solvent water molecules in the catalysis is manifested. First, the permanent dipole moments of the solvent molecules depolarize bifunctional OH-groups involved in the proton-transfer reaction. They hence decrease the efficiency of catalysis by the reacting OH-groups and the CHQ-anions in the concerted as well as step-wise mechanisms, respectively. Furthermore, in the case of ionic catalysis, solvent water exhibits a less trivial property: large aggregates of solvent molecules, can abstract protons from the protonated species and therefore prevent the formation of cationic and highly efficient zwitterionic catalytic complexes.

A second example for the importance of microsolvation on molecular properties is the phenomenon of *dual fluorescence* observed in the microhydrated gas-phase clusters of 4-*N*,*N*-dimethylaminobenzomethyl ester (DMABME) (Ref. **2**). DMABME belongs to the famous

push-pull benzene derivatives which undergo *intramolecular charge transfer* (ICT) upon excitation in the first electronically excited state. These species are known to exhibit *red-shifted* dual fluorescence in *aqueous* solutions (Ref. **18**). In contrast, single molecules of DMABME do not show dual fluorescence in the gas phase, while its hydration by two water molecules (1:2) induces dual fluorescence again. Infrared (IR) *ion-depletion* spectroscopy allowed to obtain IR spectra of the ground-state *precursors* of the particular isomer of 1:2 complex, responsible for dual fluorescence (Ref. **2**). In fact, two different isomers of the 1:2 complex were found in the molecular beam in nearly equal amounts, while only one of them induces red-shifted fluorescence.

To identify which particular isomer is responsible for red-shifted fluorescence and to investigate the underlying reaction mechanism at a microscopic level, a thorough computational study is undertaken (Chapter **3**, Ref. **3**). The calculated ground-state IR spectra made the identification of the experimentally observed isomers possible. In these complexes, water dimer is hydrogen-bonded either to the carbonyl oxygen of the ester function, or to the amino nitrogen of DMABME. Herein, the water dimer demonstrates a common property to stabilize or destabilize excited ICT states of the isomers, depending on its binding pattern, since water dimer polarizes or depolarizes the relevant electron donating or accepting groups of DMABME. This effect is conceptually similar to effect of water in the proton-transfer reactions in CHQ described above (Chapter **2**).

More surprisingly, the calculations revealed that the N-bonded isomer with the ICT state, destabilized by the water dimer, is responsible for the red-shifted fluorescence. To understand this unusual behavior of the isomers, the mechanism of *twisted intramolecular charge-transfer* (TICT) formation and energy dissipation is studied in detail. In summary, in order to induce red-shifted fluorescence, the N-bonded complex must be able to dissipate energy and stabilize itself in the TICT structure responsible for the fluorescence. In the gas phase it can only happen *nonradiatively* via *photodissociation*. In fact, arguments are given that only the N-bonded isomer dissociates rapidly enough into free DMABME and a water dimer, as a result of immediate repulsion in the TICT state between the amino nitrogen and the water dimer. Contrarily, in the O-bonded isomer the hydrogen bond becomes even stronger by additional electrostatic attraction in the ICT state. It prevents the isomer from fragmentation and therefore its deposition into the TICT structure. This example demonstrate another important but often forgotten property of solvent molecules to serve as an *energy acceptor* in the gas and liquid phase, allowing chemical reactions to follow specific ways determined by the minimum energy pathways on their potential energy surfaces (Ref. **3**).

Both examples of Chapters **2**, **3** readily support the thesis that charge-transfer processes of various mechanisms can be optimized with respect to the number and specific binding patterns of involved water molecules. The results of more efficient reaction scenarios can often be observed in the gas phase or in the *water-deficient* macromolecular architectures only, since in aqueous solutions the scenarios will be suppressed by counteraction of solvent water. *Overall, elementary reactions involving bulk solvent water often cannot be described by individual solute molecules alone and neither by those of solute molecules in polar continuum.*

The theoretical description of charge-transfer processes in solute-solvent complexes generally requires a high-level *correlated* quantum treatment of the electronic structure (Section **1.2.3**). At present, the application of correlated methodologies to *medium-sized* molecular systems is limited to those methods which are comparable, with respect to accuracy and computational cost, with second-order *perturbation theory* (Section **1.2.4**). Note, that medium-sized systems are of practical interest since they can often reproduce essential properties of larger realistic (*e.g.* biological) systems.

Most of the available high-level correlated methods operate with *atom-centered* basis sets (Section **1.4.1**). This introduces an additional computational error in the calculations – the so-called *basis-set superposition error* (BSSE) (Section **1.4.1**), which arises due to the mutual augmentation of fragment basis sets within the complex. As result, wave function and molecular properties of the complex become BSSE-contaminated, the absolute energy too negative and the *potential energy surfaces* mutilated. Ground-state potential energy surfaces of the complexes with pronounced *noncovalent* interactions (*e.g.* solute-solvent complexes) are particularly sensitive to BSSE (Section **1.4.3**). This is especially the case for the surfaces obtained at correlated level, which exhibits severe *overbinding*. To date, there are multiple examples which demonstrate that correction for BSSE significantly improves the quality of potential energy surfaces of weakly-bound, in particular – hydrogen-bonded, complexes, obtained at the level of second-order *Møller-Plesset* perturbation theory (MP2) (Section **1.2.4**) (see Ref. **19** for review).

The message of the present work is that the quality of the MP2 potential energy surfaces of hydrogen-bond complexes is not just improved by the BSSE-correction, but rather become nearly *equal* to BSSE-corrected surfaces obtained with more accurate and computationally demanding methodologies. That was shown on prototypic hydrogen-bonded systems in a benchmarking study (Section **3.7,** supporting information of Ref. **3**), which laid the ground to

decipher the IR spectrum of the 1:2 complexes of DMABME. In principle, this statement is rather straightforward, if one realizes that the *BSSE-contribution* to the *stabilization energy* of a supermolemolecular complex in the vicinity of its equilibrium structure is usually of about the same order of magnitude as the *correlation contribution* for a wide range of atom-centered basis sets. However, until recently, this fact has been greatly overseen by the quantum-chemical scientific community.

Chapter 1
Theoretical Methods: an Overview

Part 1.1
Molecular Schrödinger Equation

1.1.1 Molecular Wave-Function: General Form

Since the introduction by Erwin Schrödinger of his famous *non-relativistic* quantum equation in 1926 (Ref. **20**), its solution in application to polyatomic and molecular systems constitutes the major task of quantum chemistry. In the time-independent case, this is an *eigenvalue problem* with the *molecular Hamiltonian* $\hat{H}_{mol}$

$$\hat{H}_{mol}\Phi_{\mathrm{M}}(x,X)=\left(\hat{H}_{el}(r,R)+\hat{V}_N(R)+\hat{T}_N(R)+\underbrace{\hat{H}'(x,X)}_{\substack{small\\terms}}\right)\Phi_{\mathrm{M}}(x,X)=E_{\mathrm{M}}\Phi_{\mathrm{M}}(x,X)\,. \tag{1}$$

Its *eigenvalues* E_{M} corresponding to the *eigenfunctions* $\Phi_{\mathrm{M}}(r,R)$ provide the *energy spectrum* of molecular system. Here and further, the electronic coordinates of a molecule comprising *n* electrons and *N* nuclei are contained in the multiindices $x=(x_1,x_2,...,x_i,...,x_n)$ and $X=(X_1,X_2,...,X_I,...,X_N)$. Herein, $x_i=(\underbrace{r_i^x,r_i^y,r_i^z}_{r_i};s_i)$ with r_i and s_i are spatial (Cartesian) and spin coordinates of electron *i*, and $X_i=(\underbrace{R_I^X,R_I^Y,R_I^Z}_{R_i};S_I)$ with R_I and S_I are Cartesian and spin coordinates of nucleus *I* respectively. Spatial parts $(r_1,r_2,...,r_i,...,r_n)$, $(R_1,R_2,...,R_I,...,R_N)$ of the electronic and nuclear coordinates are designated by collective r and R, respectively. The terms within Hamiltonian (1) are the *electronic Hamiltonian*

$$\hat{H}_{el}(r,R)=\hat{V}_{el}(r,R)+\hat{T}_{el}(r)\,, \tag{2}$$

the *nuclear potential energy operator*

$$\hat{V}_N(R) = \sum_I \sum_J \frac{Z_I Z_J}{|\vec{R}_I - \vec{R}_J|} \tag{3}$$

and the *nuclear kinetic energy operator*

$$\hat{T}_N(R) = \sum_I \frac{\hat{P}_I^{\,2}}{2M_I} = \sum_I \left(-\frac{\hbar^2}{2M_I} \right) (\nabla_I, \nabla_I). \tag{4}$$

The parts of electronic Hamiltonian are the *electronic potential energy operator*

$$\hat{V}_{el}(r,R) = \sum_i \sum_{j>j} \frac{e^2}{|\vec{r}_i - \vec{r}_j|} - \sum_i \sum_J \frac{eZ_I}{|\vec{r}_i - \vec{R}_I|} \tag{5}$$

and *electronic kinetic energy operator*

$$\hat{T}_{el}(r) = \sum_i \frac{\hat{p}_i^{\,2}}{2m_i} = \sum_i \left(-\frac{\hbar^2}{2m_i} \right) (\nabla_i, \nabla_i). \tag{6}$$

In the above formulas, ∇_i, ∇_I are the *gradient operators* (vectors) with respect to the coordinates of *i*-th electron and *I*-th nuclei, respectively. Small terms in Hamiltonian (1) are usually referred to magnetic effects which are small in the case of systems, considered in the present work. The solutions of Eq. (1) comprise all quantum mechanical information about the *stationary* properties of molecular system.

Two important remarks about the properties of molecular wave-functions should be made.

1) None of the above-introduced operators within molecular Hamiltonian (1) depends on the electronic or nuclear spin. Within the non-relativistic quantum mechanics, there is no way to introduce spin of the particle from first principles. This is possible only by means of the relativistic quantum equation of Dirac (Ref. **21**). Thus, the existence of spin is postulated in the present nonrelativistic theoretical framework. Still, relativistic effects (*e.g. spin-orbital coupling*) can be often incorporated in the nonrelativistic Eq. (1) by inclusion of corresponding terms into Hamiltonian (1), only when they are small enough compared to its main part (see *e.g.* Ref. **22**, **23**, **24**).

2) An important constraint on the molecular wave-function imposes the *Pauli principle* (Ref. **25**) which is somewhat independent from the Schrödinger equation. It states that there are only two classes of particles in nature – *fermions* and *bosons*. The wave function of an

ensemble of *n identical* ferminos is *antisymmetric* with respect to the interchange (permutation) of coordinates (both spatial and spin) of any two particles

$$\Psi^F(x_1,..,x_i,...,x_j,...,x_n) = -\Psi^F(x_1,..,x_j,...,x_i,...,x_n). \quad (7)$$

Fermions possess half-integer spins and electron belongs to this class. Bosons have an integer spin and their ensemble wave function is *symmetric* with respect to the coordinates permutation

$$\Psi^B(x_1,..,x_i,...,x_j,...,x_n) = +\Psi^B(x_1,..,x_j,...,x_i,...,x_n). \quad (8)$$

Unlike electron, nuclei can belong to both classes depending on their spin.

The most general form of the molecular non-relativistic wave function would be the following product

$$\Phi(x,X) = \Phi(x_1,x_2,...,X_1^1,X_2^1,...,X_I^1,X_{I+1}^2,X_{I+2}^2,...) = \Phi^x(x,X)\cdot\Phi^{X^1}(x,X)\cdot\Phi^{X^2}(x,X)\cdot.... \quad (9)$$

Herein, Φ^x is antisymmetric with respect to the permutation of electronic coordinates, Φ^{R^1}, Φ^{X^2},… are either antisymmetric or symmetric with respect to the permutation of nuclear coordinates of the given sort X^1, X^2… .

The fact that nuclear wave function can obey to the Pauli principle is often ignored in calculations. This can be justified in many cases since nuclear wave functions are usually much more localized as compared to the electronic ones and their identity is thus not a concern. However, this is not the case, for example, in systems comprising several hydrogen atoms, or protons. It will be shortly discussed in the end of next section.

1.1.2 Adiabatic Expansion and Born-Oppenheimer Approximation

In this section, different ways of solving the molecular Schrödinger equation will be reviewed.

The famous approach, introduced by Oppenheimer (Ref. **26**) takes into account the fact of small mass ratio of electrons and nuclei ($m_{el}/M_{nuc} < 10^{-3}$). In many cases, the electronic degrees of freedom can be considered as responding *instantaneously* to the changes of nuclear configurations. This rationalizes a particularly convenient expansion of the molecular wave function into the basis set of *stationary* electronic wave-functions

$$\Phi_{\mathrm{M}}(x,X)=\sum_{\mu}\Psi_{\mu}(x,\{X\})\Theta_{\mu\mathrm{M}}(X)\,.$$

(**10**)

The expansion coefficients of Eq. (10) depend on the nuclear geometries *explicitly* and define the nuclear wave functions $\Theta_{\mu\mathrm{M}}(X)$, associated with an electronic state μ. The electronic wave functions $\Psi_{\mu}(x,\{X\})$, forming the basis set, are the stationary solutions (eigenfunctions) of the time-independent Schrödinger equation with electronic Hamiltonian (1) (Sec. **1.1.1**)

$$\hat{H}_{el}(x,X)\Psi_{\mu}(x,\{X\})=\varepsilon_{\mu}(X)\Psi_{\mu}(x,\{X\})\,.$$

(**11**)

The eigenvalues $\varepsilon_{\mu}(X)$ define energies of the electronic levels of the system and depend *parametrically* on the "fixed" nuclear geometries. Due to the parametrical dependence, the electronic wave functions are usually referred to as *adiabatic* electronic wave functions. Using the *product rule* for differentiation, it is easy to check that

$$\hat{T}_N\Psi_{\mu}(x,\{X\})\Theta_{\mu\mathrm{M}}(X)=\left(\Psi_{\mu}\hat{T}_N+(\hat{T}_N\Psi_{\mu})+\sum_I\left(-\frac{\hbar^2}{2M_I}\right)\left(\nabla_I\Psi_{\mu},\nabla_I\right)\right)\Theta_{\mu\mathrm{M}}\,.$$

(**12**)

Multiplying both sides of Eq. (1) by the conjugate electronic wave-function and integrating over all electronic coordinates $\left(\langle\phi_{\eta}|\rightarrow\int_r dx\phi_{\eta}^{*}\right)$, making use of Eq. (12) and *orthonormality* of the electronic wave functions

$$\langle\phi_{\eta}|\phi_{\mu}\rangle=\delta_{\eta\mu}\,,$$

(**13**)

one arrives at the nuclear wave function Schrödinger equations

$$\left(\varepsilon_{\eta}+\hat{V}_N+\hat{T}_N-E_{\mathrm{M}}\right)\Theta_{\eta\mathrm{M}}=-\sum_{\mu}\underbrace{\left(\langle\Psi_{\eta}|\hat{T}_N|\Psi_{\mu}\rangle+\sum_I\left(-\frac{\hbar^2}{2M_I}\right)\left(\langle\Psi_{\eta}|\nabla_I\Psi_{\mu}\rangle,\nabla_I\right)\right)}_{\hat{\Lambda}_{\eta\mu}}\Theta_{\mu\mathrm{M}}\,.$$

(**14**)

The value $\hat{\Lambda}_{\eta\mu}$ herein is the so-called *nonadiabaticity operator*. Equation (14) can be interpreted as a stationary equation for the nuclear eigenfunctions and it is still *formally exact*.

For the further analysis it is convenient to rearrange Eq. (14) as follows

$$\left(\underbrace{\varepsilon_\eta + \hat{V}_N + \hat{\Lambda}_{\eta\eta}}_{\hat{U}_\eta(R)} + \hat{T}_N - E_{\mathrm{M}} \right) \Theta_{\eta\mathrm{M}} = -\sum_{\mu \neq \eta} \hat{\Lambda}_{\eta\mu} \Theta_{\mu\mathrm{M}} \ . \tag{15}$$

Off-diagonal terms $\hat{\Lambda}_{\eta\mu}$ of the nonadiabaticity operator are termed *nonadiabatic couplings*. In fact, transitions between the electronic states in course of nuclear motion are caused by these couplings. The diagonal part $\hat{\Lambda}_{\eta\eta}$ of the operator is normally a small perturbation to the left-hand side of Eq. (15). The term $\hat{U}_\eta(R)$ in the above equation can be considered as an *effective* potential corresponding to the nuclear motion of the system in its adiabatic electronic state. It determines a *hypersurface* in the space of nuclear coordinates – the adiabatic *potential energy surface* (PES), associated with a particular electronic state. Since molecular Hamiltonian (1) (Sec. **1.1.1**) is independent on spin, PES is the function of nuclear Cartesian coordinates R only.

The solution of the coupled equations (15) for the expansion coefficients of molecular wave-function is a challenge, since it requires knowledge of all electronic adiabatic wave functions – for both ground and excited states, as well as the nonadiabaticity operator for all nuclear configurations covered during their motion. Hence, it is crucial to introduce approximations for solving Eq. (15).

The first straightforward approximation is to just neglect all the coupling terms. Under this assumption the nuclear Schrödinger equation becomes

$$(U_\eta^{BO}(R) + \hat{T}_N)\Theta_{\eta\mathrm{M}}^{BO}(X) = E_{\eta\mathrm{M}}^{BO}\Theta_{\eta\mathrm{M}}^{BO}(X), \tag{16}$$

with the adiabatic molecular wave function

$$\Phi_{\eta\mathrm{M}}^{BO}(x, X) = \Psi_\eta(x, \{X\})\Theta_{\eta\mathrm{M}}^{BO}(X) \ . \tag{17}$$

Eq. (16), (17) constitute the *Born-Oppenheimer* (BO) *approximation* (Ref. **26**) for the molecular Schrödinger equation (1).

The applicability of the BO approximation to a particular situation can be easily evaluated by means of *perturbation theory* with respect to the nonadiabaticity operator. In general, the second order corrections to the adiabatic energies of Eq. (15) have the form

$$E_{\eta\mathrm{M}}^{(2)} = E_{\eta\mathrm{M}}^{BO} + \sum_{\mu}\sum_{\mathrm{N}} \frac{\left|\left\langle \Theta_{\eta\mathrm{M}}^{BO} \middle| \hat{\Lambda}_{\eta\mu} \middle| \Theta_{\mu\mathrm{N}}^{BO} \right\rangle\right|^2}{E_{\eta\mathrm{M}}^{BO} - E_{\mu\mathrm{N}}^{BO}} .$$

(**18**)

Obviously, a breakdown of the approximation will occur when the matrix element in the numerator is large compared to the energy difference in the denominator. This can happen in two cases. (1) When $\hat{\Lambda}_{\mu\eta}\left|\Theta_{\eta\mathrm{N}}^{BO}\right\rangle$ is not small for symmetry reasons. (2) When the system approaches a region in nuclear configuration space where the adiabatic potential energy surfaces approach each other and the denominator become close to zero. Therefore, the knowledge of adiabatic PES is of paramount importance for the understanding of nonadiabatic phenomena at a microscopic level. In most cases, only a few states are involved in such crossings where the BO approximation is not valid. In this case, the nonadiabatic couplings between only these electronic states are required. Even so, implementation of the couplings is a nontrivial computational task. Moreover, within *linear response theory* for the solution of the electronic Schrödinger equation, a standard tool to obtain *excitation energies*, nonadiabatic couplings between two excited states cannot be determined, since it requires the second-order response functions (Sec. **1.3.2**) which is computationally much more demanding.

Thus, the question arises whether it is possible to avoid such a complicated representation of the nuclear Hamiltonian.

One alternative is to use electronic basis set $\Psi_{\mu}(r, R^{(0)})$ where the positions of nuclei are fixed at some point $R^{(0)}$ of configuration space. Such a point can be, for example, a *stationary point* on the adiabatic PES of an electronic state (see the next section for the classification of PES). Under this circumstance, nonadiabatic couplings vanish, whereas additional terms appear in the PES operator, what is usually easier to treat. Such basis sets are called *diabatic* ones. The *diabatization* procedure is described *e.g.* in Ref. **27** and the references herein. An undesirable consequence of the transition to fixed, with respect to the nuclear coordinates, basis set is slower convergence of the diabatic series, compared to the adiabatic ones.

Another elegant alternative to an adiabatic expansion (Sec. **1.1.1**) indeed exists. This is the so-called *nuclear-electronic orbitals* (NEO) approach (Ref. **28**, **29**, **30**, **31**). In this approach, the molecular wave function is represented by Eq. (9) (Sec. **1.1.1**). The electronic and nuclear parts are then expressed in the basis of single-particle electronic and nuclear wave functions. Consequently, the same standard theoretical methodologies as for the electronic problem are applied to the solution of the molecular Schrödinger equation. In theory, this approach has clear advantages. First, it allows to solve the *entire* molecular problem in *one pass* avoiding

expensive adiabatic expansion and nonadiabatic couplings computations. Second, it allows for taking into account nuclear quantum effects (*e.g. nuclear exchange*) explicitly. Unfortunately in practice, in order to correctly describe electron-nuclear interactions (which are much stronger than the electron-electron and the nuclear-nuclear ones), the electron-nuclear distances must be included into the molecular basis functions explicitly (Ref. **32**, **33**, **34**), *e.g.* by means of *Gaussian geminals* (Ref. **32**). Their use leads to the exponential (with respect to the number of correlated electron-nuclear pairs) rise of matrix elements in the variational optimization (Sec. **1.1.2**) of the molecular wave function and, for the moment, makes the technology compuatationally feasible only for small systems.

1.1.3 Characterization of Adiabatic Potential Energy Surfaces

Assume the adiabatic potential energy surface $U_\eta(R)$, corresponding to an electronic state η, is computed. The following two parameters of PES are of importance. First, the gradient vector towards the direction of steepest rise of PES

$$\nabla U_\eta(R) = \frac{\partial}{\partial R} U_\eta(R) = \left(\frac{\partial}{\partial R_1} U_\eta(R), ..., \frac{\partial}{\partial R_N} U_\eta(R) \right) = \\ = \left(\frac{\partial}{\partial R_1^X} U_\eta(R), \frac{\partial}{\partial R_1^Y} U_\eta(R), \frac{\partial}{\partial R_1^Z} U_\eta(R), ..., \frac{\partial}{\partial R_N^X} U_\eta(R), \frac{\partial}{\partial R_N^Y} U_\eta(R), \frac{\partial}{\partial R_N^Z} U_\eta(R) \right)^{\cdot} \quad (19)$$

Its negative value is the force along a particular direction in configuration space. Second, it is the *force constant matrix*, or, the *Hessian matrix* defined as

$$k_{I,J}^{(\eta)} = \frac{\partial^2}{\partial R_I \partial R_J} U_\eta(R) . \quad (20)$$

Since each nuclear coordinate X_I comprises three Cartesian coordinates its dimension is ($3N \times 3N$).

Often, chemical and physical properties of molecular systems are particularly important at the points $R^{(\eta)}$ of PES where the gradient vanishes

$$\nabla U_\eta(R^{(\eta)}) = 0 , \quad (21)$$

referred to as *stationary points*.

The nature of stationary points can be illuminated by analysis of the eigenvalues of the Hessian matrix calculated at a stationary point $R^{(\eta)}$. In general, any Hessian matrix has 6 eigenvalues equal to zero since there are only (3*N*-6) independent coordinates necessary to determine the energy. If all the remaining eigenvalues are positively defined then $R^{(\eta)}$ is a minimum on PES – it corresponds to an *isomer* of the molecular system. If the Hessian matrix has one negative eigenvalue than the stationary point is a *saddle point* on PES, which corresponds to a transition state connecting two isomers. Higher order derivatives of PES are also important, and their relation to molecular properties can be found in Ref. **35**.

For an efficient search for stationary points on PES, the knowledge of the gradient (19) at each step of the search is necessary. Moreover, for an efficient location of transition states, the Hessian matrix (20) is required and needs to be calculated at least in the initial step. Since the eigenvalue of the Hessian matrix corresponds to *force constants* its diagonalization is required to obtain *infrared* (IR) *spectra* (see the next section) of a molecular system.

The gradient and Hessian of PES can be calculated on computers either *numerically* by means of the *finite difference schemes*, or *analytically*. Analytic derivatives are more difficult to implement – the higher the order of the derivatives (and the higher the theoretical level for the solution of the electronic problem), the more complicated the analytic expressions are. However, analytic derivatives are more accurate and much faster in computer calculations compared to the numerical ones. Thus, the availability of analytic gradients and second derivatives of PES is an important prerequisite for an efficient stationary-point search in quantum-chemical calculations.

In the next section a common procedure for the solution of Eq. (16) around stationary points will be introduced.

1.1.4 Harmonic Approximation and Beyond

The Tailor expansion of potential $\hat{U}_\eta(R)$ around a stationary point $X^{(\eta)}$, up to the second order yields

$$U_\eta(R) = U_\eta(R^{(\eta)}) + \sum_{I,J=1}^{N} \frac{1}{2} k_{I,J}^{(\eta)} \delta R_I^{(\eta)} \delta R_J^{(\eta)} + O((\delta R)^3) . \quad (22)$$

The first derivatives vanish at stationary points due to the condition (21) (Sec. **1.1.3**). The Nuclear Hamiltonian in Eq. (16) (Sec. **1.1.2**) then becomes

$$H_\eta = U_\eta(R^{(\eta)}) + \sum_I^N \frac{\hat{P}_I^{\,2}}{2M_I} + \sum_{I,J=1}^N \frac{1}{2} k_{I,J}^{(\eta)} \delta R_I^{(\eta)} \delta R_J^{(\eta)} . \tag{23}$$

A linear transformation of the coordinates according to

$$\delta R_I^{(\eta)} = \sum_\xi \frac{1}{\sqrt{M_I}} A_{I\xi}^{(\eta)} Q_\xi^{(\eta)} , \tag{24}$$

brings Hamiltonian (16) to the diagonal form

$$H_\eta = U_\eta(Q_\xi^{(\eta)} = 0) + \underbrace{\frac{1}{2}\sum_\xi \left(\hat{P}_\xi^2 + \omega_\xi^{(\eta)2} Q_\xi^{(\eta)2} \right)}_{\hat{H}_\eta^{NM}}, \tag{25}$$

with the so-called *normal mode Hamiltonian* $\hat{H}_\eta^{NM}$. The *nomal mode coordinates* $Q_\xi^{(\eta)}$ and *normal mode frequencies* $\omega_\xi^{(\eta)}$ are introduced herein.

Representation (25) is nothing but superposition of independent *harmonic oscillators* with the equilibrium configuration $R^{(\eta)}$ corresponding to $Q_\xi^{(\eta)} = 0$

$$\hat{H}_\eta^{NM} \Theta_{\eta N}^{BO}(Q) = E_{\eta N} \Theta_{\eta N}^{BO}(Q) . \tag{26}$$

Its analytical solution is well-known

$$\Theta_{\eta N}^{BO}(Q) = \prod_\xi \left(\frac{\omega_\xi^{(\eta)} / \hbar}{\sqrt{\pi}\, 2^{N_\xi} N_\xi !} \right)^{1/2} \exp\left(-\frac{1}{2} \frac{\omega_\xi^{(\eta)}}{\hbar} Q_\xi^{(\eta)2} \right) H_{N_\xi}\left(\sqrt{\frac{\omega_\xi^{(\eta)}}{\hbar}} Q_\xi^{(\eta)} \right), \tag{27}$$

where H_{N_ξ} are the *Hermit polynomials* (see *e.g.* Ref. **36**) and $N_\xi = 0, 1, 2, \ldots$ – the *vibrational quantum numbers* for mode ξ. Eigenvalues (energy levels) of Eq. (27) then read

$$E_{\eta N} = \sum_\xi \hbar \omega_\xi^{(\eta)} \left(N_\xi + \frac{1}{2} \right). \tag{28}$$

The procedure described above is known as the *harmonic approximation* (HA) for the nuclear problem. It determines total molecular wave functions within the adiabatic BO approximation. The eigenvalues (28) determine the *infrared* (IR) *spectrum* of a molecular system within HA.

Let mention a few obvious but important implications for solving the nuclear problem within HA. First of all, according to Eq. (28), the ground-state vibrational energy ($N_\xi = 0$)

corresponding to an electronic adiabatic state η is nonzero, moreover it is positively defined. This energy is termed *zero-point vibrational energy* (ZPVE). The sum of electronic energy and ZPVE is referred to as zero temperature *enthalpy* of the molecule in the ground vibrational state (calculated within HA).

Consider an isomerisation reaction on the PES of one electronic state. A typical example of such a reaction can be inter- or intramolecular hydrogen transfer in the ground electronic state via *keto-enol tautomerism* in acetone-water clusters as is studied in Chap. **2**. The barrier of the reaction can be calculated at two levels of accuracy: as the difference of the energies between the minima and corresponding transition state obtained with and without ZPVE correction. The latter way is more computationally expensive as it requires second derivatives of the PES to be computed. In the transition state, the Hessian matrix (20) (Sec. **1.1.3**) has one negative eigenvalue (see the previous section) and one normal-mode frequency is excluded from the series (28), compared to the case of minima. As result, ZPVE in the transition state is usually smaller than in the minima. That is, taking to account ZPVE is of importance for accurate reaction energy barriers calculations, especially for the low-barrier reactions whose barriers can be modified by ZPVE considerably.

Example for the importance of ZPVE can be found in calculations of *stabilization enthalpies* of molecular complexes. The *stabilization energy* of a complex is defined as the difference in energies between the complex and its isolated fragments, while stabilization enthalpy is the same difference taking ZPVE into account. Due to additional covalent or noncovalent bonds (*e.g.* hydrogen-bonds), ZPVE of the complex is typically larger than the sum of ZPVE of its isolated fragments. Therefore, as in the case of energy barriers, absolute value of stabilization enthalpy becomes smaller than that of stabilization energy.

Further improvement of the nuclear energy calculated within HA is possible by means of perturbation theory. Assuming the solutions within HA as *unperturbed* and applying perturbation theory with respect to the higher order terms of Eq. (25), one obtains the *anharmonic correction* to HA. The procedure thus generates anharmonically-corected PES. However, it requires high-order derivatives of PES and, hence, is computationally feasible only for small systems.

Normally, nuclear energy, corrected for anharmonic effects, constitutes about 90% (Ref. **37**) of the harmonic ZPVE and can be taken to account by means of scaling by relevant constant factors. The latter can be derived from the high-level calculations on small model systems or from experimental data.

Part 1.2
Electronic Schrödinger Equation: Ground State

1.2.1 Wave function of Noninteracting Electrons

In the present paragraph, methods for the solution of the electronic problem (11) (Sec. **1.1.2**) with the Hamiltonian (2) (Sec. **1.1.1**) will be described. Beforehand, additional assumptions on the form of electronic wave function should be made

In context of the nonrelativistic theory used in this work, spin of electron was "empirically" added to its coordinate: $x_i = (r_i^x, r_i^y, r_i^z; s_i(\omega_i)) = (r_i; s_i(\omega_i))$, where r_i is the spatial part, and $s_i(\omega_i)$ is the spin part as a function of symbolic spin variable ω_i. Since electron spin is ½, the spin coordinate $s_i(\omega_i)$ comprises two *spin functions* $\alpha(\omega_i)$ and $\beta(\omega_i)$, corresponding to spin-up and spin-down, respectively. Spin functions are *complete* and *orthonormal*

$$\begin{aligned}
&\int \alpha^*(\omega_i)\alpha(\omega_i)d\omega_i = \langle \alpha | \alpha \rangle = 1 \\
&\int \beta^*(\omega_i)\beta(\omega_i)d\omega_i = \langle \beta | \beta \rangle = 1
\end{aligned}, \qquad
\begin{aligned}
&\int \alpha^*(\omega_i)\beta(\omega_i)d\omega_i = \langle \alpha | \beta \rangle = 0 \\
&\int \beta^*(\omega_i)\alpha(\omega_i)d\omega_i = \langle \beta | \alpha \rangle = 0
\end{aligned} \qquad (29)$$

– integration here is performed in a symbolic way.

Since electronic Hamiltonian (2) does not depend on spin, the assignment of spin to the wave function does not bring any actual information. However, spin-dependence of the electronic wave function becomes immediately evident in context of the antisymmetry principle (Sec. **1.1.1**). The latter requires antisymmetry with respect to the interchange of the coordinates of any two electrons, including both spatial and spin parts.

A regular way to obtain the wave-function of the system of *interacting* electrons is to start from the wave function of the *hypothetic* system of *non-interacting* electrons which will be further improved by inclusion of interactions. The latter can be constructed from the *one-electron* (*single-particle*) wave-functions – the solutions of one-electron Schrödinger equations

$$\hat{H}_{one-el}\chi_i(x_i) = \left(\hat{T}_{el}(r_i) + \hat{V}_N(r_i, R)\right)\chi_i(x_i) = \varepsilon_i \chi_i(x_i) . \qquad (30)$$

Compared to the electronic Hamiltonian of interacting electrons (2), the potential energy operator (5) (Sec. **1.1.1**) is excluded from the one-electron Hamiltonian above. Since these one-electron wave functions refer to single electrons in a molecule, they are often termed *molecular orbitals* (MO). For the *i*-th electron of the system its molecular orbital is read

$$\chi_i(x_i) = \chi_i(r_i, s_i(\omega_i)) . \tag{31}$$

Since molecular orbitals can depend on both spin and spatial coordinates, they are also named *spin orbitals*. As it was already mentioned, the nonrelativistic electronic Hamiltonian does not depend on spin, therefore molecular orbital can be separated to the product of spatially- and spin-dependent parts

$$\chi_i(x_i) = \psi_i(r_i) s_i(\omega_i) . \tag{32}$$

The spatially-dependent part $\psi_i(r_i)$ is called *spatial orbital*, $|\psi_i(r_i)|^2 dr_i$ describes the probability of finding the electron *i* in the small volume element dr_i around r_i.

The simplest expression for the waveunction of *N* noninteracting electrons, constructed from single-particle spin orbitals satisfying the antisymmetry principle, is the following determinant

$$|\Psi(x_1, x_2, ..., x_N)\rangle = \frac{1}{\sqrt{N!}} \begin{vmatrix} \chi_1(x_1) & \chi_2(x_1) & ... & \chi_N(x_1) \\ \chi_1(x_2) & \chi_2(x_2) & ... & \chi_N(x_2) \\ ... & & & \\ \chi_1(x_N) & \chi_2(x_N) & ... & \chi_N(x_N) \end{vmatrix} = |\chi_1(x_1)\chi_2(x_2)...\chi_N(x_N)\rangle . \tag{33}$$

The factor $(N!)^{-1/2}$ is the normalization factor of the wave function. The right-hand of the expression is a short-hand notation for the determinant – it displays its diagonal elements only and includes the normalization constant. This object is called *Slater determinant* (SD) (Ref. **38**). Interchange of the coordinates of two electrons corresponds to the interchange of two rows in SD. It corresponds to a sign change of the *N*-electron wave function, and SD hence fulfils the antisymmetry requirement. Occupation of the same spin orbital by more than one electron, corresponds to having at least two columns of the determinant equal, what makes it vanish. Therefore, not more than one electron in an *N*-electron system can occupy one spin orbital. Thus, SD naturally obeys the Pauli exclusion principle for fermions.

One can see that the antisymmetry principle results in a very specific kind of interaction of electrons, which makes electrons with *parallel* spin *correlated*, in some way, even at the

absence of any interaction potentials between them. This kind of interaction is termed *exchange correlation*. Within this approximation, electrons with the same spins remain *uncorrelated*, therefore a single-determinant wave function is normally referred as an uncorrelated one.

There are two types of Slater determinants used in electronic-structure calculations.

1. *Unrestricted determinants*, formed from 2*K* unrestricted spin orbitals and having 2*K* different spatial orbitals for the different spins

$$\begin{matrix} \chi_{2i+1}(x_n) = \psi_i^{\alpha}(r_n)\alpha_i(\omega_n) \\ \chi_{2i}(x_n) = \psi_i^{\beta}(r_n)\beta_i(\omega_n) \end{matrix}, \; i=1, 2, \ldots, K. \tag{34}$$

Herein, the sets of spatial orbitals with the same spin are assumed to be orthonormal

$$\left\langle \psi_i^{\alpha} \middle| \psi_j^{\alpha} \right\rangle = \left\langle \psi_i^{\beta} \middle| \psi_j^{\beta} \right\rangle = \delta_{ij}, \tag{35}$$

but the sets with different spin are not

$$\left\langle \psi_i^{\alpha} \middle| \psi_j^{\beta} \right\rangle = S_{ij}^{\alpha\beta}, \tag{36}$$

where $S_{ij}^{\alpha\beta}$ is the *overlap matrix*.

Conditions (29) for the spin parts can be generalized for the different spin orbitals *i* and *j*

$$\begin{matrix} \langle \alpha_i | \alpha_i \rangle = \langle \alpha_i | \alpha_j \rangle = \langle \beta_i | \beta_i \rangle = \langle \beta_i | \beta_j \rangle = 1 \\ \langle \alpha_i | \beta_i \rangle = \langle \alpha_i | \beta_j \rangle = 0 \end{matrix}, \tag{37}$$

what provides that unrestricted spin-orbitals form an orthonormal set, despite the condition (36).

2. *Restricted determinants*, which are formed from 2*K* restricted spin orbitals and comprise *K* spatial orbitals, each spatial orbital *i* is shared by the spins α and β

$$\begin{matrix} \chi_{2i+1}(x_n) = \psi_i(r_n)\alpha_i(\omega_n) \\ \chi_{2i}(x_n) = \psi_i(r_n)\beta_i(\omega_n) \end{matrix}, \; i=1, 2, \ldots, K. \tag{38}$$

The spatial orbitals are orthonormal

$$\left\langle \psi_i \middle| \psi_j \right\rangle = \delta_{ij}. \tag{39}$$

The conditions for the spin parts of restricted determinants are the same as for the unrestricted ones (Eq. (37)).

Restricted determinants can be further classified according to the number of spatial orbitals that are singly occupied. The determinants in which each spatial orbital is doubly occupied are the *closed-shell* determinants. The *open shell* is a singly occupied spatial orbital. The open-shell determinants can be described by the number of open shells they contain. In the *restricted open-shell* determinants one part of the electrons occupies closed-shell orbitals while another one is assigned to occupy the open shells.

In many cases, the molecules containing even number of electrons are well-described by the closed-shell restricted determinants. However, they totally fail to describe dissociation of molecules into open-shell fragments. A classical example is the dissociation of the H_2 molecule. For the description of open-shell fragments one has to use either restricted open-shell or unrestricted determinants. Both approaches have their advantages and disadvantages (see *e.g.* Part **2.5**, Ref. **39**), but a more general approach would be to use even several determinants to represent the wave function. Such a representation gives rise to the *generalized valence-bond* (GVB) (Ref. **40**) and more general *multiconfiguration self-consistent field* (MCSCF) (Ref. **41**) approaches.

In the present work, only closed-shell systems have been investigated. Thus, most of the theoretical statements of the next sections will be formulated in terms of the general spin orbitals while some particular expressions can be presented in terms of the closed-shell spatial orbitals.

1.2.2 Hartree-Fock Approximation

Hartree-Fock (HF) is the simplest method to include interactions into the system of N non-interacting electrons described by a Slater determinant. For the derivation of the HF equations it is convenient to represent the electronic Hamiltonian (2) (Sec. **1.1.1**) in the following form

$$\hat{H}_{el}(r,R) = \hat{O}_1 + \hat{O}_2 , \tag{40}$$

$\hat{O}_1$ and $\hat{O}_2$ are the single- and two-particle operators since they depend on coordinates of one and two electrons, respectively

$$\hat{O}_1 = \sum_i^N \left(-\frac{1}{2} \right) (\nabla_i, \nabla_i) + \sum_i^N \sum_J \frac{Z_I}{|\vec{r}_i - \vec{R}_I|} = \sum_i^N \hat{h}_i(r_i; \{R\}) , \tag{41}$$

with $\hat{h}_i(r_i)$, often termed *core-Hamiltonian operator*, and

$$\hat{O}_2 = \sum_{i}^{N}\sum_{j>i}^{N}\frac{1}{|\vec{r}_i - \vec{r}_j|} = \sum_{i,j>i}\frac{1}{r_{ij}}. \quad (42)$$

Here and further, all the expressions are given in *atomic units* (AU) such that mass and the Plank constant are set to unit.

It can be shown (see *e.g.* Part **2.4** Ref. **39**) that the expectation value of the electronic Hamiltonian for a single determinantal wave function, called *Hartree-Fock energy*, is given by the expression

$$E_0 = \langle \Psi | \hat{H}_{el} | \Psi \rangle = \langle \Psi | \hat{O}_1 | \Psi \rangle + \langle \Psi | \hat{O}_2 | \Psi \rangle = \sum_{i}^{N}\langle \chi_i | h_i | \chi_i \rangle + \frac{1}{2}\sum_{i=1}^{N}\sum_{j=1}^{N}\left(\underbrace{\langle \chi_i\chi_j | \chi_i\chi_j \rangle - \langle \chi_i\chi_j | \chi_j\chi_i \rangle}_{\langle \chi_i\chi_j \| \chi_i\chi_j \rangle}\right), \quad (43)$$

with *one-electron integrals*

$$\langle \chi_i | h_i | \chi_i \rangle = \int_{x_1} \chi_i^*(x_1)\hat{h}_i(r_1)\chi_i(x_1)dx_1, \quad (44)$$

and *two-electron integrals*

$$\langle \chi_i\chi_j | \chi_k\chi_l \rangle = \int_{x_1}\int_{x_2} \chi_i^*(x_1)\chi_j^*(x_2)\frac{1}{r_{ij}}\chi_k(x_1)\chi_l(x_2)dx_1dx_2. \quad (45)$$

Herein, a short-hand notation $\langle \chi_i\chi_j \| \chi_i\chi_j \rangle$ for the difference between the antisymmetrized two-electron integrals is introduced. The first term of the right-hand side of Eq. (43) comes from the kinetic energy and electron-nuclear attraction of all electrons. The second one is the classical Coulomb repulsion of two charge distributions. The last term is the so-called *exchange* energy which comes from the antisymmetry principle. Its form is such that it cancels the Coulomb energy for the system comprising only one single electron, the latter means that HF energy is *self-interaction free*. The expectation value of the single determinant (43) should then be minimized with respect to the variations of orbitals

$$\chi_{i,j} \to \chi_{i,j} + \delta\chi_{i,j}, \quad (46)$$

with an additional constraint of the orthonormality of orbitals

$$\left\langle \chi_i \middle| \chi_j \right\rangle = \delta_{ij}.$$

(47)

It can be efficiently performed by constructing the following Lagrangian

$$L = E_0 - \sum_{i=1}^{N}\sum_{j=1}^{N} \varepsilon_{ij}\left(\left\langle \chi_i \middle| \chi_j \right\rangle - \delta_{ij}\right),$$

(48)

which is the sum of the HF energy and ($N\times N$) orthonormality conditions (47). The Lagrange multipliers ε_{ij} are termed *orbital energies*. Minimization of L with respect to the orbitals

$$\delta L\left(\chi_{i,j} + \delta\chi_{i,j}\right) = 0,$$

(49)

yields the *Hartree-Fock equations*

$$\hat{f}_j \left| \chi_i(x_1) \right\rangle = \left[\hat{h}_i(r_1) + \underbrace{\sum_{j=1}^{N}\left[\hat{J}_j(x_1) - \hat{K}_j(x_1)\right]}_{\hat{\upsilon}^{HF}} \right] \left| \chi_i(x_1) \right\rangle = \sum_{j=1}^{N} \varepsilon_{ji} \left| \chi_i(x_1) \right\rangle .$$

(50)

Here $\hat{f}_j$ is the *Fock operator*, defined as a sum of the core-Hamiltonian operator, *Coulomb operator*

$$\hat{J}_j(x_1) \left| \chi_i(x_1) \right\rangle = \left[\int_{x_2} \chi_j^*(x_2) \frac{1}{r_{12}} \chi_j(x_2) dx_2 \right] \left| \chi_i(x_1) \right\rangle ,$$

(51)

and *exchange operator*

$$\hat{K}_j(x_1) \left| \chi_i(x_1) \right\rangle = \left[\int_{x_2} \chi_j^*(x_2) \frac{1}{x_{12}} \chi_i(x_2) dx_2 \right] \left| \chi_j(x_1) \right\rangle .$$

(52)

The difference $\hat{\upsilon}^{HF}$ between the two latter operators is an effective one-electron potential operator often referred as *Hartree-Fock potential*. In contrast to the Coulomb operator, the action of $\hat{K}_j(x_1)$ on $\chi_i(x_1)$ implies an "exchange" of electrons 1 and 2 (52). Since $\hat{K}_j(x_1)$ is therefore not a simple multiplicative potential uniquely defined at each point of the r_1 space, the exchange operator is a *nonlocal* operator.

Equation (50) can be brought to a more conventional form by the *unitary transformation* [1] of the spin orbitals

$$\hat{f}_i \left| \chi'_i(r_1) \right\rangle = \varepsilon'_i \left| \chi'_i(r_1) \right\rangle . \tag{53}$$

The unique set of spin orbitals obtained from the solution of the eigenvalue problem (53) with the diagonal matrix of Lagrange multipliers is called *canonical orbitals*. Since any single determinant obtained from the unitary-transformed spin orbitals differs by a phase factor from the original determinant, its expectation value will be invariant to the transformation. In this sense, the spin orbitals which minimize the HF energy are not unique and are defined up to a unitary transformation.

For the further processing, the HF equations should be expressed in terms of spatial orbitals what can be done by integrating out the spin variables. In the case of a closed-shell determinant it leads to a singular set of equations for the spatial orbitals shared by spins α and β

$$\hat{f}_i \left| \psi_i(r_1) \right\rangle = \varepsilon_i \left| \psi_i(r_1) \right\rangle . \tag{54}$$

In the spin-unrestricted case one obtains two sets of equations – one for each spatial orbital corresponding to spins α and β.

In the case of atoms, the integro-differential equation (54) can in principle be solved numerically. However, for molecules, the numerical solution is impractical. Instead, by expanding spatial orbitals into a finite *basis set* of *K* known atomic *basis functions*

$$\left| \psi_i(r_1;R) \right\rangle = \sum_{\mu=1}^{K} C_{\mu i}(R) \left| \phi_\mu(r_1;R) \right\rangle \quad i=1, 2, \ldots, K,\ K \geq N/2, \tag{55}$$

the closed-shell equation (54) can be transformed to a set of algebraic equations. Inserting (55) into (54) and multiplying by $\left\langle \phi_{\mu'} \right|$ one arrives at the matrix equation

$$\sum_{\mu=1}^{K} F_{\mu'\mu} C_{\mu i} = \varepsilon_i \sum_{\mu=1}^{K} S_{\mu'\mu} C_{\mu i} , \tag{56}$$

with the elements of the *Fock matrix*

[1] The matrix of a unitary transformation possess the property $\mathbf{U}^\dagger\mathbf{U}=\mathbf{1}$, where $\mathbf{U}^\dagger$ is the adjoint matrix. From there it follows that the determinant of a unitary matrix is defined within a complex phase factor: $\det(\mathbf{U})=e^{i\varphi}$).

$$F_{\mu'\mu} = \langle \phi_{\mu'} | h | \phi_{\mu} \rangle + \sum_{\eta'=1}^{K} \sum_{\eta=1}^{K} \left(2 \sum_{c=1}^{N/2} C_{\eta' c}^{*} C_{\eta c} \right) \left[\langle \phi_{\mu'} \phi_{\eta'} | \phi_{\mu} \phi_{\eta} \rangle - \frac{1}{2} \langle \phi_{\mu'} \phi_{\eta'} | \phi_{\eta} \phi_{\mu} \rangle \right], \tag{57}$$

and, since the atomic basis functions are not necessarily orthogonal, the *overlap matrix*

$$S_{\mu'\mu} = \langle \phi_{\mu'} | \phi_{\mu} \rangle . \tag{58}$$

The procedure was proposed by Roothan and Hall (Ref. **42**, **43**), equation (56) bears their name. In the case of unrestricted HF equations, spin α and spin β sets of spatial orbitals are represented by their own bases. This consequently gives two sets of matrix equations of type (56) named *Pople-Nesbet* equations (Ref. **44**).

Equation (56) is *nonlinear*, since the Fock matrix itself depends on the expansion coefficients (Eq. (57)) and therefore it must be solved *iteratively*. Starting from a trial set of the expansion coefficients, one calculates improved ones, forms a new Fock matrix and repeats the procedure as many times as the HF energy, expressed in terms of the coefficients, is converged to a specified criterion. The procedure is also termed *self-consistent field* (SCF). It generates *K* spatial orbitals, where *K* is the number of basis functions in the expansion (55). In the closed-shell case, *N*/2 orbitals with lowest energies are referred to as *occupied orbitals* and the remaining (*K*-*N*/2) – as *virtual orbitals*. In the unrestricted case there are, of course, *N* occupied and (2*K*-*N*) virtual orbitals, as the spatial orbitals with different spin have different energies.

Finally, it would be important to make a notice about the physical meaning of orbital energies. Assume one electron from an occupied spin orbital χ_b is removed. The energy difference between the initial *N*-electron system and the remaining (*N*-1)-electron system is called *ionization potential*. An opposite case is when one electron is added to one of the virtual orbitals χ_p. The energetic of this case is described by the *electron affinity* which is the energy difference between the initial system and the new (*N*+1)-electron system. It can be shown that in the approximation that the spin orbitals of the new system remain unchanged (only the relevant orbitals are removed/added), the ionization potential is the negative orbital energy $(-\varepsilon_b)$ of the occupied orbital, while electron affinity is the negative energy of the virtual orbital $(-\varepsilon_p)$. This property is known as *Koopmans' theorem* (Ref. **45**).

1.2.3 Electron Correlation

The Hartree-Fock energy (43) expressed in terms of the optimized orbital coefficients (Eq. (56), Sec. **1.2.2**) calculated with an infinitely-large, *i. e. complete basis set* is called *Hartree-Fock limit*. The difference between this energy and the exact nonrelativistic energy within the Born-Oppenheimer approximation is referred to as *correlation energy* (Ref. **46**), which is negatively defined. Although correlation energy is only a small fraction (normally *ca.* 1%) of the total energy, it is of paramount importance for the problems where accurate energy differences are required – in particular in chemical reactions.

It was already mentioned that the HF energy contains exchange correlations which arise from the antisymmetry principle. Since, within the nonrelativistic framework, this kind of correlations does not come from any interactions of electrons, while the electron interactions are treated merely in an average way, the HF theory is commonly referred as an *uncorrelated* theory.

There are two types of electron correlations incurring from the interactions of electrons – *static* and *dynamic* correlations (Ref. **47**, **48**). Dynamic correlations arise from the instantaneous interactions of electrons. Static correlations stem from near-degenerate effects where more than one determinant is necessary to describe the wave function. This kind of correlations is treated by the aforementioned multireference methods (Sec. **1.2.1**). As the number of determinants employed for the description of static correlations increases, the border between static and dynamic correlations blurs.

Although the HF approximation can often produce rather accurate structures and harmonic frequencies (*i.e.* around 0.01 Å for bond lengths and 10% for harmonic frequencies) for covalently-bound systems, it totally fails to describe the dispersion part of the interaction energy. The latter is essential for intermolecular bonding of weakly-bound nonpolar complexes, in particular Van-der-Waals complexes. Dispersion interactions arise from the mutual polarization of electronic densities of the molecules or polyatomic complexes. Therefore, explicit inclusion of dynamic correlations is essential for an accurate description of such interactions. In the case of *hydrogen-bonding* (H-bonding), inclusion of the dispersion energy is important to describe the anisotropy of the system correctly and, in general, to obtain more reliable structures.

Several major theoretical branches starting from the HF approximation are available for practical computations to include electron correlations.

Within the *configuration-interaction* (CI) branch (*e.g.* Chap. 4, Ref. **39**), the electronic wave function of an N-electron system is expanded in terms of the determinants constructed from $2K > N$ spin orbitals – the solutions of Hartree-Fock equations, according to

$$\Psi = \Psi_0 + \sum_{\substack{r \\ a}} c_a^r \Psi_a^r + \sum_{\substack{r<s \\ a<b}} c_{ab}^{rs} \Psi_{ab}^{rs} + \ldots + \sum_{\substack{r<s<t\ldots \\ a<b<c\ldots}} c_{abc\ldots}^{rst\ldots} \Psi_{abc\ldots}^{rst\ldots} . \quad (59)$$

Herein, *excited determinants* Ψ_a^r, Ψ_{ab}^{rs}, …, $\Psi_{abc\ldots}^{rst\ldots}$ are formed from the Hartree-Fock ground-state wave function Ψ_0 by replacement of one, two, ..., *n* occupied orbitals with virtual ones. These determinants and called singly-, doubly-, ..., *n*-tuply-excited determinants, respectively. The (*a,b,c,...*) and (*r,s,t,...*) indices sets, refer to the occupied and virtual orbitals, respectively. Applying the variational principle to the CI wave function (59), yields equations for the CI expansion coefficients c_a^r, c_{ab}^{rs}, …,. $c_{abc\ldots}^{rst\ldots}$. If all possible, for a given atomic-orbital basis set, $\binom{2K}{N}$ determinants are used in the CI expansion (59), the procedure is termed *full-CI*. Its limitation to the determinants of a specific maximal degree of excitation is named *truncated-CI*. The lowest eigenvalue obtained from the solution of the CI equations is an upper bound to the ground-state energy of the system, whereas the higher eigenvalues will be upper bounds for the excited-state energies. As the basis set approaches completeness, the full-CI energy approaches the exact electronic energy within the Born-Oppenheimer approximation. Nevertheless, even with an incomplete basis, full-CI energy is considered as “exact” within the subspace spanned by a given basis. Unfortunately, the number of determinants arising in the full-CI procedure grows exponentially with system size (*i.e.* with respect to the number of electrons and hence – the basis functions) that its application is only feasible to small benchmarking systems. It is actually a niche for full-CI in quantum chemistry. On the other hand, with truncated-CI there is another severe problem: the correlation energy does not scale correctly with respect to the number of particles in the system , thus these methods are not *size-consistent* (Ref. **49**, **50**). Size-consistency is crucial for simulations of large systems since it provides correct extrapolation of results obtained for small- and medium-sized model systems to larger ones. Owing to the above reasons, CI methods were not used in this work.

Fortunately, other viable alternatives to CI exist. Within *many-body* p*erturbation theory* (MBPT), adopted in quantum mechanics as *Rayleigh-Schrödinger perturbation theory* (RSPT), the electronic Hamiltonian is partitioned into two parts: a *zeroth-order* part having known eigenfunctions and eigenvalues, and a *perturbation* part. The exact energy is then expressed as an infinite sum over contributions of increasing order of perturbation. Those contributions which are constructed from the products of *n* such matrix elements constitute *n*-th order of perturbation theory. If the perturbation is small compared to zeroth-order energy, then the perturbation series converges fast and only a few orders are sufficient to represent the

energy of the system. Although MBPT is not variational, it is size-consistent to *all orders*. It was proved by several authors using various techniques, *e.g.* by Brueckner who employed *order-by-order* proof (Ref. **51**), by Goldstone and Hubbard using *diagrammatic techniques* (Ref. **52**, **53**) and by Coester, who proved it *by induction* (Ref. **54**). The famous *linked-cluster theorem* is indeed the most general proof of size-consistency of RSPT in each order employing a diagrammatic representation of RSPT, performed by Goldstone (Ref. **52**).

In some problematic cases the convergence of perturbation series of MBPT is not provided. This typically occurs when the perturbation in the Hamiltonian is not small compared to the zeroth-order energy. In this case, one has to resort to nonvariational but size-consistent c*oupled-cluster* (CC) theory. CC theory evolved in debates on the existence and proof of the aforementioned linked-cluster theorem and was initially formulated by Coester and Kümmel in 1958 in application to the nuclear-matter problem (Ref. **54**, **55**, **56**). In quantum chemistry CC theory was introduced by Cizek and Paldus (Ref. **57**, **58**, **59**). Within the CC methodology, the exact groundstate wave function of a many-electron system is represented by an *exponential operator* containing the *cluster operator* $\hat{T}$, acting on some zeroth-order wave function $|\Psi_0\rangle$ – usually the Hartree-Fock single-reference wave-function

$$|\Psi\rangle = e^{\hat{T}}|\Psi_0\rangle = \left(1 + \hat{T} + \frac{1}{2!}\hat{T}^2 + \frac{1}{3!}\hat{T}^3 + \ldots\right)|\Psi_0\rangle$$

$$\hat{T} = \sum_{n=1} \hat{T}_n \ . \qquad \textbf{(60)}$$

When the cluster operator $\hat{T}_n$ acts on the Hartree-Fock wave function, it produces the sum over all excitations of a given order *n,* analogously to the above CI expressions. Truncation of the cluster operator by an excitation of specific order *n* gives rise to the approximated CC schemes of increasing accuracy and computational cost: CCS, CCSD, CCSDT, CCSDTQ for the single, double, triple, quadruple excitations, respectively, included in the exponential operator. A special power of the CC approach is its rapid convergence in the cluster order *n*. The experience demonstrates that for a wide variety of many-body systems with pair interactions, about 99% of the correlation energy can be obtained at the $\hat{T} = \hat{T}_1 + \hat{T}_2$ level (CCSD), while the remaining 1% is almost entirely covered by $\hat{T}_3$ in $\hat{T} = \hat{T}_1 + \hat{T}_2 + \hat{T}_3$ (CCSDT).This was shown for closed-shell nuclei (Ref. **56**), atoms (Ref. **60**, **61**) and molecules (Ref. **61**). Unlike truncated-CI, approximated CC schemes are all size-consistent, if

the reference wave-function is size-consistent (Ref. **62**). It is provided by the exponential form of the $e^{\hat{T}}$ operator.

In summary, among correlated methodologies described in this section, CC appears to be the most systematic one and, still, a computationally accessible way to treat wide range of problems of chemical and nuclear physics.

Another correlated methodology used in this work is *density-functional theory* (DFT) introduced by Hohenberg, Kohn and Sham (Ref. **63**, **64**). It is conceptually different from the three wave function-based correlated methodologies introduced above, but structurally, it is very similar to HF theory. In DFT, electron correlation is treated by virtue of the *energy functional* $E[\rho]$ which has the *one-electron density* ρ as variable rather than the N-electron wave function. This is the reason why DFT is computationally so efficient. Unfortunately, with the present day's functionals the theory fails to describe dispersion interactions.

In conclusion of this section, the computational scalings of ground-state correlated methods, used throughout the study, are briefly discussed. Formal scaling formulas for DFT, MP2 and CCSD methods with respect to the number of particles N are $C^{\mathrm{DFT}}N^4$, $C^{\mathrm{MP2}}N^5$ and $C^{\mathrm{CCSD}}N^6$, respectively (all the formulas include relevant prefactors C). For comparison, uncorrelated HF theory, as well as DFT, formally scale as N^4 [1]. From a practical point of view it is important to realize that N^5-scaling roughly corresponds to the limit of current mainstream computational resources for studies of medium-sized molecular systems containing up to several dozens of the first-row atoms. Additional approximations can improve either the prefactors or even the scaling formulas of HF and relevant correlated methods (see *e.g.* Ref. **65**, **66**, **67** and Sec. **1.4.2**).

Perturbation, coupled-cluster and density-functional theories will be described in more detail in the next sections. A particularly useful handbook on the subject which covers most of the aspects of wave function-based methods is Ref. **39**. Reviews on analytical nuclear derivatives (see Part **1.1**) in connection to HF and correlated electronic energies can be found in Ref. **68**, **69**, **70**.

[1] This scaling of SCF is due to the necessity to calculate four-index integrals expressed in terms of a particular basis set (Eq. (57)).

1.2.4 Perturbation Theory

In Rayleigh-Schrödinger perturbation theory (Ref. **71**), the exact Hamiltonian in the *time-independent* Schrödinger equation is partitioned into a zero-order and a small perturbation part

$$\hat{H}\left|\Psi_i\right\rangle = \left(\hat{H}^{(0)} + \lambda\hat{V}\right)\left|\Psi_i\right\rangle = E_i\left|\Psi_i\right\rangle, \tag{61}$$

where λ is so-called *smallness parameter* which quantifies the magnitude of perturbation. The eigenvalues and eigenfunctions of the zeroth-order part are the known solutions of the eigenvalue problem

$$\hat{H}^{(0)}\left|\Psi_i^{(0)}\right\rangle = E_i^{(0)}\left|\Psi_i^{(0)}\right\rangle, \tag{62}$$

with the constraint on the eigenfunctions to be orthogonal

$$\left\langle\Psi_i^{(0)}\middle|\Psi_j^{(0)}\right\rangle = \delta_{ij}. \tag{63}$$

Eq. (61) can be formally solved by expanding the wave function and eigenfunction of the perturbed system into a power series with respect to the smallness parameter, treating solutions for the unperturbed system as zeroth order

$$\left|\Psi_i\right\rangle = \left|\Psi_i^{(0)}\right\rangle + \lambda\left|\Psi_i^{(1)}\right\rangle + \lambda^2\left|\Psi_i^{(2)}\right\rangle + \ldots,$$

$$E_i = E_i^{(0)} + \lambda E_i^{(1)} + \lambda^2 E_i^{(2)} + \ldots. \tag{64}$$

An additional condition for the solution requires the exact wave functions of the perturbed system and of the unperturbed one to be normalized

$$\left\langle\Psi_i^{(0)}\middle|\Psi_i\right\rangle = 1. \tag{65}$$

This property is referred to as *intermediate normalization*. It is always possible to fulfil it, unless $\Psi_i^{(0)}$ and Ψ_i are orthogonal. Expanding the eigenfunction of the perturbed system into the power series (64)

$$1 = \left\langle\Psi_i^{(0)}\middle|\Psi_i\right\rangle = \underbrace{\left\langle\Psi_i^{(0)}\middle|\Psi_i^{(0)}\right\rangle}_{1} + \lambda\underbrace{\left\langle\Psi_i^{(0)}\middle|\Psi_i^{(1)}\right\rangle}_{0} + \lambda^2\underbrace{\left\langle\Psi_i^{(0)}\middle|\Psi_i^{(2)}\right\rangle}_{0} + \ldots, \tag{66}$$

and taking to account its validity for any λ (see Eq. above), one obtains the following relation

$$\left\langle \Psi_i^{(0)} \middle| \Psi_i^{(n)} \right\rangle = 0, \;\; n = 1,\; 2,\; 3,\; \ldots.$$

(67)

Substitution of the expansion (64) into the Schrödinger equation (61) and collecting the terms at λ^n gives a system of equations for the wave functions at each order

n=0: Eq. (62)

n=1: $\left(E_i^{(0)} - \hat{H}^{(0)}\right) \left| \Psi_i^{(1)} \right\rangle = \left(\hat{V} - E_i^{(1)}\right) \left| \Psi_i^{(0)} \right\rangle$

n=2: $\left(E_i^{(0)} - \hat{H}^{(0)}\right) \left| \Psi_i^{(2)} \right\rangle = \left(\hat{V} - E_i^{(1)}\right) \left| \Psi_i^{(1)} \right\rangle - E_i^{(2)} \left| \Psi_i^{(0)} \right\rangle$

n=3: $\left(E_i^{(0)} - \hat{H}^{(0)}\right) \left| \Psi_i^{(3)} \right\rangle = \left(\hat{V} - E_i^{(1)}\right) \left| \Psi_i^{(2)} \right\rangle - E_i^{(2)} \left| \Psi_i^{(1)} \right\rangle - E_i^{(3)} \left| \Psi_i^{(0)} \right\rangle$

...

(68)

The equations above are not eigenvalue problems anymore but rather integro-differential equations. Multiplication by $\left\langle \Psi_i^{(0)} \right|$ taking to account relation (67) yields equations for the energies at each order

n=0: $E_i^{(0)} = \left\langle \Psi_i^{(0)} \middle| \hat{H}^{(0)} \middle| \Psi_i^{(0)} \right\rangle$

n=1: $E_i^{(1)} = \left\langle \Psi_i^{(0)} \middle| \hat{V} \middle| \Psi_i^{(0)} \right\rangle$

n=2: $E_i^{(2)} = \left\langle \Psi_i^{(0)} \middle| \hat{V} \middle| \Psi_i^{(1)} \right\rangle$

n=3: $E_i^{(3)} = \left\langle \Psi_i^{(0)} \middle| \hat{V} \middle| \Psi_i^{(2)} \right\rangle$

...

(69)

These equations are inserted into the equations (68). The latter then can be solved by means of a linear expansion of $\Psi_i^{(n)}$ in terms of $\Psi_i^{(0)}$

$$\left| \Psi_i^{(n)} \right\rangle = \sum_k c_{ik}^{(n)} \left| \Psi_k^{(0)} \right\rangle.$$

(70)

Due to the orthogonality of the unperturbed eigenfunctions (63), the expansion holds the following property

$$\left\langle \Psi_{k'}^{(0)} \middle| \Psi_i^{(n)} \right\rangle = \sum_k c_{ik}^{(n)} \left\langle \Psi_{k'}^{(0)} \middle| \Psi_k^{(0)} \right\rangle = \sum_k c_{ik}^{(n)} \delta_{k'k} = c_{ik'}^{(n)}.$$

(71)

Thus, the coefficients $c_{ii}^{(n)} = 0$ and are omitted from the expansion (70)

$$\left|\Psi_i^{(n)}\right\rangle = \sum_{k\neq i} c_{ik}^{(n)} \left|\Psi_k^{(0)}\right\rangle .$$

(72)

Substituting (72) into the wave function equations (68), multiplying by $\left\langle \Psi_{k'}^{(0)} \right|$ and taking into account the orthogonality condition (71) yields, up to the second order, equations for the wave functions

n=1:

$$\left|\Psi_i^{(1)}\right\rangle = \sum_{k'\neq i} \frac{\left\langle \Psi_{k'}^{(0)} \left|\hat{V}\right| \Psi_i^{(0)} \right\rangle}{E_i^{(0)} - E_{k'}^{(0)}} \left|\Psi_{k'}^{(0)}\right\rangle$$

n=2:

$$\left|\Psi_i^{(2)}\right\rangle = \sum_{k'\neq i} \left(\sum_{k\neq i} \frac{\left\langle \Psi_k^{(0)} \left|\hat{V}\right| \Psi_i^{(0)} \right\rangle \left\langle \Psi_{k'}^{(0)} \left|\hat{V}\right| \Psi_k^{(0)} \right\rangle}{\left(E_i^{(0)} - E_{k'}^{(0)}\right)\left(E_i^{(0)} - E_k^{(0)}\right)} - \frac{\left\langle \Psi_i^{(0)} \left|\hat{V}\right| \Psi_i^{(0)} \right\rangle \left\langle \Psi_{k'}^{(0)} \left|\hat{V}\right| \Psi_i^{(0)} \right\rangle}{\left(E_i^{(0)} - E_{k'}^{(0)}\right)^2} \right) \left|\Psi_{k'}^{(0)}\right\rangle .$$

(73)

By inserting these equations into Eq. (69), one finally obtains the energy-corrections up to the third order, for example

n=1: $\quad E_i^{(1)} = \left\langle \Psi_i^{(0)} \left|\hat{V}\right| \Psi_i^{(0)} \right\rangle$

n=2: $\quad E_i^{(2)} = \sum_{k'\neq i} \frac{\left|\left\langle \Psi_{k'}^{(0)} \left|\hat{V}\right| \Psi_i^{(0)} \right\rangle\right|^2}{E_i^{(0)} - E_{k'}^{(0)}}$

n=3:

$$E_i^{(3)} = \sum_{k'\neq i} \left(\sum_{k\neq i} \frac{\left\langle \Psi_k^{(0)} \left|\hat{V}\right| \Psi_i^{(0)} \right\rangle \left\langle \Psi_{k'}^{(0)} \left|\hat{V}\right| \Psi_k^{(0)} \right\rangle \left\langle \Psi_{k'}^{(0)} \left|\hat{V}\right| \Psi_k^{(0)} \right\rangle}{\left(E_i^{(0)} - E_{k'}^{(0)}\right)\left(E_i^{(0)} - E_k^{(0)}\right)} - \frac{\left\langle \Psi_i^{(0)} \left|\hat{V}\right| \Psi_i^{(0)} \right\rangle \left|\left\langle \Psi_{k'}^{(0)} \left|\hat{V}\right| \Psi_i^{(0)} \right\rangle\right|^2}{\left(E_i^{(0)} - E_{k'}^{(0)}\right)^2} \right) .$$

(74)

Derivation of the higher-order expressions can be significantly simplified by use of the *diagrammatic representation* of RSPT (Ref. **52**, **53**), initially introduced by Feynman in the field of quantum electrodynamics.

In quantum chemistry, RSPT is often used in the form of *Møller and Plesset* (MPPT) (Ref. **72**) who applied it to the Hartree-Fock wave function treated as a zeroth order in Eq.(62). It can be shown (Ref. **72**) that the Hamiltonian, whose eigenfunction is the HF wave function, is the sum of the Fock operators (Eq. (50), Sec. **1.2.2**) over all electrons

$$\hat{H}^{(0)} = \sum_i^N \hat{f}_i(r_i) = \sum_i^N \left(\hat{h}(x_i) + \hat{\upsilon}_i^{HF}(r_i)\right).$$

(75)

It is termed *Hartree-Fock Hamiltonian* and is treated as a zeroth order in (61). The zeroth order energy is thus a sum of the HF orbital energies

$$E_0^{(0)} = \sum_a \varepsilon_a \,. \tag{76}$$

The perturbation part of Eq. (61) hence can be represented as the difference between the exact electron-electron interaction and the sum of the HF potential

$$\hat{V} = \hat{H}_{el} - \hat{H}^{(0)} = \sum_i \sum_{j>i} \frac{1}{x_{ij}} - \sum_i \hat{\upsilon}_i^{HF}(r_i) \,. \tag{77}$$

It can be further shown that the ground-state first- and second-order energy contributions can be expressed as

$$E_0^{(1)} = \left\langle \Psi_0^{(0)} \middle| \hat{V} \middle| \Psi_0^{(0)} \right\rangle = -\frac{1}{2} \sum_{ab} \langle ab \| ab \rangle \,, \tag{78}$$

and

$$E_0^{(2)} = \sum_{\substack{a<b \\ r<s}} \frac{\left| \langle ab \| rs \rangle \right|^2}{\varepsilon_a + \varepsilon_b - \varepsilon_r - \varepsilon_s} = \frac{1}{4} \sum_{abrs} \frac{\left| \langle ab \| rs \rangle \right|^2}{\varepsilon_a + \varepsilon_b - \varepsilon_r - \varepsilon_s} \,. \tag{79}$$

It is interesting to notice that the HF energy (43) is the sum of zeroth- and first-order corrections (Eq. (76), (78)) of MP theory. The first correction to the HF energy (zero and first orders) is obtained in the second order *i. e.* it is MP2 energy. Thus, MP2 is often used to obtain *correlated* potential energy surfaces, as well as molecular properties resulting from its derivatives.

In its canonic form, MP2 scales as N^5 with respect to the number of basis functions in the system, although approximations giving better scaling are already available (e.g. Ref. **65**, **66**, **67**). MP2 theory is in principle capable to treat long-range interactions with sufficient accuracy, as well as dispersion, polarization, and covalent effects associated with hydrogen bonding.

One well-known shortcoming of MP2 however is a significant overbinding of weakly-bound complexes. However, numerous recent studies as well as benchmark calculations applied to typical H-bonded systems, performed in this study (Sec. **3.7**), strongly indicate that the overbinding issue of MP2 can not only be related to the lack of method itself but rather to basis-set effects (Part. **1.4**).

1.2.5 Coupled-Cluster Theory

The operators $\hat{T}_n$ contained in the cluster operator (**60**) can be compactly represented in *second-quantized* form

$$\hat{T}_1 = \sum_{\substack{r \\ a}} t_a^r a_r^+ a_a = \sum_{\substack{R_1 \\ A_1}} t_a^r a_{R_1}^+ a_{A_1} ,$$
$$\hat{T}_2 = \sum_{\substack{r<s \\ a<b}} t_{ab}^{rs} a_r^+ a_s^+ a_a a_b = \sum_{\substack{R_2 \\ A_2}} t_{ab}^{rs} a_{R_2}^+ a_{A_2} ,$$
$$\ldots$$
$$\hat{T}_n = \sum_{\substack{r<s<t\ldots \\ a<b<c\ldots}} t_{A_n}^{R_n} a_r^+ a_s^+ a_t^+ \ldots a_a a_b a_c \ldots = \sum_{\substack{R_n \\ A_n}} t_{A_n}^{R_n} a_{R_n}^+ a_{A_n} .$$

(**80**)

As in the CI case (Eq. (59), Sec. **1.2.3**), the above equations imply summation over *ordered* sets of indices referred to *n* occupied orbitals

$$A_n : \underbrace{(a,b,c,\ldots)}_{n-times},$$

and *n* virtual orbitals

$$R_n : \underbrace{(r,s,t,\ldots)}_{n-times}.$$

Here $a_{r,s,t,\ldots}^+$, $a_{a,b,c,\ldots}$ are the *creation* and *annihilation operators*, respectively. A short-hand notation for the sequence of these operators is introduced

$$a_{R_n}^+ a_{A_n} = \underbrace{a_r^+ a_s^+ a_t^+ \ldots}_{R_n} \underbrace{a_a a_b a_c \ldots}_{A_n}.$$

Their action on the Hartee-Fock reference is the following

$$a_r^+ a_a \left|\Psi_0\right\rangle = a_{R_1}^+ a_{A_1} \left|\Psi_0\right\rangle = \left|\Psi_a^r\right\rangle,$$
$$a_r^+ a_s^+ a_a a_b \left|\Psi_0\right\rangle = a_{R_2}^+ a_{A_2} \left|\Psi_0\right\rangle = \left|\Psi_{ab}^{rs}\right\rangle ,$$
$$\ldots$$
$$a_r^+ a_s^+ a_t^+ \ldots . a_a a_b a_c \ldots \left|\Psi_0\right\rangle = a_{R_n}^+ a_{A_n} \left|\Psi_0\right\rangle = \left|\Psi_{A_n}^{R_n}\right\rangle .$$

(**81**)

Thus, each $\hat{T}_n$ generates a sum over all *n*-tuply excited determinants with the CI-like coefficients $t_{A_n}^{R_n}$ called *cluster amplitudes*. Eq. (**60**) then can be explicitly written as

$$\left|\Psi\right\rangle = e^{\hat{T}}\left|\Psi_0\right\rangle = \left(1 + \hat{C}_1 + \hat{C}_2 + \hat{C}_3 + ...\right)\left|\Psi_0\right\rangle, \tag{82}$$

with

$$\begin{aligned}
&\hat{C}_1 = \hat{T}_1, \\
&\hat{C}_2 = \hat{T}_2 + \frac{1}{2!}\hat{T}_1\hat{T}_1, \\
&\hat{C}_3 = \hat{T}_3 + \frac{1}{2!}\left(\hat{T}_2\hat{T}_1 + \hat{T}_1\hat{T}_2\right) + \frac{1}{3!}\hat{T}_1\hat{T}_1\hat{T}_1,
\end{aligned} \tag{83}$$

and so on. Herein, all excited determinants of *n*-th order are grouped within $\hat{C}_n$, for example

$$\hat{T}_1\hat{T}_1\left|\Psi_0\right\rangle = \sum_{\substack{(r)(u)\\(a)(d)}} t_a^r t_d^u a_r^+ a_u^+ a_a a_d \left|\Psi_0\right\rangle = \sum_{\substack{(r)(u)\\(a)(d)}} t_a^r t_d^u \left|\Psi_{ad}^{ru}\right\rangle. \tag{84}$$

A few coments on the above procedure should be made First, Eq. (83) for $\hat{C}_n$ establishes an *analytical connection* between CI and CC methods. It brings transparent physical meaning to each term and conceptually simplifies the analysis of the equations. Second, even with low-order operators $\hat{T}_n$ included in the cluster operator $\hat{T}$, higher-order excited determinants with corresponding coefficients are generated. This is the reason for the fast convergence of the cluster operator expansion (82), at least for closed-shell references. Third, the operators $\hat{T}_n$ describe *linked clusters* of *n* particles, since they cannot be written as products of lower-order operators. In fact, the essence of aforementioned linked-cluster theorem incurs from this property.

Let finally outline the way of derivation of the CC equations.

The ground-state coupled-cluster wave-function (Eq. (82)) obeys Schrödinger equation

$$\hat{H}\left|\Psi\right\rangle = \hat{H}e^{\hat{T}}\left|\Psi_0\right\rangle = E_0^{CC}e^{\hat{T}}\left|\Psi_0\right\rangle, \tag{85}$$

with the coupled-cluster ground-state energy E_0^{CC}. As usual, the Hamiltonian includes one- and two-particle parts. To obtain equations for the cluster amplitudes one could naively multiply Eq. (85) by the singly-, doubly-, triply- , *n*-tuply-excited determinants. This allows for a convenient formal understanding of the CC methodology but brings severe

computational difficulties (Ref. **73**). Instead, multiplying (85) by inverse of the exponential operator $e^{-\hat{T}}$ first, preceding the projections, leads to significant computational simplifications

$$e^{-\hat{T}}\hat{H}e^{\hat{T}}\left|\Psi_0\right\rangle = E_0^{CC}e^{-\hat{T}}e^{\hat{T}}\left|\Psi_0\right\rangle = E_0^{CC}\left|\Psi_0\right\rangle . \tag{86}$$

In particular, multiplying the above equation by $\left\langle\Psi_0\right|$ one obtains the equation for the coupled-cluster energy

$$\left\langle\Psi_0\right|e^{-\hat{T}}\hat{H}e^{\hat{T}}\left|\Psi_0\right\rangle = E_0^{CC}, \tag{87}$$

while its projecting onto the excited determinants $\left\langle\Psi_{A_n}^{R_n}\right|$ gives the cluster amplitudes

$$\left\langle\Psi_{R_n}^{A_n}\right|e^{-\hat{T}}\hat{H}e^{\hat{T}}\left|\Psi_0\right\rangle = 0 . \tag{88}$$

Herein, normalization of the ground-state determinant and orthogonality of the ground and excited determinants have been used to derive Eq. (87) and (88), respectively.

The first obvious advantage of the above procedure is that the inverse exponential operator in equations (87) and (88) decouples energy and amplitude equations – that drastically simplifies their solution. Second advantage is less straightforward but crucial. According to so-called *Campbell-Baker-Hausdorf* expression (Ref. **74**), operator $e^{-\hat{T}}\hat{H}e^{\hat{T}}$ can be represented as a series of nested commutators of $\hat{H}$ with the cluster operator, usually referred as *Hausdorf expansion*

$$e^{-\hat{T}}\hat{H}e^{\hat{T}} = \hat{H} + [\hat{H},\hat{T}] + \frac{1}{2!}[[\hat{H},\hat{T}],\hat{T}] + \frac{1}{3!}[[[\hat{H},\hat{T}],\hat{T}],\hat{T}] + \frac{1}{4!}[[[[\hat{H},\hat{T}],\hat{T}],\hat{T}],\hat{T}] . \tag{89}$$

A special charm of the presented technique is that the series (89) is *finite* regardless of the number of particles in the system. It *naturally* terminates after the fifth term because $\hat{H}$ contains at most two-particle operators (Ref. **75**). It would not be an exaggeration to conclude that the cluster expansion of the wave-function (**60**) in combination with the finite Hausdorf expansion (89) for the $e^{-\hat{T}}\hat{H}e^{\hat{T}}$ operator constitute the essence of coupled-cluster methodology.

1.2.6 Density-Functional Theory

Consider a molecular system with the Hamiltonian (40) (Sec. **1.2.2**). In this section it will be rewritten in the conventional notation used in DFT literature

$$\hat{H} = \sum_{i}^{N}\left(-\frac{1}{2}\nabla_i^2\right) + \underbrace{\sum_{i}^{N}\hat{\upsilon}_i(r_i)}_{\hat{\upsilon}(r)} + \sum_{j>i}\frac{1}{r_{ij}}. \tag{90}$$

Here $\hat{\upsilon}_i(r_i)$ is the nuclear-electron attraction or, in general, other one-electron operators (see Eq. (41), Sec. **1.2.2**). Their sum $\hat{\upsilon}(r)$ is referred to as *external potential* in the DFT terminology.

The essence of DFT is expressed in two statements.

(1) There is one-to-one mapping between the ground-state electron density $\rho(r)$, the external potential $\upsilon(r)$, determined within an additive constant *C*, and the ground-state wave-function $\Psi(x_1, x_2, ..., x_N)$ of any *N*-electron system, defined up to a phase factor $e^{i\delta t}$

$$\rho(r) \leftrightarrow \upsilon[\rho](r) + C \leftrightarrow \Psi[\rho](r)e^{i\delta t}. \tag{91}$$

The electron density (probability density) is defined as the expectation value of the density operator integrated over spin variables

$$\rho(r) = \int_{\omega}\left\langle \Psi\middle|\sum_{i}^{N}\delta(x_i - x)\middle|\Psi\right\rangle d\omega. \tag{92}$$

Its integral over all spatial coordinates is equal to the number of electrons

$$\int_{r}\rho(r)dr = N. \tag{93}$$

Since the electronic energy is determined by the external potential and the wave function, therefore, it can be represented as a functional of the density

$$E[\rho] = \left\langle \Psi[\rho](r)\middle|\hat{H}\middle|\Psi[\rho](r)\right\rangle = T[\rho] + V_{ne}[\rho] + V_{ee}[\rho]. \tag{94}$$

Herein, $V_{ee}[\rho]$ and $T[\rho]$ are the electron-electron interactions and kinetic energy of the system of *interacting* electrons, respectively. $V_{ne}[\rho]$ corresponds to the nuclear-electron attraction (or other one-particle interactions). Ground-state expectation values of any quantum mechanical operators can be uniquely represented as a function of the density as well

$$\overline{O}[\rho] = \left\langle \Psi[\rho](r) \middle| \hat{O} \middle| \Psi[\rho](r) \right\rangle .$$

(95)

(2) The energy (94), associated with any non-negative trial density $\rho'(r)$, which integrates to the total number of electrons, cannot be lower than the exact ground state energy $E_{GS}[\rho]$ with the ground state density $\rho(r)$

$$E[\rho'] = \left\langle \Psi[\rho'](r) \middle| \hat{H} \middle| \Psi[\rho'](r) \right\rangle \geq E_{GS}[\rho] .$$

(96)

This statement provides the ground-state density-functional variational principle

$$\delta\left(E[\rho] - \mu\left(N - \int_r \rho(r) dr \right) \right) = 0 .$$

(97)

The Lagrange multiplier μ guarantees conservation of the total number of particles *N* and can be interpreted as *chemical potential* of the system.

Both statements are known as the first and second *Hohenberg-Kohn* (HK) theorems, respectively (Ref. **63**).

Successful application of the variational principle to (94) requires explicit mathematical expressions for the electron-electron interaction functional as well as the kinetic energy functional which are generally unknown. However, it is known from Hartree-Fock theory that for the special case of *N*-electron single-determinant wave function, kinetic energy can be written explicitly (Eq. (43), Sec. **1.2.2**). To utilize this property, Kohn and Sham introduced a hypothetic system of *non-interacting* particles, moving in an *effective potential* υ^{KS}, the density ρ^{KS} of which is to be equal to the density ρ of the corresponding *interacting* system (Ref. **64**). The existence of such a system is known as *υ-representability*. This system can be represented by the following Hamiltonian

$$\hat{H}^{KS} = \sum_i^N \left(-\frac{1}{2}\nabla_i^2 \right) + \sum_i^N \hat{\upsilon}^{KS}(r_i) .$$

(98)

The eigenfunction of the Hamiltonian is given as a single determinant constructed from spin-orbitals, by the solving one-electron Hartree-Fock-type equations

$$\left(-\frac{1}{2}\nabla_i^2 + \hat{\upsilon}^{KS}(r_i) \right) \left| \chi_i^{KS}(x_i) \right\rangle = \varepsilon_i \left| \chi_i^{KS}(x_i) \right\rangle .$$

(99)

These orbitals are referred to as *Kohn-Sham* (KS) *orbitals* in the DFT literature. The wave function is then represented as a single determinant constructed from the KS orbitals

$$\left|\Psi[\rho](r)\right\rangle = \left|\Psi[\rho^{KS}](r)\right\rangle = \left|\chi_1^{KS}(x_1)\chi_2^{KS}(x_2)...\chi_N^{KS}(x_N)\right\rangle . \quad \textbf{(100)}$$

According to Eq. (92), KS orbitals are related to the density of the interacting system as follows

$$\rho(r) = \rho^{KS}(r) = \int d\omega \sum_i^N \left|\chi_i^{KS}(x_i)\right|^2 . \quad \textbf{(101)}$$

For the closed-shell case it can be written

$$\rho^{KS}(r) = \sum_i^{N/2} \left|\psi_i^{KS}(r_i)\right|^2 , \quad \textbf{(102)}$$

with the spatial KS orbitals ψ_i^{KS}. The kinetic energy of the single determinant is then readily obtained by

$$T^{KS} = T^{KS}[\chi_i^{KS}] = \sum_i^N \left\langle \chi_i^{KS} \left| -\frac{1}{2}\nabla_i^2 \right| \chi_i^{KS} \right\rangle . \quad \textbf{(103)}$$

The electronic energy (94) of the reference system and, hence, the energy of real system (by virtue of the first HK theorem) can then be rearranged, taking into account the explicit expressions for the expectation value of the Hamiltonian expressed in terms of single determinant (100), to give

$$E[\rho] = E\left[\chi_i^{KS}, \rho^{KS}(\chi_i^{KS})\right] = T^{KS}[\chi_i^{KS}] + \int \rho^{KS}(r)\upsilon(r)dr + J[\rho^{KS}] + E_{xc}[\rho^{KS}] . \quad \textbf{(104)}$$

The second term describes the interaction of the electrons with the external potential (in particular – with the nuclei), the third term is the classical Coulomb interaction (Eq. (43), Sec. **1.2.2**). The last term is the so-called *exchange-correlation energy* – it comprises exchange interaction and dynamic correlations. Variation of the energy with respect to the density (KS orbitals) leads to the set of orbital *Kohn-Sham equations*

$$\hat{f}_i^{KS}\left|\chi_i^{KS}(x_1)\right\rangle = \left[-\frac{1}{2}\nabla_i^{\,2} + \hat{\upsilon}(r_1) + \int \frac{dr_2\rho(r_2)}{|\vec{r}_1 - \vec{r}_2|} + \upsilon_{xc}[\rho]\right]\left|\chi_i^{KS}(x_1)\right\rangle = \varepsilon_i\left|\chi_i^{KS}(x_1)\right\rangle , \quad \textbf{(105)}$$

with the so-called *exchange-correlation potential* defined as

$$\upsilon_{xc}[\rho] = \frac{\delta E_{xc}[\rho]}{\delta \rho}.$$

(**106**)

Formally, the KS equations are similar to the HF equations (50) (Sec. **1.2.2**) with the exception that the nonlocal HF exchange operator is replaced with a *local* exchange-correlation potential υ_{xc}. The Lagrange multipliers ε_i preserve the orthonormality of the KS orbitals and formally are similar to the HF orbital energies. However, they do not possess the same transparent physical meaning of ionization potentials and electron affinities for the negative values of occupied and virtual orbitals, respectively. Nevertheless, it can be shown that the maximal Kohn-Sham occupied orbital energy is the negative ionization energy (Ref. **76**).

The original proof of the HK theorems assumes no degeneracy in the ground state. Moreover, it requires the density in the energy expression (94) to be *υ*-representable. Later on, a more general c*onstrained-search formulation* of the theorems was suggested by Levy (Ref. **77**). It drops the limitation of nondegeneracy on the ground-state density and does not require *υ*-representability.

The flavor of KS theory is that, unlike in correlated wave function methods, electron correlation is gatheres in the exchange-correlation potential which is a functional of the one-particle electron density. This provides computational efficiency comparable to that of HF theory with the formal scaling of N^4 with respect to the number of basis set functions.

However, the exact form of exchange-correlation functional is generally unknown, this has numerous implications.

For example, the energy obtained from the KS equations is variational (*i.e.* it is an upper bound to the exact one), but only with the *exact functional*.

As it was already noticed in Sec. **1.2.2**, the HF energy is naturally self-interaction-free due to the cancellation of Coulomb and exchange terms. This is not the case in KS theory with *approximate functionals*, and special efforts are required to cope with the problem (Ref. **78**, **79**). This also has profound implications for the charge-transfer problem of the time-dependent version of DFT (see Sec. **1.3.6**).

For closed-shell systems the exchange-correlation energy can be represented as follows

$$E[\rho] = \int F_{xc}\left(\rho, \nabla\rho, \nabla^2\rho, \ldots\right) dr.$$

(**107**)

Here F_{xc} is a functional of the density and its higher spatial derivatives. In the simplest case it depends on the density alone, and constitutes the *local-density approximation* (LDA) which is derived from the *uniform electron gas* (Ref. **80**, **81**, **82**, **83**). The next class of functionals depends on the density and its gradient. This is known as *generalized gradient approximation* (GGA). Since it depends on the density gradient it simulates the two-electron character of the interactions. Inclusion of the higher-order density derivatives is in principle possible but makes all mathematic expressions and computer implementation very complicated. Even for the simplest exchange-correlation functionals, it is not possible to evaluate their integrals analytically, hence, numerical integrations must be carried out.

Further improvement of the theory is based on the fact that the exchange contribution is about an order of magnitude larger than the correlation contribution. This suggests that the HF theory can be used to treat exchange, while DFT itself should be used to treat correlations. A number of researchers have argued that exchange and correlation effects might not be easily separated (Ref. **84**, **85**, **86**). Becke has shown (Ref. **85)** that Hartree-Fock exchange can be incorporated into DFT rather rigorously by means of the *adiabatic connection method* (Ref. **87**, **88**, **89**) giving rise to *hybrid functionals*. In particular, exact HF exchange can be combined with the gradient-corrected (GGA) energy functionals (Ref. **86**). Herein, the functionals can differ in the fraction of employed exact HF exchange and in the type of exchange-correlation functional. The most successful popular hybrid functionals with GGA exchange-correlation part is the B3LYP (Ref. **86**) functional. In many cases it describes H-bonded systems very well. In the present work the majority of DFT calculations employed B3LYP.

Unfortunately, the *local* character of existing functionals in combination with the single-reference nature of the electron density prevents from a correct description of the dispersion energy. It has been shown in numerous examples that contemporary DFT methodology fails to describe potential energy surfaces of Van-der-Waals complexes where the dispersion part of the interaction is substantial (see *e.g.* Ref. **90**). Even for “normal” H-bonded systems, application of DFT requires its verification by electron-correlation methods introduced in the previous sections.

Part 1.3

Electronic Schrödinger Equation: Excited States

1.3.1 An Overview

The interaction of molecular system with light induces electronic, in general – *vibronic*, transitions. Knowledge of the energies as well as structural and other molecular properties of excited states is necessary for the explanation and interpretation of electronic spectra of molecular systems, as well as for as understanding of the excited-state dynamics. Since the interaction of molecular system with electro-magnetic fields is essentially *time-dependent*, it requires complicated theoretical methodologies for the solution of time-dependent electronic problems.

One of the primary goals of such calculations is to obtain the energies of excited states, or, alternatively, the energy differences between excited states and the ground state termed *excitation energies*. The latter are related to electronic spectra. Multireference methods (Chap. 4, Ref. **39**), MCSCF (Ref. **41**), multireference-CI (MR-CI) (Ref. **91**, **92**) include a number of excited determinants into the wave function and, in principle, allow to obtain energies of both ground and excited states explicitly, as result of variational optimization. One of the major disadvantages of these techniques is the lack of size-consistency has been already mentioned in Sec. **1.2.3**. Additionally, MCSCF methods are sensitive to the choice of relevant determinants what brings unnecessary complexity to the situations when the ground state is well described by a single reference

Alternatively, the interaction of a molecular system with a time-dependent electro-magnetic field can be treated by means of *time-dependent perturbation theory* (Ref. **93**, **94**) in terms of a power series in the field strength. The expansion coefficients of the power series determine so-called *response functions* characterizing the response of the system to the external perturbation. Such an approach has numerous advantages (Ref. **95**, **96**, **97**, **98**). For instance, when the external field is electric field, the linear, quadratic and cubic response functions have transparent physical meaning of *frequency-dependent polarizability*, *hyperpolarizability* and *second hyperpolarizability*, respectively. Additionally, the *poles*[1] of the linear response functions correspond to excitation energies, whereas the *residues*[2] determine transition dipole matrix elements – the values which characterize transition probabilities between ground and excited states. Thus, excitation energies can be calculated within the same computational procedure as transition matrix elements and polarizibilties.

Response theory combined with ground-state methodologies introduced in Part **1.2**, constitute a well-developed tool for the calculation of excited states and their properties.

[1] A pole of order n of a complex function $f(z)=g(z)(z-a)^{-n}$ is the singularity at $z=a$.
[2] The residue of a complex function is the contour integral around its isolated singularity (such as pole).

Furthermore, even aforementioned multi-reference approaches which deliver excitation energies themselves, can be combined with response theory to obtain excited-state properties and transition matrix elements. Correlated ground-state coupled-cluster methods (CCSD, CCSDT, CCSDTQ) combined with response theory give a hierarchy of accuracies for excited-state calculations and preserves advantages of the ground-state CC theory, especially size-consistency. On the other hand, less accurate DFT combined with response theory allows for the calculations of quite large systems (up to thousands of basis functions). These two methods were used in the present study (Chap. **1**, **2**) and will be described in the next sections.

There is also a possibility to obtain time-dependent molecular response properties (*e.g.* frequency-dependent polarizability) within the MP2 formalism (Ref. **99**). Unfortunately, the structure of the expressions in this case is in general not compatible with the structure of exact response functions (they will be introduced in the next section). This does not allow to obtain excitation energies and transition moments in one pass.

Another important branch of excited-state methodologies is based on the Green's functions formalism (Ref. **93**, **94, 100**) and allows for a direct evaluation of response functions by means of their perturbation expansions. For example, *algebraic diagrammatic construction* (ADC) (Ref. **101**, **102**, **103**, **104**) is a computationally-efficient correlated technique which allows to obtain the whole electronic spectrum of molecular system. Unfortunately, the Green's functions based methodologies are traditionally less popular in the chemist's world than in the physicist's one, but the situation tends to change and modern efficient implementations arrive (Ref. **105**).

1.3.2 Introduction to Response Theory

The time evolution of molecular system under time-dependent perturbations obeys the time-dependent Schrödinger equation

$$\hat{H}\left|\Psi(t)\right\rangle = i\hbar\frac{\partial}{\partial t}\left|\Psi(t)\right\rangle . \tag{108}$$

In spirit of perturbation theory (Sec. **1.2.4**), the time-dependent Hamiltonian can be represented as a sum of a time-independent part $\hat{H}^{(0)}$ and a time-dependent perturbation $\hat{V}(t)$, also named *interaction operator*, multiplied by the smallness parameter λ

$$\hat{H}(t) = \hat{H}^{(0)} + \lambda\hat{V}(t) . \tag{109}$$

Time-independent part of the Hamiltonian satisfies the egeinvalue equation

$$\hat{H}^{(0)}\left|\Psi_0^{(0)}\right\rangle = E_0^{(0)}\left|\Psi_0^{(0)}\right\rangle = E_0^{(0)}\left|0\right\rangle \tag{110}$$

for the ground state, and the equations set

$$\hat{H}^{(0)}\left|\Psi_m^{(0)}\right\rangle = E_m^{(0)}\left|\Psi_m^{(0)}\right\rangle = E_m^{(0)}\left|m\right\rangle = \hbar\omega_m\left|m\right\rangle \tag{111}$$

for the excited states of the reference system[1]. At t=-∞ the time-dependent perturbation is switched off

$$\hat{H}(t=-\infty) = \hat{H}^{(0)}, \tag{112}$$

and the system resides in its ground state

$$\left|\Psi(t=-\infty)\right\rangle = \left|\Psi_0^{(0)}\right\rangle = \left|0\right\rangle. \tag{113}$$

It is convenient for computations to express the interaction operator in Eq. (109) via its Fourier transform $\hat{V}^{\omega}$

$$\hat{V}(t) = \int_{-\infty}^{+\infty}\hat{V}^{\omega}\exp[(-i\omega+\alpha)t]d\omega. \tag{114}$$

The parameter α is a real positive small number, in mathematics called *infinitezimal*, it provides the perturbation is switched-on adiabatically. In the final expressions it is usually set to zero. The advantage of the representation of perturbation via its Fourier transform becomes evident when the external field comprise only several frequency components ω_1, ω_2, ... In this case the interaction operator becomes the sum

$$\hat{V}(t) = \left(\hat{V}^{\omega_1}\exp[(-i\omega_1+\alpha)t] + \hat{V}^{-\omega_1}[(i\omega_1+\alpha)t]\right) + \left(\hat{V}^{\omega_2}\exp[(-i\omega_2+\alpha)t] + \hat{V}^{-\omega_2}[(i\omega_2+\alpha)t]\right) + \ldots. \tag{115}$$

In the time-dependent case, the expectation value of any arbitrary operator $\hat{A}$ can be formally expressed as the power series in the field strength λ

[1] Further analysis again will be given in atomic units and the Plank constant will be set to unit in the expressions.

$$\langle\Psi(t)|\hat{A}|\Psi(t)\rangle = \langle 0|\hat{A}|0\rangle + \lambda\int_{-\infty}^{+\infty}\left\langle\left\langle \hat{A};\hat{V}^{\omega_1}\right\rangle\right\rangle_{\omega_1+i\alpha}\exp[(-i\omega_1+\alpha)t]d\omega_1 +$$
$$+\lambda^2\int_{-\infty}^{+\infty}\left\langle\left\langle \hat{A};\hat{V}^{\omega_1};\hat{V}^{\omega_2}\right\rangle\right\rangle_{\omega_1+i\alpha,\omega_2+i\alpha}\exp[(-i\omega_1+\alpha)t]\exp[(-i\omega_2+\alpha)t]d\omega_1 d\omega_2 + \ldots \quad \textbf{(116)}$$

The quantities in the double-angle brackets are Fourier transforms of the linear and quadratic response functions (Ref. **100**, **106**), respectively

$$\left\langle\left\langle \hat{A};\hat{V}^{\omega'}\right\rangle\right\rangle_{\omega'+i\alpha} = \int_{-\infty}^{+\infty}\left\langle\left\langle \hat{A}(t);\hat{V}^{\omega'}(\tau')\right\rangle\right\rangle\exp[(i\omega'+\alpha)\tau']d\tau', \quad \textbf{(117)}$$

$$\left\langle\left\langle \hat{A};\hat{V}^{\omega'};\hat{V}^{\omega''}\right\rangle\right\rangle_{\omega'+i\alpha,\omega''+i\alpha} = \int_{-\infty}^{+\infty}\left\langle\left\langle \hat{A}(t);\hat{V}^{\omega'}(\tau');\hat{V}^{\omega''}(\tau'')\right\rangle\right\rangle\exp[(i\omega'+\alpha)\tau']\exp[(i\omega''+\alpha)\tau'']d\tau' d\tau''. \quad \textbf{(118)}$$

Herein, the linear response function, alternatively called *two-time propagator*, or *Green's function*, is defined as follows [1]

$$\left\langle\left\langle \hat{A}(t);\hat{V}^{\omega_1}(\tau_1)\right\rangle\right\rangle = -i\Theta(t-\tau_1)\langle 0|\left[\hat{A},\hat{V}^{\omega_1}(\tau_1)\right]|0\rangle. \quad \textbf{(119)}$$

The quadratic response function has the explicit form

$$\left\langle\left\langle \hat{A}(t);\hat{V}^{\omega_1}(\tau_1);\hat{V}^{\omega_2}(\tau_2)\right\rangle\right\rangle = -\frac{1}{2!}\Theta(t-\tau_1)\Theta(\tau_1-\tau_2)\langle 0|\left[\left[\hat{A},\hat{V}^{\omega_1}(\tau_1)\right],\hat{V}^{\omega_2}(\tau_2)\right]|0\rangle -$$
$$-\frac{1}{2!}\Theta(t-\tau_2)\Theta(\tau_2-\tau_1)\langle 0|\left[\left[\hat{A},\hat{V}^{\omega_2}(\tau_2)\right],\hat{V}^{\omega_1}(\tau_1)\right]|0\rangle \quad \textbf{(120)}$$

Notice, in the above and further expressions, the operator $\hat{A}$ is given in the *interaction representation* $\hat{A} = e^{i\hat{H}t}Ae^{-i\hat{H}t}$, such that the explicit time dependence is moved to the exponential part.

It can be shown (see *e.g.* Ref. **107**, **108**), that the spectral representation of the response functions in a formally *complete* set of eigenstates $|m\rangle$ (Eq. (111)) can be written as

$$\left\langle\left\langle \hat{A};\hat{V}^{\omega_1}\right\rangle\right\rangle_{\omega_1+i\alpha} = \sum_m\left(\frac{\langle 0|\hat{A}|m\rangle\langle m|\hat{V}^{\omega_1}|0\rangle}{\omega_1-\omega_m+i\alpha} - \frac{\langle m|\hat{V}^{\omega_1}|0\rangle\langle 0|\hat{A}|m\rangle}{\omega_1+\omega_m+i\alpha}\right), \quad \textbf{(121)}$$

[1] $\Theta(t\text{-}\tau)$ here is the *Heaviside*, or *step* function.

and

$$\left\langle\left\langle \hat{A};\hat{V}^{\omega_1};\hat{V}^{\omega_2}\right\rangle\right\rangle_{\omega_1+i\alpha,\omega_2+i\alpha} =$$
$$\sum_{m,m'}\left(\frac{\langle 0|\hat{A}|m\rangle\langle m|\hat{V}^{\omega_1}|m'\rangle\langle m'|\hat{V}^{\omega_2}|0\rangle}{(\omega_1+\omega_2-\omega_m+2i\alpha)(\omega_2-\omega_{m'}+i\alpha)}+\frac{\langle 0|\hat{A}|m\rangle\langle m|\hat{V}^{\omega_2}|m'\rangle\langle m'|\hat{V}^{\omega_1}|0\rangle}{(\omega_1+\omega_2-\omega_m+2i\alpha)(\omega_1-\omega_{m'}+i\alpha)}+\right.$$
$$+\frac{\langle 0|\hat{V}^{\omega_2}|m\rangle\langle m|\hat{V}^{\omega_1}|m'\rangle\langle m'|\hat{A}|0\rangle}{(\omega_1+\omega_2+\omega_{m'}+2i\alpha)(\omega_2+\omega_m+i\alpha)}+\frac{\langle 0|\hat{V}^{\omega_1}|m\rangle\langle m|\hat{V}^{\omega_2}|m'\rangle\langle m'|\hat{A}|0\rangle}{(\omega_1+\omega_2+\omega_{m'}+2i\alpha)(\omega_1+\omega_m+i\alpha)}-$$
$$\left.-\frac{\langle 0|\hat{V}^{\omega_1}|m\rangle\langle m|\hat{A}|m'\rangle\langle m'|\hat{V}^{\omega_2}|0\rangle}{(\omega_1+\omega_m+i\alpha)(\omega_2-\omega_{m'}+i\alpha)}-\frac{\langle 0|\hat{V}^{\omega_2}|m\rangle\langle m|\hat{A}|m'\rangle\langle m'|\hat{V}^{\omega_1}|0\rangle}{(\omega_2+\omega_m+i\alpha)(\omega_1-\omega_{m'}+i\alpha)}\right) \quad (122)$$

These explicit expressions provide information about excitation energies and transition matrix elements of the corresponding operator $\hat{A}$ at presence of time-dependent perturbation $\hat{V}$, by means of their poles and residues.

Let discuss it in more detail. In the present work optical properties *i.e.* the interaction of molecule with light have been considered. If the light is represented by a set of several monochromatic electro-magnetic waves of frequencies ω_1, ω_2, ... then, according to Eq. (115), the interaction operator takes an explicit form

$$\hat{V}(t) = -(\vec{\mathrm{E}}_1,\hat{\vec{\mu}})\left(\exp[(-i\omega_1+\alpha)t]+\exp[(i\omega_1+\alpha)t]\right)-$$
$$-(\vec{\mathrm{E}}_2,\hat{\vec{\mu}})\left(\exp[(-i\omega_2+\alpha)t]+\exp[(i\omega_2+\alpha)t]\right)-\ldots, \quad (123)$$

where $(\vec{\mathrm{E}}_i,\hat{\vec{\mu}})$ is the scalar product of the electric dipole moment operator of the molecule and the relevant component of the electric field. In the nonrelativistic case, the force of the magnetic part of the electromagnetic wave is small compared to the electric one. Thus, magnetic terms can be excluded from the Hamiltonian since magnetic effects themselves are beyond the scope of this study.

To assign optically-relevant physical meaning to the introduced quantities, here and further, operators $\hat{A}$, $\hat{V}^{\omega_1}$, $\hat{V}^{\omega_2}$ are referred to $\hat{\mu}_i$, $\hat{\mu}_j$, $\hat{\mu}_k$ components of the electric dipole moment operator respectively, where *i*, *j*, *k* indices run over spatial coordinates *x*, *y*, *z*.

Consider the case when the external field (123) contains only one monochromatic wave of frequency ω_1. In this case the linear-response function (121) can be related to the *i*-, *j*-th components of the frequency-dependent *dipole polarizability tensor*. It describes excitation by a photon of energy ω_1 (*absorption*) and deexcitation of a photon of energy ω_1 (*emission*). First-order poles $\pm\omega_m$ of the linear response function correspond to the excitation and de-

excitation energies between the ground $(|0\rangle)$ and excited $(|m\rangle)$ states. First-order transition dipole matrix elements between the states $|0\rangle$ and $|m\rangle$ can be obtained from the residues of the linear response function at its poles $(\pm\omega_m)$. In particular, the residue at $(+\omega_m)$ corresponds to the absorption

$$\lim_{\omega_1\to\omega_m}(\omega_1-\omega_m)\left\langle\left\langle \hat{A};\hat{V}^{\omega_1}\right\rangle\right\rangle_{\omega_1}=\langle 0|\hat{A}|m\rangle\langle m|\hat{V}^{\omega_m}|0\rangle=\Gamma^{A}_{0\to m}\Gamma^{V^{\omega_m}}_{m\to 0}, \tag{124}$$

while the residue at $(-\omega_m)$ corresponds to the emission

$$\lim_{\omega_1\to-\omega_m}(\omega_1+\omega_m)\left\langle\left\langle \hat{A};\hat{V}^{\omega_1}\right\rangle\right\rangle_{\omega_1}=-\langle 0|\hat{V}^{-\omega_m}|m\rangle\langle m|\hat{A}|0\rangle=\Gamma^{V^{-\omega_m}}_{0\to m}\Gamma^{A}_{m\to 0}. \tag{125}$$

Of particular interest is the following quantity termed *oscillator strength*

$$f_I=\frac{2}{3}(\omega_I-\omega_0)\left(\left|\langle\Psi_0|\hat{\mu}_x|\Psi_I\rangle\right|^2+\left|\langle\Psi_0|\hat{\mu}_y|\Psi_I\rangle\right|^2+\left|\langle\Psi_0|\hat{\mu}_z|\Psi_I\rangle\right|^2\right). \tag{126}$$

It characterizes the probability of transition between the ground and an excited states, and can be interpreted as its "strength" (see *e.g.* Ref. **109**). The oscillator strength is related to the linear response function by means of Eq. (124). Herein, the absorption and emission oscillator strengths can be distinguished.

Although the present study is only concerned with *first-order properties*, *i.e.* properties derived from the linear-response functions, it will be informative to introduce the second-order properties. Assume the external field (123) has two monochromatic components of ω_1 and ω_2 frequency. The quadratic response function (122) in this case represents *i*, *j*, *k* components of the frequency-dependent *dipole hyperpolarizability tensor* at frequencies ω_1 and ω_2. In particular, it describes the absorption of two photons of frequency ω_1 and ω_2 and the emission of one photon of frequency $(\omega_1+\omega_2)$. The residues of quadratic-response functions at pole $(+\omega_{m'})$ determine second-order transition matrix elements between the ground and excited states (*i.e.* two-photon absorption transition matrix element)

$$\lim_{\omega_2\to\omega_{m'}}(\omega_2-\omega_{m'})\left\langle\left\langle \hat{A};\hat{V}^{\omega_1};\hat{V}^{\omega_2}\right\rangle\right\rangle_{-\omega_1,\omega_2}=\sum_m\langle m'|\hat{V}^{\omega_{m'}}|0\rangle\left(\frac{\langle 0|\hat{A}|m\rangle\left(\langle m|\hat{V}^{-\omega_1}|m'\rangle-\delta_{mm'}\langle 0|\hat{V}^{-\omega_1}|0\rangle\right)}{-\omega_1+\omega_{m'}-\omega_m}-\right.$$
$$\left.-\frac{\langle 0|\hat{V}^{-\omega_1}|m\rangle\left(\langle m|\hat{A}|m'\rangle-\delta_{mm'}\langle 0|\hat{A}|0\rangle\right)}{-\omega_1+\omega_m}\right)=\Gamma^{AV^{-\omega_1}}_{0\to m'}(\omega_1)\Gamma^{V^{\omega_{m'}}}_{m'\to 0}$$

(**127**)

Finally, the transition matrix element between two excited states $|m'\rangle$ and $|m\rangle$ can be obtained from the residue at both poles $(-\omega_m)$ and $(+\omega_{m'})$

$$\lim_{\omega_1\to-\omega_m}(\omega_1+\omega_m)\left(\lim_{\omega_2\to\omega_{m'}}(\omega_2-\omega_{m'})\left\langle\left\langle \hat{A};\hat{V}^{\omega_1};\hat{V}^{\omega_2}\right\rangle\right\rangle_{\omega_1,\omega_2}\right)=$$
$$-\langle 0|\hat{V}^{-\omega_m}|m\rangle\langle 0|\hat{V}^{-\omega_m}|m'\rangle\left(\langle m|\hat{A}|m'\rangle-\langle 0|\hat{A}|0\rangle\right)$$

(**128**)

Now, the relation between the response functions expressed in terms of the exact wave-function and excitation energies and transition matrix elements has been established. The next logical step is to specify a practical way to construct the response functions. This procedure is not unique and can be performed in several ways.

One way is to employ time-dependent perturbation theory expanding time-dependent wave-functions into the power series

$$|\Psi(t)\rangle=|\Psi_0^{(0)}\rangle+\lambda|\Psi^{(1)}\rangle+\lambda^2|\Psi^{(2)}\rangle+\ldots=|0\rangle+\lambda|0^{(1)}\rangle+\lambda^2|0^{(2)}\rangle+\ldots.$$

(**129**)

The expectation value of a relevant operator then becomes

$$\langle\Psi(t)|\hat{A}|\Psi(t)\rangle=\langle 0|\hat{A}|0\rangle+\lambda\left(\langle 0^{(1)}|\hat{A}|0\rangle+\langle 0|\hat{A}|0^{(1)}\rangle\right)+\lambda^2\left(\langle 0^{(1)}|\hat{A}|0^{(1)}\rangle+\langle 0^{(2)}|\hat{A}|0\rangle+\langle 0|\hat{A}|0^{(2)}\rangle\right)+\ldots.$$

(**130**)

Representing the expressions in parentheses via their Fourier transforms

$$\langle\Psi(t)|\hat{A}|\Psi(t)\rangle=\langle 0|\hat{A}|0\rangle+\lambda\int_{-\infty}^{+\infty}\left[\langle 0^{(1)}|\hat{A}|0\rangle+\langle 0|\hat{A}|0^{(1)}\rangle\right]_{\omega_1+i\alpha}e^{(-i\omega_1+\alpha)t}d\omega_1+$$
$$+\lambda^2\int_{-\infty}^{+\infty}\left[\langle 0^{(1)}|\hat{A}|0^{(1)}\rangle+\langle 0^{(2)}|\hat{A}|0\rangle+\langle 0|\hat{A}|0^{(2)}\rangle\right]_{\omega_1+i\alpha,\omega_2+i\alpha}e^{(-i\omega_1+\alpha)t}e^{(-i\omega_2+\alpha)t}d\omega_1d\omega_2+\ldots,$$

(**131**)

and comparing the terms of same order in λ in both Eq. (131), (116), reveals that the expressions in square brackets are the Fourier transforms of linear- and quadratic-response functions.

The second alternative for the derivation of response functions is the so-called *phase-factor approach*. It stems from the application of perturbation theory to the formal solution of the

time-dependent Schrödinger equation expressed in terms of the *evolution operator* (*e.g.* Ref. **93**) and further comparison of the terms of the same order in λ with those in Eq. (116) (Ref. **107**, **110**, **111**).

Both alternatives require the solution of time-dependent equations for the approximate wave functions associated with a particular quantum-chemical method, although the phase-factor approach is only applicable to wave function-based methods. The procedure will be briefly discussed in the next sections in application to the coupled-cluster and density-functional theories.

1.3.3 Time-Dependent Coupled-Cluster Theory

General form of the time-dependent coupled-cluster wave-function was initially proposed by Monkhorst (Ref. **110**)

$$\left|\Psi(t)\right\rangle = e^{\hat{T}(t)-i\left(E_0 t+\delta(t)\right)}\left|\Psi_0\right\rangle, \tag{132}$$

herein, $\left|\Psi_0\right\rangle$ is the ground-state variationally-optimized Hartree-Fock reference wave-function, E_0 is the ground state CC energy (Eq. (85), Sec. **1.2.5**) and $\delta(t)$ is the time-dependent phase factor. The action of cluster operator $\hat{T}(t)$ is defined in Eq. (80) (Sec. **1.2.5**) with the only difference that the cluster amplitudes contained in it are now time-dependent.

As it was mentioned in the previous section, there are two main approaches to derive CC response functions.

Within the first approach, the CC response functions can be derived directly from the coupled-cluster phase factor (Eq. (132)) (Ref. **110**, **111**). The later can be represented in perturbation manner by expanding it into the power series with respect to the field strength parameter

$$\delta(t) = \lambda\delta^{(1)}(t) + \lambda^2\delta^{(2)}(t) + \ldots. \tag{133}$$

The term at λ^0 in the above expression corresponds to the $E_0 t$ term in the exponent of time-dependent CC wave-function (132) and this fact is already taken to account there. In particular, for the external perturbation represented by a monochromatic wave of frequency ω_1 (see Eq. (115)) the linear-response function can be calculated as

$$\left\langle\left\langle \hat{A};\hat{V}^{\omega_1}\right\rangle\right\rangle_{\omega_1} = \lim_{\alpha\to 0}\frac{\omega_1}{2\pi}\int_0^{2\pi/\omega_1}\frac{\partial}{\partial\tau}\delta^{(2)}d\tau\,,$$

(**134**)

with infinitezimal α as defined in Eq. (114) (Sec. **1.3.2**).

The second approach, developed by Jorgensen and coworkers in application to the MSCSF and CC wave functions (Ref. **108**, **112**), is based on the analysis of the time evolution of the expectation value of a relevant operator (Eq. (129), (130)).

Both approaches require the solution of time-dependent CC equations for the phase factor and time-dependent cluster amplitudes. These equations can be obtained by substitution of the time-dependent CC wave function (132) into the time-dependent Schrödinger equation (108) (Sec. **1.3.2**)

$$\hat{H}(t)e^{\hat{T}(t)-i\left(E_0t+\delta(t)\right)}\left|\Psi_0\right\rangle = i\frac{\partial}{\partial t}e^{\hat{T}(t)-i\left(E_0t+\delta(t)\right)}\left|\Psi_0\right\rangle.$$

(**135**)

As usually, at t=-∞ the time-dependent perturbation is switched off and the system is described by the ground state CC wave-function (Eq. (85), Sec. **1.2.5**). Multiplying (135) by $e^{-\hat{T}(t)+i\left(E_0t+\delta(t)\right)}$ gives an intermediate equation

$$e^{-\hat{T}}\hat{H}e^{\hat{T}}\left|\Psi_0\right\rangle = i\frac{\partial\hat{T}}{\partial t}\left|\Psi_0\right\rangle + \frac{\partial\delta}{\partial t}\left|\Psi_0\right\rangle + E_0\left|\Psi_0\right\rangle.$$

(**136**)

Its subsequent multiplication by $\left\langle\Psi_0\right|$ and taking into account the normalization of the reference function $\left(\left\langle\Psi_0\middle|\Psi_0\right\rangle = 1\right)$ yields a differential equation for the time-dependent phase factor

$$\left\langle\Psi_0\middle|e^{-\hat{T}}\left(\hat{H}-E_0\right)e^{\hat{T}}\middle|\Psi_0\right\rangle = \frac{\partial}{\partial t}\delta\,.$$

(**137**)

Projecting (136) onto each n-tuply excited determinant $\left\langle\Psi_{A_n}^{R_n}\right|$ and assuming that each excited determinant is orthogonal to the Hartree-Fock ground state $\left(\left\langle\Psi_{A_n}^{R_n}\middle|\Psi_0\right\rangle = 0\right)$, yields the equations for the evolution of the time-dependent cluster amplitudes

$$\left\langle\Psi_{A_n}^{R_n}\middle|e^{-\hat{T}}\hat{H}e^{\hat{T}}\middle|\Psi_0\right\rangle = i\left\langle\Psi_{A_n}^{R_n}\middle|\frac{\partial}{\partial t}\hat{T}\middle|\Psi_0\right\rangle.$$

(**138**)

Equations (137), (138) can be solved using perturbation theory by expanding the phase factor according to (133) and the cluster operator as

$$\hat{T}(t) = \hat{T}^{(0)} + \lambda\hat{T}^{(1)} + \lambda^2\hat{T}^{(2)} + \ldots .$$

(**139**)

Herein, $\hat{T}^{(0)}$ corresponds to the time-independent cluster operator (Eq. (60), Sec. **1.2.3** and Eq. (80) (Sec. **1.2.5**)). The initial conditions for the solution of Eq. (137), (138) are

$$\delta^{(i)}(t = -\infty) = 0, \;\; i = 1, \; 2, \; \ldots$$

and

$$\hat{T}^{(i)}(t = -\infty) = 0, \;\; i = 1, \; 2, \; \ldots .$$

(**140**)

This allows to obtain the equations for time-dependent cluster amplitudes and the phase factor. The explicit forms of the linear and quadratic response functions obtained within the phase-factor or the expectation-value approach can be found in Ref. **111** and **112**, respectively.

1.3.4 Time-Dependent Density-Functional Theory: Formal Foundations

Consider molecular system with the time-dependent Hamiltonian (109) (Sec. **1.3.2**) written in the DFT manner

$$\hat{H}(r,t) = \sum_i^N \left(-\frac{1}{2}\nabla_i^2 \right) + \underbrace{\sum_i^N \hat{\upsilon}_i(r_i)}_{\hat{\upsilon}(r)} + \sum_{j>i} \frac{1}{r_{ij}} + \lambda \underbrace{\sum_i^N \hat{v}(r_i,t)}_{\hat{V}(r,t)} .$$

(**141**)

As usually, $\hat{\upsilon}(r)$ is the nuclear-electron attraction operator, or, in general, sum over other one-electron time-independent operators. $\hat{V}(r,t)$ is the sum of time-dependent one-electron operators, termed *time-dependent external potential*, analogously to time-independent DFT. The wave function $\Psi(x,t)$ of the system is determined by the time-dependent Schrödinger equation (108) with the initial condition

$$\Psi(x,t_0) = \Psi_0(x) .$$

(**142**)

Time-dependent density-functional theory (TDDFT) is formally constituted by two statements.

(1) The first statement provides that the time-dependent electron density determines the time-dependent external potential $V[\rho](r,t)$ within a *spatially-independent* the time-

dependent constant $C(t)$, therefore, the wave-function is defined within a time-dependent phase factor

$$\rho(x,t) \leftrightarrow V[\rho](r,t) + C(t) \leftrightarrow \Psi[\rho](r,t)\exp\left(-i\int C(t)dt\right). \quad \textbf{(143)}$$

This statement is known as the *Runge-Gross* (RG) theorem (Ref. **113**) which can be interpreted as a generalization of the first HK theorem (Sec. **1.2.6**) for the time-dependent case. Since the time-dependent wave function determines the expectation value of any quantum mechanical operator, the latter can be represented as

$$\overline{O}[\rho](t) = \left\langle \Psi[\rho](r,t)\middle|\hat{O}\middle|\Psi[\rho](r,t)\right\rangle. \quad \textbf{(144)}$$

In general, the expectation value (144) implicitly depends on the initial state Ψ_0 as well, so it is a functional of both ρ and Ψ_0. However, for the non-degenerate ground state, $\overline{O}[\rho](t)$ it is a functional of density alone, since in this case, Ψ_0 is a functional of the ground state density due to the first HK theorem.

(2) An equivalent of a variational principle for the time-dependent case, is provided similarly to the second HK theorem for the ground state. From general quantum mechanics it is known, that the time-dependent wave-function $\Psi(x,t)$ – the solution of the time-dependent Schrödinger equation (108) (Sec. **1.3.2**) corresponds to a stationary point

$$\frac{\delta A(t)}{\delta\Psi(r,t)} = 0 \quad \textbf{(145)}$$

of the quantum-mechanical *action integral*

$$A(t) = \int_{t_0}^{t} d\tau\left\langle \Psi(r,\tau)\middle|i\frac{d}{dt} - \hat{H}(r,\tau)\middle|\Psi(r,\tau)\right\rangle. \quad \textbf{(146)}$$

The latter is a functional of the time-dependent density by virtue of the RG theorem

$$A(t) = A[\rho](t) = \int_{t_0}^{t} dt\left\langle \Psi[\rho](r,t)\middle|i\frac{d}{dt} - \hat{H}(r,t)\middle|\Psi[\rho](r,t)\right\rangle. \quad \textbf{(147)}$$

The time-dependent density, can be then obtained from the Euler-Lagrange equation

$$\frac{\delta A[\rho](t)}{\delta \rho(r,t)} = 0,$$

(**148**)

combined with the relevant boundary conditions.

The RG theorem and the time-dependent density variational principle establish a time-dependent version of the Kohn-Sham formalism. As in the time-independent case, the main objective is to find mathematic expressions for the expectation value of the Hamiltonian operator in the action integral (147). This, again, can be achieved by introducing the hypothetic reference system of non-interacting particles, placed into the external one-electron time-dependent potential υ^{TD}, the time-dependent density ρ^{TD} of which is equal to the density ρ of the interacting system. The existence of such a system is referred to as *time-dependent υ-represenatbility*, and it is normally provided according to the later generalization of the RG theorem by Leeuwen (Ref. **114**). The wave function of the reference system is then represented by a single determinant constructed from the time-dependent spin orbitals

$$\left|\Psi[\rho^{TD}](r,t)\right\rangle = \left|\Psi[\rho^{TD}](r,t)\right\rangle = \left|\chi_1^{TD}(x_1,t)\chi_2^{TD}(x_2,t)...\chi_N^{TD}(x_N,t)\right\rangle.$$

(**149**)

The latter are the solutions of an one-electron time-dependent Schrödinger equation, also referred to as time-dependent Kohn-Sham equation

$$i\frac{\partial}{\partial t}\left|\chi_i^{TD}(x_1,t)\right\rangle = \left(-\frac{1}{2}\nabla_i^2 + \hat{\upsilon}^{TD}(r_1,t)\right)\left|\chi_i^{TD}(x_1,t)\right\rangle.$$

(**150**)

The time-dependent density and the kinetic energy has the same form as in the time-independent case (Eq. (101), (103), Sec. **1.2.6**) with the only difference that time-independent KS orbitals are replaced with the time-dependent ones. Combining action integrals (147), expressed in terms of the real and reference densities, which are assumed to be equal due to *υ*-represenatbility, and taking into account single-determinant representation for the wave function, makes it possible to write the action integral explicitly (Ref. **113**). Finally, its variation with respect to the reference density ρ^{TD} allows to express the external potential in the time-dependent KS equation (150) as

$$\hat{\upsilon}^{TD}(r_i,t) = \hat{\upsilon}(r) + \lambda\hat{V}(r,t) + \int dr_j \frac{\rho^{TD}(x_j,t)}{x_{ij}} + \frac{\delta A_{XC}[\rho^{TD}](t)}{\delta \rho^{TD}(x,t)}.$$

(**151**)

The third term here is the time-dependent Coulomb operator, A_{XC} is the "exchange-correlation" part of the action integral named *exchange-correlation kernel* (*xc*-kernel). Eq. (151) therefore can be compactly represented as

$$i\frac{\partial}{\partial t}\left|\chi_i^{TD}(x_1,t)\right\rangle = \hat{F}^{TD}(r_1,t)\left|\chi_i^{TD}(x_1,t)\right\rangle, \tag{152}$$

where $\hat{F}^{TD}$ is the time-dependent Kohn-Sham Fock operator comprising the kinetic energy operator and the external potential. Analogously to the time-independent KS counterpart, it simulates the effects of exchange and correlation on the time-dependent reference density.

The exact form of time-dependent action integral is in general unknown, therefore, approximations should be introduced. The most straightforward approximation is appropriate when the density varies slowly with respect to the external field. In this case, referred as *adiabatic local-density approximation* (ALDA), the originally nonlocal, in time, *xc*-kernel is replaced with a local, in time, *xc*-functional from the ground-state DFT with the instant values of density at a given moment

$$\upsilon_{xc}[\rho^{TD}](r,t) = \frac{\delta A_{XC}[\rho^{TD}](t)}{\delta\rho^{TD}(r,t)} \sim \frac{\delta E_{XC}[\rho_t^{KS}]}{\delta\rho_t^{KS}(r)} = \upsilon_{xc}[\rho_t^{KS}](r). \tag{153}$$

In particular, hybrid GGA functionals with the HF exchange (Sec. **1.2.6**) can be used in TDDFT.

Time-dependent KS equations (150), (152) can be expanded in a basis of *M* time-independent (unperturbed) orthonormal Kohn-Sham orbitals with the time-dependent expansion coefficients

$$\left|\chi_i^{TD}(x_1,t)\right\rangle = \sum_{\mu=1}^{M} C_{i\mu}(t)\left|\chi_\mu^{KS}(x_1)\right\rangle. \tag{154}$$

Inserting expansion (154) into the time-dependent KS equations for the spatial orbitals and multiplying by $\left\langle\chi_{\mu'}^{KS}(x_1)\right|$, one obtains a differential equations for the expansion coefficients:

$$\frac{\partial}{\partial t}C_{i\mu'}(t) = \sum_{\mu=1}^{K} C_{i\mu}(t)F_{\mu\mu'}^{KS}. \tag{155}$$

Herein, $F_{\mu'\mu}^{KS}$ are the matrix elements of the time-dependent KS Fock operator in the basis of unperturbed orbitals. Notice, that since the external potential (151) depends on the time-

dependent density, it also depends on the expansion coefficients and, therefore, as in the HF case, requires an iterative solution.

Many important aspects of TDDFT, can be found *e.g.* in review Ref. **115**.

1.3.5 Time-Dependent Density-Functional Response Theory

In order to obtain excited states within TDDFT one can either solve Eq. (152) numerically or construct the response functions according to the formalism introduced in Sec. **1.3.2**. The former method is named *time-dependent Kohn-Sham* (TD-KS), the latter is *time-dependent density-functional response theory* (TD-DFRT) (*e.g.* Ref. **116**). Since TDDFRT operates with analytical expressions having transparent physical meaning and, moreover, is robust to the numerical errors, it is usually more preferable than TD-KS, although more difficult for computer implementation.

To construct the response functions as outlined in Sec. **1.3.2,** one has to notice, that due to the single-determinant representation (149) of the time-dependent wave function, the expectation value of an operator (in particular – electric dipole operator), required for the construction of the response function, depends on the time-dependent electron density

$$\left\langle \Psi(t)\left|\hat{A}\right|\Psi(t)\right\rangle = \int dr_1 \hat{A} \sum_i^N \left|\chi_i^{TD}(r_1,t)\right|^2 = \int dr_1 \hat{A}\rho^{TD}(x_1,t)\,. \tag{156}$$

Therefore, the density response, and hence the response of the expansion coefficients due to the time-dependent perturbation

$$\delta\rho^{TD}(x_1,t) = \int d\omega \sum_{i=1}^{N}\sum_{\mu,\mu'} \delta\left(C^*_{i\mu'}(t)C_{i\mu}(t)\right)\chi_{\mu'}^{KS^*}(x_1)\chi_{\mu}^{KS}(x_1)\,, \tag{157}$$

determines the response functions. Time derivatives of the expansion coefficients can be obtained from the time-dependent KS equation (155) perturbatively. In the present study (Chap. **2**), only the first-order properties (*i.e.* excitation energies and oscillator strengths) have been of interest. They need the linear-response functions and, hence, only the first-order terms should be retained in the perturbation expansion of the coefficients. The derivatives, up to first order, can be expressed via the basis-set coefficients of the unperturbed system (zeroth order)

$$\frac{\partial}{\partial t}C_{\mu i}(t) = \sum_{p=1}^{K} C_{\mu k}^{(0)} U_{ki}\,. \tag{158}$$

The matrix of coefficients U_{ki} is called *response matrix*. In the case when the zeroth-order coefficients are variationally optimized, only the elements of the response matrix with the virtual-occupied $U_{ki} \rightarrow X_{ra}$ or occupied-virtual $U_{ki} \rightarrow Y_{ar}$ indices will be retained in the subsequent derivations. The reason is that the virtual-virtual and occupied-occupied blocks of the response matrix correspond to the orbital rotations within their subspaces and are inapt to produce new states. The property is known as *idempotency condition* for the density, while elements X_{ra}, Y_{ar} are termed TDDFT *response amplitudes*. This procedure allows to reduce the differential time-dependent KS equation (155) to a matrix equation with unknown response amplitudes. From this matrix equation, time derivatives (158) (expressed via response amplitudes) can be taken and inserted into Eq. (156). Its subsequent Fourier transform determines the linear-response function (117) (Sec. **1.3.2**) in the frequency domain. The poles of the linear-response function, when the operator corresponds to the electric dipole moment (Sec. **1.3.2**), then yield the equation for the excitation energies, while the residues provide the transition dipole matrix elements. The latter are related to oscillator strength by means of Eq. (126). In particular, the equation for the excitation energies has the following form:

$$\begin{pmatrix} \mathbf{A} & \mathbf{B} \\ \mathbf{B}^* & \mathbf{A}^* \end{pmatrix} \begin{pmatrix} \mathbf{X} \\ \mathbf{Y} \end{pmatrix} = \omega \begin{pmatrix} \mathbf{1} & \mathbf{0} \\ \mathbf{0} & -\mathbf{1} \end{pmatrix} \begin{pmatrix} \mathbf{X} \\ \mathbf{Y} \end{pmatrix}. \tag{159}$$

The elements of the above matrices are defined as follows

$$A_{ra,sb} = (\varepsilon_r - \varepsilon_a)\delta_{ab}\delta_{rs} + \langle \chi_r \chi_b | \chi_a \chi_s \rangle + \langle \chi_r \chi_b | \frac{\delta^2 E_{xc}}{\delta\rho(x_1)\delta\rho(x_2)} | \chi_a \chi_s \rangle, \tag{160}$$

$$B_{ra,sb} = \langle \chi_r \chi_s | \chi_a \chi_b \rangle + \langle \chi_r \chi_s | \frac{\delta^2 E_{xc}}{\delta\rho(x_1)\delta\rho(x_2)} | \chi_a \chi_b \rangle. \tag{161}$$

Eq. (159) is a *non-Hermitian* equation with the response amplitudes treated as its eigenvectors. The second derivative of the the *xc*-kernel with respect to the density in Eq. (160) stems from the fact that time-dependent Kohn-Sham Fock operator depends itself on the time-dependent densities.

The derivation of the linear response formalism in this section generally follows the same route as presented in Ref. **116**.

1.3.6 Time-Dependent Density-Functional Theory: Properties and Limitations

The advantages of TDDFT are widely recognized.

1. The response functions of TD-DFRT are comparable with the response functions for the exact wave-functions, what greatly simplifies their interpretation.

2. TDDFT is a computationally inexpensive procedure, *e.g.* TD-DFRT in combination with ALDA scales as N^4.

3. TDDFT describes low-lying valence excitations with good accuracy – in many cases as good as wave function correlated methods. The reason for this is that the difference in the KS orbital energies in Eq. (160) is a good approximation for the excitation energies since, unlike HF theory, the KS orbitals are correlated.

The limitations of TDDFT are well-known as well.

1. The first group of difficulties of TDDFT originates from the ALDA approximation.

The situations when ALDA is not valid, require a time-dependent *xc*-kernel. Examples of developments on time-/frequency-dependent *xc*-kernel within the TD-KS/TD-DFRT formalisms are given in Ref. **117**, **118** and **119**. Furthermore, time-dependent *xc*-kernel would allow to describe situations with *double-excitation* character, otherwise missing in the linear-response TDDFT formalism (Ref. **117**, **118**).

Further problems of the ALDA/TDDFT combination stem from the approximate character of the ground-state *xc*-functional. It transmits the approximate character of the ground-state DFT into TDDFT, making it dependent on the functional's quality. For example, often inaccurate $1/r$ (r is the electron-electron distance) behaviour of the existing ground-state functionals at long and medium distances cause severe problems in the description of *Rydberg states*[1], valence states of extended π-systems (Ref. **120**, **121**) and *charge-transfer* (CT) states[2] (Ref. **122**, **123**, **124**).

In particular, it was understood that the failure of TDDFT in the description of CT states can be attributed to the lack of nonlocal HF exchange in the standard *xc*-functionals. It causes the electron-transfer self-interaction error (Ref. **125**, **126**). Therefore, the increase of the fraction of HF exchange in the hybrid ground-state DFT functionals is a straightforward remedy against the CT failure of TDDFT. More systematic approach would be to construct

[1] Rydberg states are the upper-lying excited states which converge to the ionic states.
[2] CT excited states are the states which exhibit electron transfer from one fragment of a molecular complex to another one.

exact local Kohn-Sham exchange potential, the attempts of which are offered in Ref. **127**, **128**, **129**.

2. Other limitations of linear-response TD-DFRT have implications for nonadiabatic nuclear dynamics. In fact, within the linear-response formalism (either wave function- or density-functional-based), only the ground-to-excited and excited-to-ground transition matrix elements (Eq. (124), (125), Sec. **1.3.2**) of the nonadiabatic-coupling operators (15) (Sec. **1.1.2**) can be obtained (see Ref. **130**). The excited-to-excited matrix elements do require second-order response functions, what is computationally more demanding. This complicates the development of nonadiabatic dynamics involving transitions between excited states (Eq. (128), Sec. **1.3.2**) (Ref. **131**). The remedy would be to use TD-KS rather than TD-DFRT, but, again, this is less desirable due to the aforementioned sensitiveness to the numerical errors.

3. Unlike the case of optical phenomena considered in this work, the essentially nonlocal character of magnetic fields makes a rigorous formulation of the magnetic response properties (static or dynamic) within the TDDFT framework problematic. To describe the nonlocal and velocity-dependent potentials correctly, the theory should operate with both densities and density gradients (*current densities*) as fundamental variables. Such an extension of the formalism has been proposed and it is known as *current density-functional theory* (CDFT) (see Ref. **132**). However, this methodology is more complicated and computationally demanding than TDDFT and, hence, it is not yet clear whether it is able to compete with correlated wave function methods.

4. Finally, another interesting conceptual problem of TDDFT, which has been recently recognized (Ref. **133**, **134**) is worth to be mentioned. It was shown, that the phase-factor problem, arising from the transition from the wave function to the density, corrupts the definition of quantum-mechanical action integral (Eq. (147)). This deprives the time-dependent formulation of DFT a *strict* variational principle, and, hence, its predictive power to obtain the time-dependent densities (Eq. (148)). Indeed, it can be illustrated by the fact that response functions for wave function based methods can be equally derived from the time-dependent phase factor and expectation values of the relevant operators. That is not the case for TDDFT. Future will show what the real implications of this revision for the field are.

In summary, there are ongoing efforts in the development of new *xc*-functionals or even alternative theoretical formulations (like CDFT) to diminish the described problems of TDDFT. However, no methodology describing all states equally well is proposed so far. Therefore, the application of TDDFT to a particular problem requires a careful examination, in the best case by comparison with correlated wave function methods.

Part 1.4
Basis-Set Effects

1.4.1 Basis-Sets Types and Basis-Set Errors

From the formal quantum-mechanical perspective, many different functions can form a basis set in the expansion (55) (Sec. **1.2.2**). However, three major types of basis sets are most common in electronic-structure calculations. They are the *plane-waves*, *Slater-type functions* (SF) and *Gaussian-type functions* (GF). The first are often convenient for *periodic* calculations, the latter two – for *molecular* and *cluster* calculations.

For a given angular momentum, a Slater-type function can be written as

$$\phi_{\mu}^{SF}(\xi_m, \vec{r} - \vec{R}_I) = N_m^{SF} e^{-\xi_m |\vec{r} - \vec{R}_I|} (r^x - R_I^X)^{m_x} (r^y - R_I^Y)^{m_y} (r^z - R_I^Z)^{m_z}, \quad (\mathbf{162})$$

where N_m^{SF} is a normalization constant, ζ_m is the *Slater orbital exponent* and m_x, m_y, m_z are the exponents of the Cartesian components of the electron and nuclear coordinates. These numbers approximate the angular-momentum functions (*i.e.* the solutions of the angular part of Schrödinger equation for the hydrogen atom).

Gaussian-type functions have the form

$$\phi_{\mu}^{GF}(\alpha_{\mu}, \vec{r} - \vec{R}_I) = N_{\mu}^{GF} e^{-\alpha_{\mu} |\vec{r} - \vec{R}_I|^2} (r^x - R_I^X)^{m_x} (r^y - R_I^Y)^{m_y} (r^z - R_I^Z)^{m_z}. \quad (\mathbf{163})$$

Again, N_{μ}^{GF} is a normalization constant, α_{μ} is the *Gaussian orbital exponent* and m_x, m_y, m_z are the exponents of the Cartesian components of the electron and nuclear coordinates.

Orbital exponents for both types of functions are positive (nonzero) numbers. A larger orbital exponent determines a smaller denser function, a smaller one – a more broad function termed *diffuse function*.

In contrast to isolated molecules and clusters, periodic systems can be described by repeated boxes called *unit cells (Bravais lattices)*, containing the nuclei. The cells are characterized by three *direct lattice vectors*. Any wave function can be represented as a continuous set of plane-waves with their own wave-vectors. However, in *periodic potentials*, the *continuous* spectrum transforms to a *discrete* one. The wave function in this case can be expressed as a product of a cell-periodic part and a wave-like part. This property is known as

Bloch's theorem. (see *e.g.* Ref. **135**). The radial part of the molecular orbital in a periodic potential can therefore be written as

$$\phi_\mu(\vec{r},\vec{k}) = \frac{1}{\sqrt{\Omega}} \sum_G c_\mu(\vec{G},\vec{k}) \exp i\left(\left(\vec{G}+\vec{k}\right),\vec{r}\right), \tag{164}$$

where Ω is the volume of the unit cell and $\vec{G}$ are the *reciprocal lattice vectors* related to the direct lattice vectors by means of a linear transformation.

In course of a variational optimization, coefficients of the basis set expansion (55) are optimized, while the parameters of the basis functions (162), (163), (164) remain constant.

Skater- or Gaussian-type functions are often named *atom-centered* basis sets, the plane-waves occupying the whole space are *originless*.

Slater-type functions are more appropriate for electronic-structure calculations than Gaussian functions since the former have the correct asymptotic behaviour for atoms at large distances and hence require fewer terms in the basis set expansion (55) to reproduce the same quality of calculations. However, two-electron integrals (see Sec. **1.2.2**) are much easier to calculate with GF than with SF. The reason is that the product of two Gaussian functions, centered on two different points *A*, *B* is another Gaussian, centered on the point *C* which lies on the line connecting *A* and *B* (see *e.g.* Sec. 3.5.1 of Ref. **39**). To exploit this advantage, Slater-type functions (or other appropriate basis functions) can be represented by a linear combination of Gaussian functions termed *contracted Gaussian functions* (CGF)

$$\phi_p^{CGF}(\vec{r}-\vec{R}_I) = \sum_{\mu=1}^{L} d_{p\mu}\phi_\mu^{GF}(\alpha_{p\mu};\vec{r}-\vec{R}_I)\,. \tag{165}$$

Here L is the number of Gaussian functions, called *contraction length* and $d_{p\mu}$ are the *contraction coefficients*. Contraction length, contraction coefficients and orbital exponents are normally obtained from calculations on atoms to reproduce desirable properties (*e.g.* to approximate the Slater-type functions). During the SCF optimization, expansion coefficients are optimized while the parameters of the contractions stay fixed. Even when each Slater-type function is constructed from several Gaussians, four-electron integral calculations are still several times faster than those with Slater functions.

There exist the following strategies to construct basis sets from Gaussian-type functions.

The *minimal basis stets* are the smallest possible sets to qualitatively reproduce chemical properties of atoms within a molecule. These sets normally contain one Slater-type function per occupied atomic orbital, one per each orbital from the partially occupied subshells and one

per valence *p*-type functions for the elements from the first two groups of the periodic table. Minimal basis sets are denoted as STO-LG, where L is the contraction lenth (165) to approximate each Slater function.

Since each basis function of a given quantum number contains one Slater function, the minimal basis sets are often referred to as of *single-zeta* quality with "zeta" implying a Slater orbital exponent. Further improvement in this direction is to represent each atomic orbital by two or more Slater functions with their own coefficients (fixed during SCF): this gives rise to the double-, triple-, quadruple-zeta *etc.* quality basis sets.

While forming a chemical bond, valence orbitals of atoms alter stronger than the core orbitals. It suggests that the valence orbitals should be represented by more Slater-type functions than the core ones. This strategy emerged into the *split-valence* basis sets of Pople and co-workers (Ref. **136**).

For example, a common split-valence 6-31G basis set has six GF functions to approximate core single Slater functions, three Gaussian functions to represent the first Slater-type function and one Gaussian to represent the second Slater function for the valence orbitals. Thus, it can be seen as a double-zeta basis for the valence orbitals. Of course, there are triple-zeta split-valence bases as well. In vast number of calculations these bases perform very well whereas being much more compact than true double- and triple-zeta sets.

Aforementioned contracted basis functions are derived from the atomic HF calculations. Their further improvement can be reached by combining with *polarization* and diffuse functions. In general, polarization functions are functions having higher angular-momentum quantum numbers than those present in the occupied orbitals of a particular atom. Obviously, exponents for the polarization functions cannot be optimized from HF calculations on atoms, since they are not populated. Nevertheless, they can be derived from correlated calculations involving atoms. Addition of polarization functions to the basis sets reflects the fact that when atoms approach each other, they distort ("polarize") their normally spatially-symmetric orbitals by means of induced dipole, in general, multipole interactions. In particular, atomic *s*-type or *p*-type orbitals after chemical bonding behave rather like a superposition of *s*- and *p*-types or *p*- and *d*-types, respectively. When *p*-type orbitals and *s*-type orbitals of the 6-31G basis set are augmented by *d*-type and *p*-type orbitals, respectively, it is termed 6-31G(d,p)[1] basis set. Thus, the polarization functions are important for the quantitative description of chemical bonds as well as the effects of atomic and molecular polarization. For example, Van-der-Waals forces on noble gas complexes stem from the breaking of spatial symmetry of

[1] The latter is also often designated as 6-31G**.

the orbitals of one atom by the other one what induces nonzero dipole moment on each atom. Consequently, the two atoms attain long-range dipole-dipole attraction. Since the long-range interactions can be properly taken into account by correlated methods only, the use of polarization functions is very important in correlated calculations.

As it was mentioned above, diffuse functions have small orbital exponents and hence decay slowly with the distance from the basis-set centre. Therefore their use is again advantageous for the description of systems with long-range interactions (*e.g.* H-bonding and Van der Waals) as well as for anionic systems and in calculations of molecular properties (*e.g.* polarizabilities). Usually, diffuse functions are of *s*- or *p*-type, but diffuse polarization functions also exist.

In the Pople basis sets notation, diffuse functions are indicated by "+". For example, 6-31+G(d,p) implies addition of diffuse *s*-type and *p*-type Gaussian functions with the same exponent to the heavy atoms, while 6-31++G(d,p) means additional augmentation of hydrogens by diffuse *s*-type functions.

Finally there are so-called *correlation-consistent* basis sets of Dunning and coworkers (Ref. **137**). The bases have the same structure as described above, with the only difference that the parameters of the contracted Gaussians are optimized in correlated calculations on some atomic and molecular test sets and, by construction, include polarization functions. For instance cc-pVXZ, where "X" means triple-, quadruple-, quintuple-zeta *etc.*, while aug-cc-pVXZ means the same sets augmented by diffuse functions. The energies obtained with these basis sets have the property to converge to the *basis-set limit* (complete basis set) by means of extrapolation formulas connecting the values obtained with smaller to larger "zeta" basis sets.

One of the important consequences of adding broad Gaussians to the standard basis sets is their ability to diminish *basis-set superposition error* (BSSE) (Ref. **138**, **139**). BSSE is a peculiarity of the atom-centered basis sets which originates from the mutual augmentation of the monomer's basis sets within the supermolecule. As a result, absolute energy of the supermolecule becomes too low, while the wave function becomes BSSE-contaminated. Since BSSE corrupts virtual orbitals as well, whereas the latter are the building blocks of correlated methods (Sec. **1.2.3**), at correlated level BSSE disappears very slowly with an increase of the basis set. The BSSE phenomenon will be described in detail in course of this and the next sections.

Another kind of error in calculations with atom-centered as well as plane-wave basis sets introduced above is the so-called *basis-set incompleteness error* (BSIE). This error arises when a basis set does not describe the physical situation well *i.e.* contains insufficient, for a

particular combination of atoms in the molecule, amount of Slater exponents, polarization or diffuse functions. For a given finite basis set, BSIE leads to too high energies with respect to the complete basis set. In contrast, energies obtained with finite bases without BSSE correction are too low, compared to the BSSE-corrected results.

Plane-waves are *originless*: in contrast to the atom-centred bases they do not depend on the positions of the nuclei and, hence, are BSSE-free by construction. Therefore, one might consider plane waves as a viable alternative to the atom-centered bases in correlated electronic structure calculations. The arguments given below will show that this is not the case.

Compared to atom-centred bases, plane-wave sets are not *compact*. They require increasingly many components to resolve decreasingly small structures in real space. Most of chemical properties are determined by the valence electrons, while the core electrons remain essentially intact. It suggests that the latter can be in principle excluded from the explicit calculations whereas only the former should be represented by plane-waves. The core part, hence, can be replaced with smooth and nodeless effective potentials termed *pseudopotentials*. Introduction of pseudopotentials dramatically decreases the size of the plane-wave basis sets. Furthermore, pseudopetentials can be used in combination with atom-centered sets as well. The reviews on the subject in context of periodic and atom-centred calculations can be found in Ref. **140**, **141**, **142** and **143**, **144**, respectively. Even with pseudoptentials, the plane-wave sets are large comparing to the atom-centered sets.

Notice, in the case of plane-wave sets, a large number of waves describes an infinite number of replicas of the unit cell which may interact with each other. When a bulk, *naturally periodic* system is constructed from small- to medium-sized molecules, the computational cost due to the large noncompact plane-wave basis can in some cases be outweighted by the computational cost due to the increasingly large size of model cluster (and hence – the basis set) to reproduce continuum in calculations with atom-centered sets. In this case, *i. e.* when a small or medium molecule (or, molecular fragment) is contained in the unit cell, some advantage of the use of plane-waves can be gained. However, when the system is large enough (*e.g.* a macromolecule), when it is constructed from several weekly-bound fragments, when it is an isolated assembly of molecules[1], or it has a defect in the crystal grid[2], the unit cell size becomes increasingly large what produces huge plane-wave bases.

[1] To represent an isolated system in plane-wave calculations, its unit cell must be increased to prevent the interactions between the replicas of the system.
[2] The presence of defects in periodic system leads to continuous (infinite) basis sets. In order to avoid it, the unit cell comprising the defect, should be increased. Thus, a periodic ensemble of defects, rather than a true defect can be represented by a finite plane-wave basis.

Since correlated wave function-based methods formally scale at least as N^5 (Sec. **1.2.3**) the use of plane-waves as a versatile basis for correlated wave function calculations is limited if not prohibited. On the other hand, the magnitude of the BSSE effect in electronic structure calculations with atom-centered bases is similar to the magnitude of the correlation energy, thus, its correction is a necessary prerequisite of reliable calculations at an affordable computational effort. In the next section the methods for BSSE correction will be introduced.

1.4.2 Methods for Basis-Set Superposition Error Correction

At present, there are three feasible directions for a BSSE correction with atom-centered basis sets.

1. *Local electron-correlation methods* (Ref. **65**, **66**, **67**, **145**, **146**). The technology was initially designed to speed-up the calculations on large systems, while the decrease of BSSE is a side effect. The idea behind these methods is based on the fact that the contribution of dynamic correlation to the electron interaction decreases much faster, with respect to the interelectron distance, than the Coulomb repulsion. This suggests that the correlation contributions from neighbouring orbitals are dominant and should be taken into account in correlated calculations, whereas contributions from remote orbitals can be, to some extent, neglected. Utilization of the local-orbital approaches without the loss of physical correctness is nontrivial. A famous example of the drawbacks of early localization procedures (Ref. **65**, **66**, **67**) applied to correlated methods (Ref. **147**, **148**, **149**, **150**, **151**) is the discontinuity of potential energy surfaces (Ref. **152**), but, later on, procedures to avoid the discontinuities appeared (Ref. **145**, **146**).

Local-correlated methods are always a compromise between computational efficiency and accuracy. In particular, in the ground state, the use of local orbitals eliminates not only BSSE but also some electron correlation energy. (see Sec. I.1.1.3 of Ref. **19**). In the excited-state calculations, the use of local orbitals can affect the quality in situations where double excitations are important. In fact, the neglect of double excitations is the reason for a better scaling of local-correlated methods, compared to canonical methods. Herein, the more double excitations are neglected, the better the scaling. Therefore, a careful adjustment of the amount of neglected doubles should be done to provide the balance between the computational efficiency and accuracy in those cases, where double excitations are essential (Ref. **153**).

Turning back to BSSE, local correlation methods themselves cannot be considered as an ultimate solution to the problem. In fact, BSSE is present in the methods since the local

orbitals are normally obtained from BSSE-uncorrected HF calculations. When the error is large at the HF level, it automatically transmits to the results of local-correlated calculations.

Since at the HF level BSSE vanishes much faster with an increase of the basis-set size than at the correlated level, some researchers suggest to use a combination of large basis sets (to diminish BSSE at the HF level) and local correlation methods which are BSSE-free. In my opinion, this approach is an impasse since for the large systems with large basis sets both the HF and local correlation steps become prohibitively expensive. In contrast, utilizing approaches which correct for BSSE at both HF and correlated levels, in combination with medium-sized bases which represent the physical situation well[1], is a rational way to get accurate results and to be feasible in terms of the computational effort in correlated calculations on medium to large systems. Of course, when BSSE is corrected at the HF level (see below), its combination with local-correlated methods (BSSE free) can give an additional speedup and can be a viable alternative to both DFT and canonical correlated methods for the studies on large system.

2. *Chemical Hamiltonian approach* (CHA) introduced and developed by Mayer and coworkers (Ref. **154**). The approach is based on the decomposition of the electronic Hamiltonian (40) of a molecular complex into a sum of *intramolecular* and *intermolecular* interaction operators and further neglect of the terms responsible for BSSE in the intermolecular part. In fact, the terms introducing BSSE in SCF stem from the multi-center one- and two-electron integrals[2]. Such an analysis is easier to perform the Hamiltonian is expressed in terms of molecular orbitals in the *second-quantized* form (*e.g.* Ref. **94**). Since CHA removes BSSE not only from the energy but rather from the entire wave function, it can be treated is an *a priory* methodology for BSSE correction. At the moment, the approach seems to be the only systematic way to fully eliminate BSSE in atom-centered calculations.

The CHA methodology is rather complicated to be described within the format of this thesis. From a practical point of view, though, there are two versions of CHA to be distinguished. The first one is the so-called CHA/F (and CHA-DFT) approach (Ref. **155**, **156**) in which the terms, responsible for BSSE, are excluded directly from the Fock matrix (**57**) (Sec. **1.2.2**). The second one is the CHA-SCF approach (Ref. **157**), where the terms inducing BSSE are eliminated at the level of the molecular Hamiltonian expressed in second-quantized form. Herein, BSSE-free molecular orbitals are produced. It opens the way for the

[1] More precisely: the minimal, for a given system, basis set, which represents the physical situation adequately.
[2] In CHA one- and two-electron integrals contain at most one- and two-center integrals (over atomic orbitals), respectively. The multi-center character of the wave functions is captured *via* the overlap integrals. The neglect of multi-center integrals in CHA also provides additional speed-up for CHA-based SCF.

development of correlated methods upon CHA (Ref. **158**, **159**, **160**). Very encouraging results on closed- and open-shell hydrogen bonded systems and Van-der-Waals complexes were obtained with the BBSE-free CHA-MP2 methodology (Ref. **159**, **160**). The major disadvantage of CHA-SCF is that the Fock matrix is non-Hermitian. Although it does not affect the computational performance of the methodology, it brings an additional complexity for the analytical formulation and implementation of correlated methods and gradients upon CHA. Probably, that was a reason of the continent perception of CHA in the quantum-chemical community.

3. The *counterpoise correction* (CP) procedure introduced independently by Boys and Bernardi (Ref. **161**) and Roos (Ref. **138**). Since the CP methodology is rather intuitive, it is very useful to illustrate the essence of BSSE. It will be done in detail in the next section.

Finally, it is worth to mention that there is another promising alternative to conventional basis sets, introduced in the previous section, which is BSSE-free. This is the so-called *generalized plane-waves* defined in curvilinear coordinates (Ref. **162**, **163**). Hypothetically, these basis functions can solve the fundamental problem of compactness of conventional plane-waves while being BSSE free. Their use is supposed to be advantageous in the studies on continuous (but not necessarily periodic) systems. However, this basis set is uncommon and it needs a careful investigation to answer whether computer implementation of correlated methods with this set is practical.

Historical overview of the developments as well as many other aspects of BSSE can be found in an excellent account on the subject (Ref. **19**) and in Ref. **164**.

1.4.3 Counterpoise Correction for Basis-Set Superposition Error

Suppose there are two interacting monomers *A*, *B* assembled into the complex *AB*. Of particular interest is the energy difference between the complex and the *isolated* monomers, constituting the complex

$$\Delta E_{stab}(AB) = E_{AB}^{AB}(AB) - E_{A}^{A}(A) - E_{B}^{B}(B), \qquad (166)$$

called *stabilization energy*. Here and further, $E_{Y}^{Z}(X)$ denotes energy of the system *X* at the geometry *Y* with the basis set *Z*. This quantity characterizes the energetics of the assembly reaction. When the energies are corrected by ZPVE and temperature effects, one deals with *stabilization enthalpies* and *free energies* instead. Obviously, with atom-centered basis sets there is a problem in the definition of the stabilization energy: energies of the complex and

monomers are defined within the different basis set subspaces. This is one well-known manifestation of BSSE.

Expression (166) can be rearranged to gain more physical insight

$$\Delta E_{stab}(AB) = \underbrace{E_{AB}^{AB}(AB) - E_{A}^{A}(A) - E_{B}^{B}(B)}_{\Delta E_{stab}(AB)} + \underbrace{\left(E_{AB}^{A}(A) - E_{AB}^{A}(A)\right) + \left(E_{AB}^{B}(B) - E_{AB}^{B}(B)\right)}_{0} =$$

$$= \underbrace{E_{AB}^{AB}(AB) - E_{AB}^{A}(A) - E_{AB}^{B}(B)}_{\Delta E_{in}(AB)} + \underbrace{\left(E_{AB}^{A}(A) - E_{A}^{A}(A)\right) + \left(E_{AB}^{B}(B) - E_{B}^{B}(B)\right)}_{\Delta E_{rel}(AB)} \quad \textbf{(167)}$$

Herein, the energies of the fragments *A*, *B* in their geometries within the complex are added. The term ΔE_{in} in the final expression is termed *interaction energy*. It allows for a partition into the terms of different physical origin and, hence, for a physical interpretation of the interaction. The term ΔE_{rel} is the *relaxation energy* – it characterizes distortion of the monomer within the complex. If the fragment is an atom, its distortion is zero. Thus, interaction and stabilization energies are equivalent only for the complexes comprised from atoms.

The idea of the counterpoise correction is to add *ghost-orbitals*, borrowed from the compex *AB*, to each monomer *A*, *B* within the complex. Technically, the orbitals are obtained by setting nuclear charges of other fragments within the complex to zero and omitting their electrons. The result of the procedure is the BSSE-corrected interaction energy

$$\Delta E_{in}(AB) = E_{AB}^{AB}(AB) - E_{AB}^{A}(A) - E_{AB}^{B}(B) \rightarrow E_{AB}^{AB}(AB) - E_{AB}^{AB}(A) - E_{AB}^{AB}(B) = \Delta E_{in}^{CP}(AB). \quad \textbf{(168)}$$

In Eq. (167) interaction energy is BSSE-contaminated while the relaxation energy is BSSE-free[1]. After the correction (168), stabilization energy becomes BSSE-corrected as well

$$\Delta E_{stab}(AB) \rightarrow \Delta E_{in}^{CP}(AB) + \Delta E_{rel}(AB) = \Delta E_{stab}^{CP}(AB). \quad \textbf{(169)}$$

To get more involved interpretation of BSSE, let rearrange Eq. (169) as follows

$$\Delta E_{stab}^{CP}(AB) = \underbrace{E_{AB}^{AB}(AB) - E_{A}^{A}(A) - E_{B}^{B}(B)}_{\Delta E_{stab}(AB)} + \underbrace{\left(E_{AB}^{A}(A) - E_{AB}^{AB}(A)\right) + \left(E_{AB}^{B}(B) - E_{AB}^{AB}(B)\right)}_{\delta_{AB}^{BSSE}}$$

$$\delta_{AB}^{BSSE}(AB) = \left(E_{AB}^{A}(A) - E_{AB}^{AB}(A)\right) + \left(E_{AB}^{B}(B) - E_{AB}^{AB}(B)\right) \quad \textbf{(170)}$$

[1] Of course, this is only true when the *intramolecular* BSSE for each monomer is neglected, this case is considered here.

The first term here is the BSSE-uncorrected stabilization energy, the second one is the energy difference between the fragments in their own bases and in the basis of ghost-orbitals. This quantity itself is often referred to as BSSE energy, or, shortly, BSSE.

BSSE has the following properties.

1. Since the basis-set space is larger with the ghost-orbitals (*i.e.* $\left|E_{AB}^{A}\right|,\left|E_{AB}^{B}\right| < \left|E_{AB}^{AB}\right|$), for the variational energies BSSE is positively defined. In the limit of complete basis set, BSSE approaches to zero, however, since BSSE corrupts virtual orbitals, the convergence is much slower at correlated than at the Hartree-Fock level.

2. Since uncorrected stabilization energies are too negative, BSSE induces *overbinding*. This is especially the problem for MP2 theory for which the correlation contribution is always negative.

3. Since the ghost-orbitals employed for BSSE correction does depend on the geometry of the complex, the BSSE contribution to the stabilization energy is *not additive* with respect to the number of fragments

$$\Delta E_{stab}^{CP}(AB) = \Delta E_{stab}(AB) + \delta_{AB}^{BSSE}(AB) \neq \Delta E_{stab}(AB) + \delta_{A}^{BSSE}(A) + \delta_{B}^{BSSE}(B) . \quad (\mathbf{171})$$

Let finally make a transition from the *stabilization energy* to the *absolute energy* of the complex. This can be done by setting the energies of isolated fragments to zero $E_A^A(A) \to 0$, $E_B^B(B) \to 0$ in Eq. (170). If BSSE was additive (*i.e.* independent on the geometry of the complex), it would be zero as a result of this procedure. However, this is not the case

$$\delta_{AB}^{BSSE}(AB) \neq \delta_{A}^{BSSE}(A) + \delta_{B}^{BSSE}(B) \to 0 , \quad (\mathbf{172})$$

and, therefore

$$\Delta E_{stab}^{CP}(AB) \to E_{AB}^{AB}(AB) + \delta_{AB}^{BSSE}(AB) = E^{CP}(AB) . \quad (\mathbf{173})$$

Thus, with atom-centered basis sets, BSSE not only affects the stabilization energy of the complex, but rather its *absolute energy*. This very important consequence is often missed in common interpretation of BSSE.

Since BSSE is positively defined, its addition to the total energy (Eq. (170)) produces a "vertical shift" in the potential energy surfaces. Moreover, since BSSE depends of the nuclear positions of the complex, its gradient with respect to its nuclear coordinates is nonzero

$$\frac{\partial}{\partial R_I}\delta_{AB}^{BSSE}(AB)=\frac{\partial}{\partial R_I}\left(E_{AB}^{A}(A)-E_{AB}^{AB}(A)\right)+\frac{\partial}{\partial R_I}\left(E_{AB}^{B}(B)-E_{AB}^{AB}(B)\right)\neq 0\,. \tag{174}$$

As a consequence, the gradients of the corrected and uncorrected PES at a given point are not equal

$$\frac{\partial}{\partial R_I}E^{CP}(AB)=\frac{\partial}{\partial R_I}E_{AB}^{AB}(AB)+\frac{\partial}{\partial R_I}\delta_{AB}^{BSSE}(AB)\neq\frac{\partial}{\partial R_I}E_{AB}^{AB}(AB)\,. \tag{175}$$

This means that the stationary points of BSSE-corrected and uncorrected PES are displaced ("horizontally shifted") with respect to each other. Since any stationary point of *stabilization energy surfaces* coincides with the stationary point of potential energy surfaces, the same arguments are valid for the latter[1]. Potential energy surfaces, equilibrium structures, infrared spectrum, thermochemistry and other molecular properties employing energy derivatives can be affected by BSSE directly – like it is shown above, or indirectly – since BSSE is also presents in the wave function.

The results of the CP correction converge fast to the results of CHA with the increase of the basis-set size (Ref. **164**). At correlated level, even with moderate basis sets, very accurate PES of hydrogen-bonded systems and Van-der-Waals complexes (open- and closed-shell) can be obtained (Ref. **159**, **160**). The validity of the CP procedure was proved rigorously for the full-CI level of theory (Ref. **165**). Furthermore, since CHA determines the terms in the Hamiltonian, responsible for BSSE exactly, it can serve as a methodological pattern for the validation of the CP procedure in application to BSSE (Ref. **159**). Another advantage of CP is its easy implementation which requires energy calculations of the fragments in the basis set of the complex.

The pitfalls of the CP methodology are well-known.

1. CP is an *a posteriori* approach – it corrects for BSSE at the energy level but not at the wave function level. Wave function-specific properties (densities, magnetic properties *etc.*) can be affected by BSSE even if PES is corrected by means of CP.

2. Application of the CP correction to open-shell or charged complexes is often problematic.

In fact, the ghost-orbital calculations for open-shell fragment should describe the same spin state as for the fragment in its own basis set. Since the symmetry, and therefore spin, of the wave function of the monomers can be changed in the composite ghost-orbital basis, this

[1] Any nuclear derivative of potential energy surface is equal to the derivative of the stabilization energy surface, since the derivatives of the energies of isolated fragments with respect to the nuclear coordinates of the complex are zero.

condition is not always automatically fulfilled. This is because the minimum-energy state in the composite basis set would not be necessarily of the same multiplicity as it is in the basis of the monomer. Consequently, the SCF procedure can be difficult to converge to the same electronic spin state. This is especially the case for the complexes having several electronic states of the same symmetry.

In the case of charged, for instance, protonated complexes the charge can significantly shift electron density within the complex. Herein, the assignment of charge to the fragments (proton and the rest) to apply the CP procedure becomes ambiguous.

As both of these situations are normally present in molecules, application of CP to molecules to diminish BSSE at the *intramolecular* level is complicated. Even in such pathological cases, CP correction is often possible, although it is assumed that it diminishes only a fraction of BSSE than in the normal case of well-separated fragments (Ref. **19**).

3. The computational cost of the CP correction scales linearly with respect to the number of fragments n in the complex: the procedure requires (n+1) energy calculations in the composite basis set. This is in strong contrast to CHA which computation time is essentially independent on the number of fragments. Since the energy correction in this sense is additive, any property which requires energy derivatives (gradients, second derivatives *etc.*) needs (n+1) calculations as well. Moreover, when there are more than two monomers in the system, the definition of the fragments, necessary to apply the CP procedure, becomes ambiguous. For instance, if there are three monomers *A*, *B*, *C* in the complex *ABC*, there are four possible fragment definitions: *A*+*B*+*C*, *AB*+*C*, *AC*+*B* and *BC*+*A* within the complex. This ambiguity[1] can be circumvented by use of *hierarchical* CP, but this procedure readily becomes unfeasible with increase of the monomer number (Ref. **164**). Still, the "conventional" (*i.e.* nonhierarchic) CP correction, where each monomer is treated as a fragment, eliminates significant fraction of BSSE in the case of more than two monomers (Ref. **19**, **164**).

In the last section of this part, important but rather unexplored implications of BSSE will be discussed.

[1] The phenomenon is sometimes referred in the literature as second-order BSSE.

1.4.4 Basis-Set Superposition Error: Uncommon Implications

1. BSSE at the intramolecular level.

Despite there are very encouraging examples of the BSSE correction at *intermolecular* level, applied to Van-der-Waals and hydrogen-bonded systems, not too many studies on *intramolecular* BSSE exist by far. This is partly due to the aforementioned difficulties to apply standard CP correction to individual molecules. Another reason is that due to the strength of a chemical bond, the influence of intramolecular BSSE on the chemical bonds distances is not always immediately observable as it is the case in weakly-bound complexes. For the latter, small changes in the intermolecular forces can yield large changes in the intermolecular geometries. Unlike the structures, molecular vibrations in principle should be substantially affected by intramolecular BSSE, since vibrational frequencies are essentially determined by BSSE-contaminated surfaces.

Meanwhile, several successful attempts of the application of the CP correction to intramolecular BSSE demonstrate its paramount importance.

In Ref. **166**, significant influence of itramolecular BSSE on reaction paths and energetics of chemical reactions of several organic complexes has been reported. It was shown that the CP correction applied to both minima and transition states considerably improves the results of the calculations with moderate basis sets, while its neglect can even lead to artificial transition states.

Another prominent example of intramolecular BSSE is artificial distortion of benzene (Ref. **167**, **168**, **169**), planar arenes (Ref. **167**, **170**, **171**, **172**, **173**, **174**) and other nonrigid molecules (Ref. **175)** from planarity, observed at correlated level of theory (MP, CISD). Herein, the correct planar shapes were obtained after application of the CP correction (Ref. **176**).

In view of these findings, one would expect significant presence of BSSE in proton affinities and stabilization energies (particularly deprotonation energies) of covalently-bound complexes as well.

2. BSSE in calculations of ground-state molecular properties.

Since BSSE is also a property of wave function and not of the energy only, it is expected to be present in calculations of molecular properties. Observation of BSSE in molecular properties, in general, requires BSSE-free reference (*i.e.* obtained with CHA). For example, a recent study indicates that CHA-SCF BSSE-free densities of hydrogen-bonded systems can significantly differ from those obtained with conventional SCF (Ref. **177**). Still, those properties which require derivatives of the energy can be improved by means of conventional

CP correction, in particular, harmonic and fundamental vibrational frequencies (IR spectrum), as well as nuclear chemical shifts (NMR spectrum) (Ref. **178**, **179**). For instance, Ref. **179** indicates observable presence of BSSE in the nuclear chemical shifts of some hydrogen-bonded complexes.

In the present work, a systematic investigation of the influence of basis-set size, electron correlation and anharmonicity on the IR spectrum of typical H-bonded systems has been performed (Sec. **3.7**). CP-corrected frequencies were obtained on CP-corrected PES (*i.e.* optimized according to Eq. (175)) at the level of MP2 and CCSD with large basis sets (up to cc-pVTZ, cc-pVQZ). The study demonstrates that infrared spectra corresponding to the relevant OH stretch frequencies obtained at the CP-corrected MP2 level with moderate valence-split 6-31G(d,p) basis are well-described. The distance between the peaks, constituting the spectrum is almost unaffected by the basis set increase and improvement of electron correlations from the MP2 to CCSD levels. In contrast, IR spectra obtained at the CP-uncorrected levels of theory reveals much stronger basis-set dependence. Furthermore, the structures of the complexes obtained at the level of CP-corrected PES with MP2 and moderate basis sets are almost identical to those obtained at CP-corrected CCSD level with the cc-pVTZ basis. For the latter, BSSE error still exceeds 25% of the stabilization energy – it is larger than the differences in stabilization energies between MP2 and CCSD. *These findings suggests that transition from the second-order perturbation theory (MP2), combined with moderate basis sets, to higher levels of theory and larger basis sets does not make sense without BSSE correction of PES. The notorious overbinding problem of MP2 can hence be traced back to BSSE rather than to the lack of dynamic correlations itself.*

3. BSSE in excited-state calculations.

So far, most of the efforts around BSSE have been focused on ground-state systems. However, BSSE is present in the excited states as well. It can be easily seen for variational methods (*e.g.* full- or truncated-CI, Sec. **1.2.3**) by assignment of the CP-corrected energy (170) to the energy of a particular excited state. An ultimate solution of the problem would be to use excited-state methods with a BSSE-free CHA reference. Since such procedures are not yet implemented[1], one would consider the possibility to apply the CP correction to excited-state calculations.

In the excited-state CP correction, there are two levels of the problem.

First, in order *to apply* the CP correction, calculations on a complex and its monomers should describe the same excited state. Obviously, electronic structure of excited states of the

[1] Except single-point CHA-CI (Ref. **158**), which is limited by few-electron systems.

complex and its isolated monomers can be significantly different. For instance, excited states of the fragments in (Eq. (170)) are by construction *locally-excited* (LE) with respect to the complex. Therefore, they conceptually unable to correct *charge-transfer* (CT) excited states of the complex (if it possesses them), since CT is essentially a *collective* effect. This example readily demonstrates breakdown of the general applicability of the CP correction to excited-states. Another problem arise when a complex comprise several nearly degenerate excited states which are produced from several degenerate atomic orbitals of the fragments. This may occur in the highly symmetric cases like diatomic complexes. In this case, the assignment of an excited state of the complex to the excited state of the monomer (comprised from the degenerate orbitals) becomes ambiguous. It will be important to quantify the magnitude of this ambiguity.

Second, *to calculate* BSSE correction according to Eq. (170), MCBS and DCBS calculations for the relevant monomer should describe the same excited state. "Same" means that it should be represented by the same dominant (occupied/virtual) orbital contributions. Again, when excited states in DCBS are nearly degenerate and comprised from several degenerate orbitals of the monomer, the assignment of an excited state of DCBS to the excited state of the MCBS becomes ambiguous.

As one can see, application of the CP correction to the excited states combines the two above-mentioned problems of CP, typical for the cases of charged and open-shell complexes. In view of these arguments, it would be interesting to check for a possibility to apply CP correction within linear-response theory (Sec. **1.3.2**). In this case, the energy of a particular excited state is a sum of the ground-state total energy and the excitation energy[1]

$$E_{S_n}(R_{S_n}) = E_0(R_{S_n}) + \Delta\omega_n(R_{S_n}) . \qquad (\mathbf{176})$$

As it was mentioned above, it is often possible to apply the CP correction to the ground-state contribution, but it is not easy to establish how BSSE enters the excitation energies obtained from linear-response functions. It might occur that in some parts of PES, BSSE in the excitation energy compensates BSSE in the ground state. Thus, application of the CP procedure to the first term alone cannot be justified without the analysis of BSSE in the second term. These points need to be clearly addressed and this work is currently underway (Ref. **180**)

[1] In this notation excitation energies are designated as $\Delta\omega_n$ instead of ω_n in Sec. **1.3.2**. This is done to prevent confusion with the energies of excited states obtained variationally.

4. *BSSE-consistent* basis sets.

As it was mentioned in Sec. **1.4.1**, correlation-consistent basis sets are optimized in correlated calculations for some atomic and molecular test sets and hence, by construction, contain BSSE. This error will automatically transmit to the CHA calculations on atoms since in this case the BSSE-contamination, inherited from the basis set, cannot be removed from the atomic Hamiltonian (notice that BSSE itself is a multiatomic phenomenon). Therefore, the development of basis sets, optimized on the molecular test sets by means of BSSE-free CHA methodology is necessary for accurate atomistic calculations employing CHA.

Chapter 2

Water Deficient Environment Accelerates Proton Exchange: Acetone-Water Reaction Catalyzed by Calix[4]hydroquinone Macromolecules

2.1 Introduction

Over the past decades, *self-assembling* organic hollow and tubular structures have attracted significant interest as prospective *functional materials* in the areas of catalysis, electrochemistry, molecular recognition, and drug discovery (Ref. **181**, **182**, **183**, **184**, **185**). Most of the research in this field has been dedicated to the investigation of organic and inorganic nanotubes with *covalently-bound* architectures. Recently, Kim and coworkers discovered and investigated the self-assembly phenomenon of calix[4]hydroquinone (CHQ) monomers, which builds tubular nanostructures in the presence of water, under certain experimental conditions (Fig. **2.1**) (Ref. **186**, **187**). The tubular structures are built from the bowl-shaped non-tubular CHQ monomers, which are bound noncovalently but linked by the *hydrogen bonds* (H-bond) with the bridging water molecules. The bridging water molecules and the OH-groups of the CHQ building blocks constitute a quasi-one-dimensional (1D) H-bonded chain along the axis of the tubular structure. The CHQ tubes further aggregate in bigger porous polymers mediated by the intertubular π–π *stacking* interactions which stabilize the tubular subunits laterally. In contrast to the covalently-bound nanotubes, the ordering in the organic CHQ nanotubes is stipulated by a delicate interplay of H-bonding and π–π interactions, similarly to the situation found in biological materials like membranes and membrane proteins (Ref. **188**, **189**).

The hollow bowl shape of the aromatic CHQ molecules allows for an efficient *size-specific* trapping of organic *guest* molecules and for their subsequent chemical transformations by, for example, stereo-selective reactions (Ref. **190**). Indeed, a recent NMR/quantum chemical study has shown that CHQ nanotubes can specifically trap small organic molecules (acetone, 2-propanol, 2-methyl-2propanol). In particular, it was demonstrated that in the case of acetone, one molecule fits into one CHQ bowl (Ref. **191**, **192**). Understanding the mechanism of size-specific binding and mobility of the guest molecules in CHQ nanotubes will give insights also relevant for trans-membrane ion channels and pore structures, due to their aforementioned structural relation (Ref. **188**, **189**).

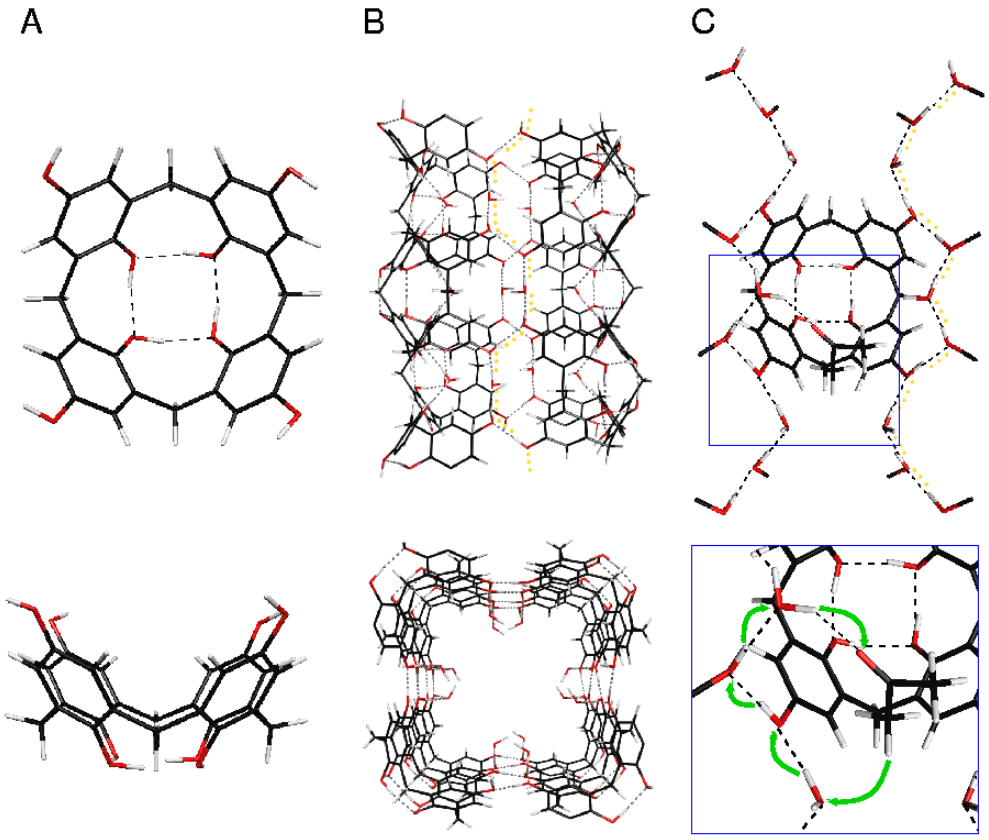

Figure 2.1. CHQ monomers (A), tubular CHQ (B) and fragment of tubular CHQ trapping acetone molecules (C), where the rest of the nanotube is removed for clarity. The 1D-H-bonded chain is highlighted by a yellow dotted line and a possible proton transport pathway is indicated by green arrows (C, bottom).

An important manifestation of the unusual chemical properties of CHQ structures (both tubular and amorphous) is its *catalytic* activity in acetone-water *proton exchange* (PE) (Ref. **193**), which has been observed at ambient conditions in two *nuclear-magnetic resonance* (NMR) experiments – the spectra are shown in Fig. **2.2**. The experiments were performed and the peaks were assigned according to Ref. **191**. In a solid state magic-angle spinning ^{1}H NMR experiment on the CHQ nanotubes (Fig. **2.2A**), the spectra were taken immediately, one day and one week after the preparation of the CHQ nanotubes. The latter were produced by evaporation of the solvent from the solution of non-tubular CHQ in deuterated acetone C_3D_6O and water. As one can see from the spectrum in Fig. **2.2A**, the intensity of the peak at 0.5 ppm, corresponding to the methyl protons of initially deuterated acetone C_3D_6O, grows during the experiment. While the peak of the protons of the OH-groups cannot be clearly resolved in the solid-state NMR experiment, it is well resolved in the corresponding solution ^{1}H-NMR experiment (Fig. **2.2B**) on nontubular, but partially-aggregated CHQ molecules in deuterated acetone. In the spectrum, a peak corresponding to water impurities is visible at about 3 ppm.

The time evolution of the solution ^{1}H-NMR spectrum reveals that the concentration of water protons decreases simultaneously with the increase of acetone methyl protons. According to these data, a proton-deuteron exchange between water and acetone takes place and, most likely, deuterated water subsequently exchanges deuterons with the OH-groups of the CHQ molecules, resulting in the observed decrease of their signals in the solution ^{1}H NMR spectrum. Since PE between acetone and water is observed in the tubular CHQ aggregates, as well as in the partially-aggregated CHQ solution, both forms of CHQ exhibit the property to catalyze the exchange.

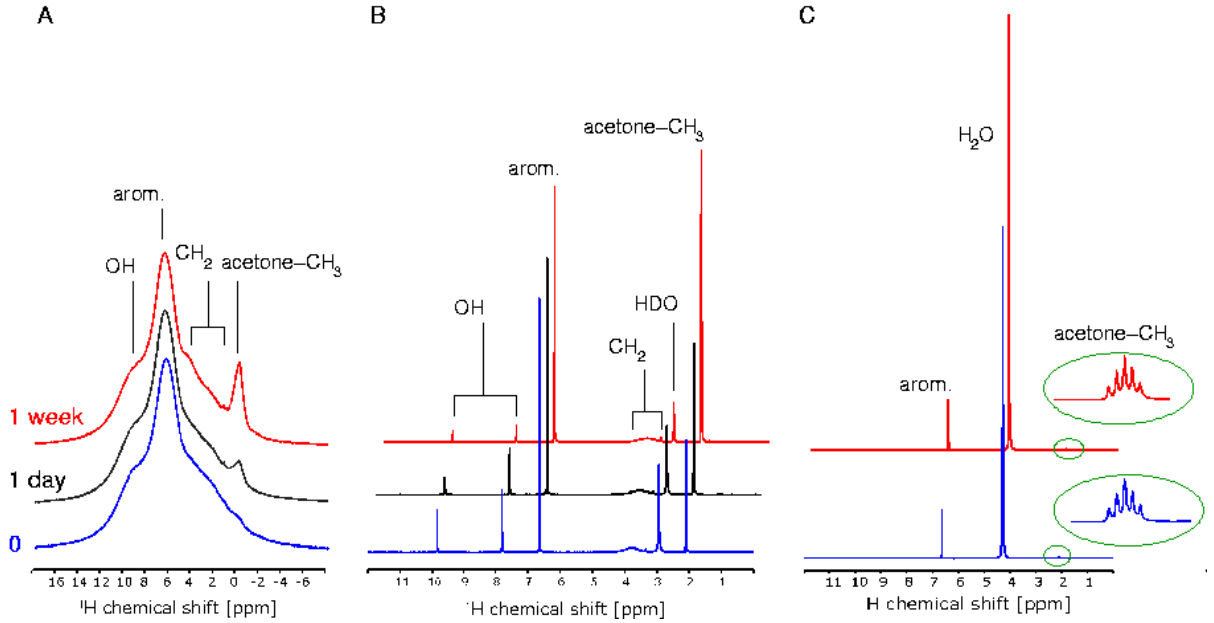

Figure 2.2. Solid state ^{1}H-NMR spectrum of tubular CHQ trapping C_3D_6O (A), solution ^{1}H-NMR spectrum of CHQ dissolved in C_3D_6O (B), solution ^{1}H-NMR spectrum of a mixture of QH_2, C_3D_6O and H_2O (C).

It is a well-established fact that acetone alone does not exchange protons with water at normal conditions (T~300 °K, pH~7) (Ref. **194**). However, acids are known to catalyze acetone *keto-enol tautomerism* (KET) (Ref. **195**) and one might suspect that the *weak acidity* of CHQ may be responsible for the observed PE. KET is an interconversion between the isomeric forms (keto and enol forms) involving a formal proton migration and a double bond (π–electron) shift (Sch. **2.1**). Since in solution, KET involves several protonation/deprotonation steps, it is reasonable to assume that it plays also a role in the PE between water and acetone, observed in the described NMR experiments.

To corroborate the weak acidity of CHQ itself is not the origin of the PE, an analogous ^{1}H-NMR experiment has been performed on the solution of hydroquinone (QH_2) in deuterated

acetone and water (in 1:1 concentrations). QH_2 has been chosen since it possesses a very similar chemical structure as CHQ and should act as a weak organic acid as well. Although the pK_a value of CHQ is not available, since the CHQ aggregates in aqueous solution immediately, the arguments that this assumption is clearly justified will be given in the next section. Surprisingly, no PE was observed (Fig. **2.2C**) in the QH_2 experiment: the spectrum taken after one week does not show any changes in the intensities of peaks corresponding to the methyl group of C_3D_6O or to the water protons. Thus, the reason of catalytic activity of CHQ in the acetone-water PE cannot be its weak acidity alone.

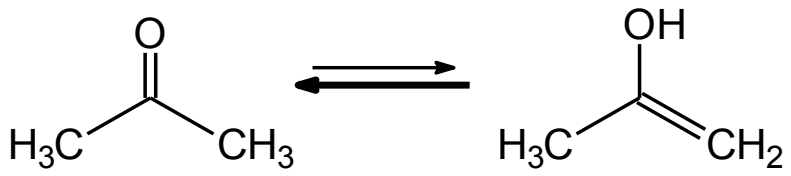

Scheme 2.1. Keto-enol tautomerism of acetone.

In order to clarify the nature and the mechanism of the catalytic function of CHQ in acetone-water proton exchange, the present computational study employing *state-of-the-art* quantum chemical methodology, have been performed.

One should notice that although QH_2 and CHQ exhibit similar acidity, they show a different catalytic function in acetone-water PE. Moreover, the concentration of dissociated CHQ species, due to the pK_a of QH_2, amounts to 10^{-5}. This means that most of CHQ in the system is present in the *neutral* form and, thus, cannot facilitate *acid-catalyzed* KET. Owing these arguments, the first step of this investigation (Sec. **2.3-2.7**) will be dedicated to the PE mechanisms via *concerted* KET of trapped acetone, without considering the formation of ionic intermediates.

Nevertheless, the concentration of ionic moieties, resulting from CHQ OH-group dissociation (~10^{-5}), can be sufficient to provide slow acid-catalyzed PE at the rates of the aforementioned experiments (hours to days). It can, in principle, occur if the *proton transfer* (PT) involving these moieties is efficient enough. This possibility thus cannot be *a priory* excluded from the consideration. Therefore, as the second step of this study (Sec. **2.8-2.13**), *ionic* mechanisms of PE, following by predissociation of CHQ OH-group, will be scrutinized.

Taking into account that water is present in all system exhibiting PE and following the title of the Thesis, special attention has been paid to clarify the role of *individual* water molecules in both considered concerted and ionic mechanisms. The latter allowed to draw general

conclusions for the case of solutions and to eventually clarify the role of supramolecular CHQ in the catalytic proton exchange.

2.2 Theoretical Methods

Description of thes proton-transfer reactions generally requires a quantum treatment of the electronic structure at highly-correlated level, combined with nuclear dynamics. However, for large systems of practical interest such calculations are presently not feasible. One thus has to resort either to the combination of computationally inexpensive electronic-structure methods combined with *nuclear dynamics*, or to *static* calculations employing correlated *ab-initio* electronic-structure methods (Sec. **1.2.3**). Since the former methods often fail to describe non-covalent interactions even qualitatively, the latter option has been chosen here.

Since the full CHQ-water-acetone complex is too large even for a comprehensive description by means of static correlated quantum-chemical methods, one has to employ molecular models. In this case, hydroquinone (QH_2) has been chosen as a model, since it represents a substructure of CHQ and was suggested as the CHQ prototype in earlier studies (Ref. **196**). The acidities of the compounds are expected to be essentially identical, since the OH-groups of CHQ and QH_2 exhibit identical polarity. Mulliken partial charges analysis revealed the charges of (-0.57) on oxygen and 0.31 on hydrogen for both systems at the DFT/B3LYP/6-31G(d,p) level of theory. Since the polarity of the OH-groups essentially determines the acidity of the compounds, one can assume that they exhibit similar pK_a values of approximately 10. Furthermore, calculation of the *deprotonation energies* (DA) of QH_2 and CHQ at the B3LYP/6-31G(d,p) level revealed that they also have nearly identical deprotonation energies of 361 and 369 kcal mol^{-1}, respectively. This confirms that QH_2 and CHQ have similar chemical properties in proton transfer processes. This rationalizes the choice of QH_2 as a prototype of CHQ. However, at first glance it contradicts the NMR experiments where CHQ and QH_2 behave differently with respect to the observed PE. As it will be shown later, their different behavior can be related to the presence and absence of solvent water aggregates in the three NMR experiments. This, and not the different structural and/or electronic properties of CHQ and QH_2, is crucial for the barriers and rates of PE.

The model systems cover the whole range of non-covalent interactions, *i.e.* dispersion interactions and hydrogen bonding, requiring high-level correlated *ab-initio* methods. However, due to the size of the largest necessary model system (QH_2 with acetone and two water molecules), the only applicable *ab-initio* method is the second-order Møller-Plesset perturbation (MP2) theory (Sec. **1.2.4**). MP2 theory is in principle capable to treat the long-

range interactions with sufficient accuracy (Ref. **197**) as well as the dispersion, polarization and covalent effects associated with hydrogen bonding (Ref. **198**).

For an efficient location of transition-state structures, as well as for the correction of proton-transfer barriers by zero-point vibrational energy (ZPVE) (Sec. **1.1.4**), the computation of analytical second derivatives is required (see Ref. **199**, **200** for review on the geometry optimization techniques). This restricts the largest possible basis set size to 6-31G(d,p) for the largest model complex (see *e.g.* Fig. **2.6**, Sec. **2.5**). Therefore, stationary-point searches and harmonic vibrational frequencies of the majority of calculations were performed at the MP2 level with the moderate double-zeta 6-31G(d,p) basis set, while the energy barriers for proton transfer were improved by means of the single-point calculations with the larger cc-pVTZ triple-zeta basis set (see Sec. **1.4.1** for details on the structures of basis sets). Comparison with existing experimental data for the reaction barrier of acid-catalyzed acetone KET (Ref. **195**) indicates that such a practical approach is quantitatively accurate enough for the investigation of the given system.

Since ZPVE is slightly overestimated within the harmonic approximation compared to ZPVE calculated on corrected anharmonic potential energy surfaces, the former was scaled by a factor of 0.9 (Sec. **1.1.4**).

Another important issue in the calculations on weakly-bound complexes is the basis-set superposition error (BSSE) (Sec. **1.4.1**). The error leads to a systematic overestimation of stabilization energies and to mutilated potential energy surfaces of the complexes. Since at correlated levels of theory, BSSE vanishes very slowly with increase of basis-set size, its correction is necessary for a quantitative evaluation of stabilization energies of weakly-bound complexes. One simple way of correction for BSSE is the counterpoise (CP) procedure (Sec. **1.4.3**). Application of the CP correction during geometry optimizations at the MP2/6-31G(d,p) level gives structures and stabilization energies of the quality similar to those obtained with much larger basis sets of triple- and quadruple-zeta quality and higher levels of theory like CCSD (Sec. **3.7**). Therefore, CP correction was employed to obtain the *absolute* values of the stabilization energies of several selected complexes.

In the second part of this study (Sec. **2.7-2.13**), proton affinities (PA) and deprotonation enthalpies (DE) of several charged protonated complexes were calculated. In general, these quantities are also sensitive to BSSE (Sec. **1.4.4**). However, in this case CP correction was not employed. In fact, the CP procedure requires an assignment of charges and multiplicities to the individual fragments of the ionic complexes, given in integer values (Sec. **1.4.3**). As it was mentioned previously (Sec. **1.4.4**), in the case of covalently-bound (*e.g.* protonated)

complexes the charge distribution over the fragments is not discrete and, thus, the assignment is not well-defined and often ambiguous. In order to avoid such ambiguities, CP correction was not applied to the calculation of PA and DE of the ptotonated complexes. Nevertheless, the neglect of CP does not affect the results since only the *relative* – not the *absolute* values of PA/DE were analyzed.

MP2 *natural-orbitals occupation number* (NOON) analysis (Ref. **201**, **202**) provides a useful criterion on the multireference nature of electronic wave functions. In some cases it can be pronounced during bond-breaking reactions, even for closed-shell reactants and thus should be controlled in proton-transfer calculations. However, the NOON analysis of all transition state structures did not reveal any deviations from the single reference. Hence, single-reference closed-shell MP2 calculations prove to be clearly adequate for the study of all model systems.

When the long-range interactions were not a major concern, density-functional theory (DFT) calculations (Sec. **1.2.6**) with the common B3LYP functional and 6-31G(d,p) basis were utilized. In particular, DFT was used to calculate deprotonation energies and partial Mulliken charge distributions in the OH-group of CHQ monomers. Alternative approaches to compute partial charges for the investigated complexes, *e.g.* Löwdin charges, NBO charges, as well as partial charges from the electrostatic-potential fitting procedures as implemented in Gaussian 03, were also employed. Since all approaches give essentially identical results, all the data are expressed in terms of Mulliken charges.

Most of the calculations were performed with the GAMESS-US (Ref. **203**) quantum chemical software package, while the computations of stabilization energies on the CP-corrected potential energy surfaces and partial charges employed the Gaussian03 package (Ref. **204**).

2.3 Proton Exchange via Concerted Proton Transfer in CHQ

A previous study of the tubular CHQ structures employing solid-state NMR and quantum-chemical calculations has given a strong evidence that only one acetone molecule is trapped within one CHQ building block (Ref. **191**). According to the derived structural model, the acetone molecule appears to be connected to the 1-D H-bonded chain of the CHQ tubes via an additional H-bond from the carbonyl group of acetone to the bridging water molecule. One particular possibility of such a connection is given in Fig. **2.1** (Sec. **2.1**). Here, a water molecule in the vicinity of the methyl group of acetone and several OH-groups, which belong either to water or to CHQ and which establishes a 1-D H-bond chain, can form a cyclic

network. Within this network, all OH-groups act as proton donors and acceptors simultaneously and, hence, they can efficiently assist PT between the moieties.

Since the OH-groups of CHQ and water molecules are the key players in the observed PE, let us discuss the differences between the tubular and nontubular CHQ aggregates, used in the described NMR experiments (A) and (B) shown in Fig. **2.2** (Sec. **2.1**) in more detail. Within the solid-state NMR experiment (A), most of the present water is bound as bridging water molecules within the 1-D networks and only a negligible amount of "free" water is available. Therefore, it is justified to assume that in the tubular CHQ rather simple proton transfer networks exist. They comprise acetone connected by its carbonyl group to one of the -OH groups of bridging water, or to the -OH groups of the CHQ molecules. This has been suggested by an analysis of previous NMR experiments on CHQ nanotubes (Ref. **191**). In the solution NMR experiment (B), nontubular CHQ aggregates were formed and water molecules were present only as impurities. Here, one can also suppose that the limited number of water molecules in the sample mediates aggregation and, thus, it is most likely bound to CHQ as bridging water. Therefore, one can assume that in both tubular and nontubular aggregates of CHQ, acetone molecules are part of very specific hydrogen bonding networks responsible for the observed PE between acetone and water. The basic mechanism of PE in tubular and nontubular aggregates of CHQ, hence, is expected to be closely related.

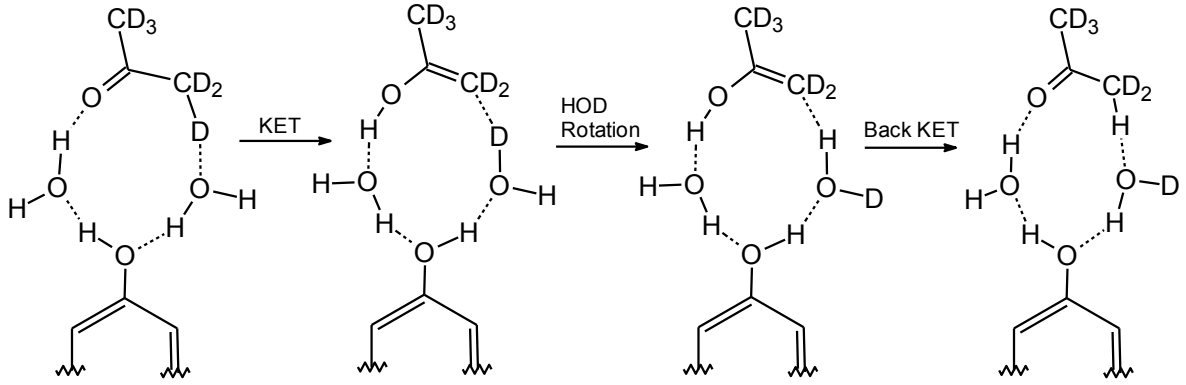

Scheme 2.2. Principal mechanism of proton exchange via concerted keto-enol tautomerism of acetone.

As it was argued in the Introduction, the absence of PE in the experiment on QH_2 (Fig. **2.2C**), having similar chemical properties as CHQ (Sec. **2.2**), as well as the low fraction of dissociated CHQ due to its weak acidity, points to the relevance of PE via concerted KET involving several OH-groups of the bridging water and CHQ. This is in contrast to acid-catalyzed KET, which requires the dissociation of an OH-group prior to PE, resulting in the formation of charged intermediates. The general idea of the mechanism of PE via concerted

KET is depicted in Sch. **2.2**. As a first step, it is assumed that concerted keto-enol tautomerism mediated by two water molecules takes place, which transfers a deuteron from the methyl group of acetone to the H-bonded water. This particular water molecule is assumed to rotate and back-KET to take place. The rotation of the deuterated water molecule is essentially barrierless, since no chemical bonds need to be broken, whereas the hydrogen bond to the methyl group is weak. The final back-KET step is fast, since the keto form is more stable than the enol form of acetone. Therefore, the initial KET step and the concomitant concerted transfer of the methyl deuteron will determine the observed proton exchange rate between acetone and water.

2.4 Keto-Enol Tautomerism via Concerted Proton Transfer in Hydrated Acetone Clusters

As it was introduced in the previous section, *bifunctional* OH-groups of water are the components of the PT networks, presumably catalyzing PE in CHQ (Sch. **2.2**). Since each water molecule possesses also a permanent dipole moment, it can *polarize* the PT agents within the networks ad, in principle, influence the catalysis of PT. Herein, the efficiency of the process can depend on the number of water molecules involved in the PT networks, as well as on their relative alignment. It means that the effect of *specific microsolvation* by water on the acetone KET should be elucidated in detail. As a first step, the question of how many waters are optimal for the catalysis of concerted PT in the networks similar to those presented in CHQ (Sch. **2.2**), was answered at first. Secondly, the influence of solvating water molecules, which are not directly involved in the concerted PT, was clarified. Having both these issues addressed, gives an insight into the molecular details of the mechanism and allows to identify the differences of the reaction mechanisms when CHQ is employed.

To answer the question about the optimal number of catalytic water molecules in the concerted KET, the hydrated clusters $C_3H_6O\bullet\bullet\bullet(H_2O)_n$ with up to three waters (n=0-3) have been constructed (Fig. **2.3**). They form the *cyclic* PT networks, in which each water acts as a proton donor and proton acceptor simultaneously, to assist KET. The equilibrium geometries of these clusters were optimized at the MP2/6-31G(d,p) level of theory in both the keto (Fig. **2.3**, top) and enol (Fig. **2.3**, bottom) forms, as well as the transition states (Fig. **2.3**, middle) corresponding to KET via concerted single-, double-, triple- and quadruple PT. All the stationary points were characterized by analysis of their harmonic frequencies (see Sec. **1.1.3**). For the transition-state structures, the latter revealed one imaginary value

corresponding to the concerted PT pathway. The energy differences between acetone keto and enol forms as well as activation energies (the energy barriers) of the PT along these pathways were further corrected by ZPVE. The calculated energy differences and the barrier values are collected in Tab. **2.1**. In addition, single-reference character of the wave-function in the transition structures was tested by computations of the NOON values (Sec. **2.2**), which, indeed, indicate no multireference character and further validates the use of closed-shell MP2.

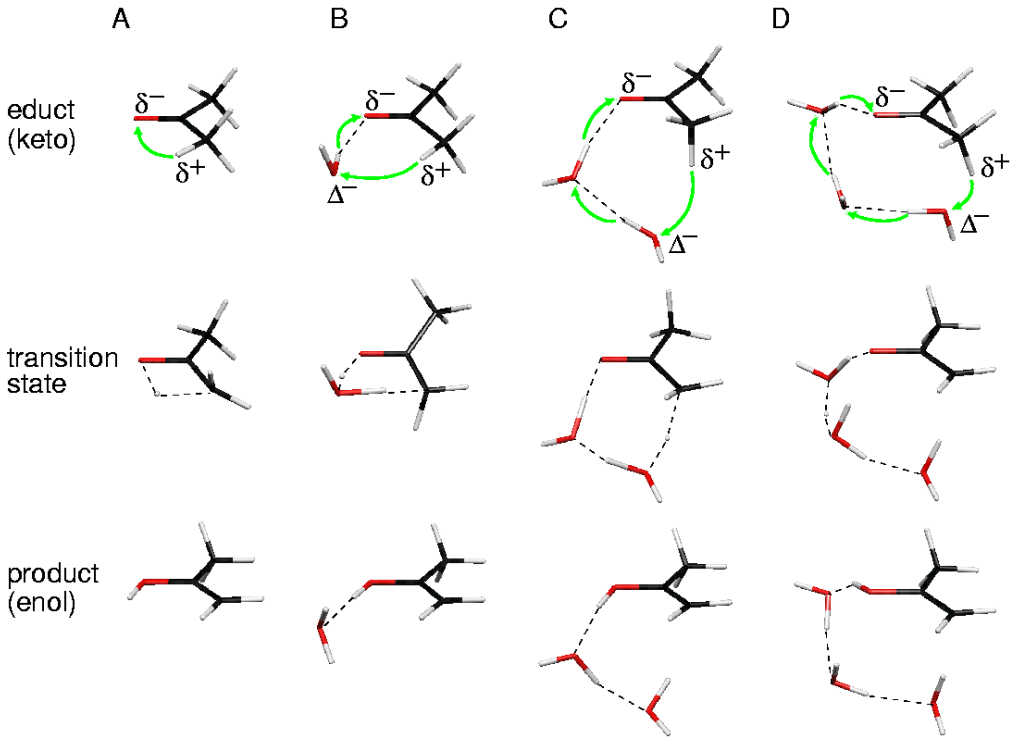

Figure 2.3. Molecular structures of the educts (top), transition states (middle) and products (bottom) along proton transfer pathways (green arrows) via keto-enol tautomerism in isolated acetone (A), $C_3H_6O\cdots H_2O$ (B), $C_3H_6O\cdots(H_2O)_2$ (C) and $C_3H_6O\cdots(H_2O)_3$ (D) clusters.

The computed energy difference between the keto and enol forms of acetone itself is 11.3 kcal mol^{-1} at the MP2/cc-pVTZ//MP2/6-31G(d,p) level of theory and increases slightly to 11.6 kcal mol^{-1} when ZPVE is employed. This agrees very favorable with a previous Car-Parinello molecular dynamics (CPMD) study at the BLYP level of theory which gave 11.8 kcal mol^{-1} (Ref. **205**). Unfortunately, neither experimental, nor benchmark theoretical data are available to evaluate directly the computed values for the hydrated acetone clusters. Instead, the averaged ZPVE-corrected energy difference between the keto and enol forms of all considered hydrated clusters $C_3H_6O\cdots(H_2O)_n$ clusters (n=1-3) was calculated to be 10.7 kcal mol^{-1}. Comparing to the experimental value of 10.3±0.4 kcal mol^{-1} found in aqueous solution of acetone (Ref. **195**), the agreement is very good. The relative energies of the keto and enol

forms are nicely reproduced with the chosen theoretical approach and this gives confidence that the PT mechanism can also be well-described with this methodology.

The calculated values for the activation enthalpy E_a in the concerted KET reveal a strong decrease of the reaction barrier height with an increase of the number of involved water molecules. While the energy barrier in isolated acetone is 64 kcal mol^{-1}, it drops already by 26.5 kcal mol^{-1} to 37.5 kcal mol^{-1}, with only one catalytic water molecule, and decreases further to 30.4 and 29.1 kcal mol^{-1} with two and three catalytic water molecules, at the level of MP2/cc-pVTZ\\MP2/6-31G(d,p) and ZPVE calculated with MP2/6-31G(d,p). This is in agreement with a previous MP2 study (Ref. **206**), which demonstrated that one water molecule leads to the reduction by 26.1 kcal mol^{-1} of the barrier of KET in acetone from 69.2 kcal mol^{-1}**,** for isolated acetone itself, to 43.1 kcal mol^{-1}.

Table 2.1. ZPVE-corrected activation energies (enthalpies) E_a (kcal mol^{-1}) for concerted keto-enol tautomerism in cyclic $C_3H_6O\bullet\bullet\bullet(H_2O)_n$ clusters (n=0-3) as well as the energy difference ΔE of keto and enol forms as function of number of catalyzing water molecules n at the theoretical level of MP2/cc-pVTZ//MP2-6-31G**. The contributions of ZPVE scaled by 0.9 for anharomonicity are given in brackets and have been computed at MP2/6-31G** level.

N	0	1	2	3
E_a(keto → enol)	64.0 (+3.0)	37.5 (+2.7)	30.4 (+3.4)	29.1 (+1.7)
E_a(enol → keto)	52.4 (+3.3)	26.5 (+2.6)	20.9 (+4.3)	17.6 (+2.9)
ΔE	11.6 (-0.3)	11.0 (+0.1)	9.6 (-0.9)	11.5 (-1.2)

In Fig. **2.4** the functional dependence of the activation energy on the number of catalytic water molecules, for the concerted KET in hydrated acetone complexes, is displayed. The barrier height is practically converged with three catalytic water molecules and one can expect only a minor decrease when a fourth water molecule is embedded in the catalytic PT network. On the other hand, due to the *anticooperative* effect of the electric dipole moment of those water molecules, which are not involved in the PT networks directly, one can expect an increase of the activation energies with increasing number of water molecules in the transition to *solution*. Indeed, previous studies on the subject corroborate this assumption. For example, an earlier research employing the *self-consistent reaction field* (SCRF) methodology to include solvent effects, showed an increase of the activation energy by about 2 kcal mol^{-1} in the $C_3H_6O\bullet\bullet\bullet H_2O$ complex, compared to the same system in the gas phase (Ref. **206**). In that study, one catalytic water molecule, involved in the PT via KET, was treated explicitly, while water as solution was represented by a *polar continuum*. In a recent *Car-Parinello molecular*

dynamics (CPMD) simulation of acetone KET in water solution (Ref. **205**), the computed activation energy of KET was 57.7 kcal mol^{-1} for the isolated acetone in the gas phase and 38.5 kcal mol^{-1} for the KET catalyzed by four water molecules in the presence of twenty four explicit solvent water molecules. It is worth to mention that the employed DFT methodology tends to underestimate reaction barriers, thus they are most likely higher in reality, as it is the in the case of the present MP2 calculations. However, this demonstrates that the activation barrier of KET of acetone in aqueous solution is higher than in isolated $C_3H_6O\bullet\bullet\bullet(H_2O)_n$ complexes with well-defined specific H-bonded networks. Summarizing, these findings already indicate that *solvent* water molecules, *i.e.* the water molecules which are not involved in the PT as proton-donor/proton-acceptors, presumably decrease the efficiency of KET. This is also in agreement with recent studies on the tautomerism of various organic molecules, where solvent water was treated explicitly (Ref. **207**).

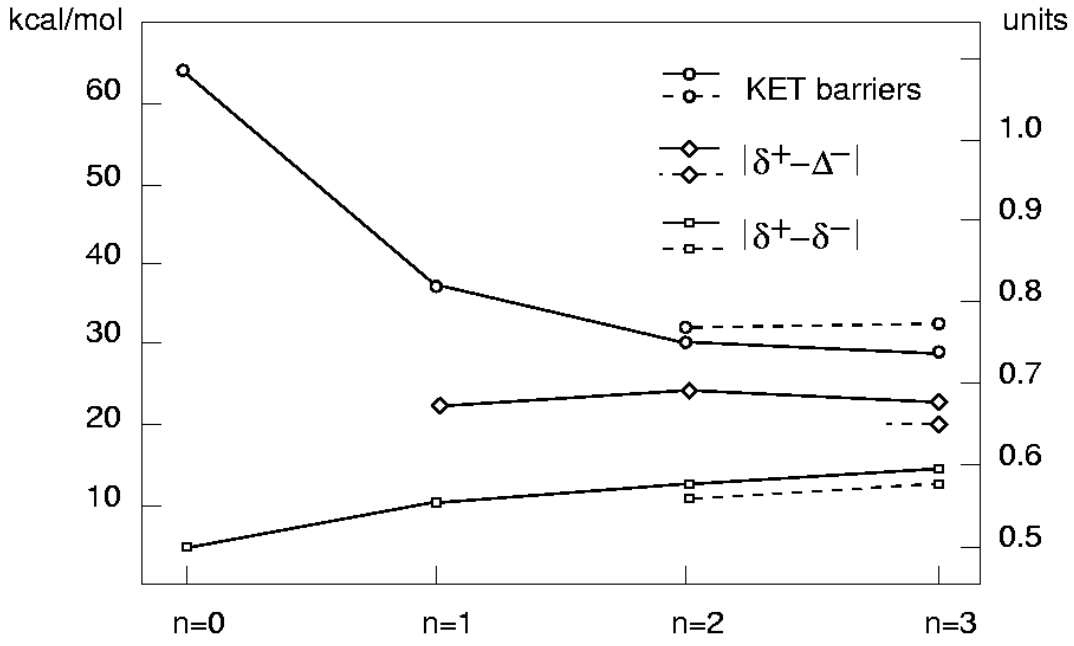

Figure 2.4. Zero-point energy corrected energy barriers of acetone-water proton transfer (circles) in $C_3H_6O\bullet\bullet\bullet(H_2O)_n$, n=1-3 (solid line) and $QH_2\bullet\bullet\bullet C_3H_6O\bullet\bullet\bullet(H_2O)_2$ (dashed line) with respect to the number of participating OH-groups. The difference between the Mulliken charges at the acetone methyl hydrogen and carbonyl oxygen (squares) as well as between methyl hydrogen and the closest water oxygen (diamonds) in $C_3H_6O\bullet\bullet\bullet(H_2O)_n$, n=1-3 (solid line) and $QH_2\bullet\bullet\bullet C_3H_6O\bullet\bullet\bullet(H_2O)_2$ (dashed line) are also given.

To corroborate these assumptions qualitatively and further clarify the *explicit* influence of solvent water on the efficiency of KET, the following complimentary study has been undertaken. Within the study, the influence of a second (solvent) water molecule on the barriers of KET in acetone$\bullet\bullet\bullet H_2O$ complexes was investigated, where KET is catalyzed by one

water and proceeds via concerted double proton transfer. For this objective, two additional acetone•••$(H_2O)_2$ complexes, in which the second water molecule is not part of the catalytic H-bonded network, but instead is bound additionally either to the carbonyl group of acetone (isomer **I**) (Fig. **2.5B**) or to the oxygen of the catalytic water (isomer **II**) (Fig. **2.5C**), were constructed. Again, keto and enol forms of the two isomers of C_3H_6O•••$(H_2O)_2$ as well as the transition states for the concerted double PT were optimized and confirmed by harmonic frequency calculations.

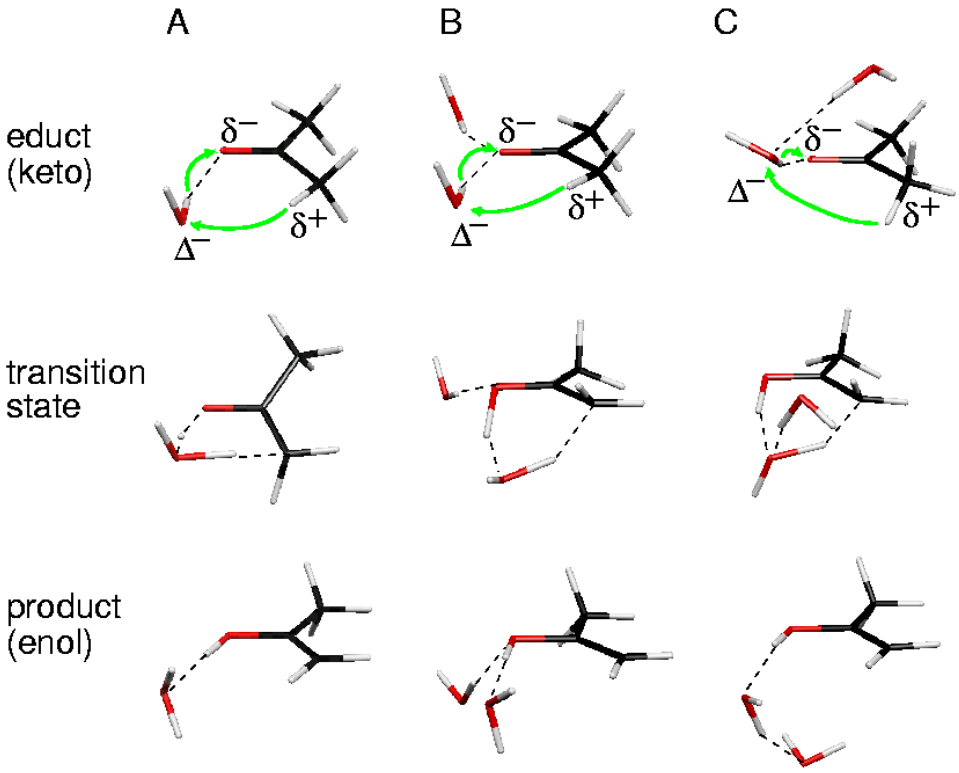

Figure 2.5. Optimized stationary structures of the educts (top), transition states (middle) and products (bottom) along the proton transfer pathways (green arrows) in C_3H_6O•••H_2O (A), C_3H_6O•••H_2O with one additional solvent water bound to acetone carbonyl (B), and C_3H_6O•••H_2O with one additional solvent water bound to water oxygen.

Computations of the activation enthalpies of KET via double proton transfer in isomers **I** and **II** show they are 37.7 and 40.7 kcal mol^{-1} at the MP2/cc-pVTZ//MP2/6-31G(d,p) level. Comparison with the value of 37.5 kcal mol^{-1} in the C_3H_6O•••H_2O complex (without the additional solvent water) (Fig. **2.5A**), reveals that the barrier is increased by 3.2 kcal mol^{-1} only when the solvent water is bound to the catalytic water directly. While the first solvent water molecule directly bound to the catalytic water network appears to have an influence of approximately 3 kcal mol^{-1}, further water molecules will still lead to an increase of the barrier, but to a smaller extent. Obviously, hydrogen bonding to the catalytic water reduces its

catalytic activity, while the hydrogen bonding to the acetone carbonyl group bears only a marginal effect. This indicates that, in principle, only those solvent water molecules, which are bound to the catalytic H-bonded networks *directly*, increase the KET energy barrier and, thereby, decrease the catalytic efficiency.

To explain this anticooperative effect of solvent water on KET in isomers **I** and **II** quantitatively, one should make one step back and elucidate the role of water molecules in the catalysis of KET (Fig. **2.3**, Tab. **2.1**). As it was supposed in the beginning of the section, *polarization* of acetone and other bifunctional OH-groups involved in PT by the permanent dipole moment of the catalytic water molecules is the most probable reason. The stronger the acetone molecule is polarized, *i.e.* the more partial positive charge is located on the hydrogen of the methyl groups and the more negative charge is located on the carbonyl oxygen, the easier the migration of the relevant protons from the methyl to the carbonyl group of acetone is. The dependence of the difference between the partial charges on the proton-accepting carbonyl oxygen and proton-donating methyl hydrogen of acetone, on the number of catalytic water molecules is presented in Fig. **2.4**. It is evident that the polarization of acetone is converged in the same way as the reaction barriers for the concerted KET. This occurs when three to four catalytic water molecules are involved. Therefore, a clear relation between the acetone polarization and the barriers for the concerted KET has been established.

A closer look at the structures of the acetone•••$(H_2O)_n$ complexes with up to three catalytic water molecules (Fig. **2.3**), indeed, explains why the activation energies converge to an optimal value of three to possibly four water molecules. An increase in the size of the cyclic H-bonded network, at some point, does not lead to an increased polarization of acetone, since a cooperative, *i.e. additive* effect of the water dipoles, is diminished due to several structural factors. In particular, the catalytic water molecules have to arrange in structures, which are far from linear alignment, which is optimal for polarization, with increasing the number of catalytic water molecules. At the same time, the distance between the catalytic water molecules and acetone increases thereby diminishing polarization.

These results allow to extrapolate the values of the energy barriers to the case of acetone KET in neutral aqueous solution. As it was shown above, the most efficient KET process with a barrier of about 30 kcal mol^{-1} assisted by three or, perhaps, by four water molecules in an isolated acetone-water complex. Solvation of this cluster in water will lead to the hydrogen-bonding of catalytic water molecules decreasing their ability to polarize acetone. If one assumes that each catalytic water molecule to be H-bonded by one solvent water, and further assumes that each solvated catalytic water molecule adds about 3 kcal mol^{-1} to the minimal

barrier of 30 kcal mol^{-1}, one would arrive at an activation energy of acetone KET in water of *ca.* 40 kcal mol^{-1}. This is consistent with the value of 38.5 kcal mol^{-1} obtained from the CPMD study mentioned previously (Ref. **205**), where on average four water molecules catalyzed KET in the presence of twenty four solvent water molecules.

Although rather simple in nature, the effect of anticooperativity of water dipoles can lead to very considerable increase of the activation energies of acetone KET in solutions. Furthermore, one would expect a similar behavior of catalytic/solvent water in other proton-transfer processes in solution pointing to the general significance of the described phenomenon.

Turning back to the initial experiments on proton exchange in CHQ, one realizes they were performed under conditions with no or only very little amount of free water, which could act as solvent and increase the barrier of KET. Therefore, based on the results for the acetone-water clusters, one can expect concerted KET to be more efficient by about 10 kcal mol^{-1} in the CHQ aggregates than in aqueous solution.

2.5 Keto-Enol Tautomerism in Hydrated Hydroquinone-Acetone Clusters

Having understood the mechanism of KET catalyzed by H-bonded networks in acetone-water complexes in detail, the next logical step is to investigate the influence of CHQ on the concerted KET. The major question to answer now is how the barrier of PT alters when one of the OH-groups of the H-bonded networks originates from CHQ and not from water. Since CHQ is too large to afford calculations at MP2 level even with only medium-size basis sets, in all calculations QH_2 was used as model system. This choice was rationalized in Sec. **2.2**.

As a first step, two model complexes comprising QH_2, acetone and one or two catalyzing water molecules, respectively, were constructed. They resemble the suggested structures of KET PT networks in CHQ (Sch. **2.2**), derived from the previous NMR experiments (Ref. **191**). The minima, corresponding to the keto and enol forms of acetone, and the transition states of the complexes were optimized at the MP2/6-31G(d,p) level of theory and were verified by analysis of their harmonic frequencies. Their structures and energetics are presented in Fig. **2.6** and Tab. **2.2**, respectively.

The smaller cluster with only one catalytic water molecule possesses two OH-groups which are involved in the concerted KET mechanism, one from QH_2 the other from the catalytic water. The results for that cluster are thus comparable with those for acetone•••$(H_2O)_2$, since in the latter, two catalytic OH-bonds (both from water) are also involved. Computed activation enthalpies along the concerted KET pathway in the

QH_2•••C_3H_6O•••H_2O complex is 31.9 kcal mol^{-1} at the MP2/cc-pVTZ//MP2/6-31G(d,p) level, which is 1.5 kcal mol^{-1} higher than in the corresponding acetone•••$(H_2O)_2$ cluster. In the larger QH_2•••C_3H_6O•••$(H_2O)_2$ cluster the activation enthalpy of concerted KET via quadruple PT is found to be even higher with 32.7 kcal mol^{-1} at the same level of theory. Compared to the corresponding value of concerted KET via quadruple proton transfer in the acetone•••$(H_2O)_2$ complex (29.1 kcal mol^{-1}), the substitution of one water by an OH-group of QH_2 increases the activation energy by 3.6 kcal mol^{-1}. Clearly, concerted acetone KET is less efficient in the QH_2 clusters than in the analogous hydrated clusters alone.

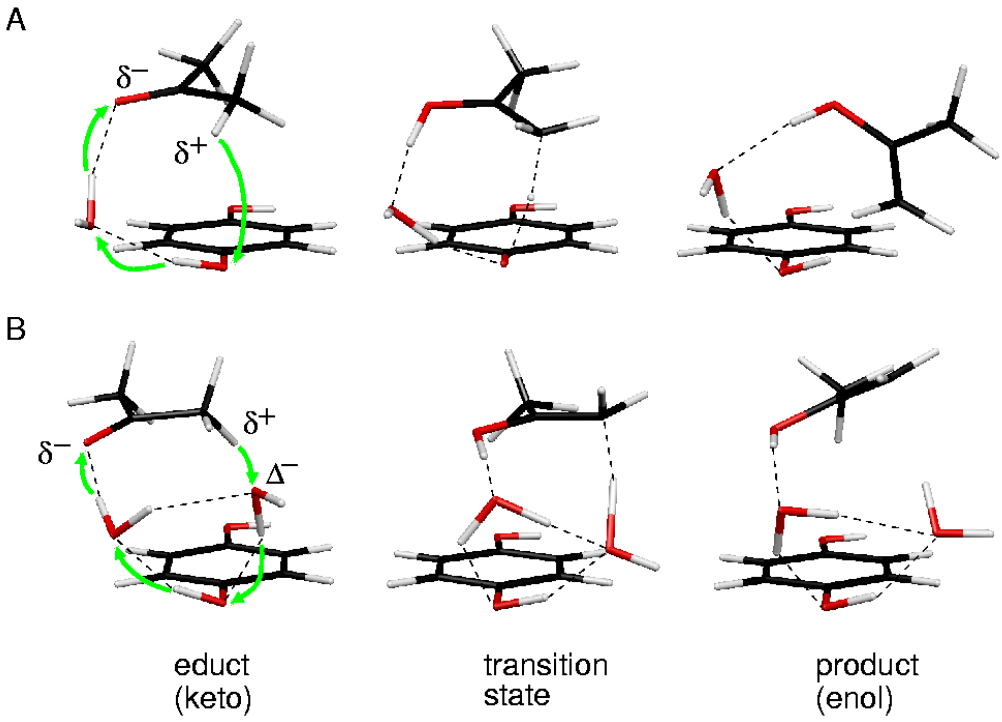

Figure 2.6. Optimized educt (left), transition state (center) and product (right) structures of the QH_2•••C_3H_6O•••H_2O model complex (A) and QH_2•••C_3H_6O•••$(H_2O)_2$ model complex (B) along the concerted acetone keto-enol tautomerism (green arrows).

Since the catalytic activity of the water molecules in the acetone-water clusters can be explained by their polarizing function, the slightly less efficient catalytic function QH_2 compared to water is readily understood in terms of the different polarity of their OH-groups. Indeed the OH-group of QH_2 is slightly less polar than the OH-group of water. It is indicated by the Mulliken charge differences between oxygen and hydrogen of 0.73 and 0.60 in H_2O and QH_2, respectively, at the SCF/cc-pVTZ//MP2/6-31G(d,p) theory level. Therefore, it is unnecessary to consider model clusters, in which both OH-groups of QH_2 are involved. In summary, in the case of QH_2•••C_3H_6O•••H_2O, the two OH-groups of the catalytic water and QH_2 are slightly less efficient in polarizing the acetone than two water OH-groups of

$C_3H_6O\bullet\bullet\bullet(H_2O)_2$. This is nicely illustrated in Fig. **2.4** (Sec. **2.4**) by relation of the partial charges on carbonyl oxygen and methyl hydrogen atoms of acetone and corresponding values of the activation energies for concerted KET in the $QH_2\bullet\bullet\bullet C_3H_6O\bullet\bullet\bullet H_2O$ and $C_3H_6O\bullet\bullet\bullet(H_2O)_2$ clusters.

The surprising, at first glance, increase of the activation energy of concerted acetone KET in the $QH_2\bullet\bullet\bullet C_3H_6O\bullet\bullet\bullet(H_2O)_2$ cluster, as compare to the $QH_2\bullet\bullet\bullet C_3H_6O\bullet\bullet\bullet H_2O$ one, can be again explained by the depolarizing function of the second water molecule. Indeed, a closer look at Fig. **2.6** reveals that the second catalytic water in the vicinity of the acetone carbonyl group of the $QH_2\bullet\bullet\bullet C_3H_6O\bullet\bullet\bullet(H_2O)_2$ complex is H-bonded to the other one in the vicinity of acetone methyl group, *i.e.* simultaneously acts a depolarizing solvent agent. This picture is also corroborated by the analyses of partial charges on the relevant groups of the $QH_2\bullet\bullet\bullet C_3H_6O\bullet\bullet\bullet(H_2O)_2$ and $QH_2\bullet\bullet\bullet C_3H_6O\bullet\bullet\bullet H_2O$ complexes (Fig. **2.4**).

Table 2.2. ZPVE corrected activation energies E_a (kcal mol^{-1}) for concerted keto-enol tautomerism in $QH_2\bullet\bullet\bullet C_3H_6O\bullet\bullet\bullet H_2O$ (n=2) and $QH_2\bullet\bullet\bullet C_3H_6O\bullet\bullet\bullet(H_2O)_2$ as well as the energy difference ΔE of keto and enol forms as function of number of catalyzing hydroxyl groups n at the theoretical level of MP2/cc-pVTZ//MP2-6-31G(d,p). The contributions of ZPVE scaled by 0.9 for anharomonicity are given in brackets and have been computed at MP2/6-31G(d,p) level.

n	2	3
E_a(keto → enol)	31.9 (-2.4)	32.2 (-3.4)
E_a(enol → keto)	7.4 (-2.9)	18.5 (-3.5)
ΔE	24.5 (+0.5)	13.7 (+0.1)

2.6 Stability of the Hydrated Acetone and Hydrated Hydroquinone-Acetone Clusters

In conclusion of this part, dedicated to the PE mechanisms via concerted KET, stabilization energies/enthalpies of the $QH_2\bullet\bullet\bullet C_3H_6O\bullet\bullet\bullet H_2O$ (Fig. **2.6**, Sec. **2.5**) and $C_3H_6O\bullet\bullet\bullet(H_2O)_2$ (Fig. **2.3**, Tab**. 2.1**, Sec. **2.4**) complexes will be compared. Both clusters have similar activation energies for KET via concerted triple proton transfer of 31.9 and 30.4 kcal mol^{-1}, respectively. The comparison will give an idea of the strength and compactness of the H-bonded PT networks assisting KET in CHQ.

To obtain reliable stabilization energies of the hydrogen-bonded complexes, their potential energy surfaces should be corrected for BSSE (see Part **1.4**). To that end, both structures have been reoptimized on the CP-corrected PES. Also ZPVE was computed in the reoptimized points with the CP correction included to produce CP-corrected stabilization enthalpies. At the level of CP-corrected MP2/6-31G(d,p), the stabilization enthalpies for the QH_2•••C_3H_6O•••H_2O and C_3H_6O•••$(H_2O)_2$ complexes amount to -12.6 and -8.4 kcal mol^{-1}, respectively. Thus, QH_2•••C_3H_6O•••H_2O is 4.2 kcal mol^{-1} stronger bound than C_3H_6O•••$(H_2O)_2$. At the level of single-point CP-corrected MP2/cc-pVTZ on the CP-corrected MP2/6-31G(d,p) structures and ZPVE, the difference is even larger with 5.7 kcal mol^{-1}.

Although the efficiency of the catalysis of KET via the OH-group of QH_2 and water is slightly weaker than the efficiency of two water OH-groups alone, the stability of the PT networks is considerably larger in the QH_2 complex – by about one H-bond strength of the water dimer (4.0 to 5.7 kcal mol^{-1}). Most likely, the origin of the additional stability are dispersion interactions between the aromatic ring of QH_2, acetone and water. In the case of CHQ, one would expect that dispersion interactions become more pronounced due to the increased number of aromatic rings. The H-bonded network in the CHQ cages hence becomes even stronger and more compactly bound. It will result in specific structures of 1D H-bond chains, observed experimentally in CHQ (Ref. **186**, **187**, **191**). Furthermore, it would explain the efficient trapping of one acetone per CHQ subunit in tubular and non-tubular CHQ aggregates as well as the observed efficient binding of other small organic molecules by CHQ.

2.7 Proton Exchange via Concerted Mechanism: Summary

In the first part of this work outlined in section 2.1, KET via concerted proton transfer was thoroughly studied as a possible precursor of the catalytic proton exchange of acetone trapped in CHQ aggregates.

At first, concerted KET of acetone in specific clusters hydrated by one to three water molecules and forming cyclic PT networks was studied at first. It was shown that three or, possibly, four water molecules are optimal for the catalysis of KET with an activation enthalpy of about 30 kcal mol^{-1}. This value appears to be about 10 kcal mol^{-1} lower than in aqueous solution. The reason for the increase of activation energy in aqueous solution can be attributed to the anticooperative effect of solvent water dipoles which depolarize the reagents involved in the proton transfer. In particular, it was shown that H-bonding of a *single* solvent

water molecule to the catalytic water involved in PT, leads to an increase of the barrier for concerted KET by about 3 kcal mol^{-1}.

Having understood the general mechanism of concerted acetone KET in detail, a specific influence of CHQ on the PT was investigated at second. For this purpose, complexes comprising QH_2, which serves as molecular model for CHQ, acetone and one or two catalytic water molecules, were used. The simulations revealed that concerted KET in these model complexes is slightly less efficient than in the corresponding hydrated acetone complexes. This is mainly due to the lower polarity of the OH-group of QH_2 comparing to that of water.

Finally, computed stabilization energies of the acetone-water and QH_2-acetone-water complexes, demonstrate that the hydrogen-transfer networks in the latter case are significantly stronger bound than in the former case.

These findings demonstrate that KET via concerted mechanism is more efficient in solvent-free environments with only a few catalytic water molecules, a condition that is provided by CHQ aggregates. Nevertheless, the Arrhenius rate constant for the concerted KET obtained using the activation enthalpy of the most efficient case $C_3H_6O\bullet\bullet\bullet(H_2O)_3$ of 29.1 kcal mol^{-1} is 10^{-13} M^{-1} s^{-1} at room temperature. This is clearly too low to explain the observation of proton exchange at the conditions of the NMR experiment. In contrast, acetone-water proton exchange in *superheated* water can be quantitatively explained by the mechanism found in the present study. In an NMR study (Ref. **194**), proton exchange between acetone and superheated deuterated water was achieved at 200° C during total exposure time of 60 min. This agrees nicely with the calculated rate constant at 473 K of about 10^{-1} M^{-1} s^{-1}, which would allow for the observation of the proton exchange under these conditions. Obviously, at room temperatures KET via concerted proton transfer, assisted by a few OH-groups is not the prevailing mechanism of the catalytic proton exchange in CHQ.

Although this part of the study was not able to identify the mechanism of the observed catalytic activity of CHQ, it has discovered that *desolvation* of the proton-transfer networks assisting KET appears to be a very important, if not a crucial feature of CHQ. This property of CHQ will reappear in the next sections, where dissociation of the CHQ OH-groups and concomitant formation of charged ionic species which are possibly involved in proton exchange via *step-wise* mechanisms, will be investigated.

2.8 Proton Exchange via Ionic Mechanism Triggered by CHQ Dissociation: Possible Scenarios

In the Introduction it was already noticed, that although the concentration of ionic species resulting from dissociation of weakly-acidic CHQ is small (of about 10^{-5}), it can still provide slow PE, observed experimentally. It may happen when PT reactions involving ionic species are efficient enough. In this section, possible scenarios and related model systems for ionic proton-exchange mechanisms will be considered. For this objective, the question where the proton goes to after dissociation of the OH-group of CHQ (or in the model complexes QH_2), will be answered. Therefore, selected *protonated* molecules and their complexes, hydrated by one water molecule, have been compared in terms of their *proton affinities* (PA). The latter are commonly defined as the differences between the total energies

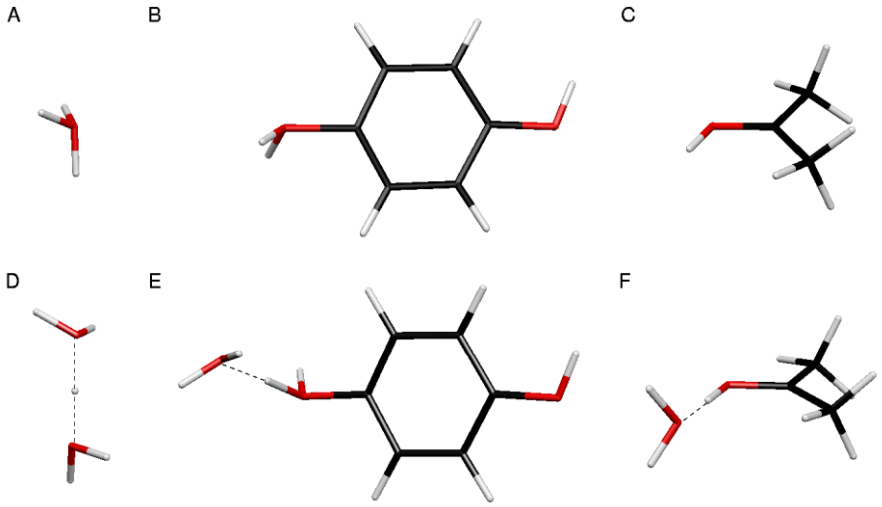

Figure 2.7. Molecular structure of the protonated water $[H_3O]^+$ (A), hydroquinone $[QH_3]^+$ (B) and acetone $[C_3H_6O]^+$ (C), water dimer $[(H_2O)_2\text{-}H]^+$ (D), mono-hydrated hydroquinone $[QH_2\text{-}H\bullet\bullet\bullet H_2O]^+$ (E) and mono-hydrated acetone $[C_3H_6O\text{-}H\bullet\bullet\bullet H_2O]^+$ (F).

of protonated and neutral systems. By inspection of the PT networks presented in the tubular CHQ aggregates, several possible protonation sites can be identified. Most likely, the proton acceptors are monomers of water, CHQ or acetone, and/or their hydrated complexes like $(H_2O)_2$, $QH_2\bullet\bullet\bullet H_2O$, $C_3H_6O\bullet\bullet\bullet H_2O$ and so on (Fig. **2.7**). In principle, one cannot *a priori* exclude larger hydrated complexes to be present in the CHQ aggregates. However, the NMR experiments on both tubular and non-tubular CHQ aggregates demonstrated that they correspond to a *water-deficient* environment. Thus, one can safely assume that additional "free" solvent water molecules, which are not bound in the H-bonded network of the tubular assembly, are scarce and are most likely spread uniformly over the OH-groups of CHQ. As a consequence, the amount of multihydrated molecular complexes in the tubular and non-tubular CHQ aggregates is probably negligible.

Equilibrium structures of the protonated complexes were optimized at the level of MP2/6-31G(d,p) and are displayed in Fig. **2.7**. Their PA were computed at the MP2/cc-pVTZ level with ZPVE calculated at the MP2/6-31G(d,p) level included (Tab. **2.3**). One can see that acetone has a higher PA than water and QH_2 by about 27 and 13 kcal mol^{-1}, respectively. Upon the addition of one water molecule to each monomer, the acetone complex $C_3H_6O{\bullet\bullet\bullet}H_2O$ still remains the best proton acceptor, but the energetic differences in the PA of the complexes decrease. The PA of the acetone-water complex, QH_2-water complex and the water dimer are now only 8 and 14 kcal mol^{-1} smaller, respectively.

Table 2.3. Zero-point energy corrected proton affinities (PA) and deprotonation enthalpies (DE) (kcal mol^{-1}) of potential proton acceptors (see text). All values were calculated as single point MP2/cc-pVTZ energies on the MP2/6-31** optimized structures. ZPE has been computed at the MP2/6-31** level and is given in parenthesis.

Complex	**PA (ZPE)**	**DE (ZPE)**
H_2O	-165.7 (+8.4)	
QH_2	-179.2 (+7.9)	+353.2 (-9.0)
C_3H_6O	-192.5 (+8.1)	+373.0 (-8.8)
$[C_3H_6O\text{-}H]^+$		+201.3 (-7.7)
$(H_2O)_2$	-197.8 (+7.2)	
$QH_2{\bullet\bullet\bullet}H_2O$	-203.2 (+7.5)	
$C_3H_6O{\bullet\bullet\bullet}H_2O$	-211.5 (+7.7)	

Comparison of the PA values of selected monomers and their monohydrated complexes suggests that the proton originating from CHQ will tend to preferentially attach to the carbonyl group of acetone. In this situation, a *zwitterionic* intermediate would be formed, which triggers the back proton transfer with a proton exchange step between the methyl group of acetone and water. This mechanism is depicted in Sch. **2.3**. The created zwitterionic intermediate will probably need quite some energy to be created (the evaluation of this energy will be given in Sec. **2.9**), whereas the further PE step should be essentially barrierless.

Since the proton affinities of selected complexes increase with the addition of water molecules, one may suspect that further hydration will lead to the protonation of surrounding water aggregates rather than acetone. Indeed, this behaviour has been previously reported for the water dimer which can abstract proton frome protonated alkenes, in contrast to a single water molecule, whose PA is insufficient for the abstraction (Ref. **208**)

To check for this option, the structures of protonated acetone-water clusters with up to three water molecules have been optimized at the MP2/6-31G(d,p) level. The structures were produced by addition of the *n*-th water molecule to the optimized structures of the $[C_3H_6O\text{-}H\bullet\bullet\bullet(H_2O)_{n-1}]^+$ cluster followed by a re-optimization step. From comparison of the optimized geometries (Fig. **2.8**) one can see that only upon addition of the third water molecule, the proton migrates from acetone to the adjacent water molecule. In the case of $[C_3H_6O\text{-}H\bullet\bullet\bullet H_2O]^+$, the proton is clearly bound to the carbonyl group of acetone exhibiting a typical bond length of 1.04 Å. Addition of one more water molecule to the $[C_3H_6O\text{-}H\bullet\bullet\bullet(H_2O)_2]^+$ cluster results to a small shift of the proton to the water. Still, it is more closely located at the acetone with an extended bond length of 1.14 Å. Finally, in the cluster hydrated by three water molecules $[C_3H_6O\text{-}H\bullet\bullet\bullet(H_2O)_3]^+$, the proton is transferred entirely to the adjacent water molecule. This is in agreement with the above supposition that a cluster of three water molecules has larger proton affinity than the acetone-water complex. In summary, the protonated acetone is stable in *water-deficient* environment (*e.g.* in the CHQ aggregates), while in the excess of water molecules around (such as in aqueous solution), protonated acetone becomes unstable and the proton moves to the water molecules.

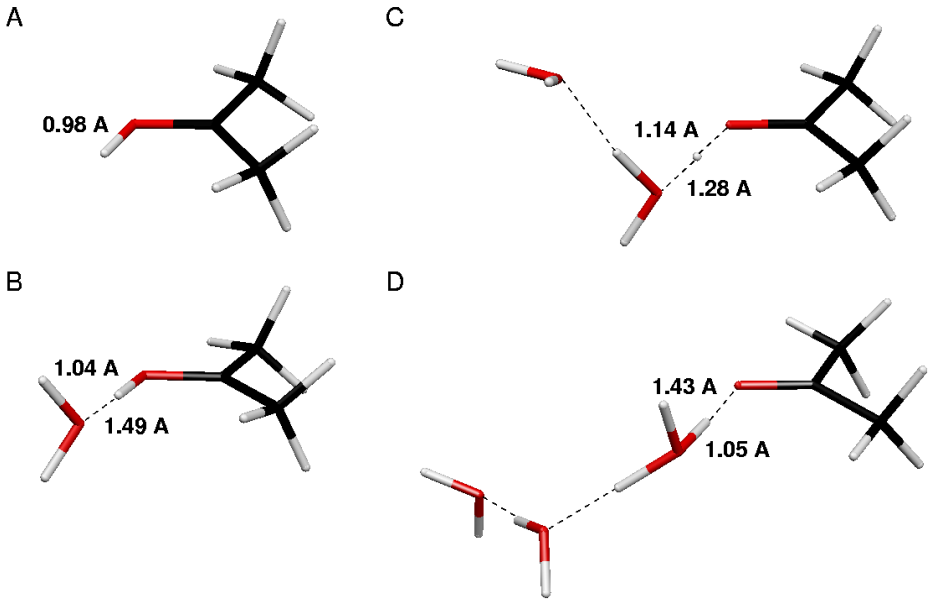

Figure 2.8. Optimized structures of protonated acetone (A) and protonated clusters of acetone hydrated by one (B) and two (C) and three (D) water molecules.

To corroborate this effect in the CHQ aggregates explicitly, the protonated clusters of acetone, QH_2 and one or two water molecules (Fig. **2.9**), were optimized. While in the $[C_3H_6O\text{-}H\bullet\bullet\bullet H_2O\bullet\bullet\bullet QH_2]^+$ cluster (Fig. **2.9A**) the proton is still bound to the carbonyl group of acetone, addition of the second water molecule results in a hydroxonium cation and neutral

acetone in the $[C_3H_6O\cdots H\text{-}(H_2O)_2\cdots QH_2]^+$ complex (Fig. **2.9B**). Therefore, the proton, again, can be released into the environment, when a sufficient number of water molecules are available. In this case, the proton could not be involved in acetone-water PE. Eventually, PE will be catalyzed by the anionic $[QH]^-$ moiety as depicted in Sch. **2.4**.

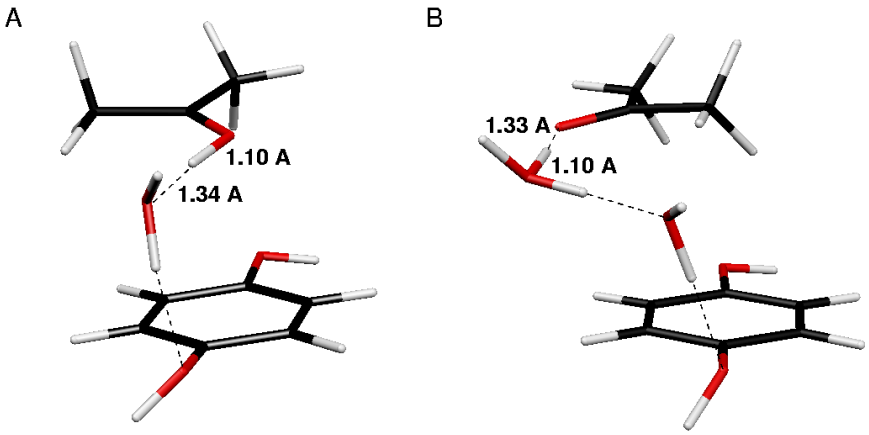

Figure 2.9. Optimized structures of the protonated clusters $[C_3H_6O\text{-}H\cdots H_2O\cdots QH_2]^+$ (A) and $[C_3H_6O\cdots H\text{-}(H_2O)_2\cdots QH_2]^+$ (B).

In summary, two general ionic scenarios appear to be relevant for the investigation of proton exchange between acetone and water in CHQ aggregates. (1) Pre-dissociated proton of the OH-group of QH_2 remains in its vicinity and protonates acetone resulting in a zwitterionic intermediate (Sch. **2.3**). This case will be realized when no or only few solvent waters surround the OH-group of CHQ. (2) The proton is released into the environment and is not directly involved in the proton exchange. The remaining anion will catalyze PE (Sch. **2.4**). The situation will occur when several solvent water molecules surround the OH-group of CHQ and screen acetone from protonation. In the next sections these two possibilities will be analyzed.

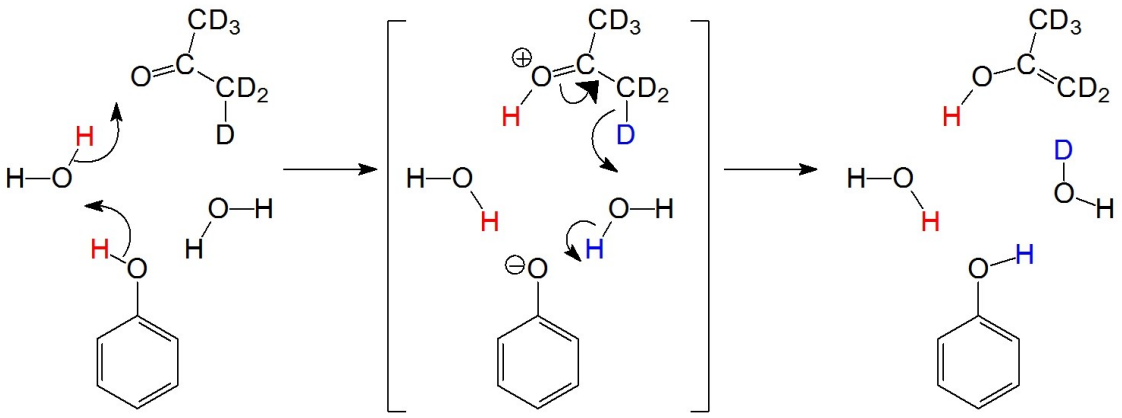

Scheme 2.3. Sketch of proposed mechanism of acetone methyl-water proton exchange initiated by OH-group dissocation of QH_2 leading to formation of a zwitterionic intermediate. Finally, a methyl deuteron is transferred to a nearby water molecule in a back proton transfer step.

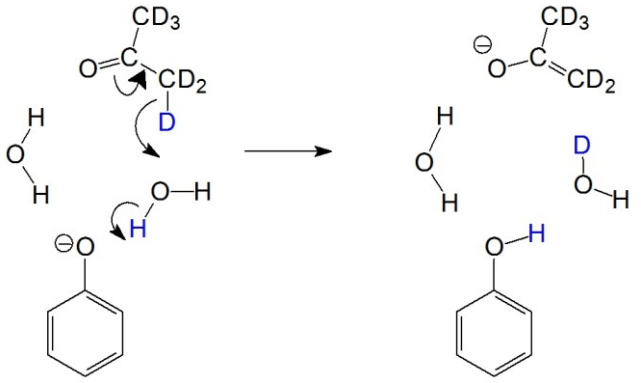

Scheme 2.4. Sketch of proposed mechanism of acetone methyl-water proton exchange catalyzed by a deprotonated CHQ moiety, where the proton has been transferred to the environment and is not immediately present.

2.9 Proton Exchange via Zwitterionic Intermediates

The quantum-chemical description of the PE reactions via zwitterionic intermediates (Sch. **2.3**, Sec. **2.8**) comprising protonated acetone cation and deprotonated $[QH]^-$ anion bears a certain challenge, since the zwitterionic structure does not correspond to a local minimum on PES. Partial geometry optimization of the zwitterionic structures is possible when the geometrical constraint is imposed that holds the proton covalently bound to the oxygen atom of the acetone molecule. For instance, the energy of a partially optimized $[C_3H_6OH]^+\cdots H_2O\cdots[QH]^-$ cluster is found to be only 24 kcal mol^{-1} above the neutral complex. Since the energy obtained by means of partial optimization constitutes an upper bound to the true energy, it manifests the feasibility of the zwitterionic catalytic pathway at ambient temperatures. Indeed, it is has been already corroborated by the liquid-phase NMR experiment on the mixture of CHQ, acetone and water, where proton exchange between the OH-groups of CHQ and water was detected (Fig. **2.2**, Sec. **2.1**). The detection of PE was possible in that case since the resolution of the liquid-state NMR signal is greater than that of the solid state. Therefore, it will be assumed in the further analysis that formation of zwitterionic intermediates occurs with the same probability as the deprotonation of QH_2 in water.

Owing to the pKa-value of weakly-acidic QH_2 (9.8), one recognizes that a fraction of only 10^{-5} of the present QH_2 molecules is deprotonated. Therefore, calculated rates of PT starting from an educt generated by the deprotonation of QH_2 must be scaled by 10^{-5} to account for the preceding deprotonation step. Taking into account the feasibility of CHQ dissociation at room temperatures as corroborated above, it is justified to assume that the influence of acetone on the pKa value is marginal.

Owing to the reasons given above, the zwitterionic complexes technically cannot be employed as defined starting points to study PT from the acetone methyl group to the attached water molecule by means of static quantum-chemical calculations. Therefore, a different strategy has been chosen to study the energetics of the mechanism and to obtain reasonable values for the energy barriers and reaction rates. Within this strategy, the as whole neutral but zwitterionic complex (Sch. **2.3**) was decomposed into two ionic fragments. On one hand, anionic complexes of neutral acetone, one or two water molecules and deprotonated $[QH]^-$ were used to investigate the influence of $[QH]^-$ on the PE mechanism (Fig. **2.10**, Sec. **2.10**). At the same time, the anionic complexes serve as a model for the second anionic mechanism, introduced in the previous section and depicted in (Sch. **2.4**, Sec. **2.8**). On the other hand, a positively charged model complex of the protonated acetone, one water molecule and neutral QH_2 was employed to study the role of protonated acetone in the proton transfer step (Fig. **2.11**, Sec. **2.11**). It is clear that both protonated acetone as well as the $[QH]^-$ anion in the zwitterionic complex together energetically support the proton-transfer step. Therefore, the obtained energy barriers for PT in the cationic and anionic model complexes are each higher than they are in the original zwitterionic intermediate (Sch. **2.3**), while the barriers for PT in the anionic complexes correspond to the true barriers in the case of the anionic mechanism (Sch. **2.4**).

2.10 Proton Exchange via Anionic Intermediates

For the investigation of the possible role of anionic clusters in the proton exchange, the complex $[C_3H_6O{\bullet\bullet\bullet}H_2O{\bullet\bullet\bullet}QH]^-$ has been constructed (Fig. **2.10A**). Calculation of the minimum energy pathway for the proton transfer from the methyl group of acetone to the water molecule reveals a concerted double proton transfer of the second water proton to the $[QH]^-$ anion via the transition state shown in Fig. **2.10A**. The product of this reaction path is a complex of the neutral QH_2, and acetone anion $[C_3H_5O]^-$ with the H-bonded neutral water molecule between them. The calculated activation enthalpy for this proton transfer amounts to 13.9 kcal mol^{-1} (Tab. **2.4**, see below) at the MP2/cc-pVTZ//MP2/6-31G(d,p) level of theory

with ZPVE calculated at MP2/6-31G(d,p). The concerted scenario in this case can be rationalized by comparison of the deprotonation enthalpy of acetone and the proton affinity of water, the potential intermediates of a step-wise process (the relevant DE and PA are given in Tab. **2.**3 (Sec. **2.7**). Since the difference between the DE and PA is about 207 kcal mol^{-1} higher in energy than the barrier for the concerted transfer, the step-wise PT via the intermediate hydronium cation $[H_3O]^+$ is unlikely to occur.

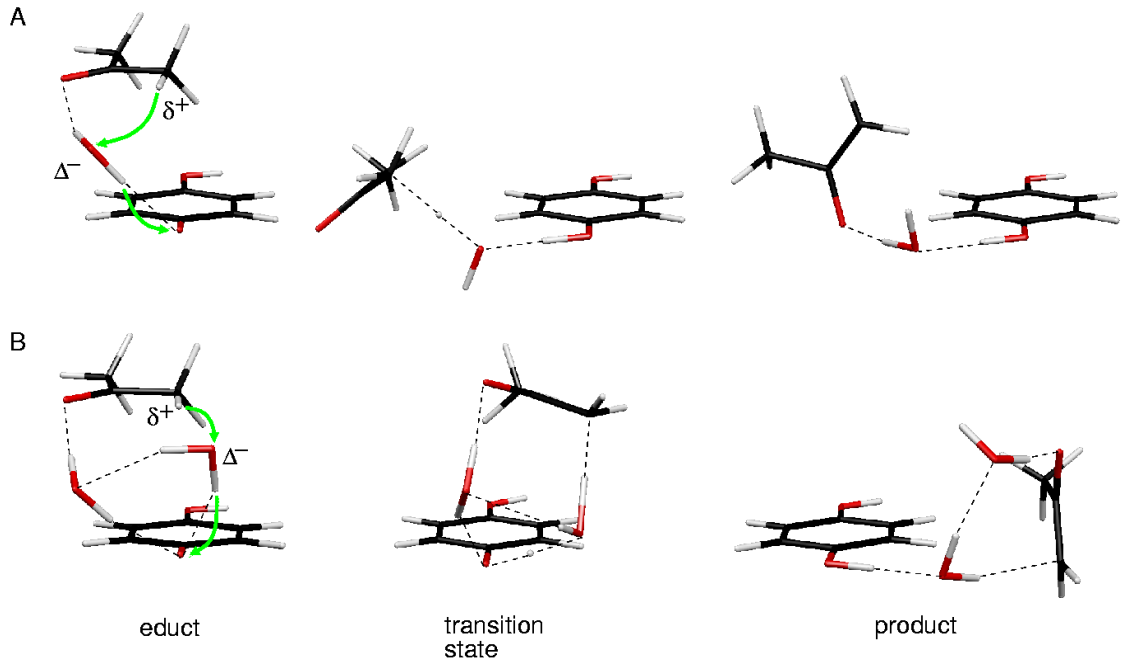

Figure 2.10. Reactants, transition states and products of the proton transfer pathways from the acetone methyl group to deprotonated hydroquinone $[QH]^-$ in $[C_3H_6O{\cdots}H_2O{\cdots}QH]^-$ (A) and $[C_3H_6O{\cdots}(H_2O)_2{\cdots}QH]^-$ (B) clusters respectively. The arrows highlight the proton transfer pathway.

The previous part of this investigation (Sec. **2.3-2.7**), dedicated to PE via a concerted mechanism in neutral complexes, revealed that additional water molecules can significantly exert the efficiency of PT. Following the same idea here, the anionic model complex $[C_3H_6O{\cdots}(H_2O)_2{\cdots}QH]^-$ hydrated by two waters, was studied (Fig. **2.10B**). The complex, again, exhibits concerted double-proton transfer like the complex with one water (Fig. **2.10A**). Again, in course of the reaction, proton is transferred from the methyl group of acetone, and simultaneously the second proton is transferred from the water to $[QH]^-$ via the transition state shown in Fig. **2.10B**. The product of this reaction is a complex of a deprotonated acetone anion and a neutral QH_2 molecule bridged by two water molecules. The calculated activation enthalpy for this pathway is 16.3 kcal mol^{-1}. Compared to the complex $[C_3H_6O{\cdots}H_2O{\cdots}QH]^-$ containing only one bridging water molecule, the barrier is higher by 2.5 kcal mol^{-1}. This

value is close to *ca.* 3 kcal mol^{-1} for the inhibition of the concerted PT via KET by a single solvent water molecule in the neutral $C_3H_6O\bullet\bullet\bullet(H_2O)_2$ complex (Fig. **2.5**, Sec. **2.4**). Thus, one additional solvent water molecule exhibits an anticooperative effect within the anionic mechanism as well.

The physical reason for the increased efficiency of the proton transfer in the anionic complexes, compared to the neutral complexes, studied in Sec. **2.3-2.7**, can be related to the polarization of the proton-donating and proton -accepting groups by the negatively charged $[QH]^-$ anion. This is readily manifested by comparison of the Mullikken charges obtained for the anionic model cluster $[C_3H_6O\bullet\bullet\bullet(H_2O)_2\bullet\bullet\bullet QH]^-$ and its neutral counterpart $C_3H_6O\bullet\bullet\bullet(H_2O)_2\bullet\bullet\bullet QH_2$. The difference of the Mullikken charges between the methyl proton of acetone and the proton-accepting oxygen atom of the adjacent water molecule (see Fig. **2.10A**) is 0.77 in the anionic complex, and only 0.65 in the corresponding neutral cluster (Fig. **2.3**, Sec. **2.4**). This correlates with the difference in the free energy barriers for the proton transfer: 16.8 kcal mol^{-1} in the case of anionic complex *vs.* 32.2 kcal mol^{-1} in the case of neutral cluster. Again, the less efficient PT in the $[C_3H_6O\bullet\bullet\bullet(H_2O)_2\bullet\bullet\bullet QH]^-$ complex can be easily explained in these terms by the influence of the second solvent water, which is not ivolved in the PT directly and depolarize the relevant proton-donating and proton-accepting groups Fig. **2.10B**.

Table 2.4. Energy difference between educt and product (ΔE_{equil}), energy barriers (ΔE_{PT}), free activation energies (ΔG_{PT}) and transfer rates (k_{PT}) calculated at ambient temperature (T=298.15 K) for the proton transfer in $[C_3H_6O\bullet\bullet\bullet H_2O\bullet\bullet\bullet QH]^-$, $[C_3H_6O\bullet\bullet\bullet(H_2O)_2\bullet\bullet\bullet QH]^-$, $[C_3H_6OH\bullet\bullet\bullet H_2O\bullet\bullet\bullet QH_2]^+$ and $C_3H_6O\bullet\bullet\bullet(H_2O)_3$ model clusters. The energies are given in kcal mol^{-1} and have been computed at MP2/cc-pVTZ level at MP2/6-31** optimized geometries. Zero point energy corrections are calculated at the MP2/6-31** level and given in parenthesis.

Complex	ΔE_{equil}	ΔE_{PT}	ΔG_{PT}	k_{PT}
$[C_3H_6O\bullet\bullet\bullet H_2O\bullet\bullet\bullet QH]^-$	4.2 (-0.4)	13.9 (-3.5)	13.0	$1.8*10^{3}$
$[C_3H_6O\bullet\bullet\bullet(H_2O)_2\bullet\bullet\bullet QH]^-$	9.2 (-0.2)	16.3 (-3.7)	16.8	2.9
$[C_3H_6OH\bullet\bullet\bullet H_2O\bullet\bullet\bullet QH_2]^+$	25.8 (-0.7)	25.6 (-2.1)	25.1	$2.6*10^{-6}$
$C_3H_6O\bullet\bullet\bullet(H_2O)_3$	11.5 (-1.2)	29.1 (-1.7)	32.0	$2.3*10^{-13}$

2.11 Proton Exchange via Cationic Intermediates

The last reaction mechanism for the proton exchange considered in this study is the cationic mechanism. It is represented by the cationic model complex of the protonated

acetone, water and neutral QH_2. The proton transfer pathway in the model cluster $[C_3H_6OH\cdots H_2O\cdots QH_2]^+$ is displayed in Fig. **2.11**. The products of the reaction are the neutral enol form of acetone, the hydronium cation H_3O^+ and neutral QH_2. In the course of the transfer, the H-bond between the protonated carbonyl group of acetone breaks and another one is created between the hydronium cation and the methylene group of the neutral enol form of acetone. Computed activation enthalpy for the PT in this pathway is 25.6 kcal mol^{-1} (Tab. **2.4**). In comparison, proton transfer between the neutral acetone and one water molecule is characterized by the energy barrier of 37.5 kcal mol^{-1} (Tab. **2.1**, Sec. **2.4**).

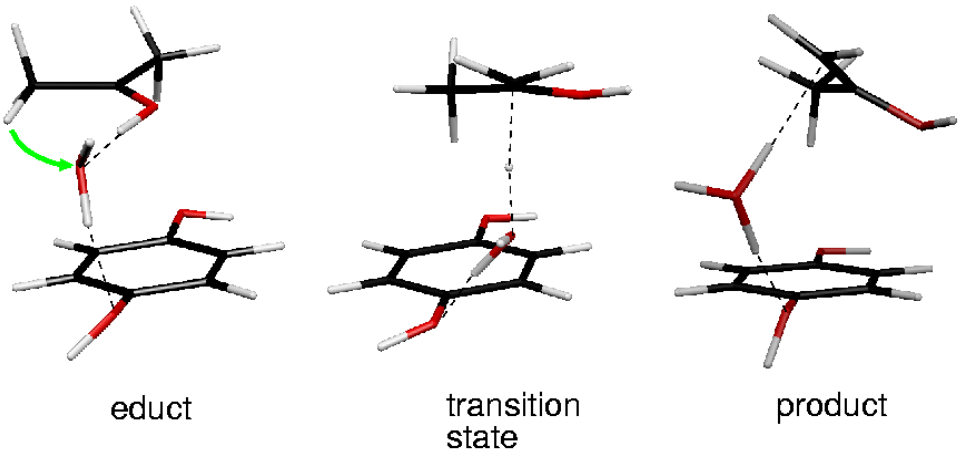

Figure 2.11. Reactant, transition state and product of the proton transfer between the methyl group of protonated acetone cation and water in the cationic complex $[C_3H_6OH\cdots H_2O\cdots QH_2]^+$. The green arrow highlights the proton transfer pathway.

Indeed, the positive charge on acetone increases the rate of the proton transfer similar to the negative charge of $[QH]^-$ considered in the previous section. However, the nature of catalysis in this case is different from the anionic one. The decrease of the barrier in the cationic cluster $[C_3H_6OH\cdots H_2O\cdots QH_2]^+$ now is not due to polarization, but due to the diminished deprotonation energy of the methyl-group of the protonated acetone cation *vs.* the neutral acetone molecule (Tab. **2.3**, Sec. **2.8**). While the deprotonation enthalpy for the neutral acetone is 373 kcal mol^{-1}, it is only 201 kcal mol^{-1} for the protonated one. The larger DE of the neutral acetone can be explained by a stronger electrostatic attraction between the proton and the remaining anion which is weaker in the case of protonated acetone since the remaining acetone is neutral. This case exhibits a special type of catalysis by means of the protonation of acetone carbonyl-group resulting in the weakening of its methyl CH-bond.

2.12 Rate Constants of the Proton Exchange via Ionic Intermediates

The Arrhenius equation (see *e.g.* Ref. **209**) has been employed to calculate proton transfer rates for the three considered ionic model complexes $[C_3H_6O\cdots H_2O\cdots QH]^-$, $[C_3H_6O\cdots(H_2O)_2\cdots QH]^-$ (Fig. **2.10A**, **2.10B**, Sec. **2.10**) and $[C_3H_6OH\cdots H_2O\cdots QH_2]^+$ (Fig. **2.11**, Sec. **2.11**)). The computed free activation energies (at 298.15° K) for the model complexes are 13.0 and 16.8 kcal mol^{-1} for the anionic complexes $[C_3H_6O\cdots H_2O\cdots QH]^-$ and $[C_3H_6O\cdots(H_2O)_2\cdots QH]^-$, respectively, and 25.1 kcal mol^{-1} for the cationic complex $[C_3H_6OH\cdots H_2O\cdots QH_2]^+$ (Tab. **2.4**, Sec. **2.10**). Comparison of these values with the lowest one of 29.1 kcal mol^{-1}, obtained for the proton transfer between the neutral acetone and water via KET, already demonstrates that ionic intermediates reduce the energy barriers considerably.

Calculated proton transfer rates for the ionic complexes are 1.8×10^3, 2.9 and 2.3×10^{-6} M^{-1} s^{-1} for the $[C_3H_6O\cdots H_2O\cdots QH]^-$, $[C_3H_6O\cdots(H_2O)_2\cdots QH]^-$ and $[C_3H_6OH\cdots H_2O\cdots QH_2]^+$, respectively. However, since CHQ (and its prototype QH_2) is a weak acid these results must be scaled by the equilibrium concentrations of the deprotonated QH_2 and protons, which can be easily estimated to be *ca.* 10^{-5} from the pK_a-value of QH_2 of 9.8. This leads to the effective rates of 1.8×10^{-2}, 2.9×10^{-5} and 2.6×10^{-11} M^{-1} s^{-1} respectively. Indeed, the rates of the anionic mechanism (1.8×10^{-2} and 2.9×10^{-5} M^{-1} s^{-1}) are comparable with the characteristic rates of the proton exchange in the NMR experiments on CHQ aggregates, and finally can explain the observation of acetone-water proton exchange in CHQ aggregates.

2.13 Catalysis of Acetone-Water Proton Exchange by Strong and Weak Acids in Aqueous Solutions

Summarizing the above findings, several remarks on general acid catalysis of acetone-water proton exchange can be made.

The analysis of the computed proton affinities (Tab. **2.3**, Sec. **2.8**), as well as the results of the calculations on the protonated hydrated acetone clusters (Sec. **2.8**), suggest that protonated acetone species are unstable in water-rich solutions of acetone and acids (either weak or strong), since larger protonated water aggregates have higher PA than protonated acetone-water clusters. Therefore, one can assume that catalysis through the anion of the dissociated acid (in this case the $[QH]^-$ anion), presented in Sch. **2.4**, Sec. **2.8**, would be a prevalent mechanism under acidic conditions. Moreover, the calculations on the anionic model complexes $[C_3H_6O\cdots H_2O\cdots QH]^-$ and $[C_3H_6O\cdots(H_2O)_2\cdots QH]^-$ have shown that the energy barrier for PT will increase by 2.5 kcal mol^{-1} upon the addition of a second solvent water

molecule. One can further estimate the barrier of this proton exchange in aqueous solution to be close to about 20 kcal mol^{-1} due to the anticooperative effect of excess solvent water molecules. In fact, the activation energy for KET of acetone catalyzed by perchloric acid, measured previously, amounts to 20 kcal mol^{-1} (Ref. **195**). This barrier leads to a rate constant of about 10^{-2} M^{-1} s^{-1} for the rate-limiting proton-transfer step from the methyl group of acetone to the anion of the dissociated acid. Analogously to CHQ, the observed rate of proton transfer will depend on the concentration of anions $[A^-]$, *i.e.* $k_{PT}^{eff} = [A^-]\times 10^{-2}$ M^{-1} s^{-1}.

These arguments eventually allow to distinguish between the limiting cases of weak and strong acids. In the former case only a fraction of the acid molecules is dissociated and hence should be scaled by $[A^-]$. In the latter case, essentially all acid molecules are dissociated ($[A^-]\sim 1$) and the PE rate is faster since it does not need to be scaled with a predissociation factor as in the case of weak acids. Consequently, in the presence of a strong acid proton exchange between acetone and water occurs with an observable rate close to 10^{-2} M^{-1} s^{-1} and should therefore be easily observable in the appropriate NMR experiments. In the presence of weak acids like QH_2, the reaction is much slower in 1 M solution since the calculated rate has to be scaled by a factor of $[A^-] \sim 10^{-5}$. This leads to a substantial decrease of the rate and makes it problematic to observe the proton exchange at the conditions of the NMR experiment.

2.14 Summary and Conclusions

In the present study, two principal mechanisms of the unique catalytic proton exchange between water and acetone, trapped in CHQ aggregates, have been investigated in detail.

The first suggested mechanism, responsible for the exchange in specific proton-transfer networks, similar to those presented in CHQ, is proton transfer via *keto-enol tautomerism* (Sec. **2.3-2.7**). The proton transfer was assumed to occur via initially *neutral* moieties and hence supposed to be *concerted*. The mechanism was explicitly studied employing model complexes of acetone, hydrated by few water molecules, as well as the complexes comprising QH_2 (served a molecular model for CHQ), acetone and one or two water molecules. It was shown, that in these networks, *bifunctional* OH-groups of water and/or of CHQ, indeed catalyze tautomeric proton transfer. Herein, the free Gibbs energy is dramatically reduced from 64 kcal mol^{-1} for the KET in isolated acetone, to *ca.* 30 kcal mol^{-1} for the transfer assisted by three water molecules. In this case, catalysis by the OH-groups involved in the proton transfer can be explained by their *cooperative* effect in polarization of proton donating/accepting groups of acetone. Furthermore, catalysis assisted by only few OH-groups appears to be about 10 kcal mol^{-1} more efficient than that in aqueous solutions. The latter was

explained by the depolarizing *anticooperative* effect of *solvent* water molecules which are not involved in the transfer. Since the CHQ aggregates, exhibiting proton exchange, are naturally *water-deficient*, one can conclude that the efficiency of the proton- exchange via concerted KET in CHQ is close to its best values observed in the model gas-phase clusters with only a few catalytic waters involved.

Nevertheless, the rate constant for the concerted mechanism, corresponding to the most efficient case of KET, assisted by three waters, is 10^{-13} M^{-1} s^{-1} at room temperature. Obviously, this value is too low to explain the observation of proton exchange at the conditions of the NMR experiments. This motivated for an investigation of the alternative *step-wise* mechanisms via formation of the *ionic* intermediates, based on the *weak acidity* of CHQ. To that end, two ionic mechanisms of proton transfer, triggered by the dissociation of CHQ OH-groups, have been studied (Sec. **2.8-2.13**). To simulate these mechanisms, the *protonated* cationic $[C_3H_6OH{\bullet\bullet\bullet}H_2O{\bullet\bullet\bullet}QH_2]^+$ and *deprotonated* anionic complexes $[C_3H_6O{\bullet\bullet\bullet}H_2O{\bullet\bullet\bullet}QH]^-$, $[C_3H_6O{\bullet\bullet\bullet}(H_2O)_2{\bullet\bullet\bullet}QH]^-$ were chosen upon the inspection of possible proton absorption sites in the proton-transfer networks of the CHQ aggregates. The feasibility of the dissociation of CHQ at room temperatures was explicitly confirmed by the partial geometry optimization of the *zwitterionic* complex $[C_3H_6OH]^+{\bullet\bullet\bullet}(H_2O)_2{\bullet\bullet\bullet}[QH]^-$ with the constrained covalent bond between the proton and carbonyl oxygen of the acetone molecule.

Computed energy barriers for the ionic proton transfer prove to be substantially smaller than those for the concerted one with activation free energies of only 13.0 and 16.8 kcal mol^{-1} in the most favorable cases of $[C_3H_6O{\bullet\bullet\bullet}H_2O{\bullet\bullet\bullet}QH]^-$ and $[C_3H_6O{\bullet\bullet\bullet}(H_2O)_2{\bullet\bullet\bullet}QH]^-$ anionic complexes. The corresponding proton transfer rates are 1.8×10^{-2} and 2.9×10^{-5} M^{-1} s^{-1}. The rates were scaled by the concentration of dissociated CHQ, owing to its weak acidity, estimated to be *ca.* 10^{-5}. In the case of isolated protonated acetone complex $[C_3H_6OH{\bullet\bullet\bullet}H_2O{\bullet\bullet\bullet}QH_2]^+$, the barrier of the reaction of 25.1 kcal mol^{-1} could, in principle, provide the proton exchange at room temperatures. However, after the scaling by the concentration of predissociated CHQ in the CHQ aggregates, this mechanism itself yields a negligible rate. Indeed, the rates associated with the anionic mechanisms are high enough to explain the observation of acetone-water proton exchange during several hours of the NMR experiments.

Herein, depending on the hydration of the CHQ OH-groups, the interplay of two principal ionic mechanisms, either involving the anionic complexes like $[C_3H_6O{\bullet\bullet\bullet}(H_2O)_2{\bullet\bullet\bullet}QH]^-$or the zwitterionic complex $[C_3H_6OH]^+{\bullet\bullet\bullet}(H_2O)_2{\bullet\bullet\bullet}[QH]^-$, can take place. The latter mechanism should be more efficient or even *barrierless* than the former one due to the presence of an

uncompensated protonated acetone cation. In contrast, in *aqueous solutions* of acids the anionic mechanism is less efficient than in the *isolated* $[C_3H_6O\bullet\bullet\bullet H_2O\bullet\bullet\bullet QH]^-$ and $[C_3H_6O\bullet\bullet\bullet(H_2O)_2\bullet\bullet\bullet QH]^-$ clusters due to the anticooperative effect of solvent water dipoles, and approaches to *ca.* 20 kcal mol^{-1}. One should notice that the *inhibiting* effect of solvent water in the case of anionic mechanism is similar to that observed in the neutral clusters via concerted KET mechanism.

These results perfectly explain why proton exchange via ionic mechanism was not observed in the aqueous solution of acetone and weakly-acidic QH_2 (having similar acidity as CHQ) and eventually allow to indentify the ionic mechanism as responsible for the proton exchange in water-deficient CHQ aggregates.

Generalizing the above findings, proton exchange should also be observable in the gas-phase acetone-water-QH_2 clusters, similar to those used for the simulations of concerted KET. This is due to the aforementioned feasibility of the formation of zwitterionic complex $[C_3H_6OH]^+\bullet\bullet\bullet(H_2O)_2\bullet\bullet\bullet[QH]^-$ at room temperature, as well as due to the lack of solvent water, suppressing the proton transfer catalyzed by the ions of $[C_3H_6OH]^+\bullet\bullet\bullet(H_2O)_2\bullet\bullet\bullet[QH]^-$. Additionally, protonated acetone-water complex $[C_3H_6OH\bullet\bullet\bullet H_2O\bullet\bullet\bullet QH_2]^+$ should exhibit proton exchange in the gas phase as well, since in this case its rate should not be scaled by the predissociation of CHQ, delivering protons.

The results obtained in Sec. **2.8-2.13** also have consequences for the understanding of acetone-water proton exchange in aqueous solutions of acids. They allow to distinguish the cases of strong and weak acids. It was shown that protonated acetone is unstable in the aqueous solution. Therefore, acetone-water proton exchange most probably will be catalyzed by the anions of dissociated acid. In the limiting case of weak acids only a fraction of the acid molecules is dissociated. Thus, predissociation of acid, determining the concentration of catalytic anions in the system is the limiting factor of proton exchange. Contrarily, in the case of strong acids, essentially all acid molecules will be dissociated and, hence, the proton-exchange rates will be determined by the activation energy of reaction itself, without further scaling by the dissociation rates. As a consequence, proton exchange should be easily observable in the relevant NMR experiments.

In conclusion of Chapter **2**, several important observations gained during the study and directly related to the main topic of the thesis, *i.e.* influence of water *microsolvation* on the proton-transfer processes, will be highlighted.

1.1. As it was shown upon the example of acetone-water proton transfer simulations via concerted keto-enol tautomerism, the role of water in this and similar proton transfer reactions is twofold. On one hand, water molecules are bifuncional and hence can be involved in the proton-transfer reactions as proton donors/acceptors. Since each water molecule at the same time bears a permanent dipole moment, the efficiency of the proton transfer can be significantly improved by *polarization* of the relevant groups, involved in the reaction. These water molecules, hence, possesses a *catalytic* function in the proton-transfer processes. On the other hand, the water molecules which are not involved in proton transfer (*i.e.* the *solvent* molecules) can *depolarize* the involved reagents and, therefore, suppress the reaction. These waters exhibits a property of the *inhibitor* of proton transfer, shared with many other *polar* solvents. Therefore, bifunctionality of water molecules is the main reason why it behaves differently from those polar solvents, which cannot participate in the proton-transfer reactions.

1.2. In comparison to the case of water catalysis (1.1), acetone-water proton transfer can be further accelerated by addition of *ionic* species into the system. In the present study, the phenomenon was observed in the predissociation of weakly-acidic CHQ which catalyzes the acetone-water proton-exchange reaction. Herein, proton transfer, leading to the catalytic proton exchange, can be treated as a *step-wise* keto-enol tautomerism via formation of ionic intermediates. In particular, addition of acidic anions into the system decreases the activation energies associated with the transfer, due to the polarization of proton-transfer reagents by the acidic anions. Since the origin of catalysis can in this case be attributed to the polarization of reagents by anions, solvent water again can inhibit proton transfer, analogously to the case of water catalysis. Furthermore, protons, resulting from the dissociation of catalytic acids can form the covalently-bound cationic complexes with the reagents of the proton transfer reaction (in particular, with the carbonyl oxygen of acetone). It alters the electronic structure of the reagent and weakens the methyl CH-bond, involved in the proton transfer between acetone and water. In this case, solvent water aggregates can also decrease the efficiency of the proton transfer reaction. However, the reason for that is not the depolarization of reagents itself, but rather the *abstraction* of protons from the reagents by larger water aggregates having larger *proton affinity*.

In summary, catalysis of proton-transfer reactions of various mechanisms can be optimized with respect to the number and specific binding patterns of water molecules involved. More efficient reaction scenarios can often be observable in the gas-phase experiments only, since in aqueous (polar) solutions the reactions will be suppressed by the action of solvent water.

The results summarized above elucidate the mechanism of acetone-water proton exchange and similar proton transfer processes in great detail. This eventually allows to clarify the catalytic role of CHQ macromolecules in this process to be the following.

2.1. Only one guest reactant molecule (acetone) is trapped by one bowl-shaped CHQ monomer. This allows its embedding into the H-bonded networks favourable for the proton transfer between the guest molecule and incorporated waters molecules. Due to the strong dispersion interaction between acetone and CHQ monomers, these catalytic networks gain additional stability.

2.2. The OH-groups of weakly-acidic CHQ can dissociate and deliver ionic intermediates (protons and anions) into the networks, which further improve the efficiency of the reaction.

2.3. Due to several structural factors, in particular, the presence of spatially-separated OH-groups, the CHQ aggregates are *naturally water-deficient*. Water-deficiency prevents from the formation of large solvent assemblies, which can inhibit proton-transfer reactions in the ways outlined in (1) and (2).

Therefore, CHQ and similar guest-host macromolecular architectures with *desolvation* function can provide conditions similar to those occurring in gas-phase experiments. It hence allows for an *optimal control* of various proton-transfer reactions, otherwise missed in aqueous solutions.

Chapter 3

Specific Microsolvation Triggers Dissociation-Mediated Red-Shifted Fluorescence of Methyl 4-*N*,*N*-dimethylaminobenzoate Ester in the Gas Phase

3.1 Introduction

Methyl 4-*N*,*N*-dimethylaminobenzoate ester (DMABME) (Sch. **3.1**) belongs to the *donor-acceptor* substituted benzene derivatives which undergo *intramolecular charge transfer* (ICT) after excitation into the first electronically-excited state. In the ICT state, the nitrogen of its amino group acts as an electron donor, while the oxygen of the carbonyl group – as an electron acceptor. Further electron transfer from the donor to acceptor imparts the system a large electric dipole moment as compared to the ground state. In polar solvents DMABME exhibits *dual fluorescence* with an additional *red-shifted* band (Ref. **18**).

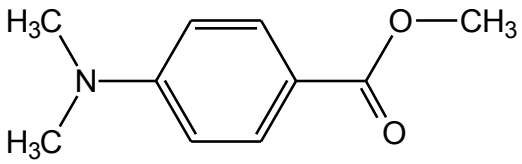

Scheme 3.1. Methyl 4-*N*,*N*-dimethylaminobenzoate ester (DMABME).

Historically, the phenomenon of dual fluorescence in polar solvents was initially discovered in another electron donor-acceptor derivative – 4-*N*,*N*-dimethylaminobenzonitrile (DMABN) (Ref. **210**). This species also possesses the dimethylamino group (electron donor) but the ester function is replaced by a nitrile group (electron acceptor). Since then, many experimental and theoretical efforts have been undertaken to elucidate the underlying molecular mechanism, responsible for the observed red-shifted fluorescence. It will be informative to briefly summarize these findings for a better understanding the situation in DMABME.

At present, it is well-established that the formation of a ICT state is responsible for the red-shifted additional fluorescence in polar environments (Ref. **9**, **18**), since the back electron transfer is suppressed due to the large structural changes in the ICT state. However, the detailed molecular structure of the fluorescing ICT state has been questionable for a long time. By now, several structural configurations of DMABN have been suggested to be

responsible for the additional red-shifted fluorescence: a *twisted* ICT (TICT) (Ref. **211**, **212**, **213**), a *planar* (PICT) (Ref. **214**, **215**), a *rehybridized* (RICT) (Ref. **216**, **217**) or a *wagged* (WICT) (Ref. **218**) configurations. The TICT and PICT states seem to be the most promising alternatives. These conformations of DMABN are also relevant for DMABME due to their structural relation.

Recent high-level *ab-initio* calculations on the excited states of DMABN revealed that the initially excited S_2 state, also referred as L_a, or the CT state, decays rapidly into the S_1 state termed *locally excited* (LE), or L_b state, via a *conical intersection* (Ref. **219**). Conical intersections are special but ubiquitous topologies of the excited-state potential energy surfaces where two states become degenerate. In general, conical intersections are responsible for the ultra-fast *nonradiative decay* processes of excited states (Ref. **220**). Indeed, it has been shown that the S_2/S_1 conical intersection is spatially and energetically very close to a planar minimum on the S_2 surface of DMABN (Ref. **219**), which allows for an ultrafast *radiationless* transition from the S_2 to the S_1 PES. On the S_1 surface, two minima are then accessible: a planar and a TICT structure. These two states hence correspond to two structural isomers of the same electronic S_1 state. In particular, the local planar minimum of the S_1 state has been assigned to a PICT state, combining the PICT and TICT models in one general mechanism for dual fluorescence in DMABN (Ref. **219**). Therefore, one can conclude that the occurrence of dual fluorescence in this and related donor-acceptor systems is controlled by the shape of the S_1 potential energy surface. It eventually depends on the relative energies of the two minima and the height of the energy barrier connecting them. These aromatic systems thus can be further classified into four groups, depending on the relative vertical excitation energies of the CT and LE states, as well as on the stabilization energy of the ICT (Ref. **221**).

Until recently, most of the experimental studies on the ICT of DMABME and similar donor-acceptor systems have been performed in solution, whereas the relevant theoretical models for understanding the effect either neglect the environment, or consider it as a *dielectric/polar continuum* (Ref. **9**, **18**). According to the models, it is assumed that the electrostatic field of a *polar* solvent stabilizes the formed ICT state due to its large dipole moment, thereby reducing the energy barrier from the LE state to the ICT state thus leading to dual fluorescence. Contrarily, an *apolar* solvent does not open the ICT channel (at least in DMABN) and hence dual fluorescence is not observed. Such an interpretation is only justified when the influence of solvent on the ICT mechanism is similar to that of a dielectric or polar continuum *i.e.* it does not have a *direct* influence on the structural or electronic properties of the molecules. In general, however, solvent molecules can directly exert ICT and dual

fluorescence (Ref. **11**, **222**, **223**). This point becomes immediately evident in context of the previous example of acetone-water proton exchange in CHQ (Chap. 2) which demonstrated that the role of solvent water in different proton-transfer reactions is not at all reproduced by a polar continuum.

Indeed, recent gas-phase experiments on donor-acceptor benzene derivatives demonstrate that dual fluorescence, common in polar solvents, is rather an exception in the *isolated* molecules (Ref. **9**). For example, jet-cooled studies on 4-*N*,*N*-diisopropylaminobenzonitrile (DIABN) detected the excited state ICT, although a red-shifted emission band was not observed under these experimental conditions (Ref. **224**). In the case of DMABN, at least five molecules of acetonitrile (the solvent) are necessary to induce red-shifted CT emission (Ref. **223**).

Earlier experimental studies of DMABME using a combination of *mass spectroscopy* and *laser-induced fluorescence* (LIF) spectroscopy recognized that at least one water molecule is necessary to stimulate dual fluorescence (Ref. **225**, **226**, **227**). It was suggested that the TICT formation is the key mechanism for the observed red-shifted fluorescence. The process is supported by microsolvation and mixing of the low-lying electronic states. Early calculations (Ref. **228**) also corroborated the suggested mechanism. Unfortunately, the employed experimental technique can only give a lower limit of the actual minimum cluster size that generates the corresponding laser-induced fluorescence spectrum. This did not allow to give an ultimate answer of how many water molecules are required for the occurrence of dual fluorescence.

To circumvent this limitation, another more accurate experiment combining LIF, *resonant two-photon ionization* (R2PI) spectroscopy and *infrared* (IR) *ion depletion spectroscopy* on DMABME clusters hydrated by one to three water molecules were performed in an ultracold supersonic jet beam (Ref. **2**). This powerful technique allows not only to establish the minimal number of water molecules necessary for dual fluorescence, but also to get the IR *footprints* of particular isomers responsible for the fluorescence, by means of IR depletion spectroscopy. Here and further, the complexes hydrated by n waters are designated as "DMABME•••$(H_2O)_n$". In the experimental terminology, this designation is equivalent to the "1:n" complex. This experimental study has demonstrated that two water molecules are needed to induce dual fluorescence at 325 and 425 nm (Fig. **3.1c**, left) (Ref. **229**). For the 1:1 complex (Fig. **3.1b**, left), red-shifted fluorescence is present only in a marginal amount. Moreover, the IR spectra revealed that two different isomers of the DMABME•••$(H_2O)_2$ complex are formed in the jet-beam (ion-depletion spectra) and only one of them is

responsible for the observed red-shifted fluorescence (fluorescence-depletion spectra). On the basis of the experiments alone, an unambiguous assignment of the vibrational bands to different isomers was not possible. In particular, the isomer which is responsible for the observed red-shifted fluorescence could not be identified. Furthermore, interpretation of the fluorescence spectrum requires the knowledge of the excited-state PES of the complexes what calls for computational support.

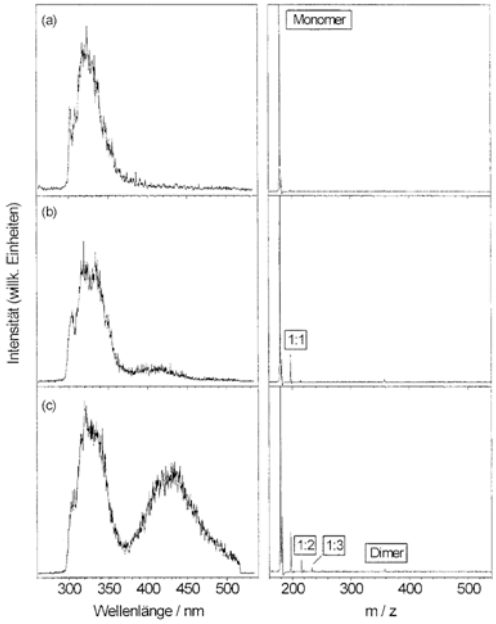

Figure 3.1. Gas-phase fluorescence (left) and mass (right) spectrum of DMABME (a), DMABME•••H_2O (b), DMABME•••$(H_2O)_2$ (c) complexes[1].

In this chapter the results of our computational investigation of the IR spectra of the DMABME•••$(H_2O)_2$ complexes, as well as of the excited states of isolated DMABME and DMABME•••$(H_2O)_2$, employing high-level quantum-chemical methodology are presented. The particular isomer of DMABME•••$(H_2O)_2$ responsible for the red-shifted fluorescence is identified. The mechanism of fluorescence in isolated DMABME, as well as in its 1:*n* (*n*=1-2) complexes is studied in detail. Hence, the direct influence of individual water molecules on the electronic and structural properties of DMABME in the CT state is illuminated. Furthermore, a complimentary benchmark study of the influence of electron correlation, anharmonic and basis-set effects on IR spectra of prototypical H-bonded systems, similar to the hydrated complexes of DMABME, has been conducted (Sec. **3.7**).

[1] Reproduced from Ref. **229**.

3.2 Theoretical Methods

One primary aim of this study is the assignment of the ground-state IR depletion spectra of the hydrated DMABME complexes to its particular isomers. In Sec. **1.4.3** it was pointed out that potential energy surfaces and, hence, IR spectra of noncovalently-bound complexes (*e.g.* H-bonded and Van der Waals) are especially sensitive to the basis-set superposition error (BSSE). Furthermore, electron correlation effects are pronounced at the characteristic distances of noncovalently-bound complexes (Sec. **1.2.3**). These arguments call for a BSSE-corrected correlated theoretical treatment of PES and IR spectrum of the H-bonded hydrated DMABME complexes.

Due to the large size of the complexes, the only applicable correlated *ab-initio* method is second-order Møller-Plesset perturbation theory (MP2) (Sec. **1.2.4**) combined with medium-sized basis sets. In particular, the minimum energy structures and harmonic frequencies of hydrated DMABME clusters were computed at the level of MP2 with the split-valence 6-31G(d,p) basis set (Sec. **1.4.1**) on the PES corrected for BSSE by means of the CP procedure (Sec. **1.4.3**). The latter implies that the CP correction was applied to both energy gradients during the geometry optimizations and to harmonic frequencies calculations. To underline this fact, the designation "CP-PES MP2" is introduced herein. Zero-point vibrational energy (ZPVE) (Sec. **1.1.4**) was taken into account at the level of CP-PES MP2/6-31G(d,p) to include nuclear effects in the relative and stabilization energies of the different DMABME•••$(H_2O)_2$ clusters.

The accuracy and reliability of this theoretical approach was extensively studied by benchmark calculations on small model clusters comprising the formic acid-water and ammonia-water complexes. These model complexes were chosen to reproduce those types of hydrogen bonds (carbonyl-water and amino-water) which are responsible for the assignment of the IR spectra of the DMABME•••$(H_2O)_2$ complexes. For these systems, theoretical levels of up to CP-PES CCSD/cc-pVTZ and CP-PES MP2/cc-pVQZ were tested (for details see Sec. **3.7**). The calculations revealed that the energetic ordering between the relevant OH stretch vibrations is nicely preserved at all levels of theory. Therefore, one can rely on CP-PES MP2 calculations with moderate 6-31G(d,p) basis set in the interpretations of the experimental IR spectra of the DMABME•••$(H_2O)_2$ clusters. Furthermore, since the benchmark complexes cover common H-bonds, the findings also allow to draw the general conclusion that BSSE-corrected potential energy surfaces, obtained with second-order perturbation theory level and moderate basis sets, are able to reproduce IR spectra of typical H-bonded systems with sufficient accuracy.

To allow for a direct comparison of the computed harmonic vibrational frequencies with the measured ones, the former were empirically scaled by factors of 0.946 and 0.940 for each isomer of the 1:2 complex. The factors were derived by comparison of the OH vibrations of two most stable DMABME•••H_2O isomers (1:1 complex), computed at the CP-PES MP2/6-31G(d,p) level, with their experimental values (see Sec. **3.7**). After the application of these shift factors to the computed OH stretch vibrations of DMABME•••$(H_2O)_2$ an excellent agreement between experiment and theory was achieved.

For the investigation of the optical properties of isolated and hydrated DMABME complexes, the two lowest excited electronic states of the complexes have been calculated using linear-response TDDFT level of theory (Sec. **1.3.2**, **1.3.5**) and were further improved by single-point calculations at the level of linear-response approximated coupled-cluster with singles and doubles, the so-called CC2 model (Ref. **230**, **231**, **232**) (see Sec. (**1.3.3**) for the linear-response coupled-cluster formalism). The equilibrium structures on the S_1 potential energy surface were optimized employing TDDFT with the B3LYP functional and TZVP basis set (triple-zeta basis augmented with polarization functions (Sec. **1.4.1**)). For consistency, the ground-state structures were also reoptimized at the DFT/B3LYP/TZVP level. Comparison of the ground state geometries of the relevant isomers of the (1:2) complex, computed at the CP-PES MP2/6-31G(d,p) and DFT/B3LYP/TZVP levels, showed that the change in geometrical parameters is small, in particular for the relevant hydrogen bonds. The maximum deviation is about 0.05 Å. One may predict that this trend will hold for the excited-state calculations as well. Nevertheless, one cannot generally expect that TDDFT/B3LYP yields reliable excited-state structures in systems with strong CT character (Sec. **1.3.6**). Therefore, the influence of HF exchange in the employed hybrid *xc*-functionals, on the geometrical parameters of the TICT structure was studied by geometry optimization with the B3LYP and BHLYP *xc*-functionals. The geometrical parameters appears to be practically independent of the amount of HF exchange, when at least 20% of HF exchange is included in the *xc*-functional, *i.e.* when at least B3LYP is employed. The largest difference is observed for the CN bond length connecting the amino group with the benzene ring. The bond has a length of 1.44 and 1.40 Å using the B3LYP and BHLYP *xc*-functionals, respectively. With increasing amount of HF exchange, the bond length becomes shorter due to the improved description of the electrostatic interaction between the separated charges in the CT state. However, the difference in the bond length has no effect on the relative position and shape of the computed excited-state surfaces. Thus, one can rely on the structures obtained with TDDFT/B3LYP.

In summary, the calculated excitation energies agree very favourably at the TDDFT/B3LYP and CC2 levels for the planar geometries. Only for the TICT states they deviate by approximately 0.8 eV. This is clearly due to the well-known CT failure of TDDFT (Sec. **1.3.6**) resulting in a strong underestimation of the excitation energies of the charge-transfer excited states. The minimum energy pathways for TICT formation in the most stable DMABME•••$(H_2O)_2$ isomers were computed at the level of TDDFT/B3LYP on the excited state PES along the dihedral angle attributed to the twist of the dimethylamino group. Again, owing to the CT failure of TDDFT for the vertical excitation energies observed in the TICT states, CC2 single-point calculations along the TDDFT/B3LYP optimized reaction pathway were performed to correct for it.

Ground state IR spectra were computed with the Gaussian 03 software package (Ref. **204**) where the CP-corrected gradients and second derivatives are implemented. The excited-states calculations employed TURBOMOLE 5.7 (Ref. **233**).

3.3 Assignment of the Infrared Spectra of DMABME•••$(H_2O)_2$ Complexes

In the previous sections it was mentioned that two water molecules are required to induce dual fluorescence of DMABME with peaks at wavelengths of 325 and 425 nm (Fig. **3.1**, Sec. **3.1**). The IR ion-depletion spectrum of the complexes with two water molecules (1:2) comprises four distinct bands at 3466, 3514, 3525 and 3550 cm^{-1} corresponding to the H-bonded OH stretch vibrations, and two bands at 3718 and 3724 cm^{-1} representing the free OH stretches (Fig. **3.2**). Therefore, two structural isomers of DMABME•••$(H_2O)_2$ are present in the molecular beam in approximately equal amounts. However only one of them with the bands of 3466, 3525 and 3718 cm^{-1} is responsible for the red-shifted CT emission.

To identify those two isomers which contribute to the IR spectrum of the beam (Fig. **3.2a**), five energetically lowest isomers of DMABME•••$(H_2O)_2$ were computed. All isomers were obtained by stationary-point searches on the ground-state PES and are verified by an analysis of their Hessian matrices (Sec. **1.1.3**). The isomers vary in the binding pattern of the water molecules to DMABME. In isomer **I**, the water dimer is bound to the amino nitrogen, while in isomer **II** it is connected to the carbonyl oxygen of the ester function (Fig. **3.3**). In isomer **III** (not shown) the water dimer is connected to the ether oxygen of the ester function. Another two possibilities is to split the water dimer and either attach one water to the carbonyl oxygen and one to nitrogen (isomer **IV**, not shown), or one water to the ether oxygen and another one to nitrogen (isomer **V**, not shown).

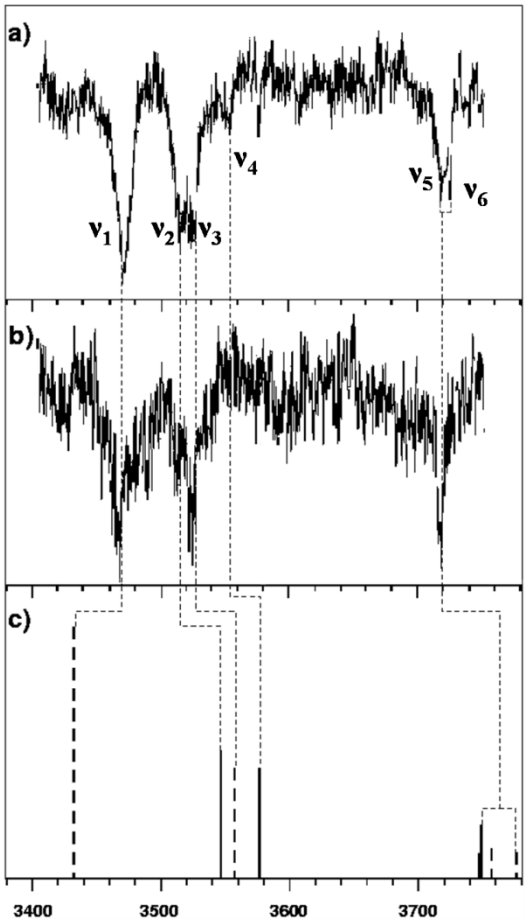

Figure 3.2. a) IR ion depletion spectra of a mixture of two isomers of DMABME·$2H_2O$ b) IR spectrum of the species responsible for CT emission measured as depletion of the red-shifted fluorescence c) calculated IR spectrum at the level of CP corrected MP2/6-31G(d,p). Dashed lines correspond to isomer **I** and solid lines to isomer **II**.

The analysis revealed that isomers **I** and **II** are the two most stable isomers of the series and being practically equal in energy (Tab. **3.1**). At the level of CP-PES MP2/6-31G(d,p) with ZPVE included, isomer **II** is slightly more stable than isomer **I** – by 0.08 kcal mol^{-1}, while at the level of single-point CP MP2/cc-pVTZ on the CP-PES MP2/6-31G(d,p) equilibrium geometry, it is -0.01 kcal mol^{-1} lower in energy. Isomer **III** is about 2 kcal mol^{-1} less stable at both levels of theory, while isomers **IV** and **V** are 3 and 6 kcal mol^{-1} higher in energy than isomers **I** and **II**, respectively (Tab. **3.1**). Since isomers **I** and **II** are nearly isoenergetic and clearly are the energetically lowest isomers, one can conclude that these two ones are observed in equal amounts in the jet-cooled beam of the IR depletion experiment. This will be further confirmed by calculations of their IR spectra.

In the case of DMABME•••H_2O, the two most stable isomers are again those where the water monomer is attached to either the amino nitrogen, or to the carbonyl oxygen. The optimized structures of isomers **I** and **II** of DMABME•••$(H_2O)_2$ are displayed in Fig. **3.3**.

Although the geometrical parameters (*i.e.* the bond distances) of the DMABME molecules within the 1:2 complexes are essentially identical, in the isomer **I** the hydrogen bonding of water dimer to the amino group leads to a strong pyramidalization of the nitrogen, and a further pre-twist of the group as a whole (Fig. **3.3**). In contrast, in isomer **II** the amino group is essentially planar and only slightly pyramidalized. The same trend is observed in the isolated DMABME, as well as in both isomers of the 1:1 complex.

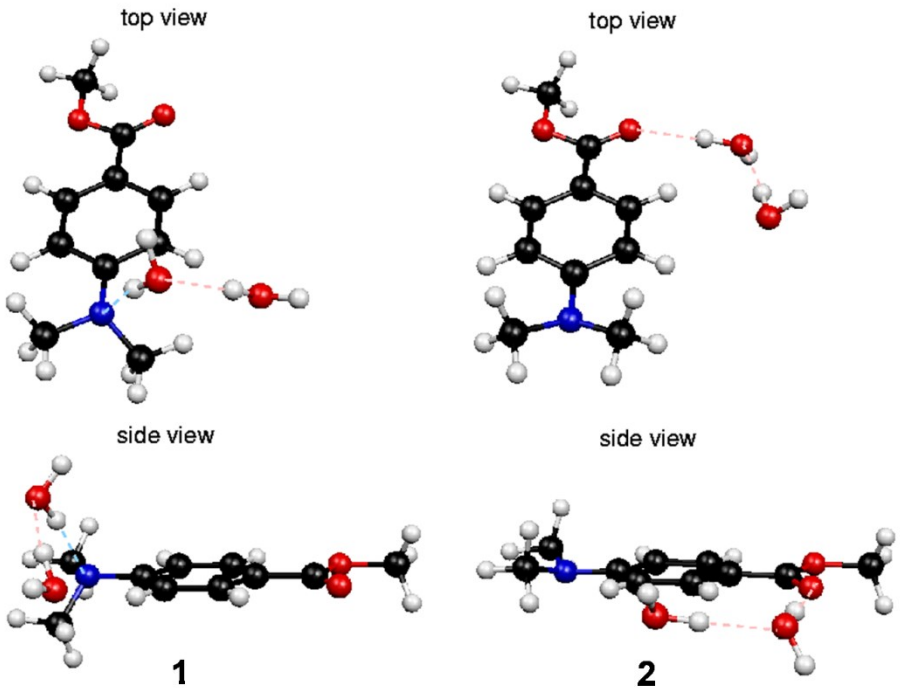

Figure 3.3. Equilibrium structures of the energetically most stable and isoenergetic isomers **I** (left) and **II** (right) of the DMABME·$2H_2O$ cluster in the electronic ground state.

To corroborate that isomers **I** and **II** are those present in the ion-depletion spectra of the molecular beam (Fig. **3.2a**), their IR spectra were calculated at the CP-PES MP2/6-31G(d,p) level of theory. The calculated harmonic frequencies of the isomers were further scaled by factors of 0.946 and 0.940, respectively, to account for basis-set effects, missing electron correlation and anharmonicity. The scaling factors were derived from comparison of calculated harmonic frequencies of the hydrogen-bonded OH vibrations of the corresponding 1:1 complexes with their known experimental values (Sec. **3.7**). Comparison of the experimental IR spectra with the calculated harmonic frequencies of the isomers **I** and **II** (Fig. **3.2c**, Tab. **3.2**) finally clarifies that the strong bands at 3466 and 3525 cm^{-1}, which are visible in both the ion-depletion IR spectrum of the molecular beam (Fig. **3.2a**) and in the IR spectrum of the precursor of the red-shifted fluorescence (Fig. **3.2b**), are due to the N•••HO and O•••HO hydrogen bonds of the water dimer in isomer **I**. The bands at 3514 and 3550 cm^{-1},

which are only found in the ion-depletion IR spectrum of the beam (Fig. **3.2a**), are due to the O•••HO carbonyl water and water dimer's hydrogen bonds of isomer **II** (Tab. **3.2**). The findings indeed confirm that both energetically lowest isomers **I** and **II** of DMABME•••$(H_2O)_2$ are present in the molecular beam. However, only isomer **I**, in which the water dimer is bound to the amino nitrogen, is responsible for the red-shifted fluorescence.

Table 3.1. Relative energies and stabilization energies (kcal·mol^{-1}) of the investigated isomers of DMABME·$2H_2O$ obtained at CP corrected MP2/6-31G** and MP2/cc-pVTZ level of theory. At the MP2/6-31G** level also ZPVE is included, and the numbers are given after the slash. The energy of isomer **I** is set to zero.

	Isomer				
	I	**II**	**III**	**IV**	**V**
Relative energies					
MP2/6-31G(d,p)	0.00/0.00	0.51/-0.08	2.56/1.93	3.77/2.70	7.02/5.45
MP2/cc-pVTZ	0.00	0.01	2.18	2.99	6.10
Stabilization energies					
MP2/6-31G(d,p)	-13.50/-9.04	-12.99/-9.11	-10.94/-7.11	-9.73/-6.33	-6.94/-3.59
MP2/cc-pVTZ	-13.08	-13.07	-10.90	-10.10	-6.98

For a preliminary guess on the CT excited states behaviour of the isomers, their ground-state *ionization potentials* (IP) and *electron affinities* (EA) were calculated and compared with those of isolated DMABME (see *e.g.* Ref. **234**, **235**, **236** for the description of diagnostics in terms of IP/EA). In the case of isomer **I**, the water dimer, hydrogen-bonded to the amino group (electron donor), increases IP and, hence, should destabilize the ICT state. On the other hand, the hydrogen bonding of water dimer to the carbonyl oxygen (electron acceptor), increases its EA and stabilizes ICT. Both give strong evidence that the electron transfer in isomer **I** should be energetically less favourable. Indeed, the vertical excitation energy of the CT state, calculated at the ground state geometries, is higher for isomer **I** (Tab. **3.3**, Sec. **3.4**) than for either isomers **II** or isolated DMABME. Therefore, the emission from this state, if it happened, would me more *blue-shifted* what contradicts to the experimental findings. From this perspective, an opposite behaviour of the isomer **I** seems to be very astonishing. However, it would be only true if one considers the phenomenon of red-shifted fluorescence merely in terms of the energetics of ICT. The next sections will show, that rather the details of gas-phase dynamics, emission and energy dissipation in the CT state together are responsible for the red-shifted fluorescence of isomer **I**.

Table 3.2. Assignment and comparison of scaled calculated harmonic frequencies of the DMABME isomers **I** and **II** at the level of CP-corrected MP2/6-31G** with the measured IR ion depletion spectrum of the mixture and of the CT emission depletion spectrum.

	Calc. OH stretch frequencies [cm^{-1}]		Expt. Frequencies [cm^{-1}]		
	Isomer I	**Isomer II**	**IR depletion**	**CT emission**	**Character**
ν_1	3432		3466	3466	N···HO
ν_2		3546	3514		=O···HO
ν_3	3557		3525	3525	H_2O···HO
ν_4		3576	3550		H_2O···HO
ν_5	3747/3749		3718	3718	free OH
ν_6		3757/3776	3724		free OH

3.4 Excited Electronic States of the DMABME•••$(H_2O)_2$ Complexes

As a first step in the investigation of excited-state properties of the energetically most stable isomers **I** and **II** of DMABME•••$(H_2O)_2$, their vertical excited states have been calculated. For this objective, geometries of the ground (S_0) and excited (S_1) states were optimized at the DFT/B3LYP and the linear response TDDFT/B3LYP level of theory, respectively, employing the standard TZVP basis set. As usual, all the minima points have been confirmed by the analyses of their harmonic frequencies. CC2 calculations generally are more reliable than TDDFT results since they do not suffer from problems with charge-transfer excitations (Sec. **1.3.6**). Thus, all TDDFT results were improved by means of single-point CC2 calculations and the following discussion will refer to these results, unless it is indicated otherwise. For comparison, the same analysis was also performed for the isolated DMABME, as well as for both 1:1 complexes.

The computed vertical excitation and deexcitation energies are summarized in Tab. **3.3**. The vertical excitation energies at the ground-state equilibrium structure are directly comparable to the experimentally observed absorption spectra (Ref. **2**), while the vertical excited states computed at the equilibrium structure of the electronic S_1 state of DMABME, 1:1 and 1:2 complexes directly relate to the wavelength of the observed red-shifted fluorescence (Fig. **3.1**, Sec. **3.1**).

At the ground-state equilibrium geometries of isomer **I**, the S_1 and S_2 states are almost degenerate with 4.78 and 4.86 eV at the level of CC2. While the S_1 state corresponds to the

locally excited (LE) state[1], the S_2 state is identified as the typical intramolecular CT state. The latter was corroborated by analysis of the molecular orbitals contributing to the S_2 state and by its dipole moment. In this CT state, electron is transferred from the amino group to the ester function, resulting in a strongly positively-charged amino nitrogen and strongly negatively-charged carbonyl oxygen. This is in agreement to the previous discussion of the ground-state IA and EA of DMABME.

Table 3.3. CC2 and TDDFT/B3LYP excitation energies (eV) and static dipole moments (Debeye) of isomers **I** and **II** of DMABME•••$(H_2O)_2$ calculated at DFT and TDDFT optimized equilibrium geometries on the ground-state S_0 and S_1 surfaces.

State	**S_0^{eq}**		**$S_1^{PICT,TS}$**			**S_1^{TICT}**		
	E_{ex} [eV]		E_{ex} [eV]		μ [D]	E_{ex} [eV]		μ [D]
	TDDFT	RI-CC2	TDDFT	RI-CC2		TDDFT	RI-CC2	
Isomer I								
LE	4.75	4.78	4.2	4.32		3.26	3.94	
CT	4.52	4.86	3.49	3.65	6.0	2.01	2.76	11.1
Isomer I								
LE	4.57	4.59	4.47	4.5		3.8	4.46	
CT	4.25	4.41	4.03	4.15	7.5	2.28	3.05	12.5
Isolated DMABME								
LE	4.55	4.57	4.36	4.45		3.88	4.56	
CT	4.43	4.64	3.6	3.82	9.05	2.56	3.37	14.0

Calculations at TDDFT/B3LYP level are consistent with single-point CC2 results. The only difference is that the order of states is reversed with the LE and CT states, exhibiting excitation energies of 4.75 and 4.52 eV, respectively, which is due to the typical underestimation of charge-transfer excited states by TDDFT (Sec. **1.3.6**). Comparison of the vertical excited LE and CT states of the isolated DMABME (Tab. **3.3**), with the excitation energies of 4.57 and 4.64 eV, respectively, reveals the CT excited state is destabilized by the water dimer in the N-bonded isomer **I** by 0.22 eV.

Unconstrained geometry optimization at TDDFT/B3LYP in the S_1 (CT) state of isomer **I** directly leads to a twisted equilibrium structure with a dihedral angle of 90° between the essentially planar dimethylamino group and the phenyl ring (Fig. **3.4**) with a large electric

[1] In contrast to the CT states, charges in the LE states are centered on specific atoms of the excited species.

dipole moment of 11.1 Debeye (Tab. **3.3**). This structure is commonly characterized as a TICT state. The TICT structure is the only minimum that could be identified on the PES of the CT state at the TDDFT level. In the TICT minimum, the CT state of isomer **I** exhibits excitation energy of only 2.76 eV. Concomitantly with the charge transfer resulting in a switch from negative to positive partial charge on the nitrogen, the hydrogen bond of the water dimer to the amino nitrogen breaks in the course of geometry optimization. Eventually, the water dimer turns around such that the oxygen of the spatially-closest water molecule interacts with the now positively-charged amino nitrogen. It can be interpreted as a transformation from hydrogen bonding to *ion solvation*. This effect should be highlighted here, since it plays a crucial role in the proposed mechanism of red-shifted fluorescence in the isomers **I**, as the next sections will show.

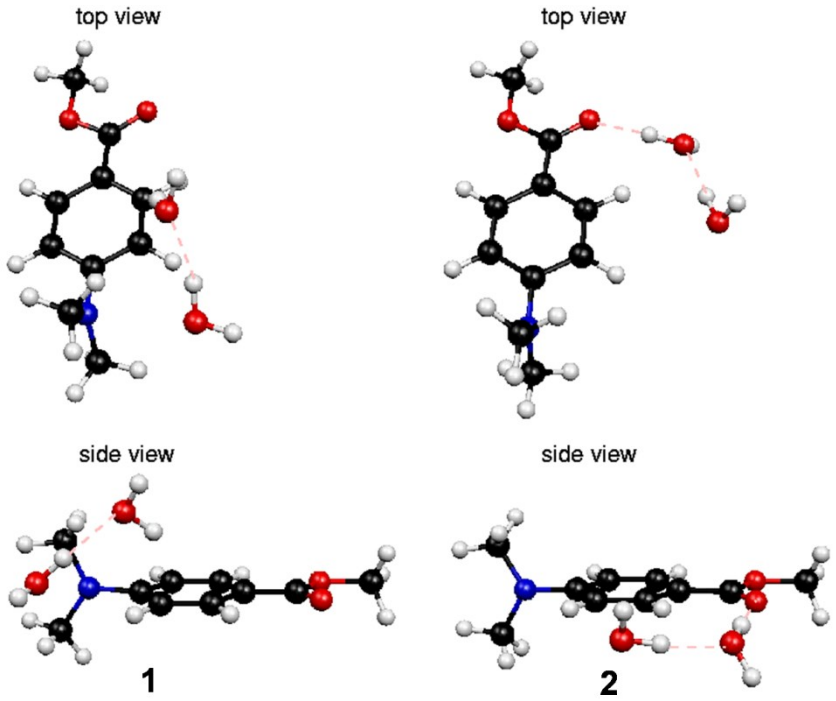

Figure 3.4. Equilibrium geometries of the TICT states of isomers **I** (left) and **II** (right) on the S_1 potential energy surfaces.

Constrained geometry optimization in the CT state, in which the dimethylamino group is not allowed to twist, leads to a planar structure which exhibits typical properties of a PICT state. However, this state is identified as a transition state on the S_1 PES at TDDFT/B3LYP level, with a single imaginary harmonic vibrational frequency corresponding to the rotation of dimethylamino group. Also, the electric dipole moment is not as large as in the TICT structure with only 6.0 Debeye at TDDFT/B3LYP level. Nevertheless, already in this planar

arrangement, the hydrogen bond between the water dimer and amino nitrogen breaks up and the water dimer rearranges in the way described above.

At the geometrically relaxed planar saddle point, the isomer **I** of DMABME•••$(H_2O)_2$ exhibits an excitation energy into S_1 of 3.65 eV at CC2 level. Notice, that at this geometry the LE (S_2) state is already 0.7 eV higher in energy than the CT state. At the equilibrium geometry of the ground state, *i.e.* at the initial excitation, the CT state has been found to possess a slightly higher energy than the LE state. Since a conical intersection has been found for DMABN (Ref. **219**), it is justified to assume that in DMABME a conical intersection is present in the vicinity of the ground-state equilibrium structure as well, allowing for an efficient radiationless transition to the S_1 CT state.

The O-bonded isomer **II** of DMABME•••$(H_2O)_2$ exhibits lower vertical excitation energies than **I**, with values of 4.41 and 4.59 eV for the CT and LE state, respectively, at CC2 level of theory. In particular, the excitation energy of the CT state is 0.45 eV lower than in isomer **I**, which is the lowest excited state at the ground-state equilibrium structure. This is mainly due to the aforementioned stabilization of the CT state by the water dimer in isomer **II**. The effect is further emphasized by comparison with the vertical excitation energy of the CT state in isolated DMABME of 4.64 eV, which is 0.23 eV higher than in isomer **II**, lacking stabilization by the water dimer. Therefore, no state crossing between CT and LE is found in isomer **II**.

It should be noticed, that based on these calculations, a further, approximately 0.4 eV red-shifted peak should exist in the absorption spectrum of DMABME•••$(H_2O)_2$ corresponding to the CT state of the O-bonded isomer. However, this peak is not detectable employing one-colour R2PI, since two photons of the required excitation energy are not sufficient for ionization. Possibly, two-colour R2PI which is currently not available would allow for its observation.

Analogously to isomer **I**, unconstrained geometry optimization of the S_1 (CT) state of isomer **II** yields a twisted equilibrium structure (Fig. **3.4**) with a dipole moment of 12.5 D, thereby representing a TICT state. The vertical excitation energy of the TICT minimum is again strongly red-shifted with a value of only 3.05 eV at CC2 level of theory. Also, in analogy to isomer **I**, a planar transition state is found, which exhibits an excitation energy of 4.15 eV. Furthermore, the excitation energy of this PICT state matches the energy of "regular" fluorescence peak at 325 nm (Fig. **3.1c**, Sec. **3.1**).

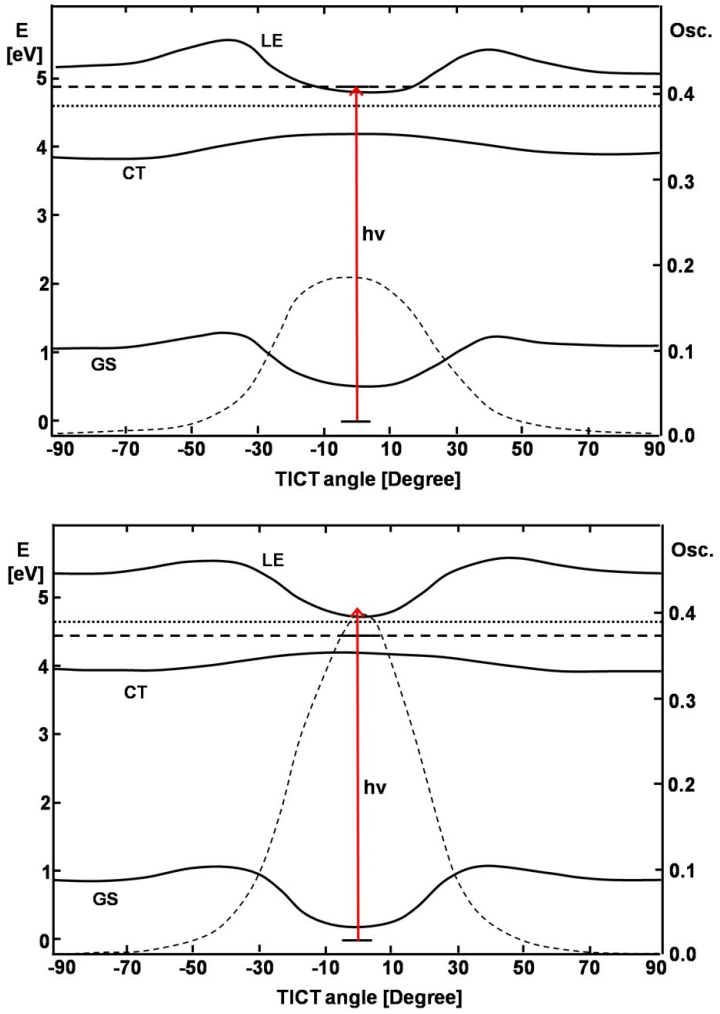

Figure 3.5. Potential energy surfaces of the ground state (GS), the locally excited (LE) and the charge-transfer (CT) state for isomers **I** (top) and **II** (bottom) at level of RI-CC2 along the TDDFT/B3LYP optimized pathway on the surface of the CT state along the TICT dihedral angle. The vertical excitation energies of the CT states as well as their dissociation energies are given as horizontal dashed and dotted lines, respectively. The energy of the ground-state equilibrium structures is set to zero. The dependence of the oscillator strength of the CT states on the TICT angle is plotted as dashed line. The vertical arrow represents the experimentally employed excitation energy.

This observation gives another hint for understanding the mechanism of dual fluorescence. It is also important to notice that in contrast to isomer **I**, the hydrogen bond does not break-up in the course of the geometry optimization but, on the opposite, becomes even stronger. This is manifested by the decrease of its bond length from 1.84 Å in the ground state to 1.72 Å in the TICT state. This is easily understood in terms of the increase of negative charge on the carbonyl oxygen in the CT excited state, which strengthens the hydrogen bond due to the additional electrostatic attraction.

Summarizing the above results for the vertical excitation energies of the CT and LE states of isomers **I** and **II** at the ground-state as well as at the TICT minimum structures, both isomers exhibit very similar properties and, in principle, could be candidates for red-shifted fluorescence. The discovered structural differences alone do not explain the observed red-shifted fluorescence in isomer **I** only, but they will become important in the discussion of possible TICT formation mechanisms.

To get more insight into the TICT formation mechanism, the S_1 potential energy surfaces of the CT excited states of isomers **I** and **II** have been computed at TDDFT/B3LYP level along the dihedral angle between the dimethylamino group and the phenyl group of DMABME. Along this twisting path, all other geometrical parameters were allowed to relax freely. The results were further improved by means of single-point CC2 calculations at the optimized structures. The curves obtained for the N-bonded isomer **I** and the O-bonded isomer **II** representing minimum energy pathways are depicted in Fig. **3.5**.

The calculated minimum-energy pathways for TICT formation in both isomers have brought another surprise, since they do not exhibit any significant difference. Both isomers can in principle form a TICT structure along the direct pathway from the initially excited structure on the electronic ground state with no energy-barriers to pass. The barrier height for the complete rotation of the dimethylamino group from the TICT state via PICT transition state is 0.25 eV for both isomers. The total energies of the CT state at the equilibrium geometries of the ground state, termed *Franck-Condon points*, are energetically above the rotation barrier by 0.85 and 0.25 eV in both isomers **I** and **II**, respectively.

At this point, one should remember that the experiments were performed in the gas phase where excess energy cannot be dissipated immediately. Therefore, the dimethylamino group can rotate freely in both isomers upon photo-excitation for a considerable time, unless the excess energy is dissipated and the molecules are cool enough to form stable TICT structures which eventually emit red-shifted fluorescence. In the case of free rotation, the emission is determined not by the minima on the PES but rather by the distribution of its *oscillator strength* (Eq. (126), Sec. **1.3.2**). It is further important to remember that the excitation energy of the PICT state of the O-bonded isomer matches the first “regular” peak in the dual fluorescence of DMABME. The computed oscillator strengths of the S_1 state of both isomers **I** and **II** , dependent on the rotational angle, is plotted in Fig. **3.5**. Indeed, for both isomers the maximum of the oscillator strength occurs at the PICT structure. Most likely, both isomers fluoresce from the PICT state, which corresponds to the “regular” fluorescence peak. Therefore, the only possible difference between the isomers, explaining why only isomer **I** is

responsible for the red-shifted emission from the TICT state, lies in their nonradiative energy dissipation mechanisms. The next section will illuminate this mechanism.

3.5 Dissociation-Mediated TICT Formation in DMABME

According to the assignment of the IR spectra and the conclusion that both isomers are present in the molecular beam of the 1:2 complexes but only the N-bonded isomer exhibits red-shifted fluorescence, energy is obviously more efficiently dissipated in the N-bonded isomer **I** than in the O-bonded isomer **II**. Thus, the key task to resolve now is how the molecules can lose their excess internal energy.

The IR and fluorescence depletion experiments described above have been performed in the gas phase and both DMABME•••$(H_2O)_2$ isomers are excited with the same laser wavelength, which was tuned to the red edge of the observed broad absorption spectrum (Ref. **2**, **225**). The calculations reveal that the CT state has a much larger oscillator strength than the LE state and, since both isomers are observed in the IR depletion spectrum, the laser energy must thus at least correspond to the higher vertical excitation energy of the CT state of the N-bonded isomer **I**, which is marked by the vertical arrows in Fig. **3.5** (Sec. **3.4**). Photo-excitation at the same laser wavelength deposits approximately equal amount (about 0.25 eV) of excess internal energy with respect to the stabilization energy of both isomers in the CT state. Thus, the only possibility for the isolated DMABME•••$(H_2O)_2$ complexes to dissipate sufficient energy and to emit via red-shifted fluorescence, can be achieved in the gas phase by fragmentation of the complex. Since the N-bonded isomer **I** exhibits red-shifted fluorescence while the O-bonded isomer **II** does not, isomer **I** obviously dissociates, whereas isomer **II** stays stable during the experiment. The latter can only emit via "regular" fluorescence from the PICT state which possesses larger oscillator strength (Fig. **3.5**).

In fact, the previous geometry optimizations of both isomers in the CT states can provide the explanation of the possible energy dissipation scenario.

As it was noticed in the previous section, the hydrogen bond between the amino nitrogen and the water dimer in isomer **I** breaks-up immediately upon photo-excitation into the CT excited state. It was manifested by the constrained geometry optimization on the CT state, with the dimethyl amino group angle fixed at its ground state value (planar). During the optimization, the water dimer is at first repelled and moves away, but rearranges and finally returns to the DMABME molecule to switch from hydrogen bonding to ion solvation. Physically, these simulations correspond to the static case of zero nuclear kinetic energy and, hence, to infinite times to adopt the equilibrium structures. However, in the dynamic case of

the real experiment, the immediate repulsion between the amino nitrogen and the water hydrogen will lead to an instantaneous dissociation of isomer **I** into twisted free DMABME, which is the only minimum on the CT PES, and to the isolated water dimer. This situation can be designated by the switch from the DMABME•••$(H_2O)_2$ to the DMABME+$(H_2O)_2$ complex. The energy difference between DMABME+$(H_2O)_2$ (*i.e.* isolated DMABME and a water dimer) and DMABME•••$(H_2O)_2$ is then added to the energy of DMABME resulting from the fragmentation. Herein, it is assumed that the water dimer absorbs this energy, exhibiting the property to serve as a kinetic energy acceptor. Thus, in the experiment, the remaining internal excess energy in DMABME after dissociation is not larger than 0.2 eV (Fig. **3.6**).

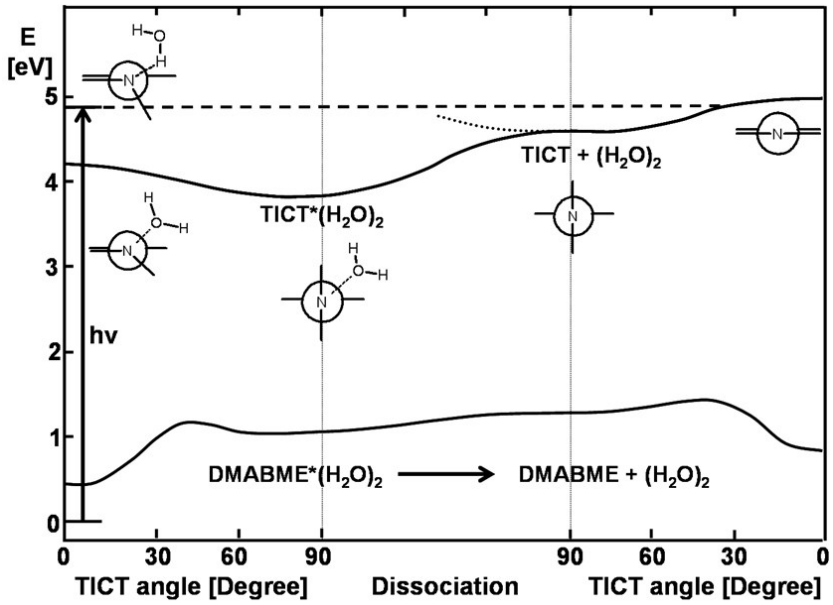

Figure 3.6. Potential energy surfaces of the CT states of the N-bonded isomer **I** along the TICT angle and dissociation pathway going from the 1:2 complexes to isolated DMABME and a free $(H_2O)_2$ dimer. The vertical energy of isomer **I** is given as dashed horizontal line, and the energy of the ground-state equilibrium structure is set to zero.

Further calculation of the potential energy curve of the CT state of isolated DMABME along its TICT formation pathway revealed that it is practically identical to the isomers of its hydrated 1:2 complexes: it possess a TICT minimum and a PICT transition state with the excitation energies of 3.37 and 3.82 eV, respectively. The maximum of the emission oscillator strength corresponds again to the PICT state. However, contrarily to the isolated species, in the case of fragmented DMABME within the DMABME+$2H_2O$ complex, the remaining internal excess energy is of around 0.2 eV, which is insufficient for the rotation of the dimethyl amino group. As a consequence, the generated free DMABME molecules are trapped in the TICT structure, from which they decay via the red-shifted fluorescence only.

As it was mentioned above, the O-bonded isomers **II** are excited with the same laser wavelength as isomers **I** in the experiment and, thus, possess enough energy to dissociate analogously to the mechanism outlined for isomer **I**. However, the experiment did not reveal red-shifted fluorescence originating from isomer **II**. The geometry optimization of the CT structures of isomer **II** again can rationalize this observation. In fact, it is seen in this isomer that the hydrogen bond between the carbonyl oxygen of the ester group and the water dimer does not break-up, but instead, is substantially strengthened upon photoexcitation. Calculation of the stabilization energy of isomer **II** in the CT state reveals that it amounts to about 0.7 eV, which is unusually strong compared to typical hydrogen-bond stabilization energies (from about 0.1 to 0.25 eV). The equilibrium bond length of the DMABME•••$(H_2O)_2$ hydrogen bond is also shorter in the ICT state than in the electronic ground state. This strongly enhanced hydrogen bond in the TICT structure of isomer **II** can be simply explained by the increase of negative partial charge on the carbonyl oxygen in the CT state and the resulting additional electrostatic attraction between the carbonyl oxygen and the hydrogen atom of water. Therefore, a direct dissociation of the water dimer in the isomer **II** should be suppressed.

Nevertheless, the fragmentation is in principle energetically feasible since the internal excess energy upon photo-excitation is 0.25 eV above the stabilization energy in the TICT state. It can occur when the excess energy is redistributed such that sufficient energy is channelled into the intermolecular hydrogen-bond dissociation coordinate. From a statistical point of view, though, it seems unlikely that almost the complete excess energy is employed for fragmentation of the complex. In fact, it has been demonstrated previously that photo-excitation with energies of 0.25 eV above the dissociation threshold can lead to delayed or metastable dissociation in much weaker Van-der-Waals complexes (Ref. **237**, **238**). However, quantum dynamic simulations, necessary for quantitative conclusions on the details of the mechanism of *internal vibrational energy redistribution* (IVR) (see *e.g.* Chap. 4 of Ref. **239**) of the isomer **II** are unfeasible at present.

In summary, photoinduced charge transfer from the dimethylamino group to the ester group in DMABME produces a positively charged nitrogen atom and a negatively charged carbonyl oxygen. This leads to a strong electrostatic repulsion between the amino nitrogen and the bound hydrogen atom in the N-bonded isomer **I** of DMABME•••$(H_2O)_2$ as well as to a strong electrostatic attraction between the carbonyl oxygen and the water dimer in the isomer **II** resulting to an unusually strong hydrogen bond. As a consequence, isomer **I** dissociates instantaneously, while the dissociation of isomer **II** is strongly suppressed, if it occurs at all. Since dissociation is required to dissipate excess energy in the gas phase for the TICT

structure, attributed to red-shifted fluorescence, to be formed, an explanation is finally provided why only the N-bonded isomer is experimentally found to exhibit red-shifted fluorescence.

A recent investigation on hydrogen-bonded phenol complexes has demonstrated that the efficiency of hydrogen bond dissociation is independent of the hydrogen bond strength (Ref. **240**). At first glance, the experiment seems to be in contradiction with the depicted mechanism in isomer **II** of DMABME•••$(H_2O)_2$. However, in that experiment, the OH stretch vibration of phenol was selectively excited with IR light. As a consequence, the internal energy, from the beginning, was directly pumped into the hydrogen bond dissociation coordinate. Furthermore, the investigated hydrogen bonds are substantially weaker with at most 0.25 eV compared to the TICT state of isomer **II** with 0.7 eV.

Owing to the above arguments, one thus cannot *a priori* expect that photo-excited complexes of O-bonded DMABME•••$(H_2O)_2$ to dissociate into DMABME and a water dimer via efficient IVR, even when the excess energy in the complexes is in principle enough for the hydrogen-bond dissociation. To corroborate the suggested mechanism of red-shifted fluorescence in the DMABME•••$(H_2O)_2$ complexes further, another IR and fluorescence depletion experiment has been proposed in the present work. In this experiment, the O-isomer **II** should be excited with its individual vertical excitation energy of 4.41 eV (computed at CC2 level), which is about 0.4 eV lower than in isomer **II**. According to the presented calculations, the stabilization energy of isomer **I** is about 0.7 eV in the excited CT state on the TICT equilibrium structures. However, the Franck-Condon point of isomer **I** is only 0.5 eV above the TICT minimum, *i.e.* its internal vibrational energy is not enough to dissociate. Therefore, this energy dissipation channel is closed. In such an experiment, one should not be able to observe red-shifted fluorescence at all, since the N-bonded isomers are not excited into the CT state because of too low photon energy, whereas the O-isomers should exhibit only a "regular" fluorescence from the PICT state.

In conclusion of this section, the question is addressed why red-shifted fluorescence is experimentally observed in very small amount (Fig. **3.1**, Sec. **3.1**) in the DMABME•••H_2O complexes hydrated by one water (1:1).

As in the case of 1:2 complexes, two most stable isomers, analogous to isomers **I** and **II** can be constructed from DMABME and water monomer. Indeed, the isomer of DMABME•••H_2O, in which the water molecule is hydrogen-bonded to the amino nitrogen, possesses essentially identical structure to the isomer **I** of the 1:2 complex. Not surprisingly, a barrierless decay into the TICT state is possible, thus red-shifted fluorescence could in

principle be observed. However, in the IR ion depletion experiment only one isomer is observed for the 1:1 clusters. Single-point CP MP2/cc-pVTZ calculations on the CP-PES MP2/6-31G(d,p) structures reveal that the O-bonded isomer of DMABME•••H_2O is thermodynamically more stable by 0.5 kcal mol^{-1} than the N-bonded one. The computed IR spectra of these isomers confirm that the only one presented in the molecular beam experiment is the O-bonded isomer. Therefore, red-shifted fluorescence is not observed for the O-bonded isomer of the 1:1 complex for the same reason as for the isomer **II** of the 1:2 complex. Thus, the weak red-shifted fluorescence, observed in the 1:1 complex (Fig. **3.1**, Sec. **3.1**) can either stem from the O-bonded isomers of the 1:2 complex, or from the N-bonded isomers of the 1:1 complex, which should present in the molecular beam at small amounts.

3.6 Summary and Conclusions

Recent experiment employing IR and fluorescence spectroscopy on the DMABME clusters hydrated by one to three water molecules revealed that two water molecules are needed to observe dual fluorescence in the gas phase. To elucidate this phenomenon the present theoretical study has been performed.

Using high-level quantum-chemical calculations, two experimentally observed isoenergetic isomers were assigned to the complexes in which a water dimer is hydrogen-bonded either to the carbonyl oxygen of the ester function or to the amino nitrogen. Moreover, the assignment proved that only N-bonded isomer exhibits unusual red-shifted fluorescence in the gas phase.

At first glance the observation seems to be intriguing, if one considers the phenomenon of the occurrence of red-shifted fluorescence merely as the result of stronger ICT. In fact, in the N-bonded isomer, the ICT formation appears to be energetically less favourable than in the O-bonded one, since the hydrogen bonding of a water dimer to the dimethylamino nitrogen increases the ionization potential, *i.e.* destabilizes ICT, whereas hydrogen bonding to the ester function increases the electron affinity, *i.e.* stabilizes ICT. Indeed, that was corroborated by the computed vertical excitation energies of the two isomers of DMABME•••$(H_2O)_2$.

To understand this surprising behaviour of the isomers, the excited-state potential energy surfaces of the two DMABME•••$(H_2O)_2$ isomers, as well as those of the isolated DMABME molecule, were computed along the dihedral angle between the dimethylamino group and the phenyl ring, representing the TICT formation coordinate. Astonishingly, all molecules possess TICT equilibrium structures on the CT excited state surface. Indeed, this TICT structure is attributed to the red-shifted peak in the fluorescence spectrum. In addition, barrierless formation of the TICT state is in principle possible for all of them.

However, the experiments were performed in the gas phase where the internal excess energy of the complexes cannot be dissipated immediately. Upon photoexcitation, the dimethylamino group can rotate freely, unless excess energy is dissipated and the molecules are localized in the equilibrium structures, *i.e.* in the TICT geometry. Under these circumstances, the emission will be determined not by the minima on the PES but rather by the distribution of its oscillator strength which maximum corresponds to the "regular" emission form the PICT state. Obviously, this fluorescence mechanism appears to be dominant for the O-bonded isomer of DMABME•••$(H_2O)_2$.

The only possibility for the N-bonded isomer to lose its excess energy radiationless and to localize in the equilibrium TICT structure can be realized by its fragmentation. Indeed, this option is energetically feasible for both isomers in the conducted experiments. However, in the N-bonded isomer the hydrogen bond breaks-up immediately upon photo-excitation into the CT state, due to strong electrostatic repulsion between the now positively-charged amino nitrogen and the hydrogen atom. In the O-bonded isomer the opposite effect is observed: the hydrogen bond is substantially strengthened due to the increased negative charge on the carbonyl oxygen leading to an unusually strong hydrogen bond suppressing dissociation of the complex. The isolated DMABME molecules resulting from the dissociated N-bonded DMABME•••$(H_2O)_2$ complexes can finally form stable TICT equilibrium structures on the CT surface and eventually decay via red-shifted fluorescence.

These results demonstrate that the phenomenon of dual fluorescence in the gas phase of the DMABME•••$(H_2O)_2$ complex is determined by specific interactions with the solvent molecules. Herein this solvent water behaves differently from conventional polar continuum. The microscopic reason for this is that the isomer **IV**[1] of the 1:2 complex, in which water could exhibit the property of a polar continuum, is less stable than the considered N- and O-bonded isomers.

Turning back to the main topic of the Thesis, the following aspects of the investigation should be highlighted in conclusion.

1. The example of dual fluorescence in DMABME demonstrates that the influence of water molecules on the charge-transfer excited states of the electron donor-acceptor systems in the gas-phase is essentially site-specific. In theoretical studies it hence cannot generally be reproduced by polar continuum models.

[1] In isomer **IV** one water molecule is attached to the carbonyl oxygen and another one to the amino nitrogen (Sec. **3.3**). Only in this case, the action of these two solvent water molecules can be similar to the action of polar continuum in the ICT state.

2. In the gas phase, when internal excess energy is larger than the energy of a particular excited state, the emission from this state will be determined by the distribution of its oscillator strength rather than by the minima on the excited-state potential energy surface. Since the latter do not necessarily fit to each other, the situation can sometimes be in contradiction to physical intuition based on minimum energy pathways alone.

3. The example highlights the property of solvent water molecules to serve as a kinetic energy acceptor in the gas phase, allowing chemical reactions to follow specific ways determined by the minima on their potential energy surfaces. Since water and hydrogen bonds are ubiquitous in nature, the identified mechanism of energy dissipation via hydrogen bond fission is expected to be not an exception, but rather a general feature of many chemical and biological processes.

4. A systematic benchmark study of computed IR spectra of suitable model systems containing typical hydrogen bonds (carbonyl-water, amino-water) that are present in the system, revealed that the basis-set superposition error (BSSE) is the leading source of error in the IR spectrum simulations (see Sec. **3.7**). At correlated, computationally-affordable MP2 level with moderate basis sets, correction for BSSE provides an accurate reproduction of the spectrum compared to higher levels of theory (CCSD) and larger basis sets (up to quadruple-zeta). This important manifestation of BSSE in calculations of spectroscopic properties is in line with recent advances in this scientific field (Part **1.4**).

3.7 Addendum

Influence of Electron Correlation, Anharmonicity and Basis-Sets on Calculated IR Spectra of H-bonded Prototype Systems

General sources of errors in quantum-chemical calculations of IR spectra

In Chapter **1**, general theoretical methods for electronic-structure calculations have been introduced. They lead to approximate descriptions of *electron correlation* (Sec. **1.2.3**) and introduce *basis-set effects* (Part. **1.4**). The latter can be divided into the *basis-set incompleteness error* (BSIE) and *basis-set superposition error* (BSSE) (Sec. **1.4.1**). Calculations of infrared (IR) spectra, as well as *stabilization*, *protonation* and *deprotonation enthalpies etc.*, in general, require the solution of the entire nuclear problem (Sec. Part **1.1**) but are usually treated in the *harmonic approximation* (Sec. **1.1.4**). In most cases it is sufficient to know the magnitude of error to draw reliable conclusions about the relation between the experimental IR bands and individual molecular vibrations. In this section, the results of a systematic study on the magnitude of aforementioned errors comprised in the computed *ground-state* IR spectra of hydrated complexes of Methyl 4-*N*,*N*-dimethylaminobenzoate ester (Fig. **3.3**, Sec. **3.3**), are presented.

Molecular model systems for benchmarking the IR spectra of hydrated DMABME complexes

A number of recent studies on the subject indicates that in most cases BSSE – not the lack of dynamic correlation, is the leading source of error in second-order perturbation theory (MP2) (Sec. **1.2.4**) calculations of potential energy surfaces (PES) of weakly-bound complexes (see references in Sec. **1.4.2**-**1.4.4**). Notice, most of these studies have been focused mainly on MP2, since it is the only wave-function correlated method which is affordable in studies on the systems of chemically relevant molecular size.

Indeed, also the size of hydrated DMABME complexes does not allow to compute their equilibrium geometries and vibrational frequencies at theoretical levels higher than MP2 with moderate basis sets and the *counterpoise correction* (CP) (Sec. **1.4.3**) for BSSE. However, the presence of hydrogen bonds, in principle, can require theoretical levels higher than MP2 to describe dispersion and polarization effects properly. Therefore, owing to the large size of the system, the primary objective of this complimentary study is to provide smaller appropriate H-bonded benchmarking systems to further evaluate the quality of their IR spectrum, *obtained*

on the CP-corrected MP2 potential energy surfaces, with respect to basis set and correlation effects.

Previous similar studies focused on the shape of PES shapes and stabilization energies of H-bonded complexes rather than on the comparison of IR spectra. Furthermore, correlated BSSE-corrected IR calculations did, in most cases, not go beyond MP2 level. This is partly due to the fact that CP-corrected gradients are implemented in Gaussian 03 only. The latter, though, does not have analytic second derivatives of PES at coupled-cluster level (Sec. **1.2.5**) what is necessary for efficient IR frequency calculations.

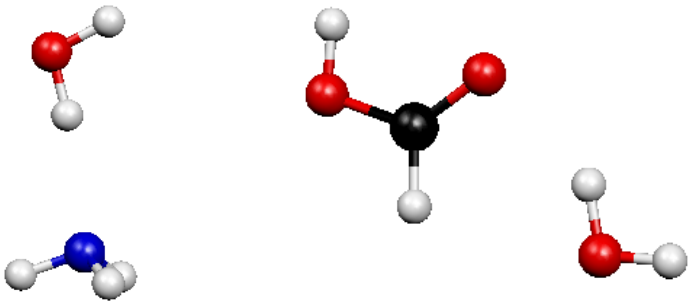

Figure A1. Ammonia-water (left) and formic acid-water (right) complexes as models for the amino- and carbonyl bound hydrogen bonds occurring in the N- and O-isomers of DMABME•••$(H_2O)_2$.

To overcome the size limitation, the following strategy has been used here. Frequency calculations, necessary for benchmarking of IR spectra (Fig. **3.2**, Sec. **3.3**), were performed for the formic-acid-water and the ammonia-water complexes, containing both types of H-bonds, required for the identification of N- and O-bonded isomers of the 1:1 and 1:2 complexes of DMABME. Herein, two relevant vibrations of each model complex (*i.e.* the two free OH stretch vibrations of both complexes, the H-bonded OH stretch vibration of the carbonyl-water dimer and the N-bonded OH stretch vibration of the amino-water dimer), computed at various levels of approximation, were plotted on the *same* graph (Fig. **A2**). The influence of the aforementioned approximations (*i.e.* the basis-set size, correlation and anharmonicity) on the IR spectrum of hydrated DMBME complexes was further tested by analysis of the relative distances between the vibrational bands of the model complexes.

The procedure can be justified to benchmark IR spectra of larger systems in those cases, when the relevant H-bonded groups are spatially-separated and their vibrations do not couple with each other. Indeed, this case is realized in the 1:1 and 1:2 hydrated complexes of DMABME in the gas phase.

Here and further, BSSE of the acid-water and ammonia-water dimer was corrected at the *intermolecular* level only. In the CP procedure for the BSSE correction (Ref. **138**, **161**), each monomer of the complexes was treated as a neutral fragment. Notice, that it means that the results still bear some *intramolecular* BSSE, especially in the computed free OH stretch vibrations and the bond lengths. However, these bands were not principal for the identifications of N- and O-bonded isomers of the 1:2 complex (see Fig. **3.3**, Sec. **3.3**).

Basis-Set Size

To assess how the basis-set size affects the computed OH stretch frequencies, CP-corrected MP2 calculations with increasingly large basis sets have been performed. They started from a relatively small split-valence 6-31G(d) basis set of double-zeta quality and went through up to the cc-pVQZ basis set of quadruple-zeta quality (see Sec. **1.4.1** for the structure of basis sets). Although the increase in the basis-set size is quite enormous, the IR spectrum constituted by the OH stretch frequencies remains rather unaffected.

In particular, addition of polarization functions to the basis set in the CP MP2 calculations, *e.g.* compare 6-31G(d) with 6-31G(d,p) or 6-31++G(d,p) with 6-31++G(d,p), shifts the absolute values of the OH frequencies upwards to higher values.

Increasing the number of diffuse functions, *i.e.* going from 6-31G(d,p) to 6-31++G(d,p), from 6-31G(d,p) to 6-31++G(d,p) or from cc-pVTZ to aug-cc-pVTZ bases, bears the opposite effect, displacing the frequencies to lower values. However, the ordering of the frequencies and even the relative energies between the peaks in this case remain essentially unchanged varying only negligibly.

Transition from the basis sets of double- to triple-zeta quality, brings the frequencies shift to higher values again. In the case of 6-311G(d,p) (triple-zeta quality) the peaks corresponding to the N•••HO and O•••HO hydrogen bonds become closer together, but are still clearly separated by 70 cm^{-1} and do not change order. Using the cc-pVTZ basis set, on the other hand, almost does not decrease their separation (100 cm^{-1}) as compare to the bases of double-zeta quality.

Obviously, the influence of basis-set size increase is strongly compensated by the application of Counterpoise correction. The computed OH stretch frequencies do change in the absolute magnitude, but their relative position is almost constant.

In contrast, the MP2 calculations, not corrected for BSSE, exhibit much less balanced description of the IR spectrum with respect to the basis-set variation. For example, addition of one polarization *p*-function to the 6-31(d) basis leads to much stronger dispersion in the

relative distances between the peaks of both N- and O-bonded isomers of DMABME, whereas application of the CP correction compensates for this effect (Fig. **A3**).

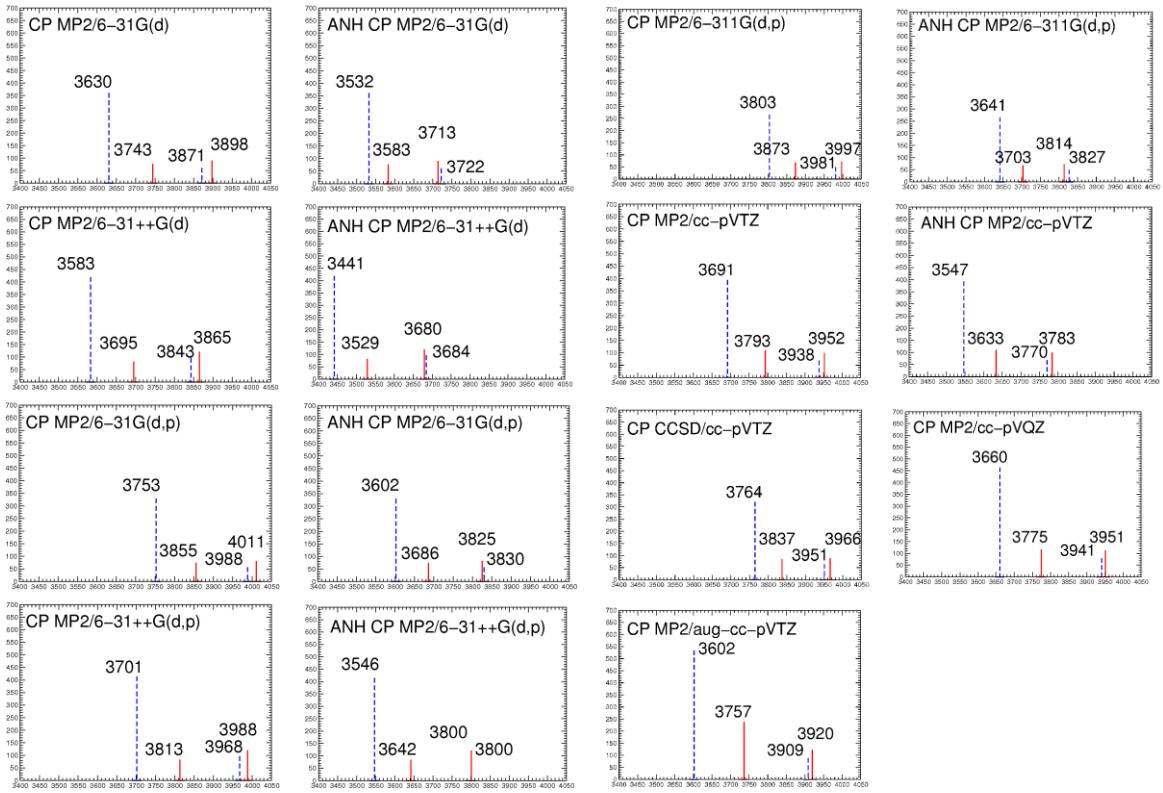

Figure A2. Influence of correlation, anharmionicity and basis-set effects on the hydrogen OH stretch frequencies of the ammonia-water complex (blue dashed lines) and the formic acid-water complex (red solid lines). The geometries have been optimized at each particular level of theory. The first two left peaks of each spectrum are of particular interest, since they correspond to the hydrogen-bonded OH stretch vibrations.

Better description of the IR spectrum, obtained on the CP-corrected PES of these hydrogen-bonded complexes, stems from the fact that the PES obtained with increasingly-large basis sets are nearly equal to those obtained with moderate sets. This is readily manifested by comparison of the relevant geometrical parameters of the model complexes. Indeed, the N•••HO H-bond lengths difference in ammonia-water dimer obtained with 6-31G(d,p) and cc-pVTZ bases is 0.02 Å (2.0581 *vs.* 2.0374 Å), while the difference in the O•••HO bond lengths of formic-acid-water dimer is 0.04 Å (2.1158 *vs.* 2.0723 Å). Single-point stabilization energies of both model complexes, computed with the cc-pVTZ basis on the 6-31G(d,p)-optimized structures, are practically identical to the stabilization energies obtained with the cc-pVTZ optimized structures itself.

As it was mentioned above, all computed frequencies bear some contribution of the *intramolecular* BSSE which was not corrected in these calculations. This is readily

corroborated by the less balanced description of the free OH frequencies of the model complexes (the right parts of the spectra of Fig. **A2**). The latter are particularly sensitive to the intramolecular BSSE. In principle, application of the CP correction to these model complexes as whole to reduce itramolecular BSSE is also possible. That would provide even more balanced IR spectrum of hydrogen-bonded complexes.

Electron Correlation

The influence of increase of electron correlations on the composite IR spectrum of hydrogen-bond frequencies of the formic acid-water and ammonia-water dimer was studied by comparison of the CP CCSD/cc-pVTZ with the CP MP2/cc-pVTZ results. CCSD theory (N^6 scaling), takes to account dynamic correlations more systematically than MP2 scaling as N^5 (see Sec. **1.2.3**), since the former includes singly-excited determinants. The calculations

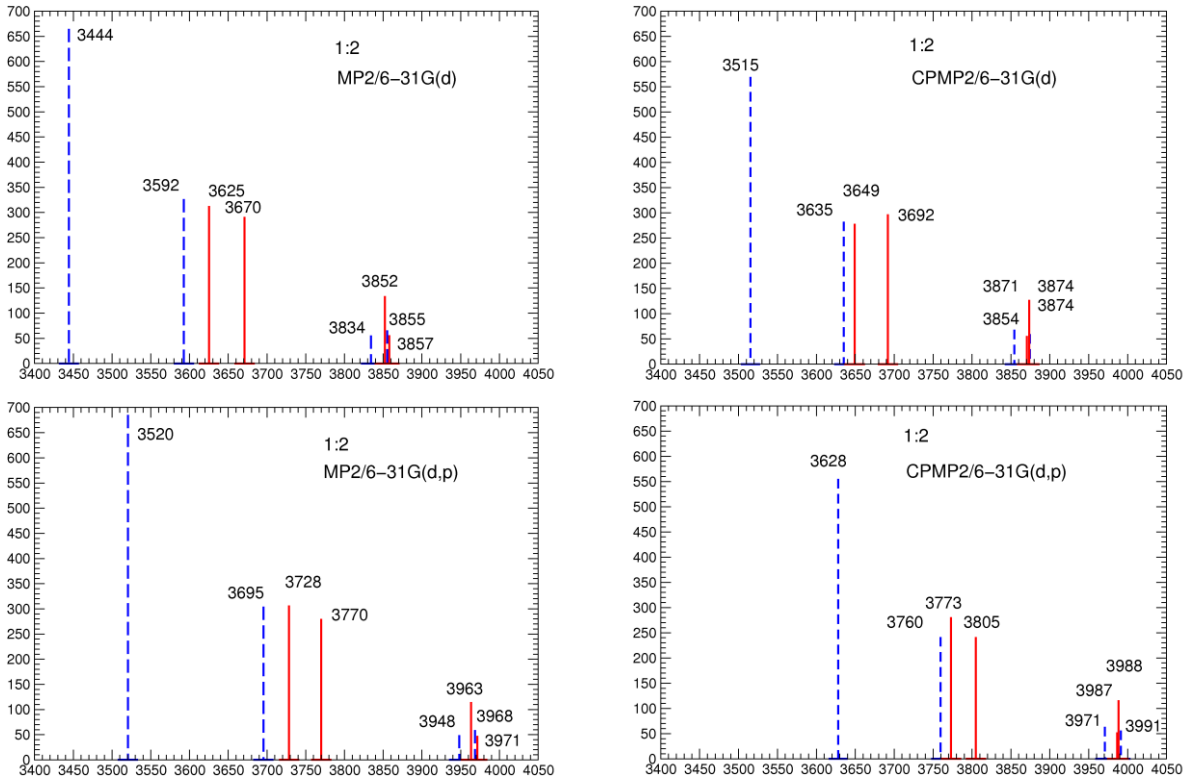

Figure A3. Comparison of computed harmonic frequencies of the OH stretch vibrations of the N- and O-isomers of DMABME•••$(H_2O)_2$: CP-uncorrected (left) *vs.* CP-corrected (right) MP2 with standard basis sets 6-31G(d,p) (top) and 6-31G(d,p) (bottom).

reveal that the CP-corrected geometric parameters of the model systems alter very slightly when going from the CP MP2/cc-pVTZ to CP CCSD/cc-pVTZ levels. The difference in the relevant H-bonds bonds obtained at MP2 and CCSD levels is negligible. The N•••HO hydrogen-bond lengths difference between the MP2 and CCSD values in ammonia-water

complex is within 0.04 Å (2.0374 *vs.* 2.0732 Å), while difference in the O•••HO bond lengths formic-acid-water dimer is only 0.03 Å (2.0723 *vs.* 2.1025 Å). This, again, indicates a nice reproducibility of the CP-corrected geometric parameters and potential energy surfaces with respect to the increase of correlation.

Harmonic OH stretch frequencies calculated at CP CCSD/cc-pVTZ level demonstrate the shift to higher absolute values, compared to the CP MP2 calculations. However, the ordering of the N-bonded OH stretch band of the ammonia-water dimer and O-bonded OH stretch band of the formic acid-water dimer, necessary to distinguish the N- and O-isomers of DMABME, remain unchanged. Hererin, the distance between the bands is reduced only slightly by about 29 cm^{-1} when going from MP2 to CCSD level. Owing to the fact that CP-corrected MP2 harmonic frequencies obtained with large basis sets are nearly equal in quality to those obtained with moderate sets of double-zeta quality, one concludes the latter are also close in quality to the frequencies obtained at CP CCSD/cc-pVTZ level.

Harmonic Approximation

In standard frequency calculations presented here, the true potential energy surfaces are approximated by harmonic ones, allowing for the computation of harmonic frequencies (Sec. **1.4.1**). The harmonic approximation introduces an additional error, which normally leads to an overestimation of frequencies as well as ZPVE magnitudes. In the stationary points it is possible to obtain corrected potential energy surfaces and their derivatives by means of the *anharmonic correction* to the harmonic approximation (Sec. **1.4.1**). However, the procedure requires high-order derivatives of PES and, hence, is computationally inapplicable to the system of the DMABME size. In practice, anharmonic effects for large systems are usually corrected by scaling of the computed harmonic frequencies with factors, derived from comparison of experimental and computed frequencies (see the next subseection).

Nevertheless, for the chosen model complexes of ammonia-water and formic acid-water dimers, the anharmonic calculations are feasible. As expected, the *fundamental* (*i.e.* corrected for anharmonicity) frequencies are systematically lower than the harmonic ones, as can be seen by comparison of the CP MP2 and ANH CP MP2 calculations with up to the cc-pVTZ basis set (Fig. **A2**). However, the ordering of the calculated peaks, responsible for identification of the N- and O-bonded isomers of DMABME does not switch in any single case.

This result, in combination with the results of the previous subsections, gives a certain confidence that harmonic frequencies, calculated at the level of CP-corrected MP2 with

moderate basis sets of double-zeta quality, allow for an *unambiguous* assignment of the experimentally-observed OH stretch frequencies to the different isomers of DMABME.

Scaling Factors for the Harmonic OH Stretch Frequencies

Calculations of DMABME•••$(H_2O)_2$

Computed harmonic frequencies demonstrate that the IR spectra, obtained on the CP-corrected MP2 potential energy surfaces with moderate basis sets, exhibit its perfect conservation *as a whole* (*i.e.* conservation of *relative* distances between the peaks) with respect to basis set, correlation and anharmonicity effects (Fig. **A2**). This is not the case for calculations that are not corrected for BSSE (Fig. **A3**). On the other hand, *absolute* values of the computed harmonic and fundamental frequencies of the model systems do not show convergence at the theory levels up to CP MP2/cc-pVQZ and CP CCSD/cc-pVTZ and, hence, cannot serve as reference points for the derivation of scaling factors for the harmonic frequencies calculations on large systems.

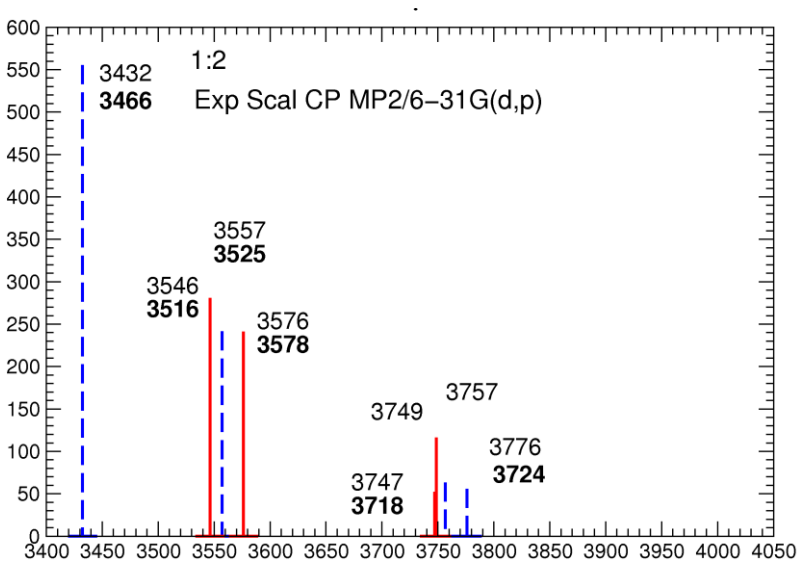

Figure A4. Scaled MP2/6-31G** IR spectrum of the N- (blue dash) and O-isomers of DMABME•••$(H_2O)_2$. The bold numbers correspond to the experimental values for DMABME•••$(H_2O)_2$.

However, a direct connection of the computed harmonic frequencies of large system to the experimental IR spectrum does require scaling factors. As it was mentioned previously, the problem in many cases can be solved by a derivation of scaling factors from comparison of computed harmonic frequencies, associated with a particular *functional group* of a molecule, with experimental IR frequencies, related to the functional groups of this, or *similar* molecules. Such scaling factors would allow for a direct comparison of calculated and

experimental values, as well as to correct for basis-set, electron correlation and anharmonicity effects. The procedure can be provided with confidence if the IR spectrum computed with available theoretical methodology is well-reproduced as a whole.

In the present study, the scaling factors for two isomers of the DMABME•••$(H_2O)_2$ complex (1:2) were derived from comparison of the experimentally available relevant OH stretch vibrations with the computed harmonic frequencies of the smaller DMABME•••H_2O complex (1:1). Herein, the N•••HO hydrogen-bonded OH vibration in the N-isomer of the 1:1 complex has an experimental frequency of 3552 cm^{-1}, while the value, calculated at the CP MP2/6-31G(d,p) level, is 3752 cm^{-1}. This gives a scaling factor for the N-isomer of $k_N = \upsilon$(CP MP2/6-31G(d,p))/υ(exp)=0.946. In the O-isomer, the corresponding experimentally determined frequency has a value of 3608 cm^{-1} compared to the calculated value of 3839 cm^{-1}. The resulting scaling factor k_O for the O-isomer is thus 0.940. The factors derived above were further applied to the CP MP2/6-31G(d,p) harmonic frequencies of the N- and O-isomers of the 1:2 complex of DMABME. The resulting IR spectrum is displayed in Fig. **A4**. Comparison of the experimental frequencies of DMABME•••$(H_2O)_2$ and the scaled computed values reveals an excellent agreement within error of 20-50 cm^{-1}. This precision is by far enough to undoubtedly assign the measured experimental IR spectra of DMABME•••$(H_2O)_2$ to the N-bonded and O-bonded isomers.

Conclusions

Numerous studies on the subject demonstrate that correction for BSSE significantly improves the quality of MP2 potential energy surfaces of weakly-bound, in particular hydrogen-bonded, complexes (see Ref. **19** for in-depth review). This benchmark study on prototypic hydrogen-bonded complexes corroborates these findings. It shows that the quality of MP2 potential surfaces and their derivatives (*e.g.* harmonic frequencies) is indeed improved by the CP correction. Unlike the case of BSSE-uncorrected MP2, harmonic frequencies of the model complexes calculated at the CP MP2 theory level with moderate basis sets (of double-zeta quality) produces a *regular*, with respect to the basis set variation (up to MP2/cc-pVQZ), IR spectrum. Its quality is sufficient to finally identify the relevant isomers of large DMABME•••$(H_2O)_2$ complexes.

Furthermore, the study reveals that the quality of CP-corrected potential energy surfaces of the prototypic H-bonded complexes computed with MP2 and moderate basis sets appears to be very close to the BSSE-corrected surfaces obtained with more accurate and computationally expensive methods like CCSD. That means that transition from the level of

second-order perturbation theory to higher levels of theory to obtain more accurate PES and their derivatives does not make sense, unless BSSE is corrected in the calculations. These findings, though, are in principle predictable, if one realizes that the *BSSE-contribution* into the *stabilization energy* of a supramolecular complex in the vicinity of its equilibrium structure is usually of the same order of magnitude as the *correlation contribution* for a wide range of atom-centered basis sets.

References

1 Zakharov, M; Masunov, A. E.; Dreuw, A. J. Phys. Chem. A 2008, 112, p. 10405.

2 Krauss, O.; Brutschy, B. Chem. Phys. Lett. 2001, 350, p. 427.

3 Zakharov, M.; Krauss, O.; Nosenko, Y.; Brutschy, B.; Dreuw, A. J. Am. Chem. Soc. 2009, 131, p. 461.

4 Mataga, N.; Kaibe, Y.; Koizumi, M. Nature 1955, 175, p. 731.

5 Herbich, J.; Waluk, J.; Thummel, R. P.; Hung, C. Y. J. Photochem. Photobiol. A 1994, 80, p. 157.

6 Mataga, N.; Miyasaka, H. Prog. React. Kinet. 1994, p. 317.

7 Chudoba, C.; Nibbering, E. T. J.; Elsaesser, T. Phys. Rev. Lett. 1998, 81, p. 3010.

8 Waluk, J. In: Conformational analysis of Molecules in Excited States; Wiley-VCH: New York 2000, p. 57.

9 Herbich, J.; Brutschy, B. TICT molecules; In: Electron Transfer in Chemistry; Wiley-VCH: Weinheim (Germany) 2001, 4, p 697.

10 Waluk, J. Acc. Chem. Res. 2003, 36, p. 832.

11 Nosenko, Y.; Kunitski, M.; Thummel, R.; Kyrychenko, A.; Herbich, J.; Waluk, J.; Riehn, C.; Brutschy, B. J. Am. Chem. Soc. 2006, 128, p. 1000.

12 Arnaut, L. G.; Formosinho, S. J. J. Photochem. Photobiol. A 1993, 75, p. 1.

13 Ormson, S. M.; Brown, R. G. Prog. React. Kinet. 1994, 19, p. 45.

14 Hammes-Schiffer, S. Acc. Chem. Res. 2001, 34, p. 273.

15 Hu, X.; Li, H.; Liang, W.; Han, S. J. Phys. Chem. B 2004, 108, p. 12999.

16 Hammes-Schiffer, S. Acc. Chem. Res. 2006, 39, p. 93.

17 Zakharov, M; Masunov, A. E.; Dreuw, A. J. Phys. Chem. C 2009, 113, p. 10395.

18 Grabowski, Z. R.; Rotkiewicz, K.; Rettig, W. Chem. Rev. 2003, 103, p. 3899.

19 Slavador, P. Ph. D. Thesis; Institute of Computational Chemistry, University of Girona 2001.

20 Schrödinger, E. Phys. Rev. 1926, 28, p. 1049.

21 Dirac, P. A. M. Proc. R. Soc. A 1928, 117 . p. 610.

22 Pitzer, K. Acc. Chem. Res. 1979, 12 (8), p. 271.

23 Christiansen, P. A.; Ermler, W. C.; Pitzer, K. S. Annu. Rev. Phys. Chem. 1985, 36, p. 407.

24 Pyykkö, P. Chem. Rev. 2002, 88 (3), p. 563.

25 Pauli, W. Exclusion Principle and Quantum Mechanics (Nobel Lecture 1946); In Nobel Lectures, Physics 1942-1962; Elsevier: Amsterdam 1964, p. 27.

26 Born, M.; Oppenheimer, R. Ann. der Phys. 1927, 84, p. 457.

27 W. Domcke, W.; Stock, G. Adv. Chem. Phys. 1997, 100, p. 1.

28 Tachikawa, M.; Mori, K.; Suzuki, K.; Iguchi, K. Int. J. Quantum Chem. 1998, 70, p. 491.

29 Tachikawa, M.; Mori, K.; Nakai, H.; Iguchi, K. Chem. Phys. Lett. 1998, 290, p. 437.

30 Tachikawa, M.; Mori, K.; Osamura, Y. Mol. Phys. 1999, 96, p. 1207.

31 Webb, S. P.; Iordanov, T.; Hammes-Schiffer, S. J. Chem. Phys. 2002, 117, p. 4106.

32 Kozlovski, P. M.; Adamowicz, L. Chem. Rev. 1993, 93, p. 2007.

33 Bochevarov, A. D.; Valeev, E. V.; Sherrill, C.D. Mol. Phys. 2004, 1, p. 111.

34 Chakraborty, A.; Pak, M.V.; Hmmess-Schiffer, S. J. Chem. Phys. 2008, 129, p. 014101.

35 Gauss, J. Molecualr Properties; In: Modern Methods and Algorithms of Quantum Chemistry; NIC Series: Jülich 2000, 3, p. 541.

36 Bohm, D. Quantum Theory; Prentice Hall: New York 1951. Reprint; Dover: New York 1989.

37 Dykstra, C. E.; Shuler, K.; Young, R. A.; Bacic, Z. J. Mol. Struct. THEOCHEM 2002, 591, p. 11.

38 Slater, J. C. Phys. Rev. 1929, 34, p. 1293.

39 Szabo, A.; Ostlund, N. S. Modern Quantum Chemistry; Dover: New York 1996.

40 Goddard III, W. A.; Dunning, T. H.; Hay, P. J. Acc. Chem. Res. 1973, 6, p. 368.

41 Wahl, A. C.; Gas, D. The Multiconfiguration Self-Consistent Field Method; In: Methods of Electronic Structure Theory; Plenum: New York 1977, p. 51.

42 C. C. J. Roothaan, C. C. J. Rev. Mod. Phys. 1951, 23, p. 69.

43 G. G. Hall, G. G. Proc. R. Soc. A 1951, 205, p. 541.

44 Pople, J. A.; Nesbet, R. K. J. Chem. Phys. 1954, 22, p. 571.

45 Koopmans, T. Physica 1933, 1, p. 104.

46 Löwdin, P. O. Adv. Chem. Phys. 1959, 2, p. 207.

47 Sinanoglu, O.; Tuan, D. F. J. Chem. Phys. 1963, 38. p. 1740.

48 Sinanoglu, O.; Tuan, D. F. J. Chem. Phys. 1964, 41, p. 2667.

49 Pople, J. A.; Binkley, J. S.; Seeger, R. Int. J. Quantum Chem. 1976, S10, p. 1.

50 Krishnan, R.; Pople, J. A. Int. J. Quantum Chem. 1978, 14, p. 91.

51 Brueckner, K. A. Phys. Rev. 1955, 100, p. 36.

52 Goldstone, J. Proc. R. Soc. A 1957, 239, p. 267.

53 Hubbard, J. Proc. R. Soc. A 1957, 240, p. 539.

54 Coester, F. Nucl. Phys. 1958, 7, p. 421.

55 Kümmel, H. Lectures in Many-Body Problem; Academic Press: New York 1962, p. 265.

56 Kümmel, H.; Lührmann, K. H.; Zabolitzky, J. G. Phys. Rep. 1978, C36, p. 1.

57 Cizek, J. Chem. Phys. 1966, 45, p. 4256.

58 Cizek, J. Adv. Chem. Phys. 1969, 14, p. 35.

59 Cizek, J.; Paldus, J. Int. J. Quantum Chem. 1971, 5, p. 359.

60 Lindgren, I.; Morrison, J. Atomic Many-Body Theory; Springer: New York 1982.

61 B. Jeziorski, B.; Monkhorst, H. J.; K. Szalewicz, K.; Zabolitzky, J. G. J. Chem. Phys. 1984, 81, p. 368.

62 Bartlett, R. J. Ann. Rev. Phys. Chem. 1981, 32, p. 359.

63 Hohenberg, P.; Kohn, W. Phys. Rev. B 1964, 136, p. 864.

64 Kohn, W.; Sham, L. J. Phys. Rev. A 1965, 140, p. 1133.

65 Pulay, P. Chem. Phys. Lett. 1983, 100, p. 151.

66 Sæbø, S.; Pulay, P. Chem. Phys. Lett. 1985, 113, p. 13.

67 Pulay, P.; Sæbø, S. Theor. Chim. Acta 1986, 69, p. 357.

68 Jørgensen, P.; Simons, J. Geometrical Derivatives of Energy Surfaces and Molecular Properties; Reidel: Dordrecht 1986.

69 Pulay, P. Adv. Chem. Phys. 1987, 69, p. 241.

70 Helgaker, T.; Jørgensen, P. Adv. Quantum Chem. 1988, 19, p. 183.

71 Schrödinger, E. Ann. der Phys. 1926, 4(80), p. 437.

72 Møller, C.; Plesset, M. S. Phys. Rev. 1934, 46, p. 618.

73. Bartlett, R. J.; Dykstra, C. E.; Paldus, J. Coupled-Cluster Methods for Molecular Calculations; In: Advanced Theories and Computational Approaches to the Electronic Structure of Molecules; D. Reidel: Dordrecht (Netherlands) 1984, p. 127.

74 Merzbacher, E. Quantum Mechanics, 2nd ed.; Wiley: New York 1970.

75 Harris, F. E.; Monkhorst, H. J.; Freeman, D. L. Algebraic and Diagrammatic Methods in Many-Fermion Theory; Oxford Press: New York 1992.

76 Parr, R. G.; Yang, W. Density-Functional Theory of Atoms and Molecules; Oxford University Press: New York 1989, p. 149.

77 Levy, M. Phys. Rev. A 1982, 26, p. 1200.

78 Perdew, J. P.; Zunger, A. Phys. Rev. A 1982, 140, p. 1133.

79 Johnson, B. G.; Gonzales, C. A.; Gill, P. M. W.; Pople, J. A. Chem. Phys. Lett. 1994, 221, p. 100.

80 Thomas, L. H. Proc. Camb. Phil. Soc. 1927, 23, p. 542.

81 Fermi, E. Rend. Accad. 1927, 6, p. 602.

82 Fermi, E. Z. Phys. 1928, 48, p. 73.

83 Dirac, P. A. M. Proc. Camb. Phil. Soc. 1930, 26, p. 376.

84 Laming, G. J.; Termath, V.; Handy, N. C. J. Chem. Phys. 1993, 97, p. 4392.

85 Becke, A. D. J. Chem. Phys. 1993, 98, p. 1372.

86 Becke, A. D. J. Chem. Phys. 1993, 98, p. 5648.

87 Harris, J.; Jones,R. O. J. Phys. F 1974, 4, p. 1170.

88 Gunnarson, O.; Lundquist, B. I. Phys. Rev. B 1976, 13, p. 4274.

89 Harris, J. Phys. Rev. A 1984, 29, p. 1648.

90 Van Mourik, T.; Gdanitz, R. J. J. Chem. Phys. 2002, 116, p. 9620.

91 Buenker, R. J.; Peyerimhoff, S. D.; Butscher, W. Mol. Phys. 1978, 35, p. 771.

92 Peyerimhoff, S. D.; Buenker, R. J. CI Calcualtions of Vertical Excitation Energies and oscillator Strength for Rydberg and Valence States of Molecules; In: Excited States in Chemistry; Reidel: Dordrecht 1978, p. 79.

93 Blinder, S. M. Foundation of Quantum Dynamics; Academic Press: London 1974.

94 Fetter, A. L.; Walecka, J. P. Quantum Theory of Many-Particle Systems; McGraw-Hill: New York 1971.

95 Bloembergen, N. Nonlinear Optics; Benjamin: New York 1965.

96 R. L. Swafford, R. L.; Uricht, A. C. A. Annu. Rev. Phys. Chem. 1978, 29, p. 421.

97 Nonlinear Raman Spectroscopy and its Chemical Applications; Ed. Kiefer, W.; Long, D. A.; Reidel: Dordrecht 1968.

98 Laser Spectroscopy of Atoms and Molecules; Ed. Walther, H.; Springer: Berlin 1976.

99 Aiga, F.; Sasagane, K.; Itoh. R. J. Chem. Phys. 1993, 99, p. 3779.

100 Linderberg, J.; Öhrn, Y. Propagators in Quantum Chemistry; Academic Press: New York 1973.

101 Schirmer, J. Phys. Rev. A 1982, 26, p. 2395.

102 Trofimov A. B.; Schirmer, J. J. Phys. B 1995, 28, p. 2299.

103 Trofimov, A. B. ; Stelter, G.; Schirmer, J. J. Chem. Phys. 1999, 111, p. 9982.

104 Trofimov, A. B. ; Stelter, G.; Schirmer, J. Chem. Phys. 2002, 117, p. 6402.

105 Starcke, J. H.; Wormit, M.; Dreuw, A. J. Chem. Phys. 2009, 130, p. 24104.

106 Zubarev, D. N. Nonequilibrium Statistical Thermodynamics; Consultant Bureau, Plenum: New York 1974.

107 Dalgaard, E. Phys. Rev. A 1982, 26, p. 42.

108 Olsen, J.; Jørgensen, P. J. Chem. Phys. 1985, 82, p. 3235.

109 Hilborn, R. C. Am. J. of Phys. 1982, 50, p. 982.

110 Monkhorst, H. J. Int. J. Quantum Chem. Symp. 1977, 11, p. 42.

111 Dalgaard, E.; Monkhorst, H. J. Phys. Rev. A 1983, 28, p. 1217.

112 Koch, H.; Jørgensen, P. J. Chem. Phys. 1990, 93, p. 3333.

113 Runge, E.; Gross, E. K. U. Phys. Rev. Lett. 1984, 52, p. 997.

114 Van Leeuwen, R. Phys. Rev. Lett. 1999, 82, p. 3863.

115 Dreuw, A.; Head-Gordon, M. Chem. Rev., 2005, 105, p. 4009.

116 Casida, M. E. Time-Dependent Density Functional Response Theory for Molecules; In: Recent Advances in Density Functional Methods, Part I; World Scientific: Singapore 1995, p 155.

117 Maitra, N. T.; Zhang, F.; Cave, R. J.; Burke, K . J. Chem. Phys. 2004, 120, p. 5932.

118 Cave, R. J.; Zhang, F.; Maitra, N. T.; Burke, K. Chem. Phys. Lett. 2004, 389, p. 39.

119 Grabo, T.; Kreibich, T.; Kurth, S.; Gross, E. K. U. Orbital Functionals in Density Functional Theory: the Optimized Effective Potential Method; In: Strong Coulomb Correlations in Electronic Structure Calculations: Beyond the Local Density Approximation; Gordon and Breach 2000, p 203.

120 Cai, Z.-L.; Sendt, K.; Reimers, J. R. J. Chem. Phys. 2002, 117, p. 5543.

121 Grimme, S.; Parac, M. Chem. Phys. Chem. 2003, 3, p. 292.

122 Tozer, D. J.; Amos, R. D.; Handy, N. C.; Roos, B. J.; Serrano-Andres, L. Mol. Phys. 1999, 97, p. 859.

123 Dreuw, A.; Weisman, J. L.; Head-Gordon, M. J. Chem. Phys. 2003, 119, p. 2943.

124 Dreuw, A.; Head-Gordon, M. J. Am. Chem. Soc. 2004, 126, p. 4007.

125 Tozer, D. J. J. Chem. Phys. 2005, 119, p. 12697.

126 Perdew, J. P.; Parr, R. G.; Levy, M.; Balduz, J. L., Jr. Phys. Rev. Lett. 1982, 49, p. 1691.

127 Görling, A. Phys. Rev. Lett. 1999, 83, p. 5459.

128 Ivanov, S.; Hirata, S.; Bartlett, R. J. Phys. Rev. Lett. 1999, 83, p. 5455.

129 Della Sala, F.; Görling, A. Int. J. Quantum Chem. 2002, 91, p. 131.

130 Chernyak , V.; Mukamel, S. J. Chem. Phys. 2000, 112, p. 3572.

131 Neepa T.; Maitra, N. T. J. Chem. Phys. 2006, 125, p. 14110.

132 Vignale, G.; Rasolt, M.; Geldart, D. J. W. Adv. Quant. Chem. 1990, 21, p. 235.

133. Schirmer J.; Dreuw, A Phys. Rev. A 2007, 75, p. 22513.

134 Dreuw, A.; Schirmer J. Phys. Rev. A 2008, 78, p.56502.

135 Ashcroft, N. W.; Mermin, N. D Solid State Physics; Harcourt: Orlando 1976.

136 Hehre W. J.; Leo Radom, L.; Schleyer, P. V.; John Pople, J. Ab Initio Molecular Orbital Theory; Wiley-Interscience: New York 1986.

137 Dunning, T. H. J. Chem. Phys. 1989, 90, p.1007.

138 Jansen, H. B.; Ross, P. Chem. Phys. Lett. 1969, 3, p. 140.

139 Liu, B.; McLean A. D. J. Chem. Phys. 1973, 59, p. 4557.

140 Pickett, W. E. Comput. Phys. Rep. 1989, 9, p. 115.

141 Singh, D. J. Planewaves, Pseudopotentials and the LAPW Method; Kluwer: Dordrecht 1994.

142. Fuchs, M.; Scheffler, M. Comput. Phys. Commun. 1999, 119, p. 67.

143 Cundari, T. R.; Benson, M. T.; Lutz, M. L.; and Sommerer, S. O. Rev. Comput. Chem. 8, p. 145.

144 Dolg, M.; Stoll, H. In: Handbook on the Physics and Chemistry of Rare Earths; Vol. 22, p. 607; Elsevier: Amsterdam 1996.

145 Subotnik, J. E.; Head-Gordon, M. J. Chem. Phys. 2005, 123, p. 64108.

146 Subotnik, J. E.; Sodt, A.; Head-Gordon, M. J. Chem. Phys. 2006, 125, p. 74116.

147 Sæbø, S.; Pulay, P J. Chem. Phys. 1987, 86, p. 914.

148 Hetzer, G.; Pulay, P.; Werner, J.-H. Chem. Phys. Lett. 1998, 290, p. 143.

149 Schütz, M.; Hetzer, G.; Werner, H.-J. J. Chem. Phys. 1999, 111, p. 5691.

150 Schütz, M.; Werner, H.-J. J. Chem. Phys. 2001, 114, p. 661.

151 Werner, H.-J.; Manby, F. R.; Knowles, P. J. J. Chem. Phys. 2003, 118, p. 8149.

152 Russ, N. J.; Crawford, T. D. J. Chem. Phys. 2004, 121, p. 691.

153 Starcke, J. H.; Wormit, M.; Schirmer, J.; Dreuw, A. Chem. Phys. 2006, 329, p. 39.

154 Mayer, I. Int. J. Quantum Chem. 1983, 23, p. 341.

155 Mayer, I.; Vibök, Á. Int. J. Quantum Chem. 1991, 40, p. 139.

156 Mayer, I.; Vibök, Á. Int. J. Quantum Chem. 1992, 43, p. 801.

157 Mayer, I.; Vibök, Á. Chem. Phys. Lett. 1987, 136, p. 115.

158 Mayer, I.; Vibök, Á.; Valliron, P. Chem. Phys. Lett. 1994, 223, p. 166.

159 Mayer, I.; Valliron, P. J. Chem. Phys. 1998, 109, p. 3360.

160 Salvador, P.; Mayer, I. J. Chem. Phys. 2004, 120. p. 5882.

161 S. B. Boys, S. B.; F. Bernardi, F. Mol. Phys. 1970, 19, p. 553.

162 Gygi, F. Europhys. Lett. 1992, 19, p. 617.

163 Gygi, F. Phys. Rev. B 1993, 48 (11) p. 692.

164 Mayer, I. Int. J. Quantum Chem. 1998, 70, p. 41.

165 Van Duijneveldt, F. B.; van Duijneveldt-van de Rijdt, J.G.C.M.; van Lenthe J. H. Chem. Rev. 1994; 94, p. 1873.

166 Kobko, N.; Dannenberg, J. J. J. Phys. Chem. A 2001, 105, p. 1944.

167 Moran, D.; Simmonett, A. C.; Leach, F. E.; Allen, W. D.; Schleyer, P. V.; Schaefer, H. F. J. Am. Chem. Soc. 2006, 128, p. 9342.

168 Martin, J. M. L.; Taylor, P. R.; Lee, T. J. Chem. Phys. Lett. 1997, 275, p. 414.

169 Goodman, L.; Ozkabak, A. G.; Thakur, S. N. J. Phys. Chem. 1991, 95, p. 9044.

170 Dkhissi, A.; Adamowicz, L.; Maes, G. J. Phys. Chem. A 2000, 104, p. 2112.

171 Lampert, H.; Mikenda, W.; Karpfen, A. J. Phys. Chem. A 1997, 101, p. 2254.

172 Michalska, D.; Zierkiewicz, W.; Bienko, D. C.; Wojciechowski, W.; Zeegers-Huyskens, T. J. Phys. Chem. A 2001, 105, p. 8734.

173 Saeki, M.; Akagi, H.; Fujii, M. J. Chem. Theory Comput. 2006, 2, p. 1176.

174 Torii, H.; Ishikawa, A.; Takashima, R.; Tasumi, M. J. Mol. Struct.: THEOCHEM 2000, 500, p. 311.

175 Simandiras, E. D.; Rice, J. E.; Lee, T. J.; Amos, R. D.; Handy, N. C. J. Chem. Phys. 1988, 88, p. 3187.

176 Asturiol, D.; Duran, M.; Salvador, P. J. Chem. Phys. 2008, 128, p. 144108.

177 Salvador, P.; Fradera, X.; Duran, M J. Chem. Phys. 2000; 112, p. 10106.

178 Chesnut, D. B.; Phung, C. G. Chem. Phys. 1990, 147, p. 91.

179 Fileti, E. E.; Canuto, S. Int. J. Quantum Chem. 2005, 102, p. 554.

180 Zakharov, M.; Dreuw, A. *On the Magnitude of Basis-Set Superposition Error in Electronic-Structure Calculations with Atom-Centered Basis Sets.* To be published.

181 Harada, A.; Li, J.; Kamachi, M. Nature 1993, 364, p. 516.

182 Ghadiri, M. R.; Granja, J. R.; Milligan, R. A.; McRee, D. E.; Khazanovich, N. Nature 1993, 366, p. 324.

183 Feldman, Y.; Wasserman, E.; Srolovitz, D.; Tenne, R. Science 1995, 267, p. 222.

184 Barbour, L.; Orr, G. W.; Atwood, J. L. Nature 1998, 393, p. 671.

185 Fenniri, H.; Mathivanan, P.; Vidale, K. L.; Sherman, D. M.; Hallenga, K.; Wood, K. V.; Stowelet, J. G. J. Am. Chem. Soc. 2001, 123, p. 3854.

186 Hong, B. H.; Lee, J. Y.; Kim, J. C.; Bae, S. C.; Kim, K. S. J. Am. Chem. Soc. 2001, 123, p. 10748.

187 Kim, K. S.; Suh, S. B.; Kim, J. C.; Hong, B. H.; Lee, E. C.; Yun, S.; Tarakeshwar, P.; Lee, J. Y.; Kim-Ihm, H.; Kim, H. G.; Lee, J. W.; Kim, J. K.; Lee, H. M.; Kim, D.; Cui, C.; Youn, S. J.; Chung, H. Y.; Choi, H. S.; Lee, C.-W.; Cho, C. J.; Jeong, S.; Cho, J.-H J. Am. Chem. Soc. 2002, 124, p. 14268.

188 Hille, B. Ionic Channels of Excitable Membranes ; Sinauer: Sunderland 1984.

189 Ghadiri, M. R.; Granja, J. R.; Buehler, L. Nature 1994, 369, p. 301.

190 Kim, K. S. Bull. Korean Chem. Soc. 2003, 24 (6), p. 757.

191 Hoffman, A.; Sebastiani, D.; Sugiono, E.; Yun, S.; Kim, K. S.; Spiess, H.-W. Chem. Phys. Lett. 2004, 388, p. 164.

192 Brunklaus, G.; Koch, A.; Sebastiani, D.; Spiess, H.-W. Phys. Chem. Chem. Phys. 2007, 9 4545, p. 4551.

193 Hoffman, A. Private Communication.

194 Kuhlmann, B.; Arnett, E. M.; Siskin, M. J. Org. Chem. 1994, 59, p. 3098.

195 Chiang, Y.; Kresge, A. J.; Shepp, N. P. J. Am. Chem. Soc. 1989, 11, p. 3977.

196 Manojkumar, T. K.; Kim, D.; Kim, K. S. J. Chem. Phys. 2005, 122, p. 14305.

197 Van Mourik, T.; Wilson, A. K. Mol. Phys. 1999, 96, p. 529.

198 Xantheas, S. S.; Arpa, E. J. Chem. Phys. 2004, 120, p. 823.

199 Schlegel, H. B. Adv. Chem. Phys. 1987, 67, p. 249.

200 Head, J. D.; Weiner, B.; Zerner, M. C. Int. J. Quantum Chem. 1988, 33, p. 177.

201 Pulay, P.; Hamilton, T. P. Chem. Phys. 1988, 88, p. 4926.

202 Gordon, M. S.; Schmidt, M. W.; Chaban, G. M.; Glaesmann, K. R.; Stevens, W. J.; Gonzales, C. J. Chem. Phys. 1999, 110, p. 4199.

203 Schmidt, M. W.; Baldridge, K. K.; Gordon, M. S.; Jensen, J. H.; Koseki, S.; Matsunaga, N.; Nguen, K. A.; Su, S.; Windus, T. L.; Dupius, M.; Montgomery, J. A. J. Comput. Chem. 1993, 14, 1347.

204 Gaussian 03, Revision C.02, Frisch, M. J.; Trucks, G. W.; Schlegel, H. B.; Scuseria, G. E.; Robb, M. A.; Cheeseman, J. R.; Montgomery, Jr, J. A.; Vreven, T.; Kudin, K. N.; Burant, J. C.; Millam, J. M.; Iyengar, S. S.; Tomasi, J.; Barone, V.; Mennucci, B.; Cossi, M.; Scalmani, G.; Rega,

N.; Petersson, G. A.; Nakatsuji, H.; Hada, M.; Ehara, M.; Toyota, K.; Fukuda, R.; Hasegawa, J.; Ishida, M.; Nakajima, T.; Honda, Y.; Kitao, O.; Nakai, H.; Klene, M.; Li, X.; Knox, J. E.; Hratchian, H. P.; Cross, J. B.; Bakken, V.; Adamo, C.; Jaramillo, J.; Gomperts, R.; Stratmann, R. E.; Yazyev, O.; Austin, A. J.; Cammi, R.; Pomelli, C.; Ochterski, J. W.; Ayala, P. Y.; Morokuma, K.; Voth, G. A.; Salvador, P.; Dannenberg, J. J.; Zakrzewski, V. G.; Dapprich, S.; Daniels, A. D.; Strain, M. C.; Farkas, O.; Malick, D. K.; Rabuck, A. D.; Raghavachari, K.; Foresman, J. B.; Ortiz, J. V.; Cui, Q.; Baboul, A. G.; Clifford, S.; Cioslowski, J.; Stefanov, B. B.; Liu, G.; Liashenko, A.; Piskorz, P.; Komaromi, I.; Martin, R. L.; Fox, D. J.; Keith, T.; Al-Laham, M. A.; Peng, C. Y.; Nanayakkara, A.; Challacombe, M.; Gill, P. M. W.; Johnson, B.; Chen, W.; Wong, M. W.; Gonzalez, C.; and Pople, J. A.; Gaussian, Inc., Wallingford CT, 2004.

205 Cucinotta, C. S.; Ruini, A.; Catellani, A.; Stirling, A. Chem. Phys. Chem. 2006, 7, p. 1229.

206 Lee, D.; Kim, C. K.; Lee, B.; Lee, I. J. Comput. Chem. 1997, 18, p. 56.

207 Hu, X.; Li, H.; Liang, W.; Han, S. J. Phys. Chem. B 2004, 108 p. 12999.

208 Laerdahl, J. K.; Uggerud, E. J. Org. Chem. 2003, 1, p. 2935.

209 Laidler, K. J. Chemical Kinetics, Third Edition; Benjamin-Cummings 1997.

210 Lippert, E.; Lüder, W.; Moll, F.; Ngele, W.; Boos, H.; Prigge, H.; Seibold-Blankenstein, I. Angew. Chem. 1961, 73, p. 695.

211 Rotkiewicz, K.; Grellmann, K. H.; Grabowski, Z. R. Chem. Phys. Lett. 1973, 19, p. 315. Rotkiewicz, K.; Grellmann, K. H.; Grabowski, Z. R. Chem. Phys. Lett. 1973, 21, p. 212 (erratum).

212 Köhler, G.; Rechthaler, K.; Rotkiewicz, K.; Rettig, W. Chem. Phys. 1996, 207, p. 85.

213 Rettig, W.; Lutze, S. Chem. Phys. Lett. 2001, 341, p. 263.

214 Zachariasse, K. A.; Grobys, M.; von der Haar, T.; Hebecker, A.; Il'ichev, Y. V.; Morawski, O.; Rückert, I.;Kühnle, W. J. Photochem. Photobiol. 1997, 105, p. 373.

215 Zachariasse, K. A.; Druzhinin, S. I.; Bosch, W.; Machinek, R. J. Am. Chem. Soc. 2004, 126, p. 8075.

216 Sobolewski, A. L.; Domcke, W. Chem. Phys. Lett. 1996, 250, p. 428.

217 Sobolewski, A. L.; Sudholt, W.; Domcke, W. J. Phys. Chem. A 1998, 102, p. 2716.

218 Gorse, A. D.; Pesquer, M. J. Phys. Chem. 1995, 99, p. 4039.

219 Gomez, I.; Reguero, M.; Boggio-Pasqua, M.; Robb, M. J. Am. Chem. Soc. 2005, 127, p. 7119.

220 Domcke, W.;Yarkony, D. R.; Kppel, H. Conical Intersections: Electronic Structure, Dynamics and Spectroscopy; World Scientific: Singapore, 2004.

221 Jamorski, C. J., and Casida, M. E. J. Phys. Chem. B 2004, 108, p. 7132.

222 Sudholt, W.; Staib, A.; Sobolewski, A. L.; Domcke, W. Phys. Chem. Chem. Phys. 2000, 2, p. 4341.

223 Krauss, O.; Lommatzsch, U.; Lahmann, C.; Brutschy, B.; Rettig, W.; Herbich, J. Phys. Chem. Chem. Phys. 2001, 3, p. 74.

224 Daum, R.; Druzhinin, S.; Ernst, D.; Rupp, L.; Schroeder, J.; Zachariasse, K.A. Chem. Phys. Lett. 2001, 341, p. 272.

225 Dedonder-Lardeux, C.; Jouvet, C.; Martrenchard, S.; Solgadi, D.; McCombie, J.; Howells, B.D; Palmer, T.F.; Subaric-Leitis, A.; Monte, C.; Rettig, W.; Zimmermann, P. Chem. Phys. 1995, 191, p. 271.

226 Rettig, W.; Dedonder-Lardeux, C.; Jouvet, C.; Martrenchard-Barra, S.; Szrifiger, P.; Krim, L.; Castaño, F. J. Chim. Phys. 1995, 92, p. 465.

227 Grégoire, G.; Dimicoli, I.; Mons, M.; Dedonder-Lardeux, C.; Jouvet, C.; Martrenchard, S.; Solgadi, D. J. Phys. Chem. A, 1998, 102, p. 7896.

228 Parusel, A. B. J.; Köhler, G.; Grimme, S. J. Phys. Chem. A 1998, 102, p. 6297.

229 Krauss, O. Photoinduzierter Ladungstransfer in Mikrosolvatclustern: Untersuchungen mit LIF-Spektroskopie und IR-UV-Doppelresonanzspektroskopie. Ph.D. Thesis, Goethe University, Frankfurt/M, Germany, 2002.

230 Christiansen, O.; Koch, H.; Jørgensen, P. Chem. Phys. Lett. 1995, 243, p. 409.

231 Hättig, C; Köhn, A. J. Chem. Phys. 2002, 117, p. 6939.

232 Köhn, A.; Hättig, C. J. Chem. Phys. 2003, 119, p. 5021.

233 Weiss, H.; Ahlrichs, R.; Häser, M. J. Chem. Phys. 1993, 99, p. 1262.

234 Kowski, K.; Luttke, W.; Rademacher, P. J. Mol. Struct. 2001, 567, p. 231.

235 Shi, T.; Ge, J.; Guo, J.; Zhu, Q. Chem. Phys. Lett. 2004, 397, p. 160.

236 Tachikawa, H. Phys. Chem. Chem. Phys. 2002, 4, p. 6018.

237 Kiermeier, A.; Ernstberger, B.; Neusser, H. J.; Schlag, E. W. J. Phys. Chem. 1988, 92, p. 3785.

238 Ernstberger, B.; Krause, H.; Neusser, H. J. Z. Phys. D 1991, 20, p. 189.

239 May, V.; Kühn, O. Charge and Energy Transfer Dynamics in Molecular Systems (Second Edition); Wiley-VCH: Berlin, 2004.

240 Kayano, M.; Ebata, T.; Yamada, Y.; Mikamia, N. J. Chem. Phys. 2004, 120, p. 7410.